Imaging mass spectrometry approaches for the detection and localisation of drug compounds and small molecules in tissue.

Eleanor Quibell Blatherwick BSc (Hons)

A thesis submitted for the degree of Doctor of Philosophy

University of Warwick

School of Life Sciences

January 2013

For my parents, Gillian and Mark, who have always encouraged and supported me to achieve the best that I can.

Table of Contents

Chapter 1 Introduction 1

1.1 Mass Spectrometry 2

1.1.1 What is a mass spectrometer? 2

1.1.2 Ionisation methods 3

1.1.2.1 Matrix-assisted laser desorption/ionisation 3

1.1.2.2 Electrospray ionisation 5

1.1.3 Mass analysers 6

1.1.3.1 Quadrupole 7

1.1.3.2 Time-of-flight 8

1.1.3.3 Ion Trap 12

1.1.3.4 Orbitrap 12

1.1.3.5 Fourier Transform ion cyclotron resonance 13

1.1.4 Detectors 13

1.1.5 Tandem mass spectrometry 15

1.1.6 Ion Mobility mass spectrometry 17

1.1.7 Travelling-wave ion mobility mass spectrometry 19

1.2 Drug Localisation 23

1.2.1 Why is drug localisation important? 23

1.2.2 Quantitative Whole Body Autoradiography 24

1.2.3 Tissue homogenisation and LC-MS/MS 26

1.2.4 Fluorescence 27

1.2.5 PET imaging 28

1.2.6 Limitations of established drug localisation approaches 28

1.3 Imaging Mass Spectrometry 30

1.4 SIMS imaging 30

1.4.1 Secondary ion ionisation 30

1.5 MALDI Imaging 32
1.5.1 Experimental overview 32
1.6 Practical considerations of MALDI imaging 34
1.6.1 Initial tissue treatment 34
1.6.2 Matrix choice and deposition 37
1.6.3 Instrumentation 41
1.6.4 Ion mobility separation 46
1.6.5 Software for imaging mass spectrometry 46
1.7 Applications of MALDI imaging 49
1.7.1 MALDI imaging for drug localisation 50
1.8 Ambient ionisation imaging 52
1.9 Desorption electrospray ionisation 52
1.10 LESA profiling 54
1.10.1 Practical considerations 56
1.10.2 Instrumentation 56
1.11 Aims of the project 58
1.12 Research Papers 59
1.13 Conference papers (peer-reviewed) 60
1.14 Invited oral presentations 60
Chapter 2 Materials and Methods 61
2.1 Overview 62
2.2 Drug detection studies (Chapter 3) 62
2.2.1 *In vivo* animal dosing 63
2.2.2 Tissue handling 63
2.2.3 Mass spectrometry analysis 64
2.2.3.2 LESA profiling 66
2.2.3.3 MALDI-MS analysis of standards 67

2.2.3.4 MALDI imaging 67
2.3 Drug and metabolite localisation studies (Chapter 4) 69
2.3.1 *In vivo* animal dosing and tissue handling 69
2.3.2 Sample preparation 70
2.3.3 Metabolite characterisation 71
2.3.4 Mass spectrometry analysis 72
2.3.5 ESI-MS analysis of standards 72
2.3.6 LESA profiling 73
2.3.7 MALDI-MS analysis of standards 74
2.3.8 MALDI profiling 75
2.3.9 MALDI imaging 75
2.4 Localisation of adenine nucleotides (Chapter 5) 77
2.4.1 Analysis of standards 77
2.4.2 Tissue handling 78
2.4.3 Heat-stabilised tissue 78
2.4.4 Experimental method 80
2.4.5 Tissue staining 81
2.4.6 Data processing 82
2.4.6.1 Relative ion intensity ratio of adenine nucleotides 82
Chapter 3 Investigation of *in vivo* drug delivery and deposition using an imaging mass spectrometry approach 83
3.1 Imaging MS approaches to drug distribution in tissue 84
3.1.1 Fenclozic Acid 85
3.1.2 Diclofenac distribution in mice 85
3.2 Results and Discussion 89
3.3 Evaluation of imaging MS approaches to drug localisation 89
3.3.1 Analysis of fenclozic acid standards 89

3.3.2 LESA-MS/MS analysis on tissue 90
3.3.3 LESA-mobility-MS/MS analysis on tissue 91
3.3.4 MALDI profiling 93
3.4 Application of imaging MS for *in vivo* drug distribution 94
3.4.1 ESI-MS analysis of diclofenac standard 94
3.4.2 LESA-MS analysis of diclofenac concentration series 97
3.5 LESA profiling of dosed whole-body tissue samples 101
3.5.1 Wild type mouse 3 hours post dose 101
3.5.2 HRN mouse 3 hours post dose 103
3.5.3 Wild type mouse 24 hours post dose 105
3.5.4 HRN mouse 24 hours post dose 107
3.6 MALDI imaging 109
3.6.1 MALDI-MS of diclofenac standard 109
3.6.2 MALDI-MS analysis of diclofenac concentration series 110
3.6.3 MALDI imaging of dosed kidney samples 114
3.7 Conclusions 115
Chapter 4 Combining industry-standard methods and imaging MS approaches for drug and metabolite distribution in rat 117
4.1 A combined Met-ID and imaging MS approach to drug and metabolite distribution in rat 118
4.1.1 Propranolol 118
4.1.2 Fenclozic Acid 121
4.2 Results and Discussion 122
4.3 Radioprofiling of tissue homogenates 122
4.4 Tissue extraction and metabolite identification 123
4.4.1 UPLC-MS 126
4.5 LESA profiling 129

4.5.1 ESI-MS analysis of fenclozic acid standard 129
4.5.2 LESA profiling of fenclozic acid dosed tissue sections 131
4.5.3 Detection of fenclozic acid metabolites by LESA-MS 135
4.5.4 ESI-MS analysis of propranolol standard 136
4.5.5 LESA profiling of propranolol dosed tissue sections 138
4.5.6 Detection of propranolol metabolites by LESA-MS 140
4.6 MALDI profiling 146
4.6.1 MALDI-MS analysis of fenclozic acid 146
4.6.2 Detection of fenclozic acid in dosed tissue sections 147
4.6.3 MALDI-MS analysis of propranolol standard 152
4.6.4 Detection of propranolol in dosed tissue sections 153
4.6.4.1 Detection of propranolol metabolites 154
4.7 MALDI imaging 156
4.7.1 Localisation of fenclozic acid in dosed tissue sections 156
4.8 Conclusions 159
Chapter 5 Localisation of adenine nucleotides in mouse brain using ion mobility enabled MALDI imaging 163
5.1 Metabolic Stress and Neuronal Function 164
5.1.1 Adenine nucleotides 164
5.1.2 Metabolic stress and adenine nucleotides 166
5.1.3 Previous work 167
5.1.4 Tissue fixation approaches 168
5.1.4.1 Ethanol fixation 169
5.1.4.2 Microwave fixation 169
5.1.4.3 Heat stabilisation 170
5.2 Results and Discussion 172
5.2.1 Analysis of adenine nucleotide standards 172

5.2.2 Identification of adenine nucleotides from a mixture 174
5.2.3 Identification of adenine nucleotides on tissue 175
5.2.4 Localisation of adenine nucleotides in mouse brain 179
5.3 Tissue fixation approaches: ethanol wash 180
5.3.1 Relative intensity of ATP:ADP:AMP in tissue 182
5.3.2 Control vs. stressed tissue 183
5.4 Tissue fixation approaches: heat stabilisation 184
5.4.1 Relative intensity of ATP:AMP 184
5.4.2 Ion distribution images of adenine nucleotides 186
5.5 Conclusions 191
Chapter 6 Conclusions and Future Work 194
6.1 Ion mobility separation 195
6.2 LESA profiling 196
6.3 MALDI imaging 197
6.4 Future directions 198
6.4.1 Quantitative imaging mass spectrometry 199
6.5 Concluding remarks 201
Appendix A: References 202
Appendix B: Dissemination of work 214

List of Figures

Figure 1.1 Schematic of a modern mass spectrometer. 2
Figure 1.2 The MALDI ionisation process. 4
Figure 1.3 The ESI ionisation process. 5
Figure 1.4 Schematic of a quadrupole mass analyser. 7
Figure 1.5 Schematic representation of a reflectron TOF instrument. 9
Figure 1.6 Simplified schematic representation of an oa-TOF reflectron system. 11
Figure 1.7 Principle of MS/MS: 16
Figure 1.8 Schematic representation of Drift-cell IMS. 18
Figure 1.9 Schematic diagram of an RF-only stacked ring ion guide (SRIG). 19
Figure 1.10 Schematic representation illustrating ion mobility separation in a TWIG. 20
Figure 1.11 The drug discovery and development process. 24
Figure 1.12 Schematic of secondary ion mass spectrometry ionisation. 31
Figure 1.13 Workflow of a typical MALDI imaging experiment. 33
Figure 1.14. Analysis of the effect of OCT on MALDI signals from rat liver. 35
Figure 1.15 Schematic of MALDI Synapt G2 HDMS Q-TOF mass spectrometer. 44
Figure 1.16 Example MALDI-mobility-MS imaging data file displayed in Driftscope as a heat map of *m/z* vs. drift time. 48
Figure 1.17 Schematic of Liquid Extraction Surface Analysis technique. 55
Figure 2.1 Schematic to show the workflow of a MALDI-mobility-MS/MS imaging experiment for the identification of adenine nucleotides in mouse brain tissue. 80
Figure 3.1 Chemical structure of fenclozic acid. 85
Figure 3.2 Chemical structure of diclofenac 85
Figure 3.3 Metabolism of diclofenac by CYP and UGT mediated pathways, forming potentially reactive intermediates. 86
Figure 3.4 QWBA images of diclofenac distribution. 87
Figure 3.5 LESA-MS analysis of fenclozic acid standard on glass slide. 89
Figure 3.6 LESA-MS/MS analysis on tissue. 90
Figure 3.7 LESA-mobility-MS/MS analysis on tissue. 92
Figure 3.8 MALDI-MS/MS profiling on tissue. 93
Figure 3.9 a) ESI-MS of diclofenac in negative ion mode. 95
Figure 3.10 Fragmentation of *m/z* 249 in negative ion mode. 96

Figure 3.11 Arrival time distribution (ATD) of diclofenac standard. 96
Figure 3.12 LESA-MS analysis of diclofenac concentration series. 97
Figure 3.13 LESA-mobility-MS/MS of diclofenac concentration series. 98
Figure 3.14. Control kidney sections for LESA-MS sampling. 99
Figure 3.15 Arrival time distribution of *m/z* 249 (red) and *m/z* 213 (black) through the mobility cell 100
Figure 3.16 LESA-IMS-MS/MS sampling of wild type mouse whole body tissue section 3 hours post-dose. 102
Figure 3.17 LESA-IMS-MS/MS sampling of hepatic P450 null reductase (HRN) mouse whole body tissue section 3 hours post-dose. 104
Figure 3.18 LESA-IMS-MS/MS sampling of wild type mouse whole body tissue section 24 hours post-dose. 106
Figure 3.19 LESA-IMS-MS/MS sampling of hepatic P450 null reductase (HRN) mouse whole body tissue section 24 hours post-dose. 108
Figure 3.20 Negative ion mode MALDI-MS of diclofenac standard. 109
Figure 3.21 MALDI-mobility-MS of diclofenac standard. 110
Figure 3.22 Schematic showing differences between a standard MALDI-MS experimental method and an enhanced selectivity MALDI-IMS-MS/MS method. 111
Figure 3.23 MALDI imaging of diclofenac concentration series on target. 112
Figure 3.24 MALDI-mobility-MS/MS imaging of diclofenac concentration series on tissue. 112
Figure 3.25 MALDI-MS imaging of diclofenac concentration series on tissue. 113
Figure 3.26 MALDI-mobility-MS/MS imaging of *m/z* 213 across dosed kidney sections. 114
Figure 4.1 Structure of propranolol 119
Figure 4.2 Metabolites of propranolol as identified in rat cryopreserved hepatocytes. 120
Figure 4.3. Structure of fenclozic acid 121
Figure 4.4 Radioactivity levels in tissue homogenate from [^{14}C]-propranolol-dosed rats at 2, 6 and 24 hours post-dose. 122
Figure 4.5 Radioactivity levels in tissue homogenate from [^{14}C]-fenclozic acid-dosed rats at 2, 6 and 24 hours post-dose. 123

Figure 4.6 Radioactivity extraction efficiency of methanol, acetonitrile and tetrahydrofuran for propranolol and fenclozic acid-dosed tissues. The percentage extraction efficiency for each stage of a two-step extraction is shown for each solvent. 124
Figure 4.7 Mean radioactivity in propranolol dosed tissue extract following methanol extraction. 125
Figure 4.8 Mean radioactivity in fenclozic acid dosed tissue extract following methanol extraction. 125
Figure 4.9 Structure of fenclozic acid taurine conjugate. 128
Figure 4.10 Analysis of fenclozic acid standard. 129
Figure 4.11 LESA-mobility-MS/MS spectra of fenclozic acid concentration series on tissue. 130
Figure 4.12 Calibration curve of fenclozic acid by LESA-MS/MS. 131
Figure 4.13 LESA-mobility-MS/MS profiling of fenclozic acid dosed rat organs 2 hours post-dose. 132
Figure 4.14 LESA-mobility-MS/MS profiling of fenclozic acid dosed rat organs 6 hours post-dose. 133
Figure 4.15 LESA-mobility-MS/MS profiling of fenclozic acid dosed rat organs 24 hours post-dose. 134
Figure 4.16 Analysis of propranolol standard. 136
Figure 4.17 Fragmentation pathway of propranolol. 136
Figure 4.18 LESA-mobility-MS/MS spectra of propranolol concentration series on tissue. 137
Figure 4.19 LESA-mobility-MS/MS profiling of propranolol dosed rat 2 hours post-dose. 138
Figure 4.20 Structures of two propranolol metabolites; 4-hydroxypropranolol and 4-hydroxypropranolol glucuronide. 140
Figure 4.21 Extracted ATD and LESA-mobility-MS/MS of *m/z* 276 from propranolol liver sample 2 hours-post dose. 141
Figure 4.22 Extracted ATD and LESA-mobility-MS/MS of *m/z* 452 from propranolol liver 2 hours post-dose. 142
Figure 4.23 Extracted ATD and LESA-mobility-MS/MS profiling of 4-hydroxypropranolol glucuronide in dosed liver at 2, 6 and 24 hours post-dose. 143

Figure 4.24 MALDI-MS/MS fragmentation of 250 fmol fenclozic acid standard spiked on tissue. 147
Figure 4.25 MALDI profiling of fenclozic acid dosed rat liver, 6 hours post-dose.148
Figure 4.26 MALDI-mobility-MS/MS profiling of *m/z* 208 fragment ion of fenclozic acid 2 hours post-dose. 149
Figure 4.27 MALDI-mobility-MS/MS profiling of *m/z* 208 fragment ion of fenclozic acid 6 hours post-dose. 150
Figure 4.28 MALDI-mobility-MS/MS profiling of *m/z* 208 fragment ion of fenclozic acid 24 hours post-dose. 151
Figure 4.29 MALDI profiling of propranolol dosed rat liver, 2 hours post-dose. ...153
Figure 4.30 ATD and MALDI-mobility-MS/MS spectra of *m/z* 452 from liver 2 hours post-dose. 154
Figure 4.31 MALDI-mobility-MS/MS imaging of fenclozic acid in liver at 2, 6 and 24 hours post-dose. 157
Figure 5.1. Chemical structures of ATP, ADP and AMP. 165
Figure 5.2 Extracted arrival time distribution and mobility-resolved MALDI MS/MS spectra for ATP standard on target. 172
Figure 5.3 Extracted arrival time distribution and mobility-resolved MALDI MS/MS spectra for ADP standard on target. 173
Figure 5.4 Extracted arrival time distribution and mobility-resolved MALDI MS/MS spectra for AMP standard on target. 173
Figure 5.5. Identification of adenine nucleotide standards from a mixture by MALDI-mobility-MS. 175
Figure 5.6. MALDI-mobility-MS/MS spectra and extracted arrival time distribution for *m/z* 506 from control mouse brain section and ATP standard. 176
Figure 5.7. MALDI-mobility-MS/MS spectra and extracted arrival time distribution for m/z 426 from control mouse brain section and ADP standard. 177
Figure 5.8. MALDI-mobility-MS/MS spectra and extracted arrival time distribution for m/z 346 from control mouse brain section and AMP standard. 178
Figure 5.9. MALDI-mobility-MS/MS images from control mouse brain sections at 50 µm spatial resolution. The intensity of parent ions at a) m/z 506 (ATP) b) m/z 426 (ADP) and c) m/z 346 (AMP) in brain are displayed. 179

Figure 5.10. MALDI-mobility-MS/MS images from washed control mouse brain sections at 50 µm spatial resolution. 181
Figure 5.11. Ion intensity percentage ratio of the adenine nucleotides in control brain sections with and without inclusion of an ethanol wash step. 182
Figure 5.12. Ion intensity percentage ratio of the adenine nucleotides in control and stressed brain sections with the inclusion of an ethanol wash step. 183
Figure 5.13 Average intensity ratios of ATP:AMP across four mouse brain sections to demonstrate the effect of heat-stabilisation. 185
Figure 5.14 MALDI-mobility-MS/MS images of adenine nucleotide localisation in a snap-frozen mouse brain. 187
Figure 5.15 MALDI-mobility-MS/MS images of adenine nucleotide localisation in a heat-stabilised mouse brain. 190
Figure 6.1 Literature search on Scopus (www.scopus.com) using the search terms ‘imaging’ and ‘mass spectrometry’ in the title, abstract or keywords. *Results up until 31st December 2012. 201

List of Tables

Table 1.1 Common matrices used in MALDI imaging. 37
Table 1.2 Matrix application techniques for imaging MS. 39
Table 1.3 A summarised list of current commercial MALDI imaging mass spectrometers.....43
Table 2.1 Experimental conditions for LESA and MALDI analysis of fenclozic acid and diclofenac. 65
Table 2.2 Tissue samples and experiments for metabolism study. 70
Table 2.3 Mouse brain samples prepared for heat-stabilisation experiments. 79
Table 2.4. Hematoxylin and Eosin staining prototcol for histological staining of tissue sections following MALDI imaging acquisition. 81
Table 4.1. Metabolites observed in selected propranolol-dosed samples. 127
Table 4.2 Summary of LESA profiling of propranolol dosed tissue sections. 144

Acknowledgements

There are many people I would like to thank for the encouragement and support they have given me throughout the course of my PhD.

I would like to start by thanking my academic supervisor Prof. Jim Scrivens, for giving me the opportunity to undertake this PhD, and for providing me with the many other fantastic opportunities that have come alongside it. His advice, support and guidance over the last three years have been invaluable. I would also like to thank my industrial supervisor, Dr. Dan Weston (AstraZeneca) for his guidance and support, despite the many ups and downs in the world of pharmaceuticals. This work was financially supported by the Medical Research Council and AstraZeneca UK. I thank everybody at AstraZeneca who looked after me during my CASE project, and who have assisted in providing me with samples over the course of the last three years.

Additional thanks goes to everyone who helped with my initial training in the world of MALDI imaging mass spectrometry, specifically Emmanuelle (Waters) and Kamila (AMOLF). I could not have started this journey without your help. I would also like to thank Mark A and Mark B at Advion for their technical expertise and for excellent dinners during ASMS. For help with the ATP work, many thanks also goes to Beatrice and colleagues at Denator.

Thanks to all members of the Scrivens Group at Warwick past and present for making this journey an enjoyable one. Special thanks to Fran, Krisztina, Nisha and Matt for their excellent company in the lab, but more importantly at coffee and lunch! Huge thanks must go to Sue, without whom I would not have entered the world of mass spectrometry in the first place. You have advised me and supported me throughout this PhD (and most importantly put up with sharing a room with me at conferences). Thank you for taking a chance on me and introducing me to biological mass spectrometry - despite highs and lows it has been a brilliant experience.

There are many friends who have shaped this experience. Thank you to Anna, Charlie and Dave for the weekends of fun that have kept me sane, especially in the

last few months. Thanks also to Cate, for coffee and catch ups that were always more successful than swimming plans!

I would like to thank my wonderful extended family (Blatherwicks and Batemans) for their unconditional love, support and an escape from the science. To my parents especially, who have always believed in me and encouraged me, despite not having understood anything I've done for a long time!

Finally, my biggest thanks is to my best friend and fiancé Perry. I cannot ever thank you enough for the love and support you have given me throughout this journey. I know you have travelled it with me, experiencing the highs and carrying me through the lows. Thank you for always being you, making me laugh and sharing this with me.

Declaration

I hereby declare that this thesis, submitted in partial fulfilment of the requirements for the degree of Doctor of Philosophy and entitled ***Imaging mass spectrometry approaches for the detection and localisation of drug compounds and small molecules in tissue*** represents my own work and has not previously been submitted to this, or any other, institution for any degree, diploma or other qualification. Work undertaken by my collaborators is explicitly stated where appropriate.

Eleanor Q. Blatherwick
January 2013

Summary

A crucial and challenging aspect of the drug development process is the requirement to measure the distribution of a pharmaceutical compound and its metabolites in tissue. Industry-standard methods used to look at total localisation of drug-related material are limited due to their dependence on labels. These labelled techniques can have difficulty in distinguishing between the drug of interest and its metabolites.

Imaging mass spectrometry is a technique that has the potential to spatially distinguish between drug and metabolites, due to its high chemical specificity and sensitivity. A number of imaging mass spectrometry approaches have been described for localisation of drug compounds in tissue, most notably matrix-assisted laser desorption/ionisation (MALDI) imaging, which can provide data complementary to existing imaging techniques.

Two imaging mass spectrometry approaches have been evaluated and compared for use in the localisation of a range of drug compounds in target tissues. The techniques used were MALDI imaging and a recently described electrospray ionisation-based technique, liquid extraction surface analysis (LESA).

Both techniques have been successfully used for the detection of drug compounds in dosed tissue sections. A major challenge associated with imaging techniques is the required selectivity of the experiment for the compound of interest, due to the complex nature of tissue sections. Combining the shape-selective method of ion mobility separation with MS/MS fragmentation has been shown to improve the selectivity of both imaging approaches for the compound of interest.

Results obtained using LESA-MS have demonstrated the suitability of this technique as a rapid and sensitive profiling technique for the detection of drugs and metabolites in tissue, but with a lower achievable spatial resolution than MALDI imaging. Higher spatial resolution was achieved with MALDI imaging; however data acquisition times were longer and required higher dosing levels for successful detection of drug compounds in tissue.

A biological application of MALDI imaging was also evaluated. Mobility-enabled MALDI imaging was used to assess differences in the localisation of important adenine nucleotides between control and metabolically stressed mouse brain sections. Tissue fixation methods were evaluated to overcome rapid post-mortem degradation of adenine nucleotides such that biologically relevant localisation images can be obtained. These studies highlight the crucial importance of appropriate biological sample preparation in MALDI imaging experiments.

List of Abbreviations

One

1D	One-dimensional

Two

2D	Two dimensional

Three

3-HPA	3-Hydroxypicolinic acid

Nine

9-AA	9-aminoacridine hydrochloride

A

ACN	Acetonitrile
ADC	Analogue-to-digital
ADP	adenosine-5-diphosphate
ADME	Absorption distribution metabolism excretion
AMP	adenosine-5-monophosphate
ATD	Arrival time distribution
ATP	adenosine-5-triphosphate

B

C

CASE	Cooperative Awards in Science and Engineering
CHCA	α-Cyano-4-hudroxycinnamic acid

CI	Chemical ionisation
CID	Collision-induced dissociation
CMC	Carboxymethylcellulose
CNS	Central nervous system
CYP	Cytochrome P450

D

Da	Dalton
DC	Direct current
DCIM	Drift cell ion mobility
DCTB	trans-2-3-(4-tert-butylphenyl)-2-methyl-(2-propenylidene)-malononitrile
DESI	Desorption electrospray ionisation
DHB	2,5-Dihydroxybenzoic acid
DIGE	Difference gel electrophoresis
DPM	Disintegrations per minute
DPMK	Drug metabolism and pharmacokinetics

E

EC	European Commission
ECD	Electron capture dissociation
EDC	Enhanced duty cycle
EI	Electron impact
EM	Electron multiplier
EMA	European Medicines Agency
ESI	Electrospray ionisation
ETD	Electron transfer dissociation
EtOH	Ethanol

F

FAB	Fast atom bombardment
FFPE	formalin-fixed paraffin-embedded
FT-ICR	Fourier transform-ion-cyclotron resonance
FTIR	Fourier transform infrared
FWHM	Full width half height maximum

G

GLP	Good Lab Practice

H

HDMS	High-definition mass spectrometry
H&E	Hematoxylin and Eosin staining
HPLC	High performance liquid chromatography
HRN	Hepatic P450 Null Reductase mice

I

ICH	International Conference on Harmonisation of Technical Requirements for Registration of Pharmaceuticals for Human Use
ICI	Imperial Chemical Industries
ID	Internal diameter
IM	Ion mobility
IM-MS	Ion mobility mass spectrometry
IMS	Ion mobility spectrometry
IR	Infrared

J

K

kV	kilo-Volts

L

LC	Liquid chromatography
LESA	Liquid extraction surface analysis
LIT	Linear ion trap
LSC	Liquid scintillation counting

M

m/z	mass-to-charge
MALDI	Matrix assisted laser desorption/ionisation
MCP	Microchannel plate
MeOH	Methanol
Met ID	Metabolite identification
MRI	Magnetic resonance imaging
MS	Mass spectrometry
MSI	Mass spectrometry imaging
MS/MS	Tandem mass spectrometry
M_w	weight-average molecular weight

N

n-ESI	nano-Electrospray ionisation
Nd:YAG	neodymium:yttrium aluminium garnet
NMR	Nuclear magnetic resonance
NSAID	Non steroidal anti-inflammatory drug

O

Oa-TOF	orthogonal acceleration time-of-flight
OCT	Optimal cutting temperature polymer
OD	Outer diameter

P

PEG	Poly(ethylene glycol)
PET	Positron Emission Tomography
pg	picogram

Q

QQQ	Triple quadrupole
Q-TOF	Quadrupole time-of-flight
QWBA	Quantitative whole-body autoradiography

R

R&D	Research and Development
RF	Radio frequency
ROI	Region of interest

S

SA	3,5-Dimethoxy-4-hydroxycinnamic acid (sinapinic acid)
SIMS	Secondary ion mass spectrometry
SRIG	Stacked ring ion guide

T

TDC	Time-to-digital
TFA	Trifluoroacetic acid
THAP	2,4,6-trihydroxyacetophenone
THF	Tetrahydrofuran
TLC	Thin-layer chromatography
TOF	Time-of-flight

T-wave	Travelling wave
TWIG	Travelling wave ion guide

U

UGT	Uridine 5’-diphospho-glucuronosyltransferase
UPLC	Ultra performance liquid chromatography
USD	United States Dollars
UV	Ultraviolet

V

W

WBA	Whole-body autoradiography
WT	Wild-type strain

X

Y

Z

Chapter 1 Introduction

1.1 Mass Spectrometry

The world's first mass spectrum, showing a plot of ion intensity against relative mass, was published over one hundred years ago, by Sir Joseph John Thomson. He obtained a mass spectrum of carbon dioxide (CO_2^+), CO^+, O^+, C^+ and H^+ using a parabola spectrograph (Thomson 1912; Budzikiewicz and Grigsby 2006). This pioneering work was extended by his student Francis W. Aston, who developed a mass spectrograph with improved resolution (Aston 1919). This instrument allowed Aston to separate chlorine isotopes and isotopes of many other non-radioactive elements (Aston 1920), for which he was awarded the Nobel Prize for Chemistry in 1922. Since then, countless improvements have been made in the field of mass spectrometry (MS). Today, mass spectrometry stands out as an analytical method with unmatched sensitivity, detection limits and speed, in use in a wide range of applications across many scientific fields.

1.1.1 What is a mass spectrometer?

Mass spectrometry can simply be defined as the measurement of the mass-to-charge (*m/z*) ratio of an ion in the gas phase. Modern day mass spectrometers consist of an ionisation source to generate ions; one or more mass analysers to separate these ions according to their mass and charge; a detector and a computer for data processing to produce the final mass spectrum. A schematic of a modern mass spectrometer is shown in Figure 1.1.

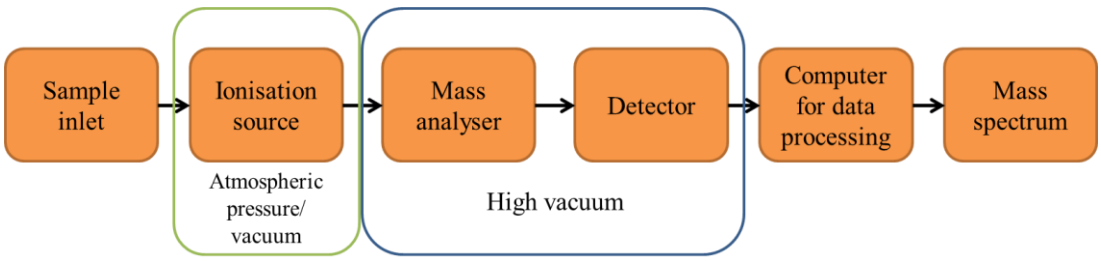

Figure 1.1 Schematic of a modern mass spectrometer.

Whilst the inlet and ionisation source may be at atmospheric pressure, the mass analyser and detector function under moderate-to-high vacuum. This allows the ions to pass through the mass spectrometer without colliding with each other, before they

reach the detector. A vacuum gradient through the mass spectrometer is generated and maintained by a series of mechanical and turbomolecular pumps. Ionisation sources can either operate at atmospheric pressure or under vacuum, depending on the approach used.

1.1.2 Ionisation methods

A wide variety of ionisation techniques have been used in mass spectrometry. The ionisation technique of choice should preserve the properties of the sample of interest, whilst converting it into gas phase ions that can be analysed in the mass spectrometer (Vestal 2001). Until the advent of soft-ionisation techniques in the 1980's, MS ionisation was commonly achieved by chemical ionisation (CI) or electron impact (EI) methods. For both ionisation methods the sample must be thermally volatile and stable. Biological molecules tend to be both thermally unstable and non-volatile, and as such, CI and EI do not prove to be useful ionisation methods for these molecules unless prior derivatisation is carried out (Griffiths, Jonsson et al. 2001).

Some progress was made in the analysis of small biological samples following the introduction of fast atom bombardment (FAB) in 1981 (Barber, Bordoli et al. 1981), but the real revolution in biological mass spectrometry came about with the development of two soft-ionisation techniques; matrix-assisted laser desorption/ionisation (MALDI) and electrospray ionisation (ESI). In 2002, the Nobel Prize in Chemistry was jointly awarded to Koichi Tanaka and John Fenn for their development of soft ionisation methods for mass spectrometric analyses of biological macromolecules.

1.1.2.1 Matrix-assisted laser desorption/ionisation

Koichi Tanaka was awarded the Nobel Prize for his work in soft laser desorption ionisation (Tanaka, Waki et al. 1988). The greatest impact in biological MS research came from the related approach of matrix-assisted laser desorption ionisation (MALDI), which was developed by Michael Karas and Franz Hillenkamp in 1988 (Karas and Hillenkamp 1988).

In MALDI, the sample of interest is embedded in a suitable matrix, typically a small organic acid that strongly absorbs UV radiation, and the two are co-crystallised together on a target plate. Under vacuum, a UV laser is focussed on the sample causing localised heating of the matrix molecules. This results in desorption of the sample and ejection of neutral and charged analyte and matrix molecules, along with analyte-matrix clusters into the gas phase as shown by Figure 1.2. Little fragmentation occurs during the MALDI process, and the majority of ions formed are singly charged. MALDI is a pulsed ionisation process.

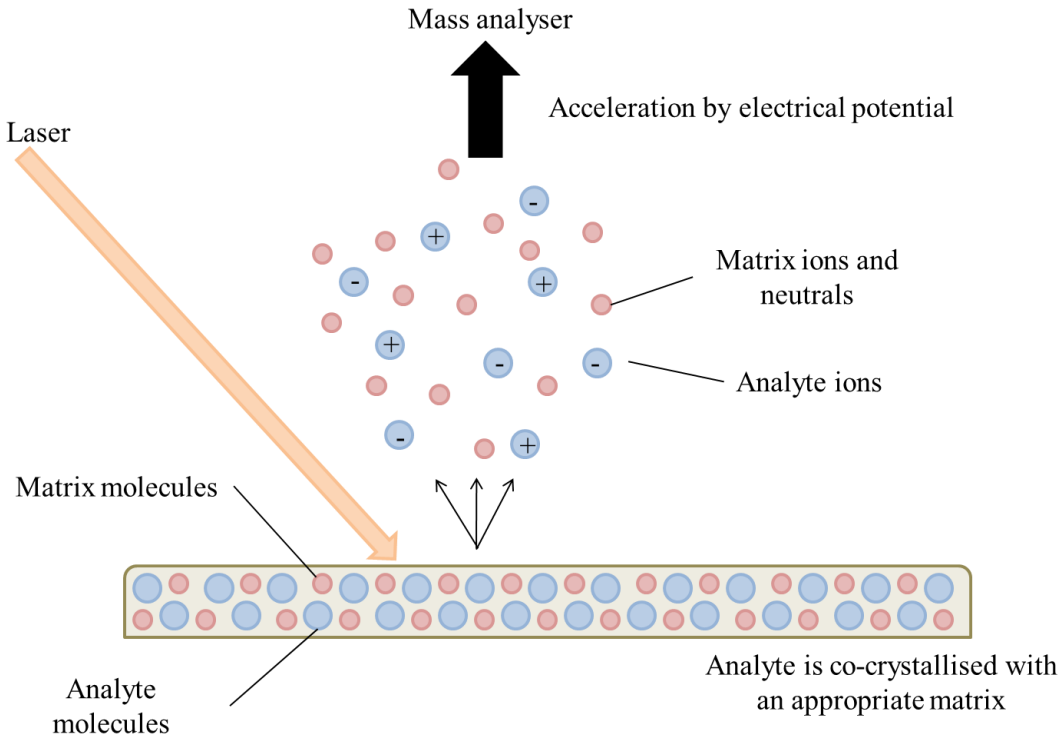

Figure 1.2 The MALDI ionisation process.
The energy from the UV laser is absorbed by the matrix molecules, which subsequently causes the desorption and ionisation of analyte molecules into the gas phase.

The exact mechanism by which ion formation occurs in MALDI remains somewhat controversial and current knowledge is not yet sufficient to allow selection of a matrix compound based on theory alone (Vestal 2001). The two most widely accepted mechanisms to explain the ionisation processes that occur during MALDI are photochemical ionisation and cluster ionisation. Photochemical ionisation describes the transfer of protons during the gas phase resulting from collision

between matrix and analyte molecules. In the cluster ionisation model, charged particles (cluster ions) are desorbed following absorption of UV light by matrix molecules. The matrix desolvates from these cluster ions, producing analyte ions (Karas and Kruger 2003; Chang, Huang et al. 2007). Although widely accepted, these two processes do not fully explain all of the ions observed during a MALDI experiment (Zenobi and Knochenmuss 1998). Secondary in-plume processes can also take place, which will also affect the final MALDI mass spectrum (Knochenmuss and Zenobi 2003). Once in the gas phase, ions are accelerated towards the analyser by an electrostatic field.

1.1.2.2 Electrospray ionisation

John Fenn was also recognised with the Nobel Prize in Chemistry in 2002, for his work on electrospray ionisation (ESI). He demonstrated that multiply charged ions could be obtained from proteins up to 130 kiloDaltons (kDa) in molecular weight using ESI. Unlike MALDI, which is a pulsed ionisation process performed under vacuum; ESI takes place at atmospheric pressure and is a continuous ionisation process.

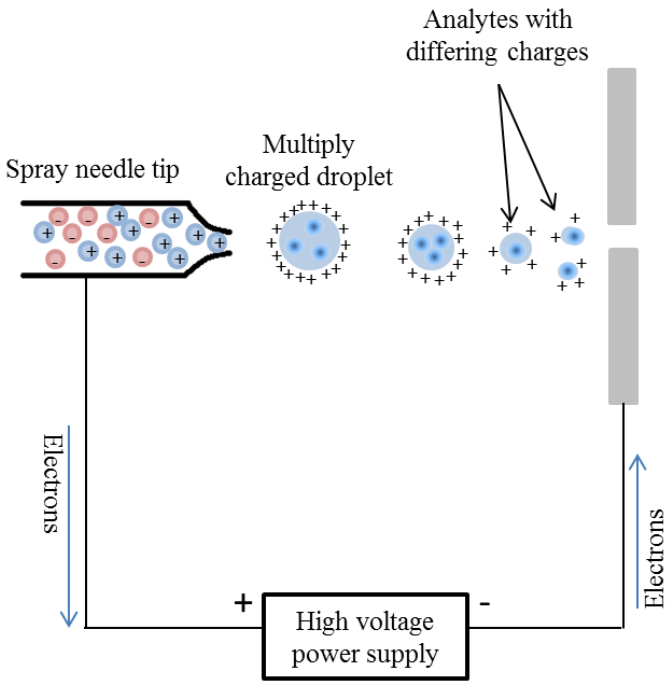

Figure 1.3 The ESI ionisation process.
Adapted from (de Hoffmann and Stroobant 2009).

For ESI, a sample is normally prepared in aqueous solution containing organic solvent such as acetonitrile (ACN) or methanol (MeOH). For positive ion analysis, a small amount of acid (formic or acetic) is commonly added to the solution to aid the ionisation process. This solution is sprayed through a capillary needle to which a high electric potential is applied. The most commonly accepted mechanisms by which ion formation takes place in ESI is represented by Figure 1.3.

The charged solution inside the capillary forms a Taylor cone at the end of the needle, which releases small highly charged droplets. The formation of these droplets is aided by a nebulising gas, such as nitrogen. Two mechanisms have been proposed that describe the formation of ions by ESI. These are the ion evaporation model (IEM) and the charge residue model (CRM). In both models charge repulsion in the droplets exceeds the surface tension causing solvent molecules to evaporate. The charge repulsion causes a Coulombic explosion and the droplets divide. In CRM this process is continuously repeated until a single, multiply-charged analyte ion is produced. For multiply charged ions at high *m/z* ratio, CRM is thought to be the dominant mechanism. In contrast, IEM is thought to be the model by which ions of low *m/z* are formed. The intial process is the same, but following the Coulombic explosion ions within the newly formed droplets are desorbed into the gas-phase and subsequently enter the mass spectrometer (Beaudry, Le Blanc et al. 1999).

The continuous ionisation offered by ES enables it to be routinely coupled to high performance liquid chromatography (HPLC) systems which are employed to separate biomolecules prior to MS analysis.

1.1.3 Mass analysers

Gas-phase ions formed during the ionisation process are subsequently separated according to their mass-to-charge (*m/z*) ratio. There are a number of mass analysers used in modern mass spectrometry, each with their own advantages and limitations. The mass analyser of choice should be considered based on the application for which it is to be used, taking into account requirements for resolving power, mass range and transmission efficiency.

Resolving power may be defined as the ability to separate two ions of near *m/z* value. For the purposes of this thesis, resolution will be defined by full width at half maximum (FWHM). This is based on a single well-resolved peak according to the equation:

$$Resolution = \frac{M}{\Delta M_x}$$

Equation 1.1

M is the mass associated with the apex of the peak, and ΔM_x is the width of the peak at a specified height, here taken to be 50% (half-maximum).

1.1.3.1 Quadrupole

A quadrupole mass analyser consists of four parallel metal rods. A combination of radio frequency (RF) and direct current (DC) voltages are applied to opposite pairs of rods, which allow the quadrupole to operate as a mass filter. The principle of the quadrupole was introduced by Paul and Steinwedel (Paul and Steinwedel 1953). Quadrupoles are low-resolution mass analysers that operate at unit mass resolution. They are often combined in series or with other forms of mass analysers, allowing them to be used for targeted analysis of specific compounds, greatly increasing the selectivity of the experiment.

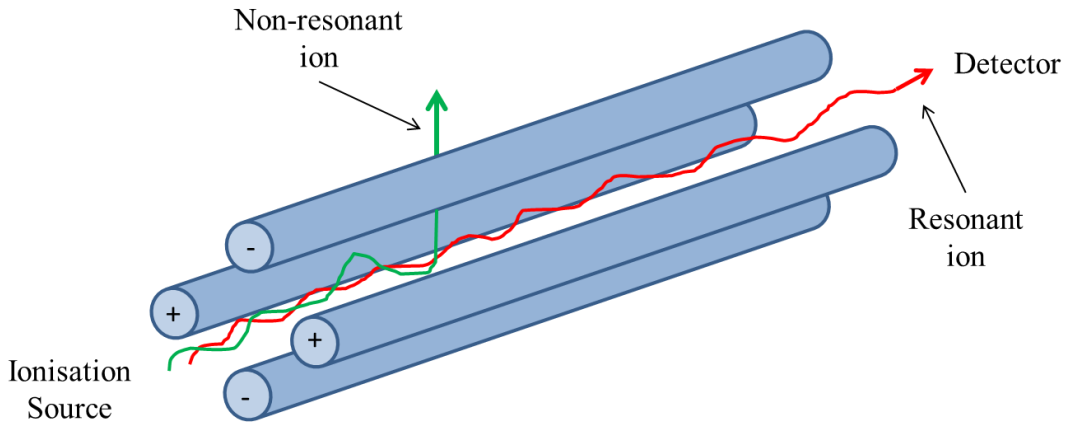

Figure 1.4 Schematic of a quadrupole mass analyser.

A combination of RF and DC voltages applied to the rods affect the trajectory of ions travelling through the quadrupole and only allow ions of a particular *m/z* to pass through with a stable trajectory. All other ions will collide with the rods or the sides of the mass analyser and will be lost. When operated in RF-only mode, the quadrupole operates as an ion guide allowing ions to pass through to reach the detector.

1.1.3.2 Time-of-flight

Time-of-flight (TOF) mass spectrometry was first described by Stephens in 1946. He outlined a new type of mass spectrometer was under construction that "should be well suited for gas composition control, rapid analysis and portable use" (Stephens 1946). The first commercial TOF instrument was based on a design published in 1955 by Wiley and McLaren (Wiley and McLaren 1955). TOF analysers are compatible with the pulsed ionisation of MALDI, and offer rapid analysis, a wide *m/z* range, and theoretically no upper mass limit. TOF mass analysers also have very high transmission efficiency and therefore high sensitivity.

Following ionisation ions are accelerated by an electric field. The ions then enter a free-field region, known as a flight tube. Here the ions are separated according to their velocity, which depends on the *m/z* ratio of the ion. The time each ion takes to traverse the flight tube is recorded by the detector; ions with smaller *m/z* move faster through the flight tube than those with a larger *m/z*. This can be described using the following equation, where t = time of flight, d = distance, m = mass, eV = accelerating voltage and z = charge.

$$t = d\sqrt{\left(\frac{m}{(2zeV)}\right)}$$

Equation 1.2

The mass resolution of TOF analysers is proportional to the flight path and time and poor resolution proved to be a major drawback with initial TOF analysers. This was in part due to a spread of kinetic energy amongst ions with the same *m/z*, caused by a number of factors including time, space and kinetic energy distribution. This kinetic energy spread results in peak broadening which, in turn, decreases resolution. The

introduction of delayed pulsed extraction and the reflectron, markedly improved the achievable resolution of TOF analysers.

When using delayed pulse extraction, in order to reduce the kinetic energy spread amongst ions with the same *m/z*, a time delay is introduced between ion formation and extraction. This technique was first considered by Wiley and McLaren and termed time-lag focusing. Delayed pulse extraction allows ions to separate according to kinetic energy following ion formation. An extraction voltage pulse is then applied to extract the ions from the source after a delay. This corrects the kinetic energy spread, thereby improving the TOF resolution. Both pulse and delay can be adjusted for the mass range of the ions of interest, to provide optimal resolution.

A reflectron design, proposed by Mamyrin in 1973 (Mamyrin, Karataev et al. 1973), can also be used to improve the resolution in a TOF analyser. This is an electrostatic reflector which acts as an ion mirror to deflect ions back through the flight tube. Reflectrons also correct the kinetic energy spread amongst ions of the same *m/z*, as ions with higher kinetic energy penetrate the reflectron more deeply than those with lower kinetic energy. This is outlined in Figure 1.5.

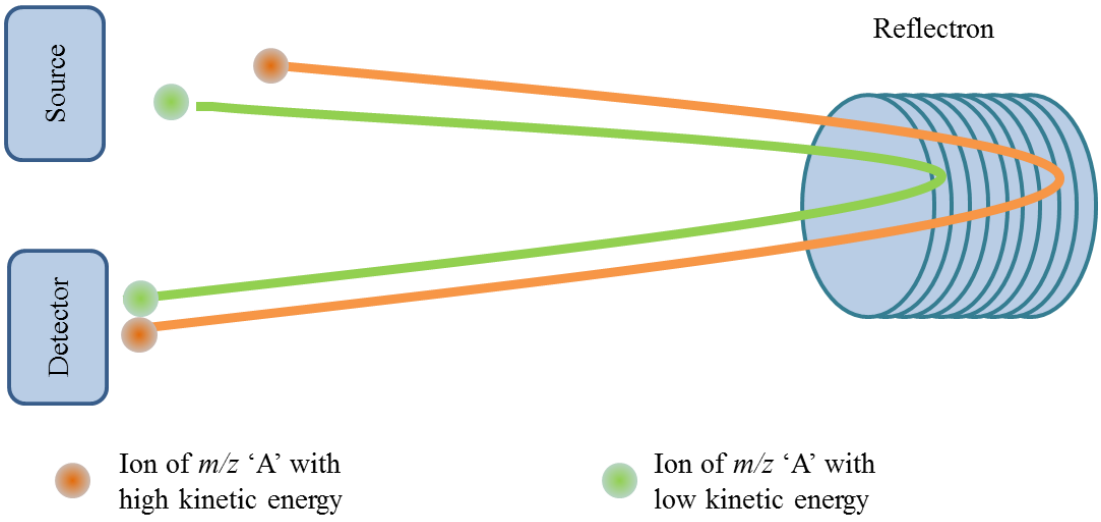

Figure 1.5 Schematic representation of a reflectron TOF instrument.
Two ions of equal *m/z*, but different initial kinetic energies, will both arrive at the detector at the same time. The ion with high kinetic energy goes deeper into the reflectron than the ion with low kinetic energy.

Ions with higher energy will therefore spend longer in the reflectron and both ions with the same *m/z* will reach the detector at the same time thereby reducing peak broadening. Whilst there is an improvement in resolution, mass range can be limited and sensitivity reduced when using a reflectron-TOF analyser. Dual-stage reflectrons may be used to improve the reflectron performance; here the first reflectron has a higher electric field to decelerate the ions and the second has a weaker field. Dual-stage reflectrons may also suffer from lower transmission efficiency, but can correct a wider range of kinetic energy spread and provide higher mass resolution (de Hoffmann and Stroobant 2009).

The development of orthogonal acceleration (oa) in TOF analysers has, to an extent, overcome the difficulties in combining TOF with continuous ionisation sources (e.g. ESI) that do not produce packets of ions. Orthogonal acceleration was first proposed in 1964 (O'Halloran, Fluegge et al. 1964), but its full potential was not realised until much later with the work of Guilhaus and Dodonov (Dawson and Guilhaus 1989; Coles and Guilhaus 1993). In an oa-TOF instrument, the ion source generates an ion beam that is directed into an orthogonal accelerator region, perpendicular to the TOF. An electrostatic field is created by applying a large voltage pulse, and a packet of ions is pushed at a right-angle away from the ion beam and into the strong acceleration field towards the TOF. This is shown in Figure 1.6.

When using reflectron TOF analysers, the detector can be conveniently located next to the orthogonal accelerator for improved resolution. The introduction of oa-TOF analysers has allowed ESI applications to benefit from the high mass range, speed, sensitivity and mass accuracy of TOF analysers (Guilhaus, Selby et al. 2000; McLuckey and Wells 2001).

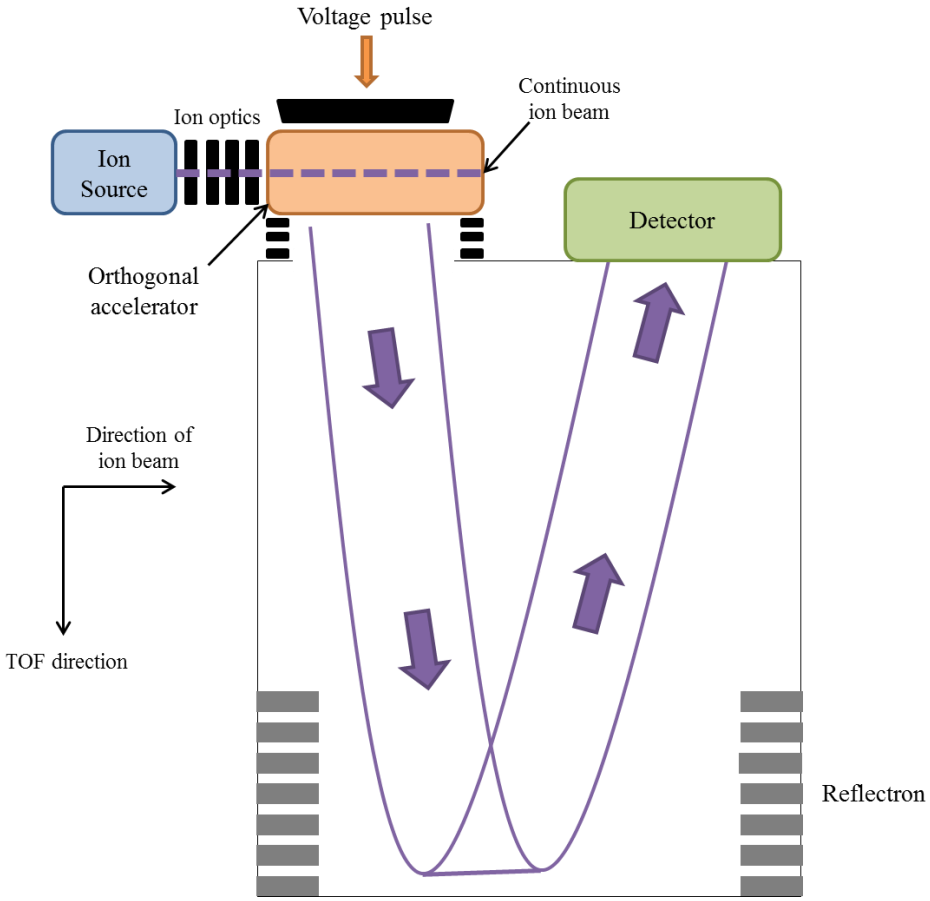

Figure 1.6 Simplified schematic representation of an oa-TOF reflectron system. The ion beam enters from a source at the left and enters the orthogonal accelerator (oa). A voltage pulse is then applied, perpendicular to the ion beam, which sends a packet of ions into the accelerator region and towards the TOF. Here a single-stage reflectron is represented. Whilst the ion packet traverses the TOF the oa refills with the next packet of ions. Adapted from (Guilhaus, Selby et al. 2000).

1.1.3.3 Ion Trap

Ion trap analysers use an oscillating electric field to store ions, which are then ejected from the trap according to their *m/z* values in order to create the spectrum. Two types of ion trap exist, the 2D or linear ion trap and the 3D ion trap. Paul and Steinwedel had patented an ion trap instrument in 1960 (Paul and Steinwedel 1960), but it was not until Stafford *et al*. modified the design that ion traps were used more widely (Stafford, Kelley et al. 1984).

The 3D ion trap consists of a circular electrode, with ellipsoid caps on either end. Ions are pulsed into the trapping region, where they are held in a 3D trajectory by overlapping DC and RF voltages. Ions of different masses are contained in the trap and released based on their *m/z*. With many ions present in the trap, they may repel each other causing an expansion of their trajectories. This is known as space charging and can result in ion losses. To remove excess energy from the ions, the trap is maintained at pressure using helium gas, which collides with the ions and prevents losses from the trap. The number of ions within the trap is maintained by a gating lens; too few ions may cause a loss of sensitivity, whilst too many may cause a loss of resolution through the introduction of space charge effects.

2D or linear ion traps (LIT) are similar in principle to the quadrupole mass analyser, consisting of four parallel rods with lenses at each end. These lenses repel the ions and trap them inside the rods. LITs have an advantage over 3D ion traps in that they have a much higher trapping capacity, which reduces the space-charge effect. Ions are selectively ejected from the trap either perpendicularly to or along the axis of the trap (de Hoffmann and Stroobant 2009).

1.1.3.4 Orbitrap

In June 2005 a new mass analyser, known as the Orbitrap, was introduced by the Thermo Electron Corporation. This was based on a concept initially proposed by Makarov in 2000, which involved trapping ions within an electrostatic field. Mass spectra are obtained using a Fourier Transform (FT) of the induced ion current (Makarov 2000). Ions orbit around a central axial electrode, in the absence of either magnetic or RF fields. These orbiting ions perform harmonic oscillations along this

electrode at a frequency proportional to $(m/z)^{-½}$ and independent of energy and spatial spread. These oscillations are detected using image current detection before conversion into mass spectra using FT (Hu, Noll et al. 2005).

The Orbitrap can be characterised as a high-resolution and high mass accuracy instrument; though it should be noted that Orbitrap resolution is dependent both on *m/z* and scan time. The resolution is currently specified at 60,000 (FWHM) at *m/z* 400 with a scan time of 1 second. This increases linearly with scan time and can reach over 100,000. The achievable resolution is inversely proportional to $(m/z)^{-½}$, and so decreases as the mass range is increased (de Hoffmann and Stroobant 2009).

1.1.3.5 Fourier Transform ion cyclotron resonance

Fourier Transform ion cyclotron resonance (FT-ICR) or Fourier Transform mass spectrometry (FTMS) determines the *m/z* of ions based on their cyclotron frequency when subjected to a magnetic field. Ions are trapped in a Penning trap and excited into a cyclotron radius. The ions circle with a frequency that is inversely proportional to their *m/z*. As the ions experience cyclotron motion, they pass near a pair of plates which detect and record image currents; these are then converted into a mass spectrum using a Fourier Transform.

FT-ICR offers the highest mass resolution and mass accuracy of all current mass analysers (>300,000 for *m/z* 200-1000, at 9.4 Tesla). This is due to the fact that *m/z* is detected as frequency during an FT-ICR experiment; and frequency can be measured more accurately than any other experimental parameter. The resolution of FT-ICR is inversely proportional to *m/z*, and is dependent on both scan time and magnetic field. The larger the magnetic field, the higher the potential resolution of the analyser (Henry, Williams et al. 1989; Marshall and Hendrickson 2002).

1.1.4 Detectors

Detectors record the arrival of ions through the mass analyser and transform the measurement into a usable signal. A number of different detectors have been used in mass spectrometry and vary according to instrument type or application. Mass spectrometry detectors were reviewed in 2005 (Koppenaal, Barinaga et al. 2005).

The most common type of detector used in mass spectrometry is the electron multiplier (EM). This detector improves detection efficiency by accelerating ions from the analyser to a high velocity. An electrode (conversion dynode) is held at a high potential (between 3 and 30 kV), opposite to the charge on the ions to be detected. When ions hit the conversion dynode, secondary particles are emitted (of the opposite charge to the detected ion). These are then accelerated into the electron multiplier to produce a current. Electron multipliers can either be a discrete dynode or continuous dynode, such as a microchannel plate (MCP).

An MCP detector is a plate in which parallel, cylindrical channels have been formed. Each individual channel is 4-25 μm in diameter, a few millimetres in length and coated in a semiconductor substance that is able to emit secondary electrons. When an ion strikes the surface of the plate, a burst of electrons is initiated that can be directed onto an anode for electronic detection of the current. An electron can be multiplied by a factor of 10^5 using just one channel. Multiple plates can be used to provide amplification up to 10^8. The MCP is the detector of choice for TOF systems, since the short electron path and fast response time allow for precise arrival times and the narrow pulse widths required. MCP detectors are capable of detecting a large number of ions at one time, which make them suitable for the analysis of complex biological samples. The plates can be fragile and sensitive to environmental conditions such as air (Koppenaal, Barinaga et al. 2005; de Hoffmann and Stroobant 2009). MCP channels must have time to recover between ion signals. This is known as dead time. They should therefore not be saturated with large signals since that may mask smaller signals which could follow shortly afterwards.

The electrical signal from the detector must be digitised using a data acquisition system. The most common detection systems operate as analog-to-digital (ADC) or time-to-digital (TDC) converters. TDC systems operate in pulse counting mode, where the time that each ion that strikes the detector is recorded and acquisitions are summed together to produce the spectrum. ADCs register the ion current, amplify the signal and employ a filter to remove high frequency noise. This signal is converted to a digital value and plotted on an *m/z* scale (de Hoffmann and Stroobant 2009).

TDC detectors are commonly used in oaTOF instruments, and are used on Waters (Waters, Manchester, UK) mass spectrometers. The latest Waters instruments, including the Synapt G2 HDMS, now use an ultrafast electron multiplier with hybrid ADC/TDC detector electronics to provide high resolution, low noise and an improved dynamic range.

1.1.5 Tandem mass spectrometry

Tandem mass spectrometry (MS/MS) involves at least two stages of mass analysis. Most commonly, in the first stage of mass analysis a precursor ion is selected and the ion is fragmented, giving product ions and neutral fragments. Product ions are subsequently analysed using a second stage of mass analysis. This process is schematically represented in Figure 1.7.

More than two stages of analysis may be employed to perform MS^n experiments (where *n* refers to the number of stages of mass analysis). Tandem mass spectrometry can either be performed in space; coupling two mass analysers together that are physically distinct, or in time; by performing a number of events within an ion storage device, or a combination thereof; in hybrid instruments.

An example of tandem MS in space is provided by the quadrupole-time of flight (Q-TOF) mass spectrometer. This can be operated in different modes. To obtain full spectra the quadrupole is set to RF-only mode; allowing a wide mass range of ions through prior to mass analysis in the TOF. In MS/MS mode the quadrupole is used to select a precursor ion from the *m/z* value; the ions are fragmented in a collision cell and product ions analysed using the TOF. This takes full advantage of the selectivity of the quadrupole for a set *m/z*, and the virtually simultaneous analysis of all product ions using the TOF.

In Q-TOF instruments fragmentation of the precursor ion is normally achieved using collision induced dissociation (CID). This was pioneered by Jennings in the 1960s (Haddon and McLafferty 1968; Jennings 1968). Ions selected by the quadrupole are subjected to collisions with an inert gas such as argon, in a collision cell located between the two mass analysers. As ions collide with the gas, energy is transferred to the selected precursor ion resulting in fragmentation. The product ions are detected

using the TOF and are formed from the precursor ion. The fragment ions can provide important information regarding, or can be used to confirm the identity of, the precursor ion selected.

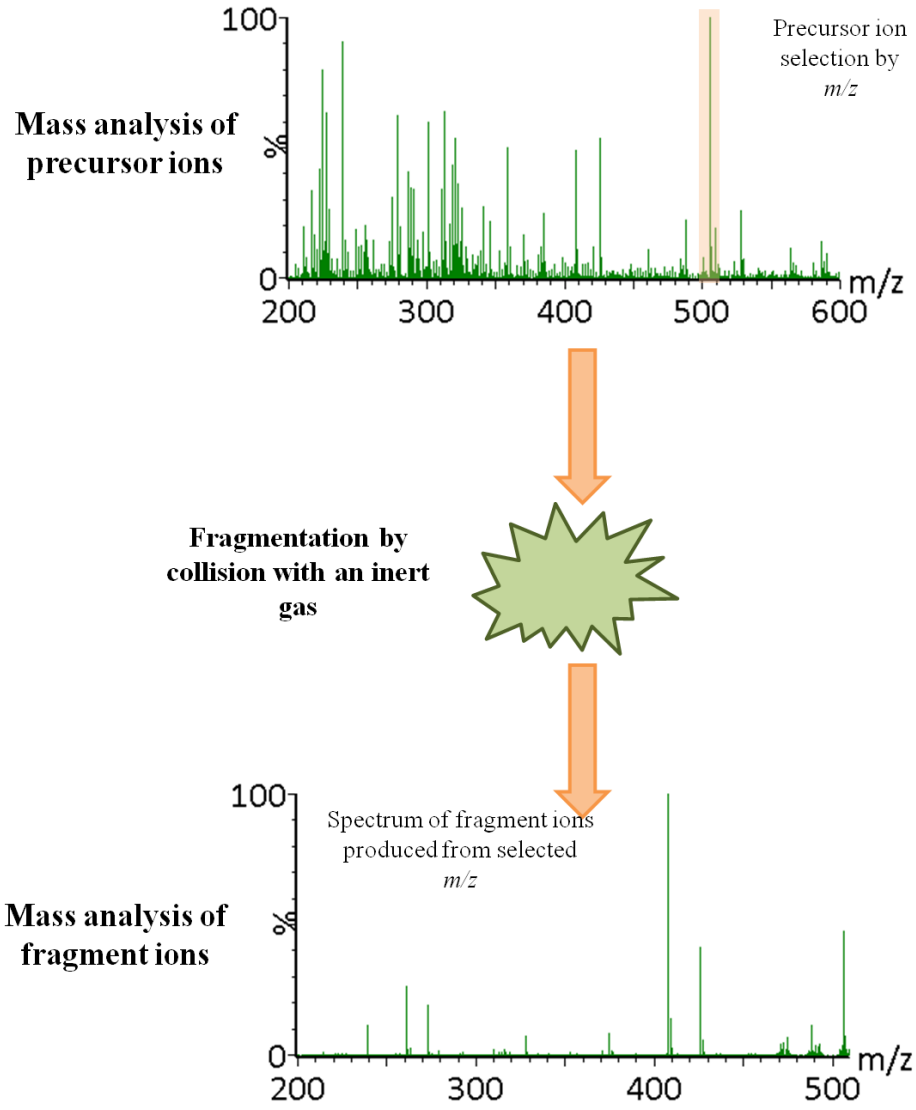

Figure 1.7 Principle of MS/MS:
A precursor ion is selected by the first mass analyser based on *m/z*; fragmented via collision and the resulting fragment ions analysed by the second mass analyser to give an MS/MS spectrum.

Tandem mass spectrometry in time can be performed with ion trap, Orbitrap and FT-ICR mass spectrometers. In an ion trap this is achieved by selecting ions of a particular *m/z*, by expelling all other ions from the trap. Fragmentation is then

performed by allowing collision of the precursor ions with helium (CID) and the resulting product ions analysed. Both precursor selection and product ion analysis occur with the same mass analyser. Following the first fragmentation, a product ion can be selected for further fragmentation to perform MS^n experiments (de Hoffmann and Stroobant 2009).

1.1.6 Ion Mobility mass spectrometry

Ion mobility spectrometry (IMS) is an electrophoretic technique that allows gas-phase analytes to be distinguished on the basis of their mass, charge and collisional cross-section (size and shape) (Upthagrove, Hackett et al. 1999; Djidja, Francese et al. 2009). Originally developed as a method for the detection and identification of compounds in the security and military fields; the combination of ion-mobility spectrometry and mass spectrometry (IM-MS) has resulted in a powerful analytical tool with a wide range of potential applications in biological research (Borsdorf and Eiceman 2006; Kanu, Dwivedi et al. 2008).

Drift-time IMS was the originally introduced method of mobility separation. Here the time it takes an ion to migrate through a buffer gas in the presence of a low electric field was measured. The mobility of the ion (K; $cm^2s^{-1}V^{-1}$) is demonstrated by the following equation:

$$V_d = KE$$

Equation 1.3

This is determined by the velocity (V_d; $cm^2\ s^{-1}$) attained under the influence of the electric field gradient (E, V cm^{-1}) in the presence of a drift gas. The time taken to traverse a drift cell of length d (cm) is t_d (s), therefore:

$$K = \frac{d}{t_d E}$$

Equation 1.4

A combination of gas flow and electric field is used to move the ions towards the drift tube, where they are then pulsed into the tube in discrete ion packets. Once in

the drift tube the ions are then subjected to a uniform and low electric field, which accelerates them towards a detector. Inside the drift tube a drift gas (or buffer gas) is maintained at a constant pressure. As ions pass through the buffer gas they experience collisions that hinder their progress towards the detector. Larger ions (greater collision cross-section) encounter more collisions than smaller ions and so take longer to reach the detector. Ions are thereby separated according to shape. A representative schematic of a drift-time IMS is shown in Figure 1.8.

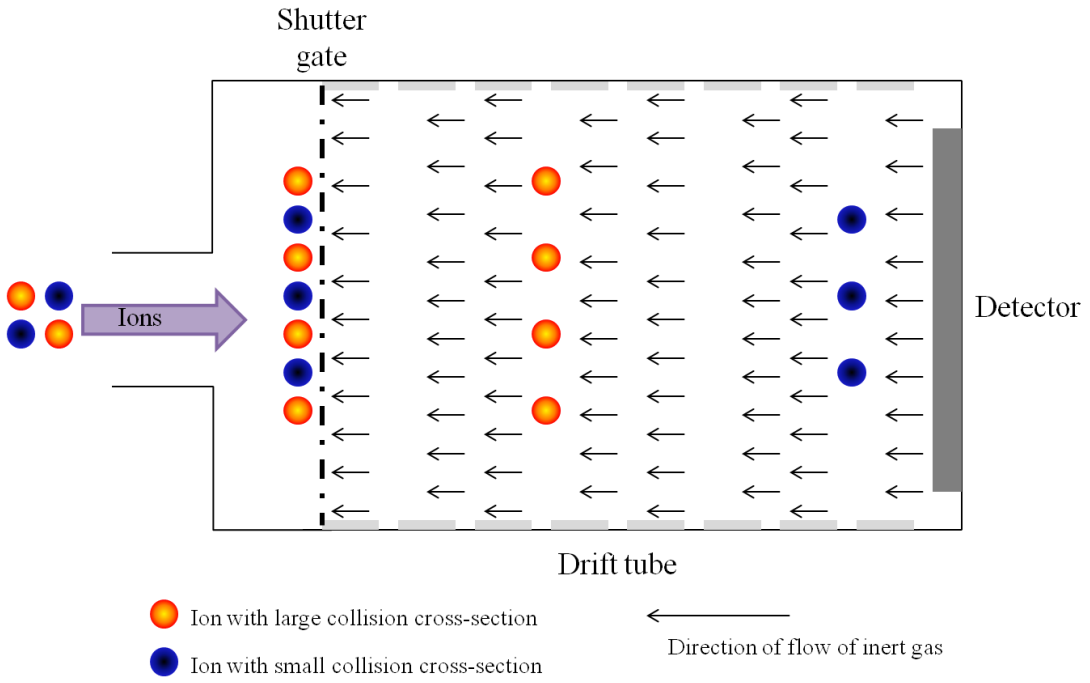

Figure 1.8 Schematic representation of Drift-cell IMS.
Packets of ions are pulsed into the drift tube where they encounter a weak electric field and buffer gas. Ions with large collision cross-sections encounter more collisions with the drift gas and take longer to traverse the drift tube and reach the detector than ions with a small collision cross-section. (Adapted from (Borsdorf, Mayer et al. 2011)).

Under low field conditions, the velocity of the ion is directly proportional to the electric field and so ion mobility under these conditions can be considered as directed diffusion. Drift time IMS is the only mobility experiment where collision cross-sections of ions can be determined directly from the drift time through the cell (Creaser, Griffiths et al. 2004; Kanu, Dwivedi et al. 2008).

Drift-time IMS has been coupled to a range of mass spectrometers, but in general these instruments are home-built or modified commercial instruments in academic

laboratories (Thalassinos, Slade et al. 2004; McCullough, Kalapothakis et al. 2008). A commercial drift-cell IM-MS instrument is not currently available. Ion mobility and mass spectrometry are complementary, in that mass spectra can be acquired on the microsecond time scale, with mobility separation performed on the millisecond timescale. This can allow multiple mass spectra to be acquired during a mobility experiment.

1.1.7 Travelling-wave ion mobility mass spectrometry

A significant development in the field of ion mobility mass spectrometry was the introduction of a commercial IM-MS instrument, the Synapt HDMS mass spectrometer, by Waters Corporation (Manchester, UK). This system incorporated a travelling-wave ion mobility separation device (TWIMS) (Pringle, Giles et al. 2007).

In contrast with the uniform low electric field used in drift-time IMS, in TWIMS a field is applied to one region of the IMS cell and passed sequentially through the cell towards the detector. Ions are moved through the cell by this electrical field wave and separated according to their mobility (Kanu, Dwivedi et al. 2008). The TWIMS device uses a stacked ring ion guide (SRIG). This consists of a series of ring electrodes as shown in Figure 1.9. Opposite phases of RF voltages are applied to adjacent rings to stabilise the trajectory of ions as they travel through the SRIG.

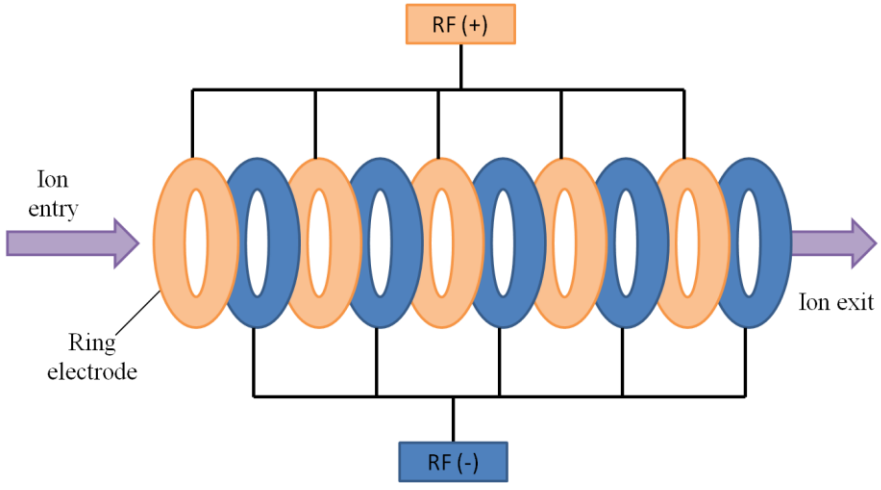

Figure 1.9 Schematic diagram of an RF-only stacked ring ion guide (SRIG). Adapted from (Giles, Pringle et al. 2004).

In order to propel ions through the SRIG, a DC potential is superimposed on the RF of each electrode. This creates the moving electrical field previously described; providing a travelling wave on which the ions can surf through the ion guide. For this reason the ion guide is referred to as a travelling wave ion guide (TWIG). When an inert gas is present in the TWIG the ability of an ion to surf the travelling wave is dependent on its mobility. For a given gas pressure, wave height and wave velocity the TWIG device can therefore be used for ion mobility separation. Ions with a low mobility roll over the wave as it passes through the TWIG and take longer to traverse the cell than ions with a high mobility, which surf the wave and pass through more quickly. This is shown more clearly in Figure 1.10.

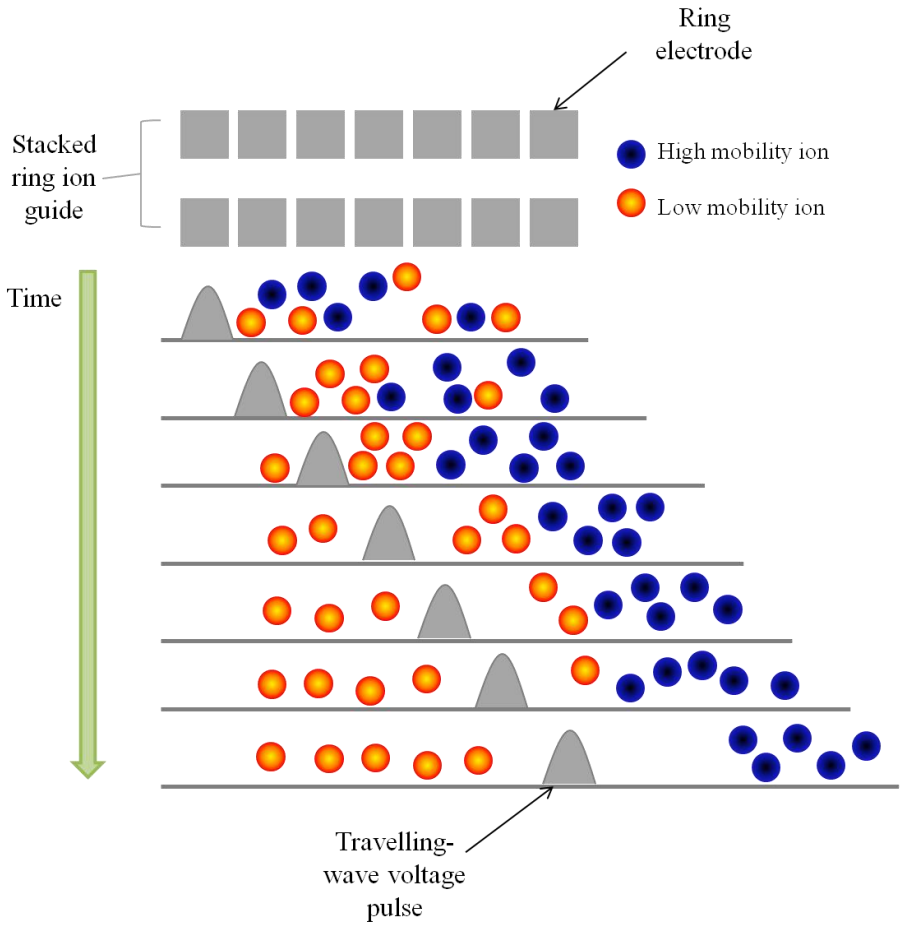

Figure 1.10 Schematic representation illustrating ion mobility separation in a TWIG. Here low mobility ions rollover the travelling wave voltage pulse, whilst high mobility ions keep up with the wave and traverse through the TWIG more quickly. Adapted from (Giles, Pringle et al. 2004).

The travelling wave device was described in 2004 (Giles, Pringle et al. 2004) and first used in IMS-MS experiments to determine the collisional cross-section of an RNA binding protein in 2005 (Ruotolo, Giles et al. 2005). In 2007 this TWIMS device was incorporated into a new hybrid quadrupole ion mobility orthogonal acceleration time-of-flight mass spectrometer to create the first commercial ion mobility mass spectrometer (Synapt HDMS, Waters, Manchester, UK) (Pringle, Giles et al. 2007). The TWIMS device is located between the quadrupole and oaTOF mass analysers in the mass spectrometer and consists of three TWIGs, referred to as a Triwave (or T-wave).

The first and third TWIGs are the trap and transfer regions, respectively. The trap is used to release ion packets into the mobility cell and does not have a travelling wave pulse voltage applied to it. The transfer region has a travelling wave voltage applied in order to maintain the mobility separation of the ions from the IMS cell as they are transferred to the oaTOF. The second TWIG (between the trap and transfer) is used as the IMS cell. A travelling wave voltage pulse is applied in the presence of an inert buffer gas within the cell. The travelling wave height (V) and velocity (m/s) can be adjusted for each sample to provide optimal IMS separation. The release of ion packets into the IMS cell is synchronised with the oaTOF pusher; one IMS gate pulse corresponding to 200 orthogonal acceleration pushes. This allows the arrival time distribution (ATD) of ions to be recorded at the same time as their mass spectra.

The trap and transfer ion guides can also be used as collision cells for tandem mass spectrometry experiments either before or after mobility separation (or both). This allows for a wide range of experiments to be performed; mobility separation of product ions, fragmentation of mobility separated precursor ions and further fragmentation of mobility separated product ions can be performed in an MS^3 type experiment (Pringle, Giles et al. 2007).

TWIMS has limited mobility resolving power when compared to drift-cell instruments, however the sensitivity of the mass spectrometer is not compromised when operating in ion mobility mode and high transmission efficiency is achieved (Pringle, Giles et al. 2007; Kanu, Dwivedi et al. 2008). Recently a second-generation Synapt has been introduced (Synapt G2 HDMS, Waters, Manchester, UK), with significantly improved mobility resolution. This was achieved by increasing the

pressure in the IMS cell to allow higher electric fields to be used to improve resolution. A helium gate has also been incorporated prior to the high-pressure nitrogen filled IMS cell, as a buffer between this and the low-pressure trap cell (filled with Argon). This allows ions to be injected against a pressure gradient, reducing collisional activation and heating of the ions (Wallace 2010; Giles, Williams et al. 2011).

IMS-MS experiments using the Synapt and Synapt G2 systems have been used in a range of mass spectrometry applications in biological research including determination of collision cross-sections of peptides and proteins (Bush, Hall et al. 2010), structural studies of proteins (Scarff, Patel et al. 2009; Hilton, Thalassinos et al. 2010) and the characterisation of protein complexes (van Duijn, Barendregt et al. 2009), characterisation and separation of phosphorylated peptides (Thalassinos, Grabenauer et al. 2009), oligosaccharides and glycans (Williams, Grabenauer et al. 2010), imaging mass spectrometry experiments (Trim, Henson et al. 2008; Stauber, MacAleese et al. 2010) and more recently in mobility-enabled proteomics experiments (Slade, Gethings et al. 2012; Vafadar-Isfahani, Patel et al. 2012).

1.2 Drug Localisation

The drug discovery and development process can take a long time and cost pharmaceutical companies an ever-increasing amount of money to get a new drug to market. Whilst a number of investigations into the cost of drug development have been published (DiMasi, Hansen et al. 2003; Adams and Brantner 2006; Paul, Mytelka et al. 2010), it remains difficult to pinpoint a single estimated figure of the total cost. A recent review into published estimates of drug development costs indicate that the total cash cost may range from $92 million (USD) up to $884 million (Morgan, Grootendorst et al. 2011). A large proportion of these costs relates to the development of compounds that fail during clinical trials. This indicates that improvements in the pre-clinical development stages are required to better assess drug candidates early on in order to identify successful compounds and eliminate others (Khatib-Shahidi, Andersson et al. 2006).

One of the most important questions to be addressed during drug discovery and development is whether the drug reaches its target site of action. A drug may meet every requirement surrounding potency, safety and efficacy, but if it is not made available at the target site, it will not be useful in the treatment of disease or infection. Knowing the distribution of a drug and its metabolites within tissues is also important in providing biological information that can help in understanding drug action and toxicity.

1.2.1 Why is drug localisation important?

During the drug discovery and development process, pharmaceutical companies are required to assess the absorption, distribution, metabolism and excretion (ADME) of potential drug candidates. Establishing the ADME properties of drug candidates helps to determine the toxicity levels of the compound and to establish dosing levels prior to human clinical trials, as well as investigating the pharmacokinetic properties of the drug.

In the European Commission (EC), United States and Japan, tissue distribution studies are considered essential during non-clinical drug development processes in

order to determine the distribution and accumulation of drug compounds and their related metabolites. This is especially important in relation to potential sites of action of the drug compound. Figure 1.11 shows a simplified schematic of the drug discovery and development process, indicating where drug localisation studies fit into the process.

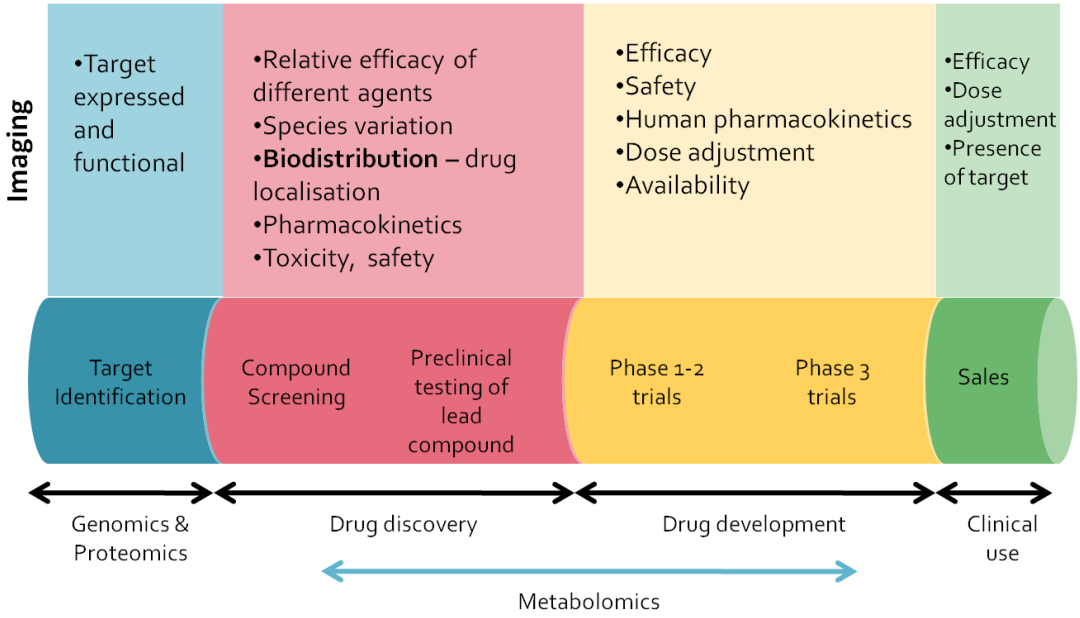

Figure 1.11 The drug discovery and development process.
Adapted from (Rudin and Weissleder 2003)

The European Medicines Agency (EMA: 3BS11a, 1994) and ICH (ICH: M3(R2) 2009) regulatory guidelines state that the levels of drug compound and metabolites must be assessed in blood, body fluids and organs before testing compounds on a large number of human subjects. This distribution data can be obtained by physical, chemical or biological methods, and there are a number of approaches used by the pharmaceutical industry to determine drug localisation in animal models.

1.2.2 Quantitative Whole Body Autoradiography

The most commonly used technique and industry gold-standard for drug distribution studies is quantitative whole-body autoradiography (QWBA). The modern version of this technique is based on a method first described by Sven Ullberg in 1954 investigating the distribution of ^{35}S-labelled benzylpenicillin in the body (Ullberg

1954). Whole-body autoradiography (WBA) involves the preparation of radiolabelled drug compounds, commonly incorporating carbon-14 (^{14}C) or hydrogen-3 (^{3}H) isotopes into drug compounds during synthesis. These radiolabelled compounds are then administered to laboratory animals, which are sacrificed at different time points post-dose. The carcasses are frozen and then sectioned using a cryotome to produce whole-body sections at 30-50 µm thickness and imaged, originally using X-ray film. An autoradiography image is produced by the pattern of decay emissions from the radioactive label, showing the distribution of the radiolabel in the whole-body section. The original method was not suitable for quantitative analysis owing to limitations with the X-ray film used for imaging. Exposure over a number of weeks or months was required to produce images (Solon 2012).

The development of phosphorimaging systems (Luckey 1975) facilitated quantitative analyses of beta-radiation in whole-body sections and transformed WBA from a lengthy, qualitative process to a much shorter, quantitative method that was adopted by the pharmaceutical industry. Prior to this, the standard method consisted of tissue homogenisation followed by liquid scintillation counting (LSC) to determine levels of radioactivity present in dissected tissues. In QWBA the spatial distribution of drug compounds can be determined and quantified in a whole body section. For quantitation, ^{14}C-spiked blood standards across a range of concentrations are produced allowing for calibration of the images produced (Schweitzer, Fahr et al. 1987).

The methods used for QWBA and phosphorimaging instrumentation were validated in a study published in 2000. Formal guidelines were published for this procedure according to Good Lab Practice (GLP) (Coe 2000; Kolbe and Dietzel 2000; Maas, Binder et al. 2000). This led to most pharmaceutical companies adopting QWBA as the gold-standard for tissue distribution studies, which is widely accepted and often requested by regulatory agencies around the world. The use of QWBA for drug tissue distribution has been discussed in depth in a number of recent reviews and will not be covered further here (Solon, Schweitzer et al. 2010; Solon 2012).

It should be noted that QWBA images show the distribution of the radioactive atom. Despite the numerous advantages of QWBA, its major limitation is the inability to

distinguish between the distribution of the parent drug compound and any metabolites. When the drug compound is metabolised, only those metabolites retaining the radiolabel are detected. It remains important to determine the sites at which metabolism occurs, how the drug compound travels through the body and the ratios of metabolites that are generated (Shigematsu, Motoji et al. 1995). As such, metabolite identification data are obtained from tissue extracts using LC-MS/MS experiments to support QWBA data (Solon, Schweitzer et al. 2010).

1.2.3 Tissue homogenisation and LC-MS/MS

In order to identify parent drug compound and metabolites, dissected tissues are homogenised and extracted for analysis by LC-MS/MS. Identification of compounds can be aided by using exact mass measurement in LC-MS mode, but more commonly a tandem MS experiment is performed to fragment the ions and provide structural information (Solon, Schweitzer et al. 2010).

This method can identify drug compounds and metabolites at different time points post-dose, without the need for labelling; however, detailed spatial localisation information is lost (Wang, Jackson et al. 2005). This approach does not provide information about the drug distribution within the tissue or information relating to the interaction of the drug or metabolites with other biological molecules (Hsieh, Chen et al. 2007).

To analyse tissues by LC-MS/MS, they must first be homogenised in a suitable medium (e.g. buffer, water). The compound of interest and associated metabolites are then extracted from the homogenate using a suitable solvent. This can be optimised in order to increase the recovery of analytes during extraction (Holcapek, Kolarova et al. 2008). This extracted sample is then analysed by LC to separate metabolites and parent compound. The LC is then coupled to a mass spectrometer to perform fragmentation MS/MS experiments to identify metabolites.

Quantitation of parent drug compounds is possible using LC-MS methods, but it is limited with respect to the quantitation of metabolites unless pure standards of these metabolites are available (Prasad, Garg et al. 2011). Radiolabelled metabolites can also be quantified by radiochemical detection of high performance (HPLC) or ultra-

performance liquid chromatography (UPLC) separated metabolites using an online radiochemical flow detector (Chen, Monshouwer et al. 2007). This mixes liquid scintillant with the eluent as it passes through the cell, and allows for high throughput of sample analysis. The method has poor sensitivity owing to the short period of time that the radioactive components are in the cell at conventional UPLC and HPLC flow rates. This can be improved by fraction collection and off-line scintillation counting, but this removes the high-throughput nature of the approach (Prakash, Shaffer et al. 2007).

1.2.4 Fluorescence

In vivo fluorescence imaging detects fluorescence emission from fluorophores in whole-body living small animals. The energy from an external source is absorbed and almost immediately emitted at a longer wavelength of lower energy. A low-light camera and appropriate filters are used to collect this fluorescence emission light from a whole-body small animal sample (Rudin and Weissleder 2003). A fluorescent probe is injected, which is then specifically activated in the presence of a target (e.g. receptor or enzyme). This allows mapping of the spatio-temporal distribution of active drug targets. This optical imaging technique offers the advantages of being cheap, highly sensitive and robust, but suffers from limited spatial resolution (mm) and depth sensitivity (Gross and Piwnica-Worms 2006). The fluorophores used must remain biologically stable following injection, accumulate at the target and offer an imaging contrast specific for that target (Rao, Dragulescu-Andrasi et al. 2007).

Site specific reporter gene expression has been described for *in vivo* fluorescence imaging. A reporter mouse that ubiquitously expresses a fluorescent protein (e.g. green-fluorescent protein, GFP) upon Cre-mediated recombination is crossed with a mouse that expresses Cre under the control of a site-specific promoter. The fluorescent protein is thereby expressed at the target site, and is monitored using *in vivo* fluorescence imaging (Rudin, Rausch et al. 2005). *In vivo* fluorescence imaging is predominantly used to assess drug targets and tissue characterisation rather than drug localisation, though the distribution of a photosensitiser compound within a tumour has been described (Mitra and Foster 2008).

1.2.5 PET imaging

Positron Emission Tomography (PET) is an *in vivo* imaging approach used for drug distribution studies in live animals, without the need for sacrifice. Whilst autoradiography studies are initially performed *in vivo*, distribution studies require the animal must be sacrificed. PET imaging can also offer the possibility of performing studies before and after drug treatment in the same animal (Eckelman 2003).

PET uses short-lived positron emitting radionuclides to label molecules, such as new drug compounds, that are intravenously administered and traced through the body at low (sub-picomolar, 10^{-12}M) concentrations. External detectors are used to monitor the three-dimensional (3D) distribution and kinetics of these labelled molecules. The radionuclide label emits a positron (e^{+}) that annihilates to produce two gamma rays at 180˚, which are detected by the PET scanner (Aboagye and Price 2003; Eckelman 2003). A range of radionuclides have been described for PET imaging, including ^{15}O, ^{11}C, ^{13}N and ^{18}F. ^{11}C is commonly used as it does not alter the biochemistry of pharmacology of the drug molecule (Farde 1996).

Whilst commonly used for medical imaging approaches in humans, PET imaging has been proposed as a tool that could help to reduce drug development costs by improving the efficiency of preclinical and clinical stages of drug research (Burns, Hamill et al. 1999). PET imaging has a spatial resolution of 1-3 mm and provides both 3D localisation of the radionuclide and determination of absolute radioactivity concentrations in tissue (Port and Wolf 2003). Using PET imaging for small animals allows a connection between *in vitro* science approaches and *in vivo* human studies, which could provide a better assessment of pharmacokinetics and efficacy of drugs under development (Aboagye 2005).

1.2.6 Limitations of established drug localisation approaches

Many chemical imaging techniques can be used during development to assess drug distribution. Established approaches (discussed above) to drug and metabolite distribution are widely used and have a number of advantages, however there are limitations associated with each method that should be considered. Most of the

methods lack sufficient sensitivity, spatial and chemical resolution for widespread use in the pharmaceutical industry and also require labelling of the analytes (Rubakhin, Jurchen et al. 2005).

LC-MS/MS techniques can be used for the detection of non-labelled drugs in homogenised tissue and can also distinguish between parent drug and metabolites in a sample. A major disadvantage of this approach is that specific spatial information is lost during the tissue homogenisation process, limiting distribution information to dissected tissues.

QWBA provides quantitative localisation data, at high spatial resolution, but involves the preparation of radioactively labelled drugs; which is both expensive and time consuming. The nature of radioactive labelling means the tag will be detected whether it is attached to the parent drug, or a metabolite of the drug. This method cannot therefore distinguish between the localisation of the drug or a labelled metabolite (Wang, Jackson et al. 2005; Stoeckli, Staab et al. 2007). This limitation is also true for PET imaging which, despite the ability to perform *in vivo* imaging, requires a radionuclide label and cannot distinguish between parent drug and metabolites. PET imaging also suffers from poor spatial resolution, in the order of millimetres (Wiseman, Ifa et al. 2008).

Another imaging technique used for the non-invasive monitoring of drug and small molecule distribution *in vivo* is nuclear magnetic resonance spectroscopy imaging (MRSI). MRSI utilises the phenomenon of NMR to measure changes in proton/nuclei excitation and relaxation of various metabolites (Port and Wolf 2003; Pysz, Gambhir et al. 2010). MRSI is more commonly used in pharmacological research to determine the effects of a drug on tissues rather than to study the fate of drug compounds in an organism and as such has not been considered further here (Rodríguez, Pérez-Rial et al. 2008).

1.3 Imaging Mass Spectrometry

Imaging mass spectrometry is a technique that combines the specificity and sensitivity of mass spectrometry with imaging capability. Multiple analytes across a wide range of molecules can be detected simultaneously and combined with spatial coordinates to produce a molecular image without the need for labelling (McDonnell and Heeren 2007). There are many potential advantages in using mass spectrometry for molecular imaging, since it has high sensitivity (femtomole) and chemical specificity that is unmatched by other techniques.

Imaging mass spectrometry has been used for a wide range of applications, predominantly in the field of material science using secondary ion mass spectrometry (SIMS), but recent developments have led to the application of imaging MS directly on biological tissue samples using matrix assisted laser desorption/ionisation (MALDI) mass spectrometry and ambient ionisation techniques.

1.4 SIMS imaging

Imaging MS using secondary ion mass spectrometry has been established since the 1960s and has been mainly used for the analysis of inorganic species on surfaces. Although not originally developed for the analysis of biological surfaces, SIMS has been successfully used for imaging of biological tissue, but has significant limitations.

1.4.1 Secondary ion ionisation

SIMS analyses the secondary ions emitted when an energetic primary ion beam is used to irradiate a surface. A schematic of this process is shown in Figure 1.12. The primary ions are focused and accelerated by an electric field to form a continuous ion beam, (usually pulsed) to produce the ionisation event. When the ions hit the sample surface, a collision cascade takes place affecting the substrate atoms within a few nanometres of the impact point. Some of the primary ion kinetic energy is turned back towards the surface causing the ejection of analyte molecules and ions from the

surface of the sample into the gas phase as charged and neutral particles. Small characteristic fragments are detected by the mass analyser, which is commonly a time-of-flight (TOF) analyser. As mentioned in 1.1.3.2, this analyser offers high sensitivity, high detection efficiency and effectively parallel detection (Rubakhin, Jurchen et al. 2005; McDonnell and Heeren 2007).

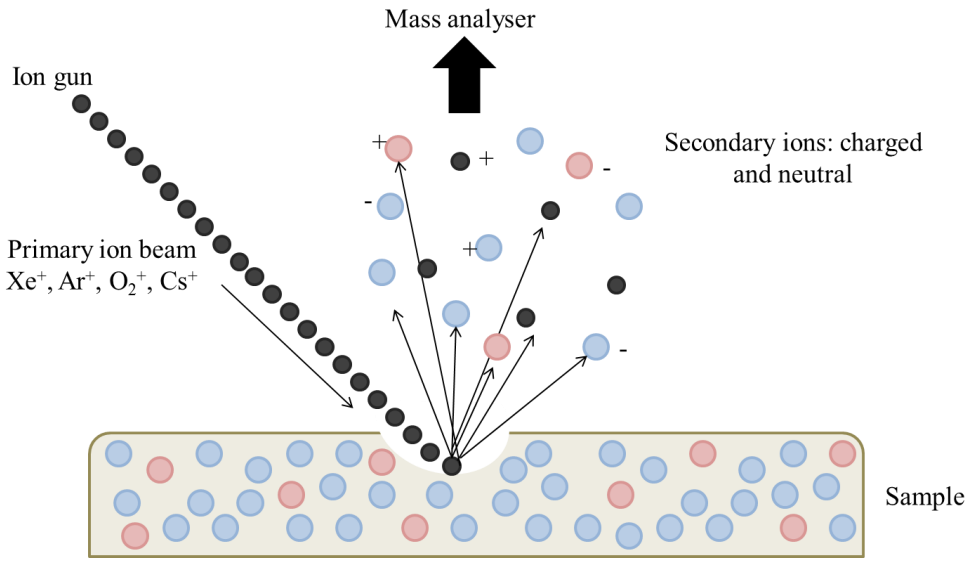

Figure 1.12 Schematic of secondary ion mass spectrometry ionisation. Adapted from Rubakhin *et al.* (2005).

SIMS experiments can provide a wealth of information at subcellular spatial resolution, but this is strongly dependent on sample preparation and surface conditions that are often poorly understood. Many drugs and their metabolites have relatively low molecular weights and low mass ions have much greater signal intensity than higher mass ions in a SIMS experiment. The high energy of a SIMS experiment produces many low molecular weight fragment ions that can in theory be used to identify the compound of interest, but these fragment ions often do not have sufficient chemical specificity for biological applications.

SIMS instrumentation also remains expensive and highly specialised, so although it can offer excellent analytical capabilities, progress in biological applications has been limited. (Heeren, McDonnell et al. 2006; Fletcher, Lockyer et al. 2009; Heeren, Smith et al. 2009)

1.5 MALDI Imaging

Recent developments have led to the application of imaging MS directly on biological tissue samples using matrix assisted laser desorption/ionisation (MALDI) mass spectrometry. MALDI-MS can be used to analyse hundreds of biological molecules directly from tissue sections. When combined with spatial coordinates, the distributions of these molecules can be determined, without the need for labelling. Two-dimensional ion intensity maps can be created to show the localisation of a particular ion across the tissue sample.

Molecular imaging of biological samples using MALDI MS was first demonstrated in 1997 (Caprioli, Farmer et al. 1997) and since then has gained increasing interest in a number of different application areas. These application areas include proteomics, lipidomics and pharmacology. Imaging using MALDI-MS can cover a much greater molecular ion mass range than SIMS, but has a lower spatial resolution often limited by the size of the laser used in the experiment and the sample preparation. When imaging low molecular weight molecules, such as drugs, interference from matrix ions can cause difficulties in assigning spectra. This can be overcome by the use of tandem MS experiments or the use of an ion mobility separation step as discussed in section 1.6.4.

1.5.1 Experimental overview

In a typical MALDI imaging experiment, a frozen tissue sample is sectioned and mounted onto a suitable MALDI target plate. The tissue section is then coated with an organic matrix solution, creating a homogenous layer of small analyte-matrix crystals on the tissue surface. A number of different methods can be used for matrix deposition onto the tissue and matrix choice also plays an important part in the success of the imaging experiment. This is discussed in further detail in section 1.6.2.

A raster or grid is created over the tissue. This determines the region of the sample to be analysed, and the distance between each sampling point. The tissue slice is then analysed using MALDI-MS, firing a focused laser in an ordered array across the surface of the tissue. The spatial coordinates and the mass spectrum obtained at each

position are recorded. This continues until the entire area of the tissue has been analysed and a mass spectrum is associated with each position of the raster.

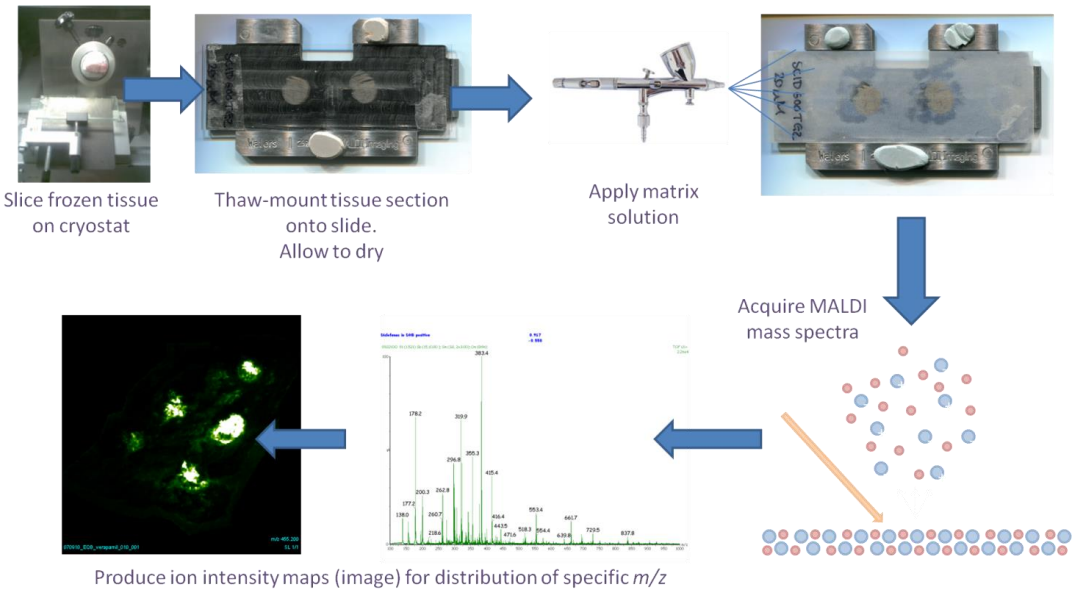

Figure 1.13 Workflow of a typical MALDI imaging experiment.
Different types of MS-acquisition can be used to increase selectivity for a compound of interest.

From the data, molecular images are reconstructed across the tissue creating 2D ion intensity maps of a particular ion of interest. The spatial dimensions of the sample are plotted against relative abundance of a selected ion. This can be used to investigate the localisation of a particular compound (e.g. a drug compound, peptide or lipid of interest) within a tissue section. Profiling experiments may also be conducted where a discrete region of the tissue section is analysed, rather than the entire tissue section. A workflow of a typical MALDI imaging experiment and sample preparation is shown in Figure 1.13. (Stoeckli, Chaurand et al. 2001; Chaurand, Schwartz et al. 2005; Reyzer and Caprioli 2007; Chughtai and Heeren 2010).

1.6 Practical considerations of MALDI imaging

The success of an imaging mass spectrometry experiment relies on sample preparation techniques, especially when maintaining the spatial integrity of the sample. In a MALDI imaging experiment spatial resolution is limited by two key parameters – crystal size and laser diameter.

A number of different methods of sample preparation have been reported in the literature, and suitable sample preparation techniques must be optimised in each experiment for the compounds of interest and the tissue type. Some aspects of sample preparation that need to be considered include optimisation of matrix parameters, such as the type of matrix used, matrix concentration, solvent composition and importantly, deposition of the matrix onto the tissue. Sample handling methods including tissue storage, sectioning and mounting of the tissue onto the target plate are also very important in an imaging experiment. A number of papers reviewing sample preparation techniques for MALDI imaging of biological tissues have been published (Atkinson, Prideaux et al. 2005; Heeren, Kukrer-Kaletas et al. 2008; Kaletas, van der Wiel et al. 2009; Chughtai and Heeren 2010). Key aspects of sample preparation for the localisation of small molecules in tissue using MALDI imaging are discussed here.

1.6.1 Initial tissue treatment

Mishandling of tissue samples early on in the sample preparation process can lead to sample degradation or delocalisation of the analytes on the tissue surface. From the moment the tissue is harvested, careful handling is required in order to maintain the integrity of the localisation of the analytes. Tissue degradation can also be a vital consideration. Once blood and oxygen supply to the tissue is stopped, tissue degradation begins immediately. Organs need to be dissected quickly and freshly harvested tissue should be snap-frozen by immersion in liquid nitrogen, ethanol or isopropranol to prevent rapid tissue degradation. The tissue may be loosely wrapped in aluminium foil prior to freezing to avoid sample damage and to maintain the tissue shape.

Once frozen, the tissue sample is sliced into thin sections in a microcryotome before being mounted onto a MALDI target plate for analysis. The tissue sample is normally sliced to between 10 and 20 µm, the diameter of a mammalian cell, so that the majority of the cells in the tissue are sliced open and can reveal their contents. Traditional histological tissue sectioning protocols involve embedding mediums such as agar or optimal cutting temperature (OCT) polymer. Tissues sectioned for subsequent analysis by mass spectrometry should avoid contamination of the tissue surface with these mediums since they can suppress ion formation. This is shown in Figure 1.14. Instead, ice or gelatine can be used to attach tissues to the sample stage prior to sectioning. Embedding tissues in 10 % gelatine can prevent damage to the tissue during freezing and aid in the sectioning process.

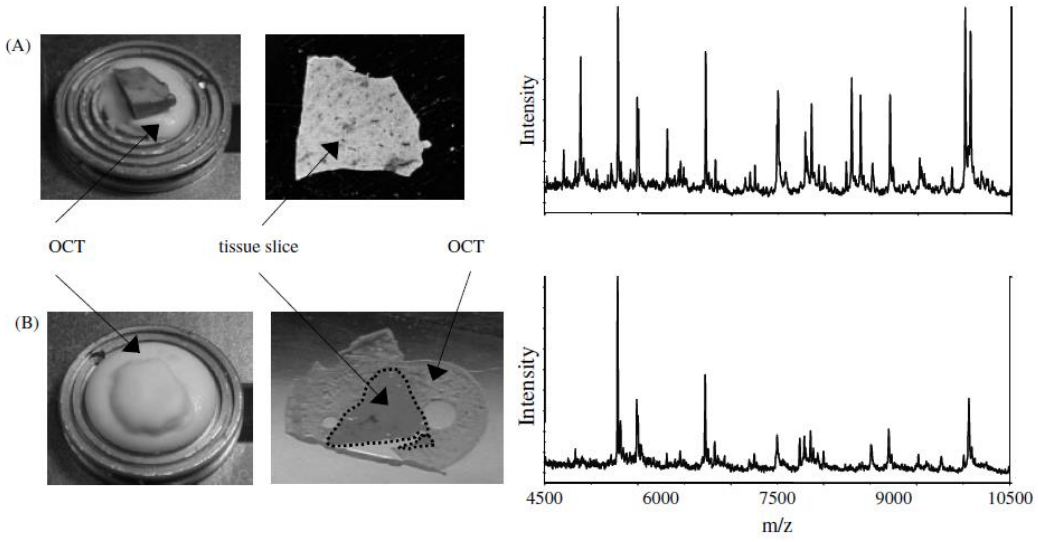

Figure 1.14. Analysis of the effect of OCT on MALDI signals from rat liver.
(A) Procedure where OCT is used to adhere the tissue to the sample stage but does not come into contact with the sliced tissue. The resulting spectrum shows many intense signals between *m/z* 4500 and 10 500.
(B) The tissue was embedded in OCT and attached to the sample stage. The resulting spectrum contains only about half of the signals as that in part A. Reproduced from Schwartz *et al.* 2003.

Tissue sections need to be mounted onto a suitable target plate for MALDI analysis. This can be a stainless steel MALDI target or a glass microscope slide. Stainless steel targets provide good contrast between the tissue section and target, however glass slides allow for subsequent microscopic visualisation of the sections.

Transfer of the tissue slice onto the plate can be done in a number of ways but must be executed with great care to prevent deformities, scratches, tears or rolled up edges of the tissue sample since these cause complications with analysis. Both commonly used methods involve thaw-mounting the tissue section onto the target plate. The first method uses a paintbrush or forceps to carefully transfer the tissue section onto a cold target plate or glass slide. The tissue section and target are then quickly warmed together to thaw mount the section onto the target. This method ensures any ice crystals formed during sectioning are transferred with the section, preventing the loss of water-soluble compounds onto the sectioning blade. The second method involves placing a warm target plate (at room temperature) over the tissue section. As the tissue section thaws it adheres to the target plate, but this approach can leave behind ice crystals on the surface of the cryotome blade.

Once mounted onto the target plate the samples need to be placed in a closed container (such as a petri-dish sealed with parafilm) on dry ice and stored at -80 ˚C until required for matrix deposition and further analysis. Prior to analysis, mounted sections should be brought slowly to room temperature in a vaccuum dessicator to prevent condensation forming on the surface of the tissue that could cause delocalisation of molecules.

Chemical washing has been employed in imaging MS protocols to remove salts and other unwanted molecules from the surface of the tissue. This has been shown to greatly improve resulting mass spectra, especially for proteins and peptides. The standard washing protocol uses an increasing percentage of an ethanol solution. This is not expected to cause delocalisation of proteins due to the fixation and dehydration properties of the solution. Washing the tissue improves signal quality from tissue due to improved crystallisation of the matrix on the surface of the tissue. Washing protocols are generally avoided for analysis of small molecules such as drug compounds, due to the potential for altering the spatial integrity of both drugs and drug-related compounds (Schwartz, Reyzer et al. 2003; Hsieh, Chen et al. 2007; Heeren, Kukrer-Kaletas et al. 2008; Kaletas, van der Wiel et al. 2009; Chughtai and Heeren 2010).

1.6.2 Matrix choice and deposition

The choice of the correct matrix and the optimisation of the method used to apply the matrix to the tissue are vital for obtaining high quality mass spectra directly from the tissue samples whilst maintaining the spatial integrity of the tissue surface. The complex nature of the tissue surface means that the matrix used must crystallise effectively and homogenously across the surface of the tissue in order to yield high quality spectra.

There are three components that make up the matrix solution: the matrix compound, an organic solvent and normally trifluoroacetic acid (TFA). TFA is added in many cases to increase the number of available protons for ionisation. The matrix compound is normally an organic acid with a strong absorbance at the wavelength of the laser used for ionisation. As the organic solvent extracts molecules from tissue, it evaporates and allows for the formation of matrix-analyte crystals on the surface of the tissue (Kaletas, van der Wiel et al. 2009; Chughtai and Heeren 2010).

Table 1.1 summarises the most commonly used matrix compounds for imaging mass spectrometry and highlights the type of molecules analysed using these matrices. For drug localisation studies the most commonly used matrices are DHB and CHCA.

Matrix	Abbreviation	Application
2,5-Dihydroxybenzoic acid	DHB	Sugars, peptides, nucleotides, glycopeptides, glycoproteins, small molecules and small proteins.
α-Cyano-4-hydroxycinnamic acid	CHCA	Peptides, small proteins, glycopeptides, small molecules.
3,5-Dimethoxy-4-hydroxycinnamic acid (Sinapinic acid)	SA	Peptides and large proteins, lipids.
2,4,6-Trihydroxyacetophenone	THAP	Oligonucleotides.
3-Hydroxypicolinic acid	3-HPA	Oligonucleotides, peptides and glycoproteins.

Table 1.1 Common matrices used in MALDI imaging.
Adapted from Kaletas *et al.* 2009.

Matrix concentration is an important consideration since it affects both signal quality and matrix coverage across the tissue. Higher matrix concentrations generally result in improved quality mass spectra from direct tissue analysis. Solvent composition needs to be optimised based on the compound of interest and the tissue type being analysed. Many different combinations of organic solvent have been shown to be successful for imaging experiments. For the analysis of small molecules the solvent composition should be chosen carefully for effectiveness of analyte extraction and crystal formation for the target compound (Schwartz, Reyzer et al. 2003; Hsieh, Chen et al. 2007).

In a MALDI profiling experiment, small droplets of matrix solution are deposited onto the surface of the tissue at discrete locations. For an imaging experiment the entire surface of the tissue is coated with matrix to provide a homogenous layer of small matrix crystals. Smaller crystals mean that the image resolution is limited by the laser diameter. There are a number of methods currently in use for matrix deposition onto tissue, which aim to produce high resolution images by minimising crystal size. These matrix application techniques were reviewed by Kaletas *et al.* in 2009, and a summary of these techniques are shown in Table 1.2. The most popular matrix application methods tend to be manual or automated pneumatic nebulisation and spraying methods, alongside automated spotting methods. The most important protocol features of commercially available matrix deposition devices are discussed in further detail below.

Applying the matrix solution by using an automated spotting device prevents diffusion of analytes beyond the spot size. Manual spotting is limited to profiling type experiments, as spot size is limited to around a millimetre and difficult to control, whereas automated devices deposit picolitre (pL) droplets, thereby producing a spot size of around around 100-200 micrometres. An advantage of automated spotting devices is that they can also be used for on-tissue digestion protocols, where a digestive enzyme like trypsin can be spotted across the tissue surface. A number of automated spotting devices, using different types of droplet ejectors, are commercially available for MALDI imaging. These include the Portrait 630 (Labcyte Inc, California, USA), ChIP 1000 (Shimadzu Scientific Instruments, Columbia, USA) and the TM iD (LEAP Technologies, Carborro, NC, USA). Spotting protocols tend to

Technique	Droplet Diameter	Advantanges	Disadvantages
Pneumatic nebulisation (airbrush)	Variable, mostly small (aerosols)	Fast, simple, homogenous layer, cheap.	Limited environmental control, low concentrations of matrix solution can be used; quality varies from person to person, droplet size not consistent.
Chemical inkjet printer - ChIP	~ 150 µm (100 pL)	Uniform droplets, precision of placement, conditions can be controlled, automated, high signal quality, reproducible.	Slow, nozzle tip clogging, expensive.
Acoustic reagent multi-spotter	180-230 µm (170 pL)	Uniform droplets, precision of placement, automated, no clogging, fast, good reproducibility.	Matrix applied in droplets, few experiences in the use of it.
Electrospray deposition	Small	Homogenous layer, equally sized crystals.	Limited time for analyte-matrix interaction, quality varies from person to person.
Pneumatic sprayer	Variable, but small	Homogenous layer, automated, controlled environment, suitable for large area.	Vary large amounts of matrix solution used (50-150 ml), droplet size not constant.
ImagePrep (Bruker)	Variable, but small (~20-50 µm)	Conditions can be varied and controlled, automated, homogenous layer.	Slow, small area, membrane clogging, droplet size not constant, expensive.
Dry-coating	20 µm (crystal size)	Cheap, very homogenous, high purity of organic matrix, reproducible, fast.	Limited time for matrix-analyte interaction – only lipids detected so far.

Table 1.2 Matrix application techniques for imaging MS.
Adapted from Kaletas *et al.* 2009.

be slower than spraying methods, but require less carefully designed application protocols (Kaletas, van der Wiel et al. 2009; Chughtai and Heeren 2010; McDonnell, van Remoortere et al. 2010).

Spray coating is designed to coat the entire sample surface with a fine distribution of droplets of matrix solution, with the aim of producing a homogenous layer of small matrix crystals. Spraying devices cover the tissue surface with much smaller droplets than those produced by spotting devices, generating smaller crystal sizes and allowing for better spatial resolution. Both manual and automated spraying techniques have been developed, with a few automated devices commercially available. Whilst automated methods give more reproducible results, they tend to be significantly more expensive than the manual methods.

Bruker Daltonics have developed an automated vibrational sprayer system for matrix application (ImagePrep, Bruker Daltonik GmbH, Bremen, Germany) (Schuerenberg, Luebbert et al. 2007). This device produces small droplets in the region of 20 – 50 µm and allows control over a number of conditions during spraying. The thickness of the matrix crystal layer is monitored during application and the drying time between each layer is carefully controlled, but application time is slow and limited to a small sample area. The ImagePrep device is also expensive when compared with other matrix application methods (Kaletas, van der Wiel et al. 2009). Other automated sprayers commercially available are the TM-Sprayer (LEAP Technologies, Carborro, NC, USA) and SunCollect spotter/sprayer system (KR Analytical, Cheshire, UK).

The simplest and cheapest method for spray coating is manual spraying, using a commercially available artists airbrush or thin-layer chromatography (TLC) sprayers. Manual spray coating using an airbrush is a fast and simple method for producing a homogenous layer of relatively small matrix crystals across the surface of the tissue. A number of parameters need to be controlled for reproducible results by manual spraying. Spraying should be done at a constant room temperature and humidity, and beginners should practice their technique to achieve homogenous and reproducible matrix coverage (Setou 2010). The sprayer should be held approximately 20 – 30 cm from the target, mounted vertically. As the matrix is sprayed, the airbrush needs to

be moved parallel to the target. This ensures an even coverage of matrix and prevents overwetting of the tissue. Typically, the matrix is applied in a series of cycles where small volumes of matrix solution are sprayed across the tissue per cycle, with time allowed between each cycle to allow the matrix to dry. Around ten cycles provides sufficient coverage of matrix, though this can vary with sample type. In order to increase incorporation of analytes into matrix crystals, the final cycle can consist of matrix solvent in order to recrystallise the matrix previously applied (Schwartz, Reyzer et al. 2003).

1.6.3 Instrumentation

Initially all MALDI imaging experiments were performed on home built or modified commercial mass spectrometers, limiting the opportunity of many groups to undertake imaging mass spectrometry research. By 2004, the first commercially available MALDI imaging instruments had been introduced and now most instrument vendors sell MALDI mass spectrometers capable of MALDI imaging, each with their own approach and data output.

A comprehensive list of commercial imaging instruments past and present can be found on the MALDI MSI interest group website (http://www.maldi-msi.org/). This website is a valuable resource, dedicated to sharing information on MALDI imaging experiments among the research community. A summary of commercial imaging mass spectrometers currently available is covered in Table 1.3. There are a range of different mass analysers employed for imaging mass spectrometry instrumentation, the most commonly used for MALDI imaging are TOF, FTMS, ion traps and hybrid combinations of the above. Each mass analyser, discussed in section 1.1.3, has strengths and weaknesses in terms of resolving power, mass range, speed of acquisition and detection.

MALDI imaging experiments have been largely carried out using TOF systems. MALDI-TOF systems alone can have limitations in resolving power, mass measurement accuracy and are unable to perform forms of tandem mass spectrometry experiments (Kutz, Schmidt et al. 2004). The coupling of two TOF mass analysers allows for precursor ion fragmentation by the first TOF system,

followed by rapid parallel fragment analysis using the second TOF system. Q-TOF systems can provide improved mass accuracy and allow for effective CID tandem mass spectrometry experiments to be performed (Chughtai and Heeren 2010).

The high mass accuracy and resolution of FT-ICR instruments provides a number of potential advantages for imaging experiments; details may be revealed that would not be seen with lower resolution instruments. The much longer measuring time required for FT-ICR to image a whole tissue section has limited the use of this approach to small, defined regions of interest highlighted by traditional TOF imaging experiments (Taban, Altelaar et al. 2007).

One of the potential limitations of an imaging experiment is separation of isobaric species from tissue in the low mass region, where matrix clusters reside. Instruments offering improved mass resolution and mass accuracy are often used for imaging experiments to overcome this limitation. Ion traps are included in hybrid imaging instruments coupled with an Orbitrap analyser to provide high resolution data for small molecule analysis. The linear ion trap is then used for multistage MS/MS fragmentation in order to identify compounds (Landgraf, Conaway et al. 2009). Ion traps have also been combined with TOF analysers (Hayasaka, Goto-Inoue et al. 2008; Shimma, Sugiura et al. 2008).

Instrument	Vendor	Type	Laser	Mass Range	Resolution (st[1],la[2])	Software	Data Format
4800/5800 MALDI TOF-TOF™ Analyzer	**AB Sciex**	TOF-TOF	Nd:YAG 200 Hz/1 kHz	Full	1 µm, 50 µm	4800 Img, TissueView	Analyze
ultrafleXtreme	**Bruker**	TOF-TOF	Smartbeam-II	Full	5 µm, 10 µm	flexImaging, CreateTarget, AnalyzeThis!, BioMap	XMass, XML
Solarix MI		Hybrid FTMS	1 kHz	100 – 10 kDa	5 µm, 20 µm		
AXIMA QIT™	**Shimadzu**	Ion trap – TOF	N2	< 20 kDa	10 µm, 100 µm	Axima2Analyze	Analyze
AXIMA Assurance		TOF		< 500 kDa (linear)			
AXIMA Confidence/Performance		TOF/ TOF-TOF	50 Hz	< 500 kDa (linear)/< 80 kDa (reflectron)			
MALDI LTQ XL	**Thermo Fisher Scientific**	Ion Trap	N_2	50 - 4000 Da	1 µm, 60 µm	LTQ Tune, ImageQuest	RAW, ImzML
MALDI LTQ Orbitrap Discovery/XL		Ion trap – orbitrap hybrid	60 Hz				
MALDI Synapt G2 HDMS	**Waters**	Q-TWIMS-oaTOF	Nd:YAG 200 Hz / 1 kHz	< 40 kDa	3.5 µm, 60/200 µm	MassLynx/BioMap HDImaging	XML
MALDI Synapt HDMS							

Table 1.3 A summarised list of current commercial MALDI imaging mass spectrometers. Adapted from (http://www.maldi-msi.org/)

1. Mechanical resolution limited by sample stage positioning
2. Approximate laser beam diameter on sample

Ion mobility separation provides an alternative approach for the separation of isobaric species. All MALDI imaging experiments in this study were performed on a MALDI Synapt G2 HDMS travelling-wave ion mobility (TWIM) quadrupole time-of-flight (Q-TOF) mass spectrometer (Waters Corporation, Manchester, UK). This mass spectrometer was used because it is the only commercially available MALDI imaging instrument with the ability to perform ion mobility separation.

The MALDI Synapt G2 is a second generation quadrupole orthogonal acceleration TOF mass spectrometer, with an IMS cell located between the quadrupole and TOF analyser. A schematic of the MALDI Synapt G2 is shown in Figure 1.15. The travelling wave IMS device is described in detail in 1.1.7. The location of this Triwave device allows a number of different experimental modes to be explored. When operated in TOF mode, without mobility separation, the Triwave region of the mass spectrometer acts as an ion guide to transfer ions from the quadrupole into the TOF mass analyser. Collision gas can be introduced into the trap or transfer sections of the Triwave cell for MS/MS fragmentation.

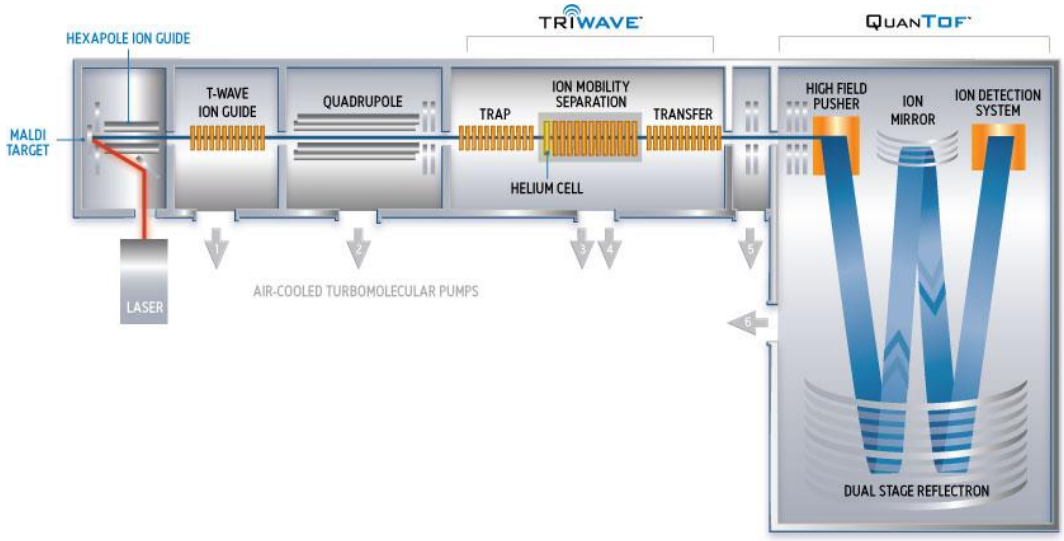

Figure 1.15 Schematic of MALDI Synapt G2 HDMS Q-TOF mass spectrometer.

In mobility mode, the IMS cell, which separates ions based on their shape and charge state, is filled with nitrogen gas. Ions with smaller collisional cross-sections encounter less drag when passing through the IMS cell, and therefore have an earlier arrival time than larger ions. Collision gas can be introduced into the trap region, for

MS/MS fragmentation prior to mobility separation; or can be introduced into the transfer region, for MS/MS fragmentation after mobility separation, or both.

The instrument is equipped with an interchangeable MALDI source region, allowing other modes of AP ionisation to be employed, such as ESI or nESI. The MALDI source is operated at an intermediate pressure (9×10^{-2} mbar) and has a 200 Hz neodymium:yttrium aluminium garnet (Nd:YAG) laser system with a wavelength of 355 nm. During an imaging experiment the laser position remains fixed whilst the tissue section is moved in a raster pattern on an x/y sample stage, relative to the laser.

In the QuanTof region of the Synapt G2 there is a high field pusher and dual stage reflectron combined with a novel ion detection system, to provide high resolution and higher dynamic range. There are three modes of operation, each providing differing levels of resolution. In both sensitivity and resolution modes, the QuanTof region is operated as a single stage reflectron ('V'-mode). In resolution mode, voltages are used to limit the space in the pusher region to form a tighter packet of ions, increasing the resolution to 20,000 FWHM. In sensitivity mode, a greater number of ions can fit in the pusher region but are able to move more freely, offering a resolution of 10,000 FWHM, but with greater sensitivity as an increased number of ions are detected. In high-resolution mode, the Quan-Tof region operates using a dual stage reflectron (W-mode) offering a resolution of 40,000 FWHM. Fewer ions reach the detector in this mode and so there is a reduction in sensitivity. The majority of MALDI imaging experiments for drug localisation require the instrument to be operated in sensitivity mode, however imaging of more abundant species can be performed in resolution mode. Ion detection is achieved using an ultra-fast electron multiplier and hybrid ADC detector electronics, providing high sensitivity and dynamic range.

In MS/MS experiments, the mass spectrometer can be operated with an Enhanced Duty Cycle (EDC) mode to increase the sensitivity of the MS/MS experiment. This is done by coupling the pusher in the TOF mass analyser with the preceding ion guide, enhancing sensitivity for ions with a particular mass-to-charge (m/z).

1.6.4 Ion mobility separation

MALDI-MS can have some limitations when imaging small molecules. Most drugs are of low molecular weight (<1000 Da) which can lead to signal interference by both the matrix and low mass molecular ions present in the tissue. Tandem MS experiments can be used to distinguish the drug from matrix ions, but only a limited number of analytes can be sequenced at each sample position before the sample is consumed. This is made more difficult when spatial resolution is increased and the amount of sample at each point decreases (McLean, Ridenour et al. 2007).

Ion mobility mass spectrometry (IM-MS) can be used to provide separation of ions on the basis of their molecular structure as well as their mass-to-charge ratio (*m/z*). Coupling ion mobility with MALDI imaging allows for the separation of ions according to their size, shape and charge state. This means that different compound classes can be separated, providing a unique advantage over MALDI imaging experiments alone. MALDI-IMS-MS can be used to produce clearer images reducing interference from background ions of similar mass. This gives additional confidence that the true distribution of an ion of interest has been observed and can distinguish the drug compound from matrix, giving more precise localisation (McLean, Ridenour et al. 2007; Snel 2007).

The advantages of ion mobility MALDI imaging experiments when compared to conventional MALDI MS, MS/MS imaging and WBA have recently been published for the imaging of an anticancer drug in rat whole body tissue sections (Trim, Henson et al. 2008). The use of ion mobility as a further separation technique allowed the drug to be separated from interference by endogenous ions.

1.6.5 Software for imaging mass spectrometry

Large amounts of complex, multi-dimensional data are collected during an imaging mass spectrometry experiment. Imaging data from one tissue section can be in the region of a few gigabytes, and this size is increased when ion mobility separation data are included. Specialised software is required at each step of an imaging experiment, from controlling experimental methods and data acquisition to processing and visualising these data as images. Each instrument manufacturer has

different propriatory data formats highlighted in Table 1.3 and there are a number different software packages available. Some of these have been evaluated by Jardin-Mathé *et al.* (Jardin-Mathe, Bonnel et al. 2008). Software packages used throughout this project are discussed in more detail below.

All imaging experiments in this thesis were carried out using the MALDI Synapt G2 HDMS. After matrix application, an optical image of the target plate and tissue were obtained using a flatbed scanner (Epson Perfection V30, Epson, UK). The tissue region to be imaged was then selected using MALDI Imaging Pattern Creator (Waters) and the required spatial resolution defined. This was then saved as a pattern definition metafile file (.pdm) and a pattern definition file (.pat) was generated, specifying sample acquisition points. Once the pattern file has been created, an experimental method was set up using MassLynx (Waters). This experimental method defines the mass range, acquisition type (MS, MS/MS, HDMS, HDMS/MS), scan time and the pattern file for the region to be imaged. Data acquisition was then carried out using MassLynx software. For MS or MS/MS data without mobility separation, data files were simply converted to .img files for image reconstruction with Biomap (Novartis, Basel, Switzerland) using MALDI Imaging Converter (Waters).

Experiments with an ion mobility separation step required the data to be further interrogated prior to conversion, in order to extract arrival time distribution information. Mobility data was analysed using Driftscope (Waters), which displayed *m/z* data vs. drift time as a 2D heat map (shown in Figure 1.16). Ions were selected based on their drift time and *m/z.* This allowed for separation of an ion of interest from background noise, providing that the drift time through the mobility cell was known for that ion. This could be be determined during optimisation experiments using standards. For MS/MS experiments where fragmentation was performed following ion mobility separation, daughter ions were selected based on the drift time of the parent ion. This added an extra degree of selectivity to the experiment.

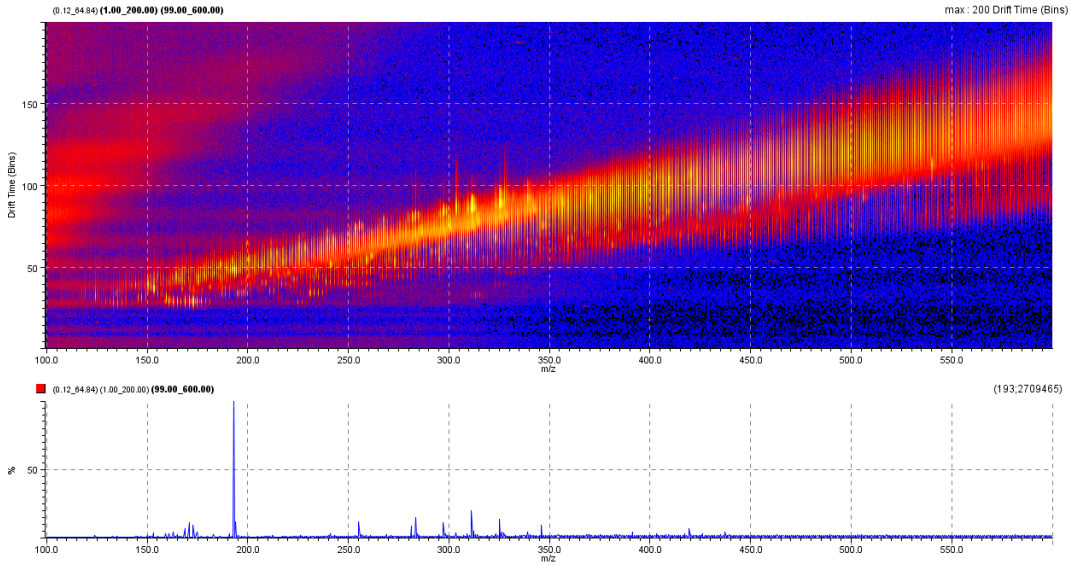

Figure 1.16 Example MALDI-mobility-MS imaging data file displayed in Driftscope as a heat map of *m/z* vs. drift time.

Regions of the mobilogram selected, based on drift time and *m/z*, were exported to MassLynx, retaining the x/y spatial coordinate information from the imaging experiment. These data were then converted using MALDI Imaging Converter for image visualisation.

Image reconstruction was achieved using Biomap (Novartis, Basel, Switzerland) which is freely available at www.maldi-msi.org. This is an image processing application written in IDL™ (Research Systems, Boulder, CO) developed originally by Martin Rausch for MRI data in biomedical research that has been developed for a number of imaging data formats, including imaging MS data (Stoeckli, Staab et al. 2002). Biomap is compatible with data from a number of instrument vendors, providing an input filter exists for that data format. It allows single points or regions of interest (ROIs) to be selected on the MS image, displaying the mass spectrum corresponding to that position. Selecting a specific *m/z* of an ion of interest displays an intensity map of that ion across the tissue surface (Rohner, Staab et al. 2005). Data processed in Biomap was then stored in Analyze format.

A complete software package for MALDI ion mobility imaging named HDImaging was recently introduced by Waters. This comprises a number of features from the original imaging software, including Pattern Creator and Converter, but also contains new features for experimental setup, data processing and image reconstruction. It also removes the need to process mobility data in Driftscope, incorporating ion mobility separation data within the imaging analysis. The raw data can be processed using the algorithm Apex 3D to create a peak list with *m/z* and drift time information. Aside from the requirement of MassLynx for the control of data acquisition, this software package contains everything required for running a MALDI imaging experiment and analysis of results using Waters instrumentation. This software package may also be used to reprocess data previously acquired (Waters 2011).

1.7 Applications of MALDI imaging

Since MALDI imaging was first introduced by the Caprioli group in 1997, the technique has been used in a wide range of applications. These applications include imaging of proteins, drug localisation experiments, lipidomics and metabolite distribution studies for a range of tissue types.

The localisation of peptides and proteins in biological samples has been of great interest. Initial work by the Caprioli group reported localisation of insulin in a rat pancreatic tissue section (Caprioli, Farmer et al. 1997) and the first ion images followed closely in 2001, showing localisation of proteins in glioblastoma tumour sections and ion distributions in mouse brain sections (Stoeckli, Chaurand et al. 2001). In 2004 Chaurand *et al.* published an overview of protein profiling and imaging in tissue sections by mass spectrometry (Chaurand, Schwartz et al. 2004). A protocol for the identification of proteins directly from tissue sections was published in 2007 using enzymatic digestion performed *in situ* using MALDI MS/MS analysis to determine the peptide sequence (Groseclose, Andersson et al. 2007). Introducing an ion mobility separation step into the MALDI imaging experiment for protein imaging has been shown to add confidence to protein identification directly from tissue. Using mobility arrival time information to separate ions of similar *m/z* can allow specific fragmentation patterns to be observed which can improve peptide identification (Stauber, MacAleese et al. 2010).

1.7.1 MALDI imaging for drug localisation

Drug distribution techniques employed by pharmaceutical companies can suffer from a number of limitations. These have been highlighted in section 1.2.6. These imaging approaches rely on labels, such as radioactivity or fluorescent tags, which may not distinguish between the drug of interest and its metabolites. A number of mass spectrometry-based imaging approaches have been described for the localisation of drug compounds and metabolites in tissue. These experiments can provide data complementary to existing imaging techniques.

MALDI-MS was first used to directly study pharmaceutical compounds in tissue by Troendle *et al*. but specific localisation of the drug could not be determined. The authors used MALDI quadrupole ion trap mass spectrometry to detect an anticancer drug in human ovarian tumour tissue and an antipsychotic drug in spiked sections of rat liver tissue. They reported that tandem MS experiments were required to identify the drug compounds at trace levels, due to the complex nature of the tissue (Troendle, Reddick et al. 1999). The first example of drug localisation in a tissue section by MALDI-MS was demonstrated in 2001 by the Caprioli group (Todd, Schaaff et al. 2001). They showed the distribution of clozapine, an anti-psychotic drug, in rat brain.

In 2003, the Caprioli group studied the distribution of anti-tumour drugs in mouse tumour tissue and rat brain. These studies demonstrated the advantages of performing fragmentation (using collision induced dissociation (CID)) on ions of interest. The selectivity of the technique was improved and allowed the characterisation of small molecules without interference by matrix ions. Localisation of drug compounds in the tissue samples was also demonstrated (Reyzer, Hsieh et al. 2003). Hsieh and workers compared the imaging outcomes of traditional autoradiography techniques with MALDI imaging (looking at the distribution of clozapine in rat brain tissue) and demonstrated good correlation between the results (Hsieh, Casale et al. 2006). Imaging by MS has an advantage in that the drug may be distinguished from its metabolites. In autoradiography techniques, the radioactive tag is observed and this could be attached to a metabolite rather than the compound of interest. The first demonstration of simultaneous drug and metabolite distribution within whole body tissue sections was by Khatib-Shahidi *et al* in 2006, who showed the distribution of olanzapine (another antipsychotic drug) and metabolites at various

time points following administration. The distributions also showed good correlation with previous whole body autoradiography studies of olanzapine (Khatib-Shahidi, Andersson et al. 2006).

Work by Stoeckli *et al*. further demonstrated good correlation between WBA and MALDI imaging experiments. The distribution of a ^{14}C labelled compound in rat whole body tissue sections was determined at different time points post-dose. The authors highlighted the benefit of having WBA data available to validate the results obtained by imaging mass spectrometry and commented on the complementary nature of the two techniques (Stoeckli, Staab et al. 2007).

Since these initial studies, a number of other studies have been published which show the use of MALDI experiments to localise pharmaceuticals in a number of different tissue samples, including rat brain (Reyzer, Hsieh et al. 2003; Wang, Jackson et al. 2005; Hsieh, Casale et al. 2006; Goodwin, Pennington et al. 2008), mouse brain (Shin, Dong et al. 2011), skin (Bunch, Clench et al. 2004), human tumour xenographs (Atkinson, Loadman et al. 2007), rat spleen (Drexler, Garrett et al. 2007), rabbit lungs (Prideaux, Dartois et al. 2011) and rat whole-body tissue sections (Khatib-Shahidi, Andersson et al. 2006; Stoeckli, Staab et al. 2007; Trim, Henson et al. 2008).

As described in 1.6.4, use of ion mobility separation during MALDI imaging drug localisation studies can add an extra degree of selectivity. This may allow an ion of interest to be separated from endogenous ions, providing confidence that the ion detected is the drug of analyte of interest (Trim, Henson et al. 2008).

1.8 Ambient ionisation imaging

Ambient ionisation methods operate under atmospheric pressure, unlike traditional ionisation techniques such as MALDI or SIMS, which operate under high vacuum conditions. Alongside developments in MALDI imaging, significant progress has also been made in the field of ambient ionisation imaging.

1.9 Desorption electrospray ionisation

Desorption electrospray ionisation (DESI) is an ambient ionisation method, developed by Graham Cooks in 2004; that has been successfully used for imaging mass spectrometry experiments. In a DESI experiment electrosprayed charged droplets and ions of solvent are directed onto the surface to be analysed. The impact of these charged particles on the surface produces ions of material present on the surface via a solvent pick up mechanism. (Takats, Wiseman et al. 2004). Unlike MALDI and SIMS, minimal sample preparation is required for DESI imaging; no matrix compounds are required, and the composition of the solvent can be altered to target analytes of interest. Samples can either be mounted onto a target or analysed *in situ* for DESI imaging.

The first example of the use of DESI for the profiling of biological tissues was reported in 2005. This showed the detection of lipids in mouse pancreas and adenocarcinoma tissue (Wiseman, Puolitaival et al. 2005). The first DESI imaging paper followed closely in 2006 from the same group. This showed negative ion lipid distributions from a rat brain section with a spatial resolution of less than 500 μm (Wiseman, Ifa et al. 2006). An experimental method for DESI imaging has been published in Nature Protocols in 2008 by Cooks *et al* and since then DESI imaging has been used for a range of applications with significant improvements in spatial resolution having been achieved (Wiseman, Ifa et al. 2008).

DESI has predominantly been used for the mass spectrometric imaging of lipids in a range of tissue types. Early DESI imaging work in the field of lipidomics was reviewed in 2009 (Dill, Ifa et al. 2009). Since this there have been a number of other examples of lipid imaging in atheroma tissue (Manicke, Nefliu et al. 2009), rat spinal

cord (Girod, Shi et al. 2010) and in mouse brain, where a 3D visualisation of the brain was achieved by lipid analysis (Eberlin, Ifa et al. 2010). The strengths and limitations of DESI imaging for lipid characterisation and imaging have been described by the Cooks group in a recent review (Eberlin, Ferreira et al. 2011).

DESI imaging has also been used for localisation of pharmaceutical compounds in dosed tissue sections. The distribution of clozapine has been demonstrated in rat kidney, lung, testis and brain tissue sections, with spatial resolutions of 250 µm achieved. The authors detected the presence of a metabolite in lung sections using the DESI method (Wiseman, Ifa et al. 2008). DESI imaging for drug localisation has also been compared with whole body autoradiography (WBA) for the localisation of the drug propranolol in mouse whole body tissue sections (Kertesz, Van Berkel et al. 2008). Since 2008, there has been surprisingly few reports of the use of DESI imaging for localisation of drug compounds in tissue. This may be due to the lack of appropriate commercially available DESI imaging sources.

Until recently, DESI imaging has had a distinct disadvantage in achievable spatial resolution when compared to MALDI and SIMS imaging. Routinely, spatial resolutions have been reported between 200-400 µm. An investigation into imaging resolution of the DESI experiment was first performed in 2008. This work used printed patterns on paper and thin-layer chromatography plate surfaces. Resolutions close to 40 µm were described, indicating the potential of DESI imaging (Kertesz and Van Berkel 2008), although such results have not been similarly reported for DESI imaging of biological tissue. The recent development of nanospray DESI shows great promise in improving spatial resolution in ambient ionisation imaging experiments. The authors demonstrate a spatial resolution for tissue sections in the region of 12 µm (for lipid imaging), which forms a significant improvement on that which had been achieved in previous ambient ionisation imaging studies (Roach, Laskin et al. 2010; Laskin, Heath et al. 2011).

1.10 LESA profiling

An electrospray-based technique for tissue analysis, termed liquid extraction surface analysis (LESA), has recently been described. This experiment uses a chip-based robotic nanoelectrospray platform (TriVersa NanoMate, Advion) (Kertesz and Van Berkel 2010).

An extraction solvent is brought into contact with the surface of a sample (e.g. tissue section) in a pre-defined position held by the NanoMate. The droplet is held on the surface to allow analyte compounds to be extracted from the surface, before being aspirated and sprayed through an ESI chip into the mass spectrometer. This process is shown by the schematic shown in Figure 1.17.

The authors have shown the application of this technique for a number of different sample types including MALDI spots, dried blood spots and detection of drugs from thin tissue sections. This work has been extended to include a high pressure liquid chromatography (HPLC) separation step after extraction of analytes from the tissue surface and prior to introduction into the mass spectrometer. The chromatography separation step allowed for the detection of isomeric metabolites of propanolol from whole body tissue slices. These were not observed without the HPLC separation (Kertesz and Van Berkel 2010).

Recently, MALDI-MS and LESA-MS have both been shown to be able to successfully determine the degree of penetration in skin of a topically applied glucocorticosteroid drug, known to cause skin blanching (Marshall, Toteu-Djomte et al. 2010). The advantages of LESA-MS as a profiling tool for drug distribution and metabolism in tissue sections have been demonstrated, and the results compared to a quantitative whole body autoradiography experiment. (Eikel, Vavrek et al. 2011)

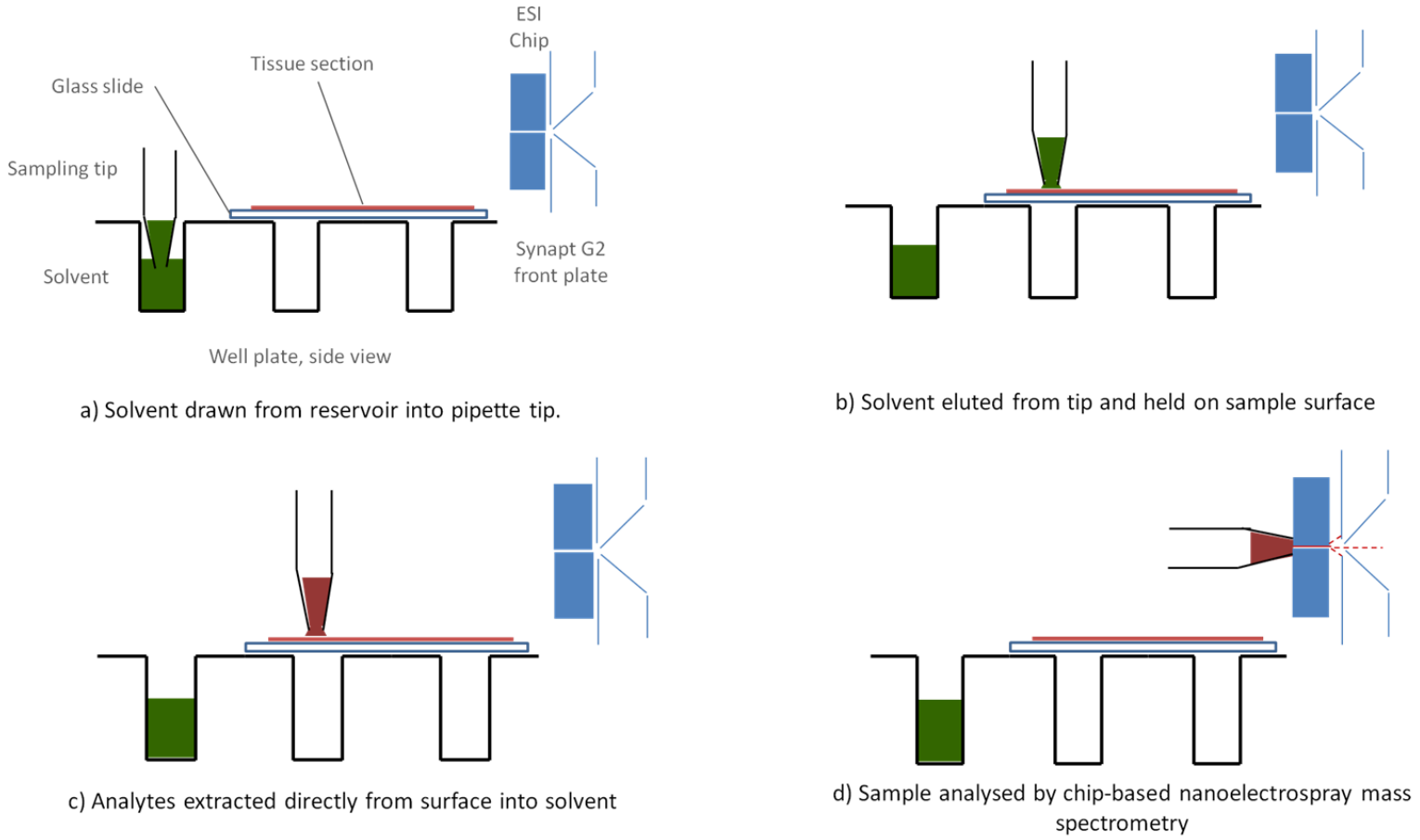

Figure 1.17 Schematic of Liquid Extraction Surface Analysis technique. Adapted from (Kertesz and Van Berkel 2010).

1.10.1 Practical considerations

The spatial resolution of LESA is dependent on the size of the solvent droplet held on the tissue surface. This is approximately 1-2 mm in diameter in contrast to MALDI imaging experiments, which can achieve spatial resolution on the micrometre scale, dependent on matrix crystal size and laser diameter. Despite these drawbacks in spatial resolution, LESA-MS possesses a number of advantages over conventional MALDI imaging experiments, including little sample preparation and no matrix requirements. At the present time, LESA-MS remains a tissue profiling technique, partly due to the lack of available software for image reconstruction.

The extraction solvent used must be optimised using standard compounds, balancing the requirements of compound extraction from tissue and the ability to maintain a stable spray through the nanoESI chip. Very little sample preparation is required for the LESA experiment aside from the choice of the extraction solvent. The sample stage is relatively large when compared with MALDI targets, and can easily hold a mouse whole-body section, making this technique amenable to a wide range of sample types. As LESA is an ESI-based technique, optimisation of extraction solvent and other experimental conditions can be performed by ESI-MS and transferred to the LESA experiment.

It has been noted that the extraction process of compounds from tissue sections using LESA is poorly understood. The sensitivity of the technique may be due to ionisation efficiency of particular compounds, and the effects of ion suppression have not yet been fully investigated. Differences in extraction and ionisation efficiency may prove to be a stumbling block with regards to relative quantitation across a tissue section (Eikel, Vavrek et al. 2011).

1.10.2 Instrumentation

The NanoMate device can be attached to a number of different mass spectrometers, enabling the use of a variety of MS experiments to be carried out following LESA sampling and ionisation. The NanoMate has been combined with a variety of MS instrumentation including an Orbitrap (Eikel and Henion 2011; Eikel, Vavrek et al. 2011), a triple quadrupole (Eikel and Henion 2011), an ion trap-orbitrap hybrid

(Schadt, Kallbach et al. 2012), a triple quadrupole-ion trap hybrid (Walworth, ElNaggar et al. 2011) and a QTOF instrument (Marshall, Toteu-Djomte et al. 2010).

All LESA-MS experiments performed in this research were conducted on a Synapt G2 HDMS mass spectrometer as previously described in 1.6.3. Instead of the MALDI interface, the instrument was operated with an ESI source equipped with a TriVersa Advion NanoMate system. Coupling the LESA surface sampling technique with the Synapt G2 instrument formed a novel approach that provided the opportunity to perform ion mobility separation, enhancing selectivity and enabling a range of tandem MS experiments to be carried out.

1.11 Aims of the project

The work presented in this thesis involved the evaluation of imaging mass spectrometry-based approaches for the localisation of drug compounds and small molecules in animal tissue. The advantages of including an ion mobility separation step in imaging mass spectrometry protocols has been addressed for both MALDI imaging and LESA profiling.

The field of MALDI imaging was first described around fifteen years ago in 1997 and the imaging mass spectrometry community continues to grow year on year. The use of ion mobility enabled MALDI imaging remains a small field, as only two commercial instruments exist which are capable of these experiments. The MALDI Synapt G2 HDMS system was made commercially available in June 2010. The use of this system for drug localisation in tissue sections has been assessed and compared both with the novel approach of LESA profiling and traditional drug localisation techniques. These studies were conducted, in part, at the Alderley Park site of AstraZeneca UK, under the supervision of Dr. Daniel Weston. The combination of LESA profiling and ion mobility separation for the detection of drug compounds in tissue has not previously been described. The advantages and limitations of combining these techniques has been discussed.

A critical evaluation of the applicability of these techniques for drug localisation across the target tissue, which includes important experimental considerations such as spatial resolution, time of acquisition, fit-for-purpose assessment and complementarity vs. traditional drug distribution techniques, has been evaluated for both MALDI imaging and LESA profiling, with and without the inclusion of ion mobility separation.

MALDI mobility imaging, in collaboration with the group of Prof. Bruno Frenguelli, has been applied to the localisation of endogenous energy metabolites in mouse brain. This research had the objective of detecting differences between normal brains and those subjected to metabolic stress.

The aims of this project were to:

1. Evaluate the applicability of two ion mobility imaging mass spectrometry approaches for the localisation of the common non-steroidal anti-inflammatory drug (NSAID), diclofenac, in whole body mouse sections and to compare these approaches with QWBA experiments (Chapter Three).

2. The comparison of industry-standard drug localisation and metabolite identification techniques with ion mobility enabled MALDI imaging and LESA profiling for the localisation of two drug compounds in rat, fenclozic acid and propranolol (Chapter Four).

3. The investigation of the use of ion mobility enabled MALDI imaging experiments for the localisation of important energy metabolites in mouse brain. Tissue fixation techniques were evaluated in order to to prevent rapid post-mortem changes in brain tissue (Chapter Five).

1.12 Research Papers

The research presented in this thesis has resulted in the publication of three peer-reviewed papers.

Blatherwick, E.Q., Van Berkel, G.J., Pickup, K., Johansson, M.K., Beaudoin, M., Cole, R.O., Day, J.M., Iverson, S., Wilson, I.D., Scrivens, J.H. and Weston, D.J. (2011) Utility of spatially-resolved atmospheric pressure surface sampling and ionization techniques as alternatives to mass spectrometric imaging (MSI) in drug metabolism. *Xenobiotica.* **41**, 720-734.

Blatherwick, E.Q., Pickup, K.J., Wilson, I.D., Weston, D.J. and Scrivens, J.H. Improved identification of drug compounds in tissue using a combination of liquid extraction surface analysis and ion mobility separation. *Rapid Communications in Mass Spectrometry* (in press).

Blatherwick, E.Q., Svensson, C.I., Frenguelli, B.G., Scrivens, J.H. (2013) Localisation of adenine nucleotides in heat-stabilised mouse brains using ion mobility enabled MALDI imaging. *International Journal of Mass Spectrometry* (doi: 10.1016/j.ijms.2013.02.004).

1.13 Conference papers (peer-reviewed)

Blatherwick, E.Q., Frenguelli, B.G. and Scrivens, J.H. Localisation of adenine nucleotides in mouse brain using ion mobility enabled MALDI imaging. *Proc.1st OurCon, Ourense Conference on Imaging Mass Spectrometry, 2012, Ourense, Spain.*

Blatherwick, E.Q., Frenguelli, B.G. and Scrivens, J.H. Localisation of adenine nucleotides in mouse brain using ion mobility enabled MALDI imaging. *Proc. 60th ASMS Conference on Mass Spectrometry and Allied Topics, 2012, Vancouver, BC, Canada.*

Blatherwick, E.Q., Pickup, K.J., Sarda, S., Schulz-Utermoehl, T., Wilson, I.D., Weston, D.J. and Scrivens, J.H. Imaging mass spectrometry based approaches to the localisation of drugs and drug metabolites in animal tissue. *Proc. 59th ASMS Conference on Mass Spectrometry and Allied Topics, 2011, Denver, CO, USA.*

Blatherwick, E.Q., Day, J.M., Johansson, M.K., Weston, D.J. and Scrivens, J.H. Mass Spectrometry-Based Imaging Approaches to Spatial Localisation of Drugs in Tissue. *Proc. 31st Annual Meeting of the British Mass Spectrometry Society, 2010, Cardiff, UK.*

Ray. A., **Blatherwick, E.Q.,** Snelling, J.R., Weston, D.J. and Scrivens J.H. Investigating liquid extraction surface analysis (LESA) for the analysis of pharmaceutical tablets. *Proc. 31st Annual Meeting of the British Mass Spectrometry Society, 2010, Cardiff, UK.*

1.14 Invited oral presentations

Blatherwick, E.Q., Johansson, M.K., Pickup, K., Weston, D.J. and Scrivens, J.H. Improved identification of drug compounds in tissue using a combination of LESA and ion mobility separation. *Advion Biosciences User's Meeting at the 60th American Society of Mass Spectrometry Conference on Mass Spectrometry and Allied Topics, May 2012, Vancouver, BC, Canada.*

Chapter 2 Materials and Methods

2.1 Overview

The work presented in this thesis focused on two different applications of imaging mass spectrometry approaches. The first evaluated the potential applicability of MALDI imaging and LESA profiling experiments for drug localisation in dosed tissue sections. These experiments were compared with the industry-standard methods; QWBA and tissue homogenisation followed by LC-MS/MS. This work has been completed as part of the MRC funded CASE award in collaboration with AstraZeneca, Alderley Park, Cheshire, UK. Results are presented in Chapters 3 and 4.

A biological application of MALDI imaging has also been investigated. The use of mobility enabled MALDI imaging experiments for the localisation of adenine nucleotides in tissue sections was carried out, with the aim to detect differences between control and metabolically stressed brain tissue. Results of this work are presented in Chapter 5.

All imaging mass spectrometry experiments have been conducted on a Synapt G2 HDMS travelling wave ion mobility (TWIM) quadrupole time-of-flight (Q-TOF) mass spectrometer (Waters Corporation, Manchester, UK) operated with either a MALDI interface, ESI source or ESI source coupled with a LESA-enabled TriVersa Advion NanoMate system (Advion BioSciences, Inc. Ithaca, NY, USA).

2.2 Drug detection studies (Chapter 3)

Two different imaging mass spectrometry approaches have been used for the detection of different drug compounds in dosed tissue sections. Optimisation experiments were performed for each approach, using drug standards on or off tissue. These experiments were performed in order to determine the most selective method of detection of each compound. These selective methods were then used to detect drug compounds in dosed tissue sections.

All MALDI matrices and diclofenac sodium salt standard were obtained from Sigma-Aldrich. Fenclozic acid standard (purity > 98 %) and [^{14}C]-fenclozic acid (8.77 mBq/mg; radiochemical purity 99 %) were synthesised by AstraZeneca R&D, Alderley Park (Cheshire, UK). [^{14}C]-diclofenac dosed whole body tissue sections

and dosed organs were obtained from AstraZeneca R&D, Alderley Park (Cheshire, UK). [^{14}C]-fenclozic acid dosed tissue sections were obtained from AstraZeneca R&D, Södertälje (Södertälje, Sweden). All solvents were purchased from J.T.Baker at the highest purity grade available and used without further purification.

2.2.1 *In vivo* animal dosing

The detection of two drug compounds (fenclozic acid and diclofenac) by means of imaging mass spectrometry experiments has been assessed. All *in vivo* dosing procedures and preparation of whole-body tissue sections for LESA-MS analysis were undertaken by industrial collaborators at AstraZeneca. Dosing protocols have been outlined with reference to the origin of these samples. QWBA data has been acquired by collaborators, from a previous study at AstraZeneca, Alderley Park. These data have been used here, with permission, to enable a comparison with imaging MS approaches.

Fenclozic Acid: Fenclozic acid was administered orally at 10 mg/kg (10MBq/kg) in 0.1 M phosphate buffer (pH 7.4) to Wistar Hannover Galas rats supplied by Taconic M&S, Denmark, which were sacrificed 24 hours post-dose. Liver tissue was prepared at 30 µm for LESA-MS analysis and 12 µm for MALDI experiments using a Microm microtome (Cellab, Sweden). Control animals (dose vehicle only) were treated likewise to provide control tissue sections.

Diclofenac: [^{14}C]-diclofenac was dosed at 10mg/kg to wild type (WT) mice (strain C57BL/6J) and HRN (hepatic P450 Null Reductase) mice (strain B6.Cg-*Portm1Wolf*Tg(Alb-cre)21Mgn N7) aged between 7 and 10 weeks and weighing between 15 and 30 g. Wild-type mice were supplied by the Rodent Breeding Unit, Alderley Park and HRN mice were supplied by Taconic USA. Mice were sacrificed at 3 and 24 hours post-dose**.**

2.2.2 Tissue handling

To obtain organs, animals were subjected to necropsy for tissue harvesting after sacrifice. The tissues were snap-frozen in either dry-ice and ethanol or liquid nitrogen and stored at -80 ºC. For whole-body sections, whole animals were

embedded in a carboxymethylcellulose (CMC) solid scaffold support, frozen at -70 ºC. Whole-body sections were prepared at 30-40 µm for LESA analysis using a CM3600 Cryostat (Leica Microsystems). CMC tissue blocks were maintained at -20 ºC during sectioning. Sections were mounted onto double sided tape, dehydrated and stored at room temperature prior to analysis.

Unless otherwise stated, all frozen tissue sections were thaw-mounted onto glass slides for MALDI mass spectrometry analysis. Sectioned tissue was frozen and stored at -80 ºC prior to analysis. Tissue sections were slowly allowed to thaw to room temperature under vacuum, in order to prevent the formation of condensation prior to matrix application.

2.2.3 Mass spectrometry analysis

All experiments have been conducted using a Synapt G2 HDMS travelling wave ion mobility (TWIM) quadrupole time-of-flight (Q-TOF) mass spectrometer (Waters). The details of specific experimental conditions used for each drug compound using MALDI and LESA have been summarised in Table 2.1.

In all experiments the Synapt G2 was operated in either positive or negative ion sensitivity (V) mode. The TOF mass analyser was operated at a resolution of approximately 10000 (FWHM), with spectra acquired at an acquisition rate of one spectrum every second. For MALDI-MS/MS experiments spectra were acquired at a rate of one spectrum every two seconds.

For IMS experiments the instrument was operated in mobility-TOF mode, with a wave height of 40 eV. The travelling wave voltage was optimised using standards of each compound. Nitrogen was used as the gas in the ion mobility cell.

For all MS/MS experiments, argon was used as the collision gas and the collision energy used for MS/MS experiments was optimised for each compound. For MS/MS mobility experiments the CID was carried out in the trap cell of the mass spectrometer (prior to mobility separation) or in the transfer cell (after mobility separation).

				LESA experiments		MALDI experiments	
Drug Compound	**Ionisation Mode**	**Mass Range (*m/z*)**	**Travelling wave IMS voltage (m/s)**	**Extraction Solvent**	**Collision Energy (eV)**	**Matrix Compound**	**Collision Energy (eV)**
Fenclozic Acid	Positive	50-300	800	50 % ACN + 0.1 % formic acid	23	CHCA	20
Diclofenac	Negative	100-600	600	80 % ACN	25	CHCA	25/33[1]

Table 2.1 Experimental conditions for LESA and MALDI analysis of fenclozic acid and diclofenac.

[1] Dependent on the MS/MS transition followed

2.2.3.1 ESI-MS analysis of standards

Standard solutions of each drug compound were prepared at 0.5-1.0 $mgmL^{-1}$ in distilled water, diluted 1:1 in 50% ACN and analysed using ESI-MS with and without mobility separation. A capillary voltage of 1.0-1.2 kV was applied. The TOF mass analyser was calibrated using sodium formate solution in 90% propan-2-ol. In mobility-TOF mode instrument acquisition parameters were adjusted to provide an optimal ion mobility separation. These conditions were used for all subsequent LESA experiments.

Diclofenac sodium standard was prepared at 1 $mgmL^{-1}$ in distilled water, with a range of concentrations between 1 $\mu g\mu L^{-1}$ and 10 $pg\mu L^{-1}$ produced by serial dilution. 1 µL of each diclofenac concentration was spotted onto glass slides or control tissue sections as two 0.5 µL droplets for limit of detection experiments.

2.2.3.2 LESA profiling

The LESA enabled TriVersa NanoMate device was operated using Chipsoft (v8.3.1) and sampling positions were selected using LESA Points (v1.1) software. A nano-ESI voltage of 1.55-1.65 kV and a gas pressure of 0.45-0.50 psi were applied in all experiments. The extraction solvent was optimised for each drug compound as indicated in Table 2.1. 1 µL droplet of extraction solvent was used on-tissue and the liquid microjunction was sustained on the tissue surface for 5 seconds before aspiration back into the tip. For diclofenac-dosed samples, a 1 second delay was introduced prior to infusion into the mass spectrometer.

Infusion was performed through a nanofabricated sample introduction chip with 400 spray-nozzles (each 5.5 µm ID x 28 µm OD x 75 µm long). On tissue spot size was approximately 2 mm in diameter, sample positions were manually selected at appropriate distances to avoid spot overlap.

The time-of-flight (TOF) mass analyser was calibrated using sodium formate solution in 90 % propan-2-ol. After acquisition, data evaluation was performed using Driftscope and MassLynx (v4.1).

2.2.3.3 MALDI-MS analysis of standards

Standard solutions of each drug compound were prepared at 0.5 – 1.0 $mgmL^{-1}$ in distilled water for optimisation experiments. Solutions for matrix optimisation experiments were prepared as follows:

CHCA matrix: 3.6 $mgmL^{-1}$ in 50 % ACN + 0.05% TFA (v/v)

DHB matrix: 10 $mgmL^{-1}$ in 50% ACN + 0.05% TFA (v/v)

For positive ion experiments the TOF mass analyser was calibrated using sodiated PEG solution mixed 1:1 (v/v) with 3.6 $mgmL^{-1}$ CHCA matrix in 50 % acetonitrile with 0.05 % trifluoroacetic acid (v/v). For negative ion experiments the TOF mass analyser was calibrated using 40 $mgmL^{-1}$ caesium triiodide mixed 1:2 (v/v) with 25 $mgmL^{-1}$ DCTB (*trans*-2-[3-(4-*tert*-Butylphenyl)-2-methyl-2-propenylidene] malononitrile) matrix.

Fenclozic Acid: 0.5 µL of a 0.5 $mgmL^{-1}$ fenclozic acid solution was co-spotted onto a glass slide with 0.5 µL of CHCA matrix solution prepared at 3.6 $mgmL^{-1}$ in 50:50 (v/v) acetonitrile: water with 0.05 % trifluoroacetic acid.

Diclofenac: Diclofenac sodium standard was prepared at 1 $mgmL^{-1}$ in distilled water, and a range of concentrations between 1 $\mu g\mu L^{-1}$ and 10 $pg\mu L^{-1}$ produced by serial dilution. For MALDI optimisation experiments 1 µL of each diclofenac concentration was spotted onto a stainless steel MALDI target, followed by 1 µL of each matrix solution. 1 µL of each diclofenac concentration was spotted onto control tissue sections as two 0.5 µL droplets followed by 1 µL of matrix, applied as two 0.5 µL droplets, for MALDI profiling experiments.

2.2.3.4 MALDI imaging

For profiling and imaging experiments CHCA matrix was prepared at 15 $mgmL^{-1}$ in 50 % ACN with 0.05% TFA (v/v).

Profiling experiments: 0.5 µL of matrix solution was spotted manually onto control or dosed tissue sections. Matrix spots were analysed by MALDI-MS with a spatial resolution of 75 µm and 1 second scan time.

Imaging experiments: 15 cycles of 5 passes of 15 $mgmL^{-1}$ CHCA matrix were applied to mounted tissue sections using an airbrush (Iwata). Time was allowed between each cycle of application to allow the matrix to dry, to prevent overwetting of the tissue sample. Glass slides with mounted tissue sections were imaged optically using a scanner (Epson Perfection V30) before and after matrix application.

The area to be imaged was selected using MALDI Imaging Pattern Creator for profiling and imaging experiments. The instrument was operated as previously described using a spatial resolution of 150 μm between sampling positions (pixel). Each position was sampled for 2 seconds at a laser repetition rate of 200 Hz. After acquisition, data evaluation was performed using Driftscope and MassLynx (v4.1). For mobility imaging experiments, the ion of interest was selected in Driftscope by *m/z* and drift time and extracted to MassLynx. Data were then converted into Analyze file format using MALDI Imaging Converter for image analysis using BioMap (Novartis, Basel). Ion intensity maps were produced for the ion of interest, with the lowest 5 % intensity ions removed. Coregistration of optical tissue image and ion intensity maps was achieved using BioMap for clarity.

2.3 Drug and metabolite localisation studies (Chapter 4)

Two drug compounds have been dosed to rats for separate metabolism studies comparing traditional metabolite identification protocols at AstraZeneca with LESA profiling and MALDI imaging. Tissue homogenisation and metabolite identification experiments were completed during placement at AstraZeneca, Alderley Park during March-April 2012. QWBA studies have been completed alongside this work on the same compounds and resultant whole body sections.

[^{14}C]-fenclozic acid and [^{14}C]-propranolol were synthesised by AstraZeneca R&D, Alderley Park, Cheshire, UK. Propranolol standard was purchased from SigmaAldrich. Fenclozic acid standard (purity > 98 %) and [^{14}C]-fenclozic acid (8.77 mBq/mg; radiochemical purity 99 %) were synthesised by AstraZeneca R&D, Alderley Park (Cheshire, UK).

2.3.1 *In vivo* animal dosing and tissue handling

[^{14}C]-propranolol and [^{14}C]-fenclozic acid were dosed orally at 25 mg/kg to male Wistar Hannover rats weighing 180-220 grams, supplied by the Rodent Breeding Unit, Alderley Park. Rats were sacrificed at 2, 6 and 24 hours post-dose by anaesthetic inhalation (halothane). Two rats were prepared for each time point: one for QWBA and preparation of whole-body tissue sections, the other for tissue harvesting, homogenisation and metabolite identification experiments.

Carcasses were frozen in a mixture of solid CO_2 and hexane immediately after sacrifice. Liver, kidneys, lung and brain were harvested, frozen and kept at approx -20 until analysed. Whole animals were embedded in a CMC solid scaffold support and frozen at -80 ºC, prior to sectioning at 30 µm for LESA profiling experiments and 12 µm for MALDI imaging experiments. CMC tissue blocks were maintained at -20 ºC during sectioning. Sections were mounted onto double sided tape, dehydrated and stored at room temperature prior to analysis. Table 2.2 summarises the samples collected for these experiments.

<table>
<tr><td></td><td></td><td colspan="6">Samples</td></tr>
<tr><td>Drug Compound</td><td>Time Point</td><td>Liver</td><td>Kidney</td><td>Lung</td><td>Brain</td><td>Blood</td><td>Whole Body</td></tr>
<tr><td rowspan="3">Propranolol & Fenclozic Acid</td><td>2 hr</td><td colspan="5" rowspan="3">Tissue homogenisation, extraction and metabolite identification experiments.</td><td rowspan="3">QWBA, MALDI and LESA analysis</td></tr>
<tr><td>6 hr</td></tr>
<tr><td>24 hr</td></tr>
</table>

Table 2.2 Tissue samples and experiments for metabolism study.

2.3.2 Sample preparation

Tissues from each time point for each dosed animal were homogenised 1:1 (w/w) with distilled water. 0.1 mg aliquots of homogenate were prepared in paper cones for oxidisation to determine radioactivity levels in each tissue sample. Oxidiser efficiency was checked using [^{14}C]-glucose standard before and after analysis of homogenates. Once oxidised, levels of [^{14}C] in each homogenate were determined using a liquid scintillation counter.

Three extraction solvents were tested for the extraction of drug related compound from each tissue homogenate for both fenclozic acid and propranolol. These solvents were ACN, MeOH and tetrahydrofuran (THF), and were tested using homogenates with the highest level of radioactivity as determined by oxidisation experiments. The extraction efficiency of each was calculated for both drug compounds. The optimal extraction solvent for both drug compounds was MeOH.

Methanol was added in three-fold excess to each homogenate sample and centrifuged at 3000 rpm for 10 minutes. The supernatant was removed and stored at 4 ^{o}C and the extraction process repeated twice more. The radioactivity of each extract was counted using liquid scintillation and percentage efficiency calculated. Only samples obtained from the first extraction step were used for metabolite identification experiments.

2.3.3 Metabolite characterisation

Metabolite characterisation experiments were carried out on selected tissue homogenate samples using ultra-performance liquid chromatography (UPLC) with accurate mass LC-MS detection. UPLC eleuent was split post-column for LC-MS detection and sample collection for offline TopCount radioactivity detection. Tissue homogenate samples (20 µL) were injected onto a UPLC column (Waters BEH C18 2.1 mm x 100 mm, 1.7 µm) and chromatographed using a reversed-phase gradient (0.5 mL/min) of aqueous ammonium acetate with 0.1 % (v/v) formic acid (5 mmol/L, J.T. Baker, mobile phase A) and methanol and ammonium acetate with 0.1 % (v/v) formic acid (5 mmol/L, J.T. Baker, mobile phase B). Gradient parameters; time 0 mins (5% B), 1 min (5% B), 12 min (45% B), 12.5 min (99% B), 13 min (5% B), 15 min (5% B).

Mass spectrometric detection was carried out using positive ion electrospray with FTMS detection routines (ThermoFisher Scientific Orbitrap Discovery), carried out using automatic gain control (AGC) and preset ion targets to preserve ion statistics and accurate *m/z* measurement. Tandem mass spectrometry was performed in the ion trap part of the instrument, with alternating tube lens voltage (30 V or 80 V) to provide fragmentation data. The ion trap was set at unit resolution and controlled by AGC to prevent space charging effects.

TopCount data was acquired using a modified CTC autosampler (2.1 s/well) collecting into 96 well LumaPlates, detecting [^{14}C] at 10 min/well (offline) radioactivity counting time using a TopCount NXT HTS (Perkin Elmer Life Sciences, USA).

Reconstructed [^{14}C]-radiochromatograms were produced by importing ASCII format TopCount data into Laura software (v.4.12, LabLogic, Sheffield, UK) or Excel (Microsoft).

2.3.4 Mass spectrometry analysis

All Warwick based experiments were conducted using a Synapt G2 HDMS travelling wave ion mobility (TWIM) quadrupole time-of-flight (Q-TOF) mass spectrometer (Waters) operated with either a MALDI interface or ESI interface coupled with a LESA-enabled TriVersa NanoMate. Details of specific experimental conditions used are summarised in the following sections.

For all experiments the Synapt G2 was operated in positive ion sensitivity (V) mode with data acquired between *m/z* 100-600. The TOF mass analyser was operated at a resolution of approximately 10000 (FWHM), with spectra acquired at an acquisition rate of one spectrum every second unless otherwise stated. For IMS experiments the instrument was operated in mobility-TOF mode, with a wave height of 40 eV. The travelling wave voltage was optimised using standards for each compound of interest. Nitrogen was used as the gas in the ion mobility cell.

For all MS/MS experiments, argon was used as the collision gas and the collision energy used for MS/MS experiments was optimised for each compound. For MS/MS mobility experiments the CID experiments were performed in the trap cell of the mass spectrometer (prior to mobility separation) or in the transfer cell (after mobility separation).

2.3.5 ESI-MS analysis of standards

Propranolol standard was prepared at 0.5 $mgmL^{-1}$ in distilled water for LESA and MALDI optimisation experiments. A serial dilution of propranolol was prepared in distilled water to give a concentration range between 0.5 $\mu g\mu L^{-1}$ and 500 $fg\mu L^{-1}$.

Fenclozic acid standard was diluted to 0.5 $mgmL^{-1}$ in 50 % ACN for both LESA and MALDI optimisation experiments. A serial dilution of fenclozic acid was prepared in distilled water to give a final concentration range between 0.5 $\mu g\mu L^{-1}$ and 500 $fg\mu L^{-1}$.

Standard solutions of each drug compound were prepared at 25 $ng\mu L^{-1}$ in 50 % ACN with 0.1 % HCOOH and analysed by ESI-MS with and without mobility separation. Data were acquired using a Synapt G2 HDMS mass spectrometer operated in ESI positive ion mode with and without mobility separation. A capillary voltage of 1.2

kV was applied. The TOF mass analyser was calibrated using sodium formate solution in 90% propan-2-ol. In mobility-TOF mode instrument acquisition parameters were varied to provide an optimal ion mobility separation. Optimal separation was achieved with a wave velocity of 800 m/s and a wave height of 40.0 V for both propranolol and fenclozic acid and was used in all subsequent LESA experiments.

Fragmentation of fenclozic acid was carried out using a collision energy of 20.0 eV, whilst fragmentation of propranolol required a collision energy of 28.0 eV. For MS/MS mobility experiments the CID was carried out in the trap cell of the mass spectrometer (prior to mobility separation) and these conditions were used for all LESA profiling experiments.

2.3.6 LESA profiling

For limit of detection experiments, 0.5 µL of each drug compound concentration was spiked onto glass slides and control rat kidney tissue sections to give a final amount of drug ranging from 0.25 µg to 250 fg.

The LESA enabled TriVersa NanoMate device was operated using Chipsoft (v8.3.1) and sampling positions were selected using LESA Points (v1.1) software. A nano-ESI voltage of 1.55-1.65 kV and a gas pressure of 0.45-0.50 psi were applied in all experiments. 50 % ACN with 0.1 % HCOOH (v/v) was used as the extraction solvent in all experiments. 1 µL droplet of extraction solvent was used on-tissue and the liquid microjunction was sustained on the tissue surface for 5 second before aspiration back into the tip.

Infusion was performed through a nanofabricated sample introduction chip with 400 spray-nozzles (each 5.5 µm ID x 28 µm OD x 75 µm long). On tissue spot size was around 2 mm in diameter, and sample positions were manually selected at appropriate distances to avoid spot overlap.

Data were acquired for a minimum of 2 minutes per sample, in MS/MS mobility mode from 100-600 *m/z*, with mobility separation after MS/MS fragmentation for all

experiments. After acquisition, data evaluation was performed using Driftscope and MassLynx (v4.1).

2.3.7 MALDI-MS analysis of standards

Propranolol at 0.5 $mgmL^{-1}$ was diluted ten-fold and prepared 1:1 (v/v) with matrix solution. 1 µL of propranolol and matrix mix was spotted onto stainless steel target plates for MALDI analysis. CHCA (3.6 $mgmL^{-1}$ in 50 % ACN + 0.05 % TFA (v/v)) and DHB (10 $mgmL^{-1}$ in 50 % ACN + 0.05 % TFA (v/v)) were tested as matrix compounds across the propranolol concentration range. Matrix solution and propranolol standard were mixed 1:1 (v/v) to give a final concentration range between 0.25 $\mu g\mu L^{-1}$ and 250 $fg\mu L^{-1}$.

Fenclozic acid was diluted to 0.5 $mgmL^{-1}$ in 50 % ACN; diluted ten-fold in distilled water and prepared 1:1 (v/v) with matrix solution. 1µL of fenclozic acid and matrix mix was spotted onto stainless steel target plates for MALDI analysis. CHCA (3.6 $mgmL^{-1}$ in 50 % ACN + 0.05 % TFA (v/v)) was used as the matrix compound for fenclozic acid. Matrix solution and fenclozic acid standard were mixed 1:1 (v/v) to give a final concentration range between 0.25 $\mu g\mu L^{-1}$ and 250 $fg\mu L^{-1}$.

1 µL of each drug standard concentration were spotted onto control tissue sections (rat kidney) as 2 x 0.5 µL droplets. 1 µL of matrix solution was applied as 2 x 0.5 µL droplets to the same positions to determine limits of detection on tissue and establish the most selective method for successful detection of each drug.

Data were acquired using a Synapt G2 HDMS mass spectrometer operated in MALDI positive ion mode from 100-600 *m/z* with and without mobility separation. The TOF mass analyser was calibrated using phosphorus red (10 $mgmL^{-1}$) prepared in acetone. In mobility-TOF mode instrument acquisition parameters were adjusted to provide an optimal ion mobility separation. Optimal separation was achieved using a wave velocity of 800 m/s and a wave height of 40.0 V for propranolol and fenclozic acid. These conditions were used for all subsequent MALDI experiments.

MS/MS fragmentation was optimised using drug standards, with and without mobility separation. A collision energy of 30.0 V was applied in the transfer region

of the mass spectrometer after mobility separation, with 27.0 V applied in the trap region for MS/MS experiments without mobility separation for propranolol. Fragmentation of fenclozic acid was achieved using a collision energy of 20.0 V applied in the trap region of the mass spectrometer for MS/MS experiments with and without mobility separation.

Ion mobility separation following MS/MS fragmentation was determined to be the most selective approach for the identification and localisation of fenclozic acid and propranolol over a range of concentrations on tissue. Fenclozic acid was successfully detected at 250 fg spiked on tissue, whilst propranolol was successfully detected at 2.5 ng spiked on tissue. This method was used for all subsequent profiling and imaging experiments on dosed tissue.

2.3.8 MALDI profiling

CHCA matrix solution at 15 $mgmL^{-1}$ in 50 % ACN with 0.05 % TFA was spotted onto 30 µm thick freeze-dried, dosed whole-body tissue sections as two 0.5 µL droplets. Once dry, these spots were analysed using MALDI-mobility-MS/MS between *m/z* 100-600, with fragmentation performed in the trap region prior to ion mobility separation for either fenclozic acid or propranolol. A spatial resolution of 75 µm and a scan time of 2 seconds was used to image the matrix spots on tissue.

Acquired data have been processed and analysed using HDImaging™ (v1.0) software. This was achieved by extracting the ten most abundant ions, of intensity greater than 1000 counts, within the drift time window for the fragment ion characteristic of the drug of interest (Fenclozic acid: *m/z* 208, arrival time scan 61-65, Propranolol: *m/z* 183, arrival time scan 57-61). The experimental type was defined as IMS-MS/MS. MALDI profiling images were produced by the selection of detected MS/MS fragment ions based on their *m/z* and mobility drift time. The intensity of these ions was then displayed across the tissue to create an image.

2.3.9 MALDI imaging

Organs of interest were excised from the 12 µm fenclozic acid dosed whole-body tissue section and mounted to a standard microscope glass slide using double-sided

sticky tape. 10 mL of CHCA matrix solution at 15 $mgmL^{-1}$ in 50 % ACN with 0.05 % TFA was applied to mounted tissue sections using an airbrush for MALDI imaging experiments.

An optical image of the slide and tissue section was obtained using a flatbed scanner (Epson Perfection V30). The tissue region to be imaged was then selected using the Pattern Creator function of the HDImaging™ software package (Waters, Manchester, UK) using a spatial resolution of 75 µm. Data were acquired using a Synapt G2 HDMS mass spectrometer operated in MALDI HDMS/MS positive ion mode from 100-600 *m/z* with mobility separation following MS/MS fragmentation and a scan time of 2 seconds.

Acquired data were processed and analysed using HDImaging™ (v1.0) software. Data were processed by extracting the ten most abundant ions, of intensity greater than 1000 counts, within the drift time window for the fragment ion characteristic of the drug of interest (Fenclozic acid: *m/z* 208, arrival time scan 61-65). The experimental type was defined as IMS-MS/MS. Ion intensity MALDI images were produced using the same software, with the selection of detected MS/MS fragment ions based on their *m/z* and mobility drift time. The intensity of these selected ions was then displayed across the tissue.

2.4 Localisation of adenine nucleotides (Chapter 5)

MALDI imaging mass spectrometry has been used for the localisation of the adenine nucleotides ATP, ADP and AMP in mouse brain. Experimental methods have been optimised in order to determine the most selective method for identification and localisation of the adenine nucleotides in tissue. Different methods for tissue fixation have been evaluated in order to prevent rapid changes in the levels of adenine nucleotides post-mortem. These methods have then been applied to control and stressed tissue sections in order to identify changes in localisation of adenine nucleotides that occur during periods of metabolic stress.

9-aminoacridine hydrochloride (9-AA), adenosine-5-triphosphate (ATP) disodium salt hydrate, adenosine-5-diphosphate (ADP) sodium salt and adenosine-5-monophosphate (AMP) disodium salt standards were purchased from Sigma-Aldrich. Ethanol was purchased from Fisher Scientific at the highest purity grade available and used without further purification. Water was purchased from J.T. Baker at the highest purity grade available and used without further purification.

Harvesting of whole mouse brain samples for all experiments was performed by collaborators, either in-house at Warwick or Sweden. Tissue harvesting and preparation protocols are outlined with reference to the origin of these samples.

2.4.1 Analysis of standards

Standards of ATP, ADP and AMP were prepared at 1 $mgmL^{-1}$ in water. 9-AA was prepared at 10 $mgmL^{-1}$ in 70 % ethanol with 0.1 % TFA (v/v). Each adenine nucleotide solution was diluted 1:1 (v/v) with 9-AA matrix solution as described. 1 µL was spotted onto a stainless steel target plate and allowed to dry prior to MALDI-MS analysis.

Data were acquired using a Synapt G2 HDMS mass spectrometer operated in MALDI negative ion mode from 100-600 *m/z* with and without mobility separation. The TOF mass analyser was calibrated using phosphorus red (10 $mgmL^{-1}$) prepared in acetone. In mobility-TOF mode instrument acquisition parameters were adjusted to provide an optimal ion mobility separation. Optimal separation was achieved

using a wave velocity of 650 m/s and a wave height of 40.0 V. These conditions were used for all following MALDI experiments.

MS/MS fragmentation was optimised using adenine nucleotide standards, with and without mobility separation. Collision energies of 30.0 V, 30.0 V and 31.0 V were applied in the transfer region of the mass spectrometer after mobility separation for ATP, ADP and AMP respectively.

2.4.2 Tissue handling

Male wild-type mice aged 12-15 weeks were sacrificed by cervical dislocation in accordance with the Animals (Scientific Procedures) Act 1986 and with local ethical review guidelines. Brains were harvested within 1 minute and snap-frozen in liquid nitrogen (~10 minutes) before storage at -80 ˚C prior to sectioning and mass spectrometry analysis. For test stressed brain experiments, following dissection, the brains were left at room temperature for 10 minutes prior to snap-freezing. Frozen brain sections were prepared at 12 µm using an OFT 5000 Cryotome (Bright Instruments, Cambridge) and thaw-mounted onto glass slides for mass spectrometry analysis.

Frozen sections were washed sequentially for 1 minute in ice-cold 70 % and 95 % ethanol before being brought to room temperature in a vacuum dessicator. Untreated tissue sections were brought to room temperature in a vacuum dessicator without an ethanol wash step.

10 $mgmL^{-1}$ 9-aminoacridine hydrochloride (9-AA) matrix in 70 % ethanol with 0.1 % TFA was applied using an airbrush (Iwata) for all imaging experiments.

2.4.3 Heat-stabilised tissue

12-week old male CBA mice were sacrificed using deep isofluorane anesthesia and decapitation in accordance with protocols approved by the ethical committee for animal experiments in Sweden (Stockholms Norra Djurförsöksetiska Nämnd). Mice were obtained from an in-house breeding program at the Karolinska Institute,

Stockholm, Sweden. Brains were quickly dissected and prepared according to Table 2.3.

Sample	Abbreviation	Preparation
Snap-frozen	SF	Immediately snap frozen on dry ice.
Heat-stabilised	HS	Immediately heat-stabilised prior to snap-freezing on dry ice.
30 + snap-frozen	30+SF	Left at room temperature for 30 minutes following dissection, before snap-freezing.
30 + heat-stabilised	30+HS	Left at room temperature for 30 minutes prior to heat-stabilisation and snap-freezing.
Heat-stabilised + 30	HS+30	Immediately heat-stabilised following dissection, then left at room temperature for 30 minutes prior to snap-freezing.

Table 2.3 Mouse brain samples prepared for heat-stabilisation experiments.

Heat stabilisation was performed using the Stabilizor™ (Denator, Sweden) operated in the structural preserve fresh auto mode. Stablilisation was performed at 95 °C with minimal compression and cavity vacuum. Stabilisation time was optimised based on sample height.

Frozen brain sections were prepared at 14-20 µm using an OFT 5000 Cryotome (Bright Instruments, Cambridge) and thaw-mounted onto glass slides for mass spectrometry analysis. Heat-stabilised brain tissues proved to be more fragile during sectioning than non-treated tissue, and as such the sectioning procedure was altered slightly to produce thicker sections for analysis.

Frozen sections were washed sequentially for 1 minute in ice-cold 70 % and 95 % ethanol before being brought to room temperature in a vacuum dessicator. 10 $mgmL^{-1}$ 9-aminoacridine hydrochloride (9-AA) matrix in 70 % ethanol with 0.1 % TFA was applied using an airbrush (Iwata) for all imaging experiments.

2.4.4 Experimental method

All MALDI imaging experiments were conducted using a Synapt G2 HDMS travelling wave ion mobility (TWIM) quadrupole time-of-flight (Q-TOF) mass spectrometer (Waters Corporation, Manchester, UK) operated with a MALDI interface. Ion mobility separation prior to MS/MS fragmentation and mass spectrometry detection (IMMS) was used to confirm the identification of adenine nucleotides in control and stressed mouse brain sections, outlined in the schematic shown in Figure 2.1. This experimental method was determined to be the most selective approach for the identification and localisation of adenine nucleotides over a range of concentrations on tissue.

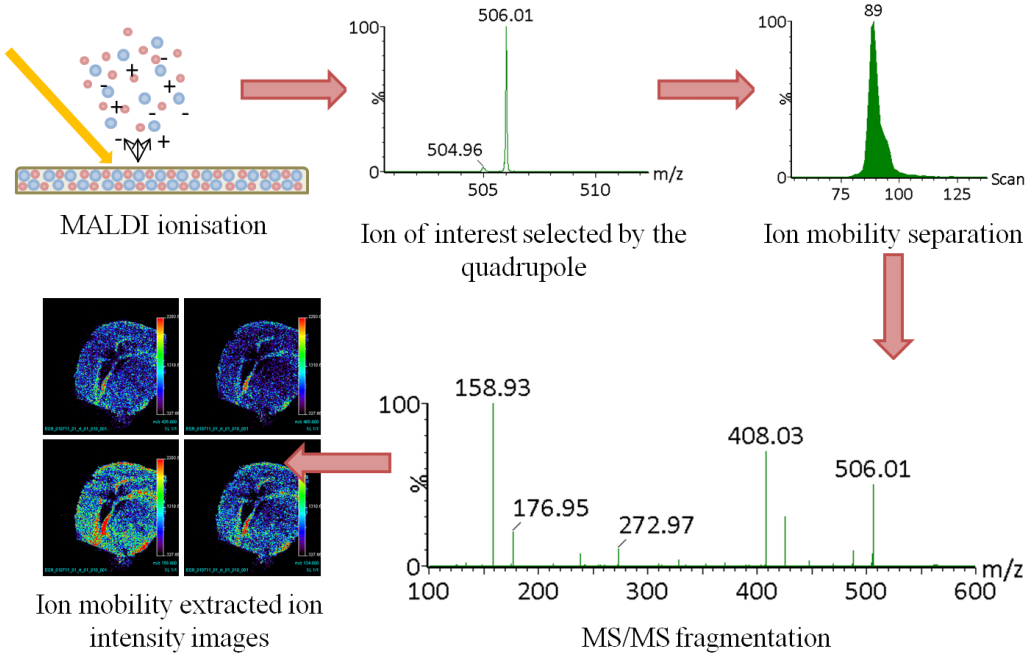

Figure 2.1 Schematic to show the workflow of a MALDI-mobility-MS/MS imaging experiment for the identification of adenine nucleotides in mouse brain tissue. These ions are then separated by ion mobility separation before fragmentation by CID. Mobility-resolved MS/MS spectra are recorded and used to produce ion intensity images.

An optical image of the slide and tissue section was obtained using a flatbed scanner (Epson Perfection V30). The tissue region to be imaged was then selected using the Pattern Creator function of the HDImaging™ software package (Waters, Manchester, UK) with a spatial resolution of 50 µm employed. Data were acquired using a Synapt

G2 HDMS mass spectrometer operated in MALDI HDMS/MS negative ion mode from 100-600 *m/z* with mobility separation carried out prior to MS/MS fragmentation.

Acquired data were processed and analysed using HDImaging™ (v 1.0) software. Data were processed in HDImaging™ by extracting the ten most abundant ions, of intensity greater than 1000 counts, within the drift scan window for the adenine nucleotide of interest (ATP: scans 85-95, ADP: scans 79-89 and AMP: scans 68-78). The experiment type was defined as IMS-MS/MS. Ion intensity MALDI images were produced using the same software, selecting detected MS/MS fragment ions based on their *m/z* and drift time and displaying their intensity across the tissue.

2.4.5 Tissue staining

Histological staining was performed on tissue sections following analysis by MALDI imaging. Matrix was washed off the slide and tissue sections by immersion in 70 % EtOH with 0.1 % TFA for approximately 1 minute with mild agitation. Hematoxylin and Eosin (H&E) solutions were purchased from Sigma Aldrich. The protocol followed for H&E staining is outlined below in Table 2.4:

Solution	Time (minutes)
Hematoxylin	3
Warm running tap water	0.5
95 % Ethanol	0.5
Eosin solution	1
95 % Ethanol	0.5
95 % Ethanol (fresh)	0.5

Table 2.4. Hematoxylin and Eosin staining prototcol for histological staining of tissue sections following MALDI imaging acquisition.

Following H&E staining the slides and tissue sections were allowed to dry at room temperature prior to obtaining optical images of the stained sections for reference. These images were obtained using a flatbed scanner (Epson Perfection V30) at 600 x resolution.

2.4.6 Data processing

To assess differences between control and stressed tissue sections it was important to measure the relative intensity ratio of ATP:ADP:AMP in tissue sections. Although MALDI imaging is not a quantitative technique, it can be used to provide an indicative relative intensity ratio of ions in a sample. For these experiments the relative ion intensity ratio of adenine nucleotides in tissue was determined as follows.

2.4.6.1 Relative ion intensity ratio of adenine nucleotides

Three regions identical in sampling area were selected on a single mouse brain section. Each section was analysed using MALDI-mobility-MS/MS imaging at a spatial resolution of 50 µm targeting ATP, ADP or AMP. This method was repeated across four brain sections, altering the region targeted for each compound to account for any small localisation differences across the surface of the brain.

The data acquired for each region were combined and mobility extracted MS/MS spectra produced for each compound in one brain section. The intensity of the two most intense product ions from these MS/MS spectra for each nucleotide were summed together giving a total intensity for each of ATP, ADP and AMP in one brain section. These intensities were divided by the total intensity of adenine nucleotides and used to create a percentage ratio of ATP:ADP:AMP in the brain section. These ratios were averaged across the four brain sections and a standard deviation calculated for each adenine nucleotide.

Chapter 3 Investigation of *in vivo* drug delivery and deposition using an imaging mass spectrometry approach

3.1 Imaging MS approaches to drug distribution in tissue

Information regarding the distribution of drug-related material in target tissue may provide important biological information during the drug development process. Industry-standard methods used to look at total localisation of drug-related material can have limitations due to their dependence on labels, either fluorescent tags or radioactivity (e.g. quantitative whole body autoradiography (QWBA)). These approaches may have difficulty in distinguishing between the drug of interest and its metabolites. Mass spectrometry imaging (MSI) is a technique that has the potential to distinguish spatially between the drug of interest and its metabolites. A number of mass spectrometry-based imaging experiments have been described for localisation of drug compounds and metabolites in tissue. These experiments have been shown to provide data complementary to existing imaging techniques.

In this work, two-mass spectrometry based imaging approaches have been evaluated for the identification and localisation of two drug compounds. The first section focused on the identification and localisation of fenclozic acid, with evaluation and comparison of two imaging MS experiments. This work has been published in the peer-reviewed journal Xenobiotica (Blatherwick, Van Berkel et al. 2011).

The second section investigated other applications. Optimisation experiments were performed in order to determine the most selective method for the localisation of diclofenac (a common non-steroidal anti-inflammatory drug). These methods were evaluated for their ability to localise diclofenac in dosed whole body tissue sections and harvested tissue, for comparison with existing QWBA data.

The ionisation techniques used in the imaging MS experiments were Matrix-Assisted Laser Desorption/Ionisation (MALDI) and liquid extraction surface analysis (LESA). This was employed using a chip-based robotic nanoelectrospray platform (TriVersa NanoMate, Advion).

3.1.1 Fenclozic Acid

Fenclozic acid is a low molecular weight acidic non-steroidal anti-inflammatory drug (NSAID) (ICI 54, 450: Myalex) (Hepworth, Newbould et al. 1969). The chemical structure of fenclozic acid is shown in Figure 3.1. This drug was withdrawn from the market following documented hepatotoxicity (Hart, Bain et al. 1970). It is important, therefore to gain a better understanding of its disposition in tissues and metabolic fate.

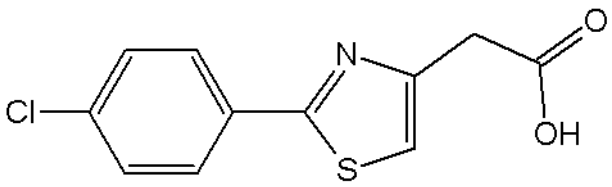

Figure 3.1 Chemical structure of fenclozic acid.

An original study into fenclozic acid metabolism showed five metabolites that were identified in rats and dogs. These metabolites included decarboxylated fenclozic acid and metabolites with oxidation and hydroxylation at the chlorine substituent (Foulkes 1970).

3.1.2 Diclofenac distribution in mice

Diclofenac is a common non-steroidal anti-inflammatory drug (NSAID), often used as a painkiller for arthritis. The chemical structure of diclofenac is shown in Figure 3.2 below.

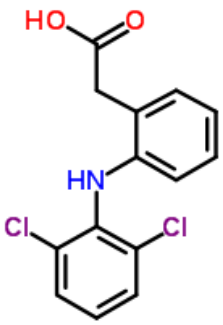

Figure 3.2 Chemical structure of diclofenac

Diclofenac has been shown to undergo hepatic metabolism in mice via both cytochrome P450 (CYP2C9) and uridine 5'-diphospho-glucuronosyltransferase (UGT) mediated pathways to produce potentially reactive intermediates shown in Figure 3.3. Other major metabolites of diclofenac have been shown to include 4'-hydroxydiclofenac and 5'-hydroxydiclofenac (Tang 2003).

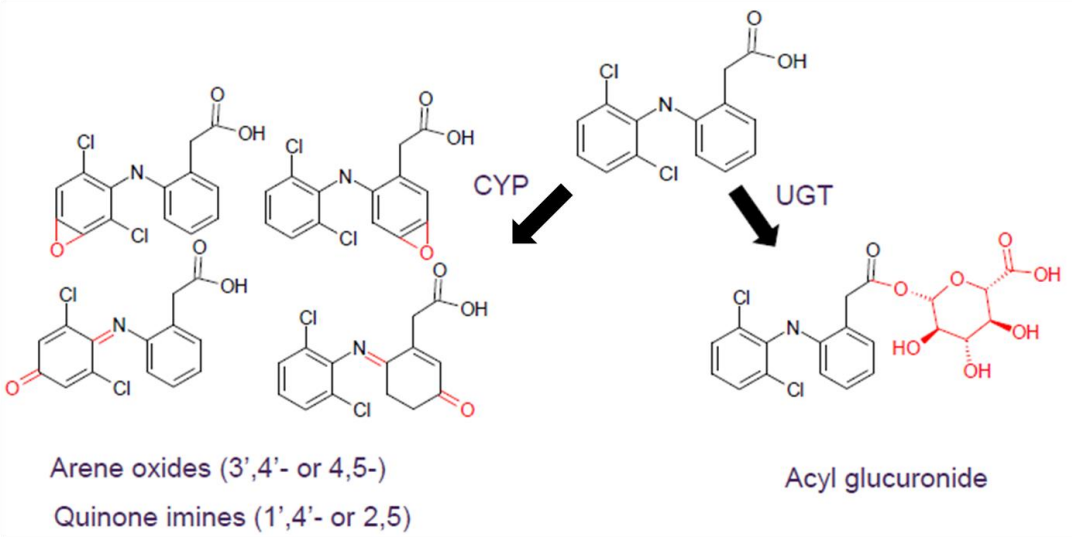

Figure 3.3 Metabolism of diclofenac by CYP and UGT mediated pathways, forming potentially reactive intermediates.

A study was completed by AstraZeneca UK in order to assess the differences in disposition and hepatic effects of ^{14}C-diclofenac in hepatic P450 null reductase (HRN) mice compared with wild-type mice. These mice do not have the cytochrome P450 enzyme in the liver. This prevents metabolism via the CYP-mediated pathway. The study used a combination of techniques: QWBA, for drug localisation and conventional metabolite identification from urine using LC-MS methods.

These metabolite identification results highlighted a lack of oxidative metabolites identified from the HRN mice. An increase in glucuronide and taurine conjugation of metabolites was also observed. This was expected based on known metabolism pathways.

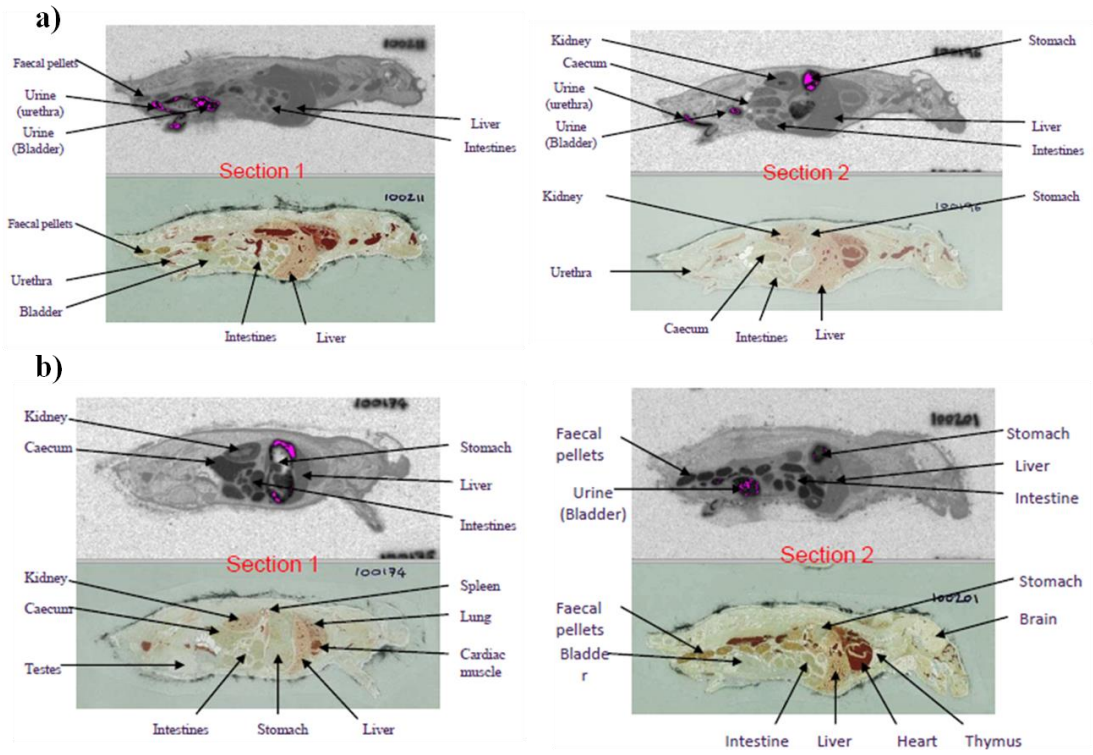

Figure 3.4 QWBA images of diclofenac distribution.
a) QWBA results showing radioactivity distribution in a 14C-diclofenac dosed wild-type mouse sacrificed 3 hours post-dose.
b) QWBA results showing radioactivity distribution in a 14C-diclofenac dosed hepatic P450 null reductase (HRN) mouse sacrificed 3 hours post-dose.
Darker regions represent higher levels of radioactivity. Pink areas represent over-exposure of the phosphor-imaging plate as a result of high concentrations of radioactivity. QWBA images reproduced with permission from AstraZeneca.

Significant differences in metabolism and rates of excretion were observed between the wild type and HRN strains. QWBA results showed widespread radioactivity distribution for wild type and HRN mice sacrificed 3 hours post-dose, these are shown in Figure 3.4 a) and b) respectively.

The QWBA results for the wild-type mouse in Figure 3.4 showed widespread radioactivity throughout the tissues, with a moderate presence in the liver and elevated presence in the caecum, kidneys, intestines and the stomach. The section shown on the right indicated high levels of radioactivity present in the urine and the faecal pellets. Noticeably the brain showed little presence of radioactivity.

QWBA results for HRN mice showed widespread radioactivity throughout the tissues, with a moderate presence observed in the liver, caecum, heart, lung, kidneys, intestines and faecal pellets. Over-exposure was observed in the urine and stomach.

The QWBA results showed differences in the distribution of radioactivity between wild type and HRN mice, but they could not determine whether this was due to the presence of parent drug, or metabolite compounds within the tissue. Mass spectrometry imaging approaches may help to distinguish between parent drug and metabolites in tissue, and answer important questions surrounding the observed differences in distribution between the two groups of mice.

Here, optimisation experiments have been performed both on and off tissue using two different imaging mass spectrometry approaches, to identify the most selective method for localisation of diclofenac. The optimised MALDI-MS and LESA-MS methods have been used for the detection and localisation of diclofenac in whole body tissue sections and kidney sections from dosed mice. Both techniques were coupled to a travelling wave ion mobility (TWIM) Q-TOF (Synapt G2, Waters) mass spectrometer.

3.2 Results and Discussion

For all materials and methods please refer to Chapter 3.

3.3 Evaluation of imaging MS approaches to drug localisation

The applicability of imaging MS approaches for the detection of drugs in tissue must be assessed before comparison with established drug localisation techniques. LESA and MALDI profiling methods have been evaluated for the detection of fenclozic acid in dosed tissue sections. Optimisation of these methods has been performed using standards of the drug target of interest.

3.3.1 Analysis of fenclozic acid standards

Fenclozic acid parent drug contains a single chlorine atom, which results in a characteristic isotope pattern (3:1) in the mass spectrum of the protonated parent drug ion at *m/z* 254 (Cl^{35}) and 256 (Cl^{37}) (shown in Figure 3.5). MS/MS fragment ions of the drug that retain the chlorine also display this characteristic isotope pattern, which enhances spectral selectivity.

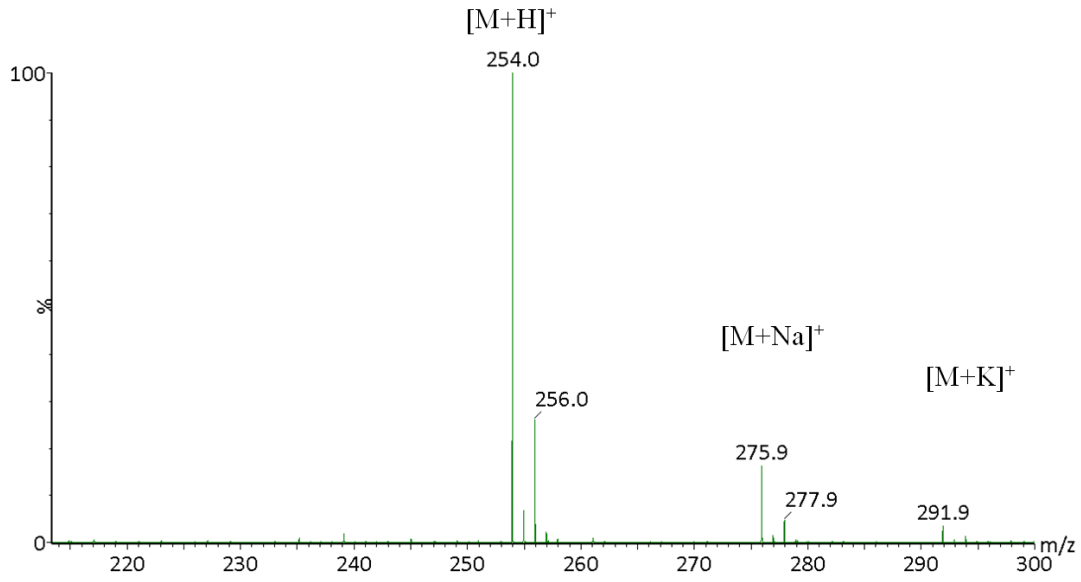

Figure 3.5 LESA-MS analysis of fenclozic acid standard on glass slide. Protonated fenclozic acid is shown, with the characteristic isotope pattern of chlorine containing compounds. Sodiated and potassiated forms of fenclozic acid are also detected.

3.3.2 LESA-MS/MS analysis on tissue

Dosed and control liver sections of 40 µm thickness were analysed using LESA-MS and LESA-MS/MS. The protonated parent ion at *m/z* 254 was selected for MS/MS fragmentation and the resulting MS/MS spectra (*m/z* 50-245 zoom) for fenclozic acid standard, dosed liver tissue and control liver tissue are displayed in Figure 3.6. The parent ion at *m/z* 254 was fully fragmented and not detected in the MS/MS spectra. Fenclozic acid could not be confidently identified from dosed tissue sections using LESA-MS alone since the intensity of the *m/z* 254 parent ion was very low. Quadrupole selection and MS/MS fragmentation of the *m/z* 254 ion was required in order to confidently detect fenclozic acid in tissue.

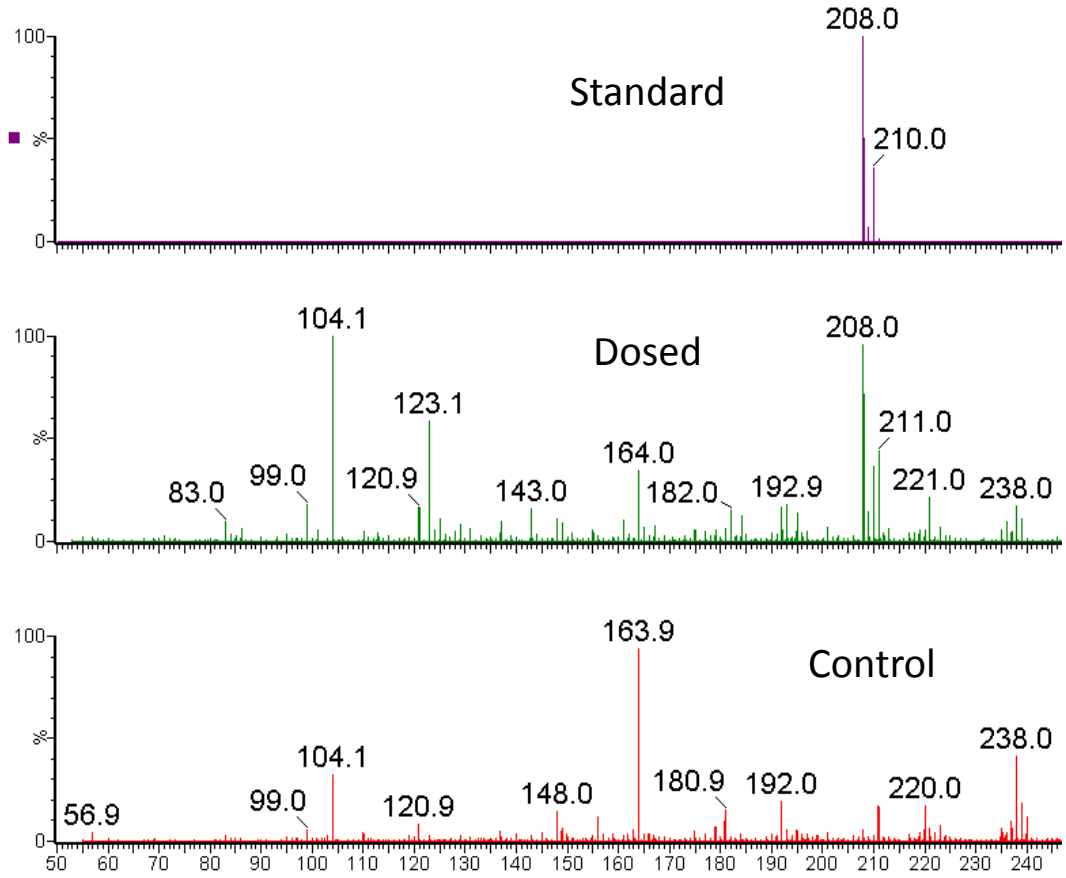

Figure 3.6 LESA-MS/MS analysis on tissue.
MS/MS spectra of (a) fenclozic acid standard, (b) fenclozic acid dosed tissue, and (c) control tissue.

The MS/MS spectrum of the ion at *m/z* 254 of the fenclozic acid standard showed a base peak fragment ion with a corresponding chlorine isotope peak at *m/z* 208 and 210, respectively. These fragment ions were also present in the MS/MS spectrum from dosed tissue sections, but absent in the MS/MS spectrum from control tissue. These results indicate that fenclozic acid could be detected in the dosed liver tissue using the LESA-MS/MS method.

3.3.3 LESA-mobility-MS/MS analysis on tissue

LESA-MS/MS was coupled with an ion mobility separation step prior to MS/MS fragmentation. This improves the selectivity of the experiment for the compound of interest. Figure 3.7 shows the extracted arrival time distribution (ATD) of the parent *m/z* 254 generated from fenclozic acid standard, dosed tissue and control tissue together with the resulting MS/MS spectra.

Comparison of the extracted ATDs of *m/z* 254 from fenclozic acid standard, dosed tissue and control tissue provided evidence that fenclozic acid had been detected in tissue. The same arrival time was observed for the drug standard and dosed tissue in the ATD. The arrival time of *m/z* 254 from control tissue was different, indicating different ion mobility. This indicates that the ion from control tissue may have arisen from an endogenous ion or chemical noise. The *m/z* 254 ion from dosed tissue was confidently identified as fenclozic acid, as it displayed the same ATD as that of the standard drug. The MS/MS spectrum also contained the characteristic *m/z* 208 and 210 fragment ions. Ion mobility separation provided cleaner mass spectra with increased experimental selectivity for the analyte of interest.

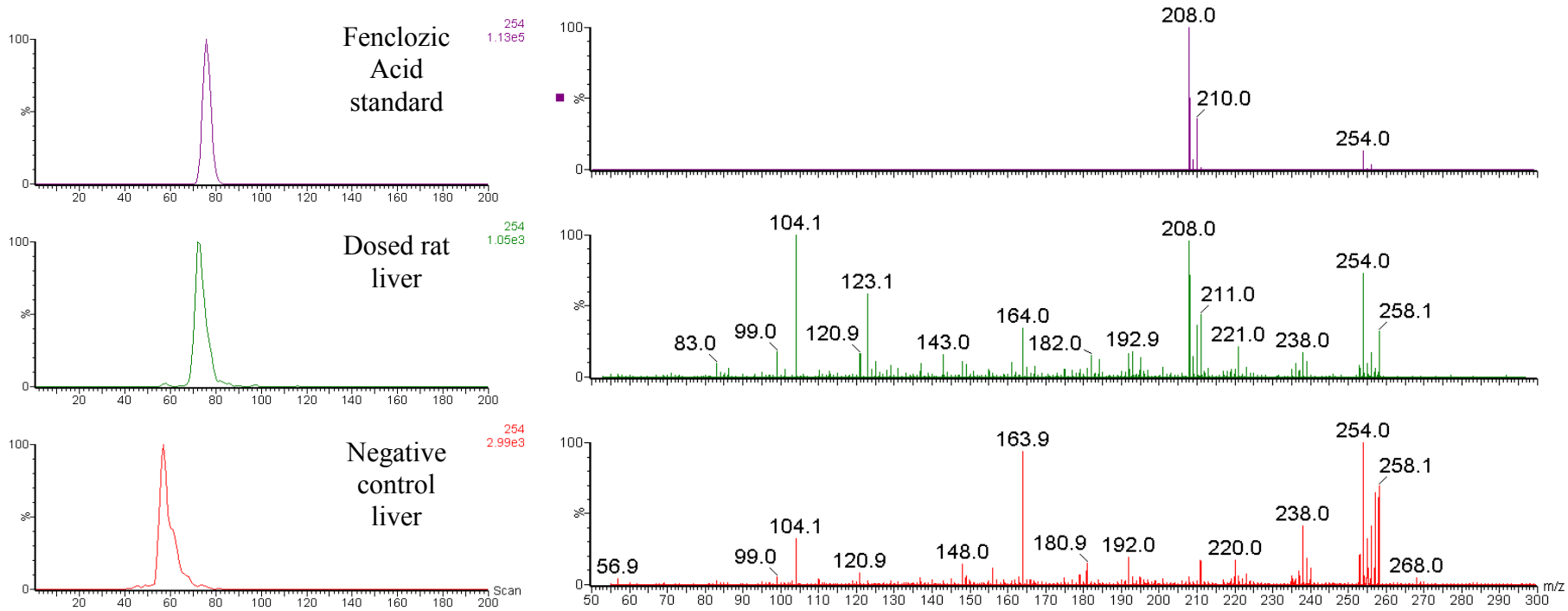

Figure 3.7 LESA-mobility-MS/MS analysis on tissue.
a) Arrival time distribution of 254 *m/z* ion. **b)** MS/MS of 254 *m/z* after mobility separation. Fenclozic acid standard is shown at the top (purple), dosed tissue in the middle (green) and control tissue at the bottom (red).

3.3.4 MALDI profiling

Dosed and control liver sections of 12 µm thickness were analysed using a MALDI-MS/MS profiling experiment. The protonated parent ion at *m/z* 254 was selected for fragmentation. MALDI-MS/MS spectra obtained are shown in Figure 3.8 for fenclozic acid drug standard, dosed tissue and control tissue respectively. MALDI-MS profiling alone was not able to confidently identify fenclozic acid from dosed tissue sections, similar to the results obtained from the LESA-MS experiment. The extra selectivity provided by the inclusion of an MS/MS fragmentation step was required in order to detect fenclozic acid in dosed tissue sections.

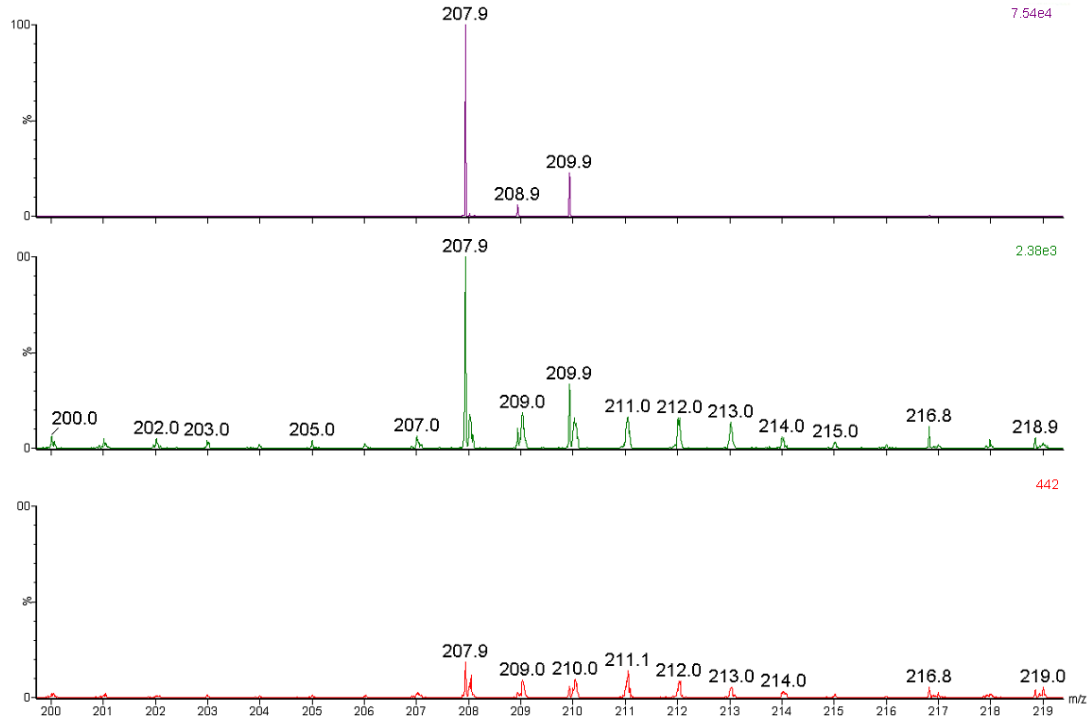

Figure 3.8 MALDI-MS/MS profiling on tissue.
Zoomed MS/MS spectra of fragmented *m/z* 254 from fenclozic acid standard (top), dosed tissue section (middle) and control tissue section (bottom).

MALDI-MS/MS spectra from drug standard and dosed tissue sections showed the presence of major MS/MS fragments at *m/z* 208 and 210. This indicated that parent drug was detectable in the dosed tissue sections using a MALDI profiling approach. These fragment ions were absent in the MS/MS spectra from control tissue sections. The use of ion mobility as an additional separation step was not investigated for the

MALDI profiling approach. An attempt to image the distribution of fenclozic acid in dosed tissue sections was unsuccessful due to the low dosing levels of the drug.

3.4 Application of imaging MS for *in vivo* drug distribution

Following on from these initial experiments, LESA profiling and MALDI imaging have been used for the detection and localisation of a common NSAID, diclofenac, in dosed mouse whole body and kidney sections from two strains of mice. A previous study at AstraZeneca had identified differences in radioactivity distribution during QWBA and differences in the metabolite profiles from the two strains of mice.

3.4.1 ESI-MS analysis of diclofenac standard

A solution of diclofenac standard was analysed by ESI-MS. An ion corresponding to deprotonated diclofenac was detected at *m/*z 293, shown in Figure 3.9 (a). A suggested fragmentation pathway of deprotonated diclofenac by ESI-MS/MS is shown in Figure 3.9 (b).

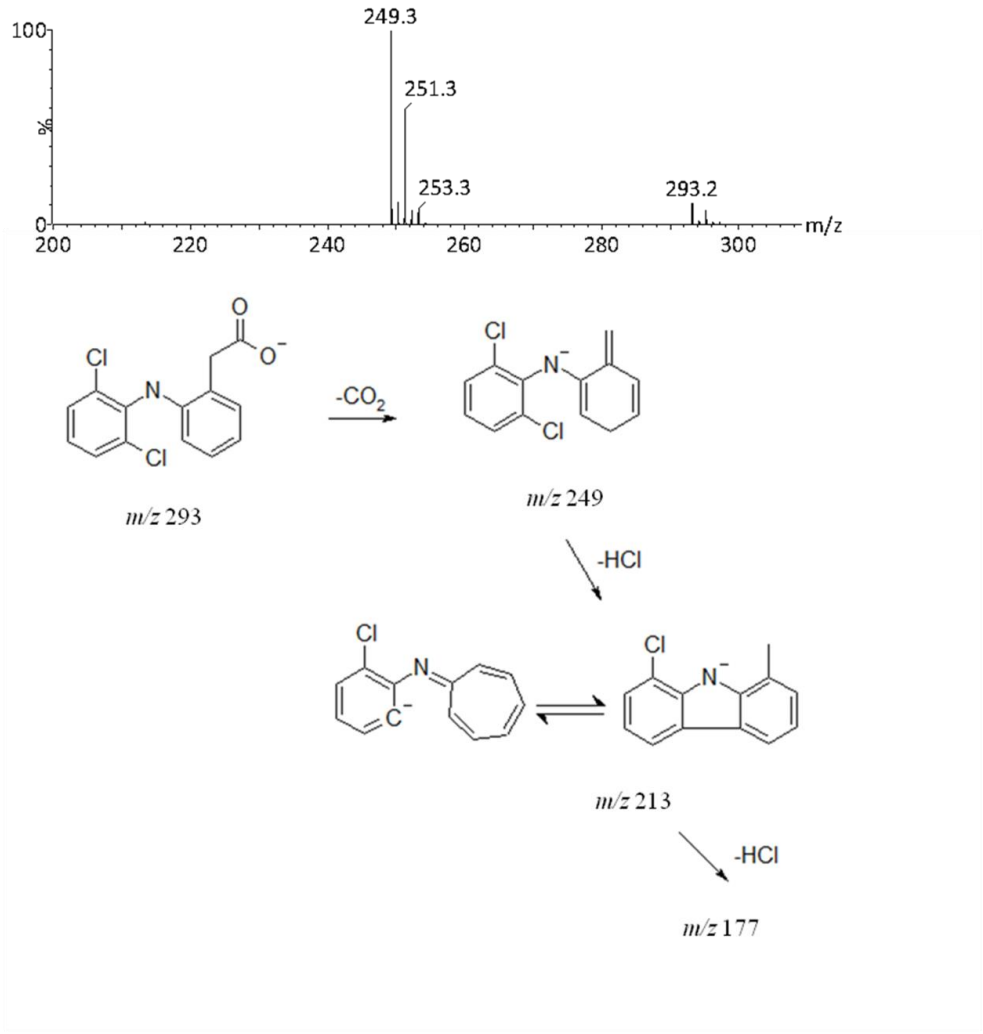

Figure 3.9 a) ESI-MS of diclofenac in negative ion mode.
b) Proposed fragmentation pathway of deprotonated diclofenac by means of ESI-MS/MS in negative ion mode.

The base peak observed in the spectrum was at *m/z* 249. This is consistent with the loss of CO_2 from diclofenac and indicated that in the absence of any collision energy diclofenac will readily fragment to form the *m/z* 249 ion.

Further fragmentation of *m/z* 249 using ESI-MS/MS produced ions at *m/z* 213 and *m/z* 177, shown by Figure 3.10. These ions correspond to subsequent losses of HCl from the decarboxylated diclofenac ion.

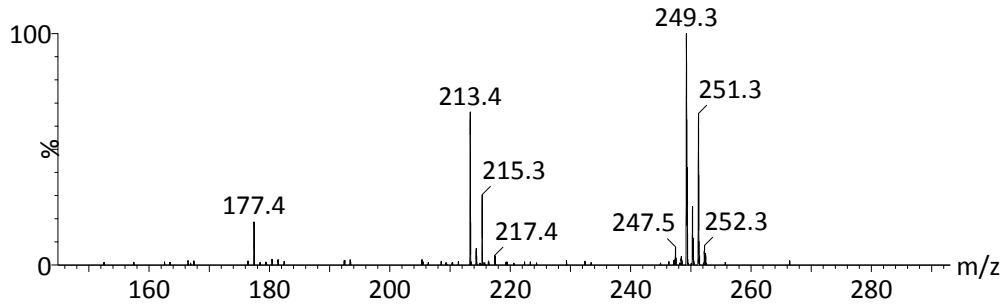

Figure 3.10 Fragmentation of *m/z* 249 in negative ion mode.

Analysis of diclofenac using ESI-MS/MS was repeated. An ion mobility separation step was included in the experiment after MS/MS fragmentation of the *m/z* 249 ion in order to determine the arrival times of the fragment ions through the mobility cell. The extracted ATDs are shown below in Figure 3.11.

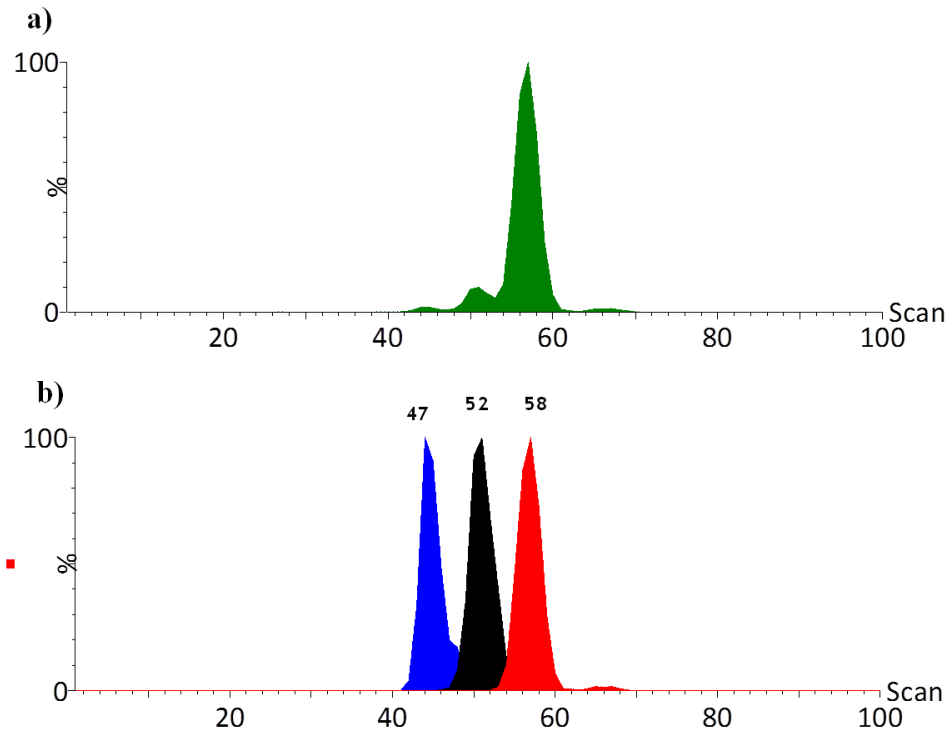

Figure 3.11 Arrival time distribution (ATD) of diclofenac standard.
a) Diclofenac in negative ion ESI-MS/MS mode
b) extracted ATDs of *m/z* 249 (red) *m/z* 213 (black) and *m/z* 177 (blue) fragment ions.

3.4.2 LESA-MS analysis of diclofenac concentration series

A concentration series of diclofenac was spotted onto control rat kidney tissue in order to assess the detection limits of the LESA technique. ESI-MS analysis of diclofenac standard revealed that a readily occurring decarboxylated diclofenac ion at *m/z* 249 was the most intense ion produced. Each doped position was sampled using LESA and analysed by means of nano ESI-MS, with *m/z* 249 selected by the quadrupole (set to also allow through the ^{37}Cl isotope peaks). The resulting spectra are shown in Figure 3.12 with the *m/z* 249.3 ion of decarboxylated diclofenac highlighted in yellow. The confidence in this ion being assigned to diclofenac decreased with lower than 1ng spotted on tissue (e-f).

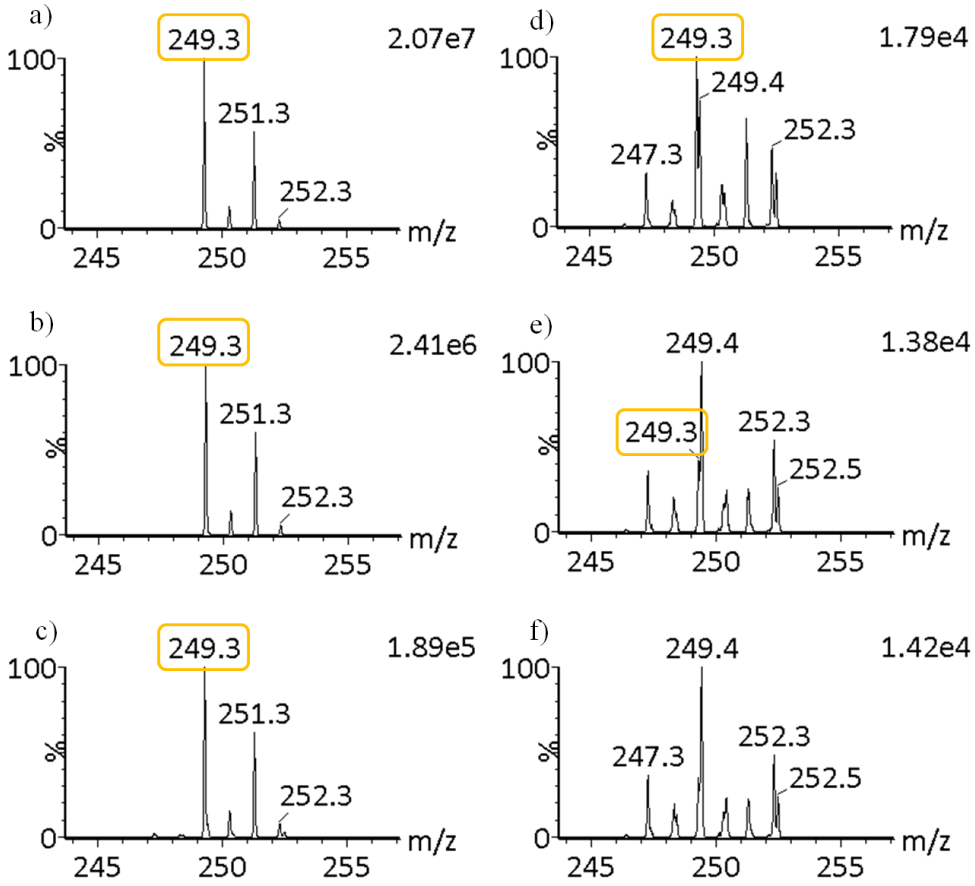

Figure 3.12 LESA-MS analysis of diclofenac concentration series.
MS spectra of quad-selected *m/z* 249 sampled at **a)** 1 µgµL^{-1} **b)** 100 ngµL^{-1} **c)** 10 ngµL^{-1} **d)** 1 ngµL^{-1} **e)** 100 pgµL^{-1} **f)** 10 pgµL^{-1} of diclofenac spotted on tissue.
At lower concentrations an interfering ion at *m/z* 249.4 can be seen. *m/z* 249.3 from decarboxylated diclofenac is highlighted in yellow and the total ion count for the zoomed spectra is displayed.

In order to improve confidence in the detection of diclofenac on tissue at lower concentrations, an ion mobility separation step following MS/MS fragmentation of the *m/z* 249.3 ion was included. Each doped position was sampled using LESA and analysed by obtaining the MS/MS spectrum of *m/z* 249, followed by mobility separation of the fragment ions. Fragmentation was performed in the trap region. Figure 3.13 shows the arrival time distribution of the *m/z* 249 ion selected for fragmentation, and the resulting *m/z* 213 and *m/z* 177 ions through the mobility cell.

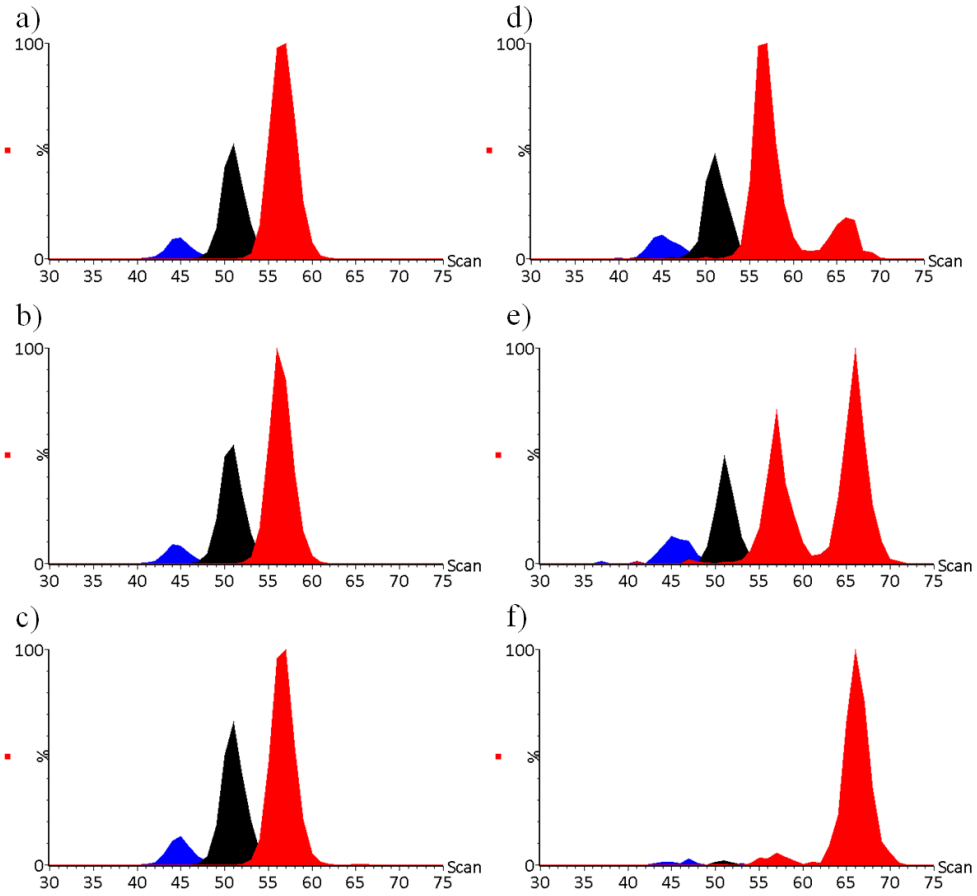

Figure 3.13 LESA-mobility-MS/MS of diclofenac concentration series.
ATDs of *m/z* 249 (red), *m/z* 213 (black) and *m/z* 177 (blue) through mobility cell after MS/MS of *m/z* 249 of diclofenac at **a)** 1 µgµL^{-1} **b)**100 ngµL^{-1} **c)** 10 ngµL^{-1} **d)** 1 ngµL^{-1} **e)** 100 pgµL^{-1} **f)** 10 pgµL^{-1}.
Diclofenac can be detected on tissue at 100 pg spotted on tissue by following an MS/MS transition, with mobility separation after fragmentation of *m/z* 249.

These results showed that LESA was successfully used to detect diclofenac on tissue with as low as 100 pgµL^{-1} spotted onto tissue (Fig. 4.5 (e)). All three ions *m/z* 249, *m/z* 213 and *m/z* 177, with the correct ATDs were present in the mobility spectrum.

At the lowest amount of diclofenac on tissue (Fig 4.5 (f)), 10 ngµL^{-1}, these distributions were less obvious and detection of diclofenac was less confident.

These results showed that by including MS/MS fragmentation and an ion mobility separation step, the selectivity of the LESA experiment was enhanced. This allowed more confident detection of diclofenac on tissue at low concentrations of diclofenac.

In order to demonstrate that this method was selective for diclofenac, three different concentrations of diclofenac were spotted onto three control rat kidney sections. Five positions on each kidney section were sampled using the selective method described above; these positions are shown in Figure 3.14.

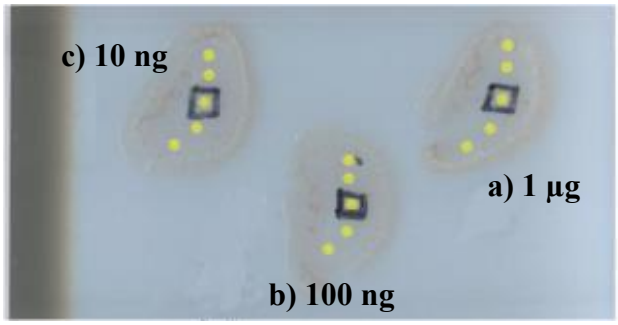

Figure 3.14. Control kidney sections for LESA-MS sampling.
a) 1 µg diclofenac dosed on tissue. **b)** 100 ng diclofenac on tissue. **c)** 10 ng diclofenac on tissue. Yellow dots indicate a sampling position. Black box indicates where diclofenac standard was spotted onto tissue.

The extracted ATDs obtained from *m/z* 249 and the fragment ion at *m/z* 213 are displayed in Figure 3.15 for two samplings from each tissue section. Where the diclofenac was present on the tissue, the arrival times for these ions were consistent with those seen from the diclofenac standard. Where control tissue was sampled, there was an ATD for a *m/*z 249 ion. This had a different mobility to that seen for diclofenac standard, and no ion at *m/*z 213 was observed. These results confirmed that the method is selective for diclofenac. This significantly reduces the risk of false positive results from tissue.

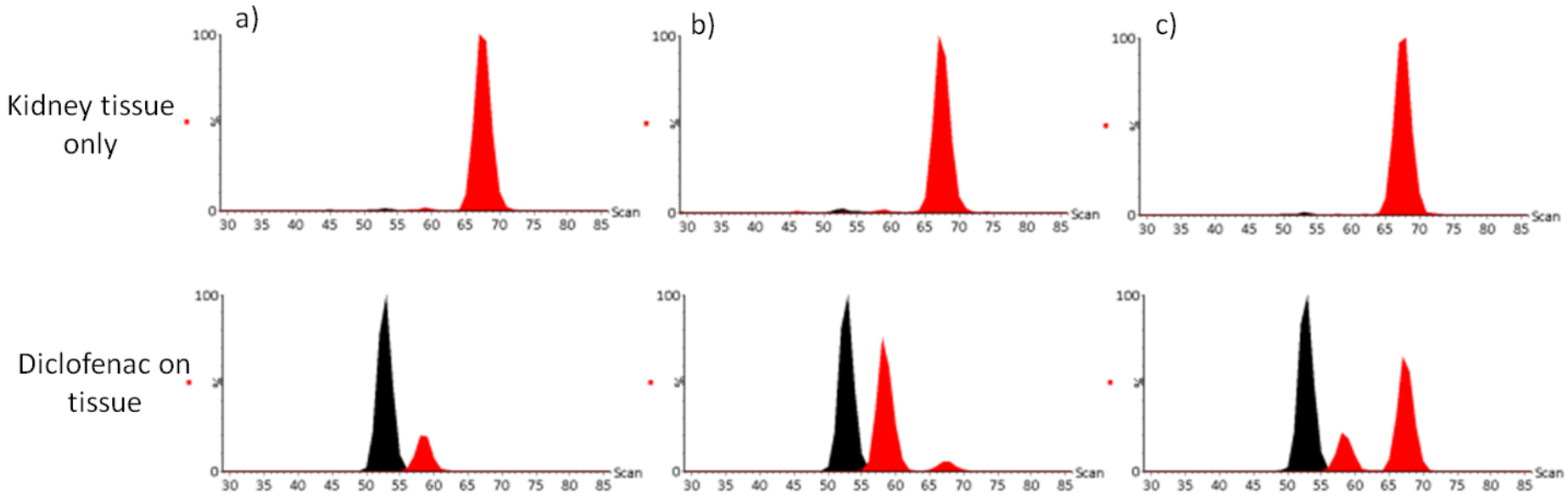

Figure 3.15 Arrival time distribution of *m/z* 249 (red) and *m/z* 213 (black) through the mobility cell.
a) 1 µg diclofenac dosed on tissue. b) 100 ng diclofenac on tissue. c) 10 ng diclofenac on tissue. *m/z* 213 is not present in the ATD from sampling positions of kidney tissue alone.

3.5 LESA profiling of dosed whole-body tissue samples

LESA profiling has been used to detect and localise parent drug compound in whole-body tissue sections to compare with existing QWBA data. This has been achieved using experimental methods optimised on diclofenac standard.

3.5.1 Wild type mouse 3 hours post dose

Kidney and liver regions of whole-body tissue sections from dosed wild type mice sacrificed 3 hours post-dose were sampled with LESA-MS using the selective method previously described. QWBA data from dosed wild type mice indicated moderate radioactivity (from diclofenac or metabolites) in the liver and elevated radioactivity in the kidney. The brain noticeably showed little or no radioactivity and so was also sampled for comparison as a control region.

The extracted ATDs (Figure 3.16) from wild type kidney and liver showed the presence of *m/z* 249 and *m/z* 213, with mobility similar to that observed for the standard diclofenac spotted on tissue (ATD scan 55-60 and 50-54, for *m/z* 249 and 213) respectively. The ATD from brain revealed an ion at *m/z* 249, with a similar mobility to that of the diclofenac standard. No ion at *m/z* 213 was present. This peak was potentially due to an endogenous species present in the tissue. These results indicated that a small amount of parent diclofenac drug was present in both the kidney and liver of the wild type mouse, but none present in the brain. This is consistent with QWBA studies, which showed radioactivity distribution in both organs, but none in the head region or brain of the mouse.

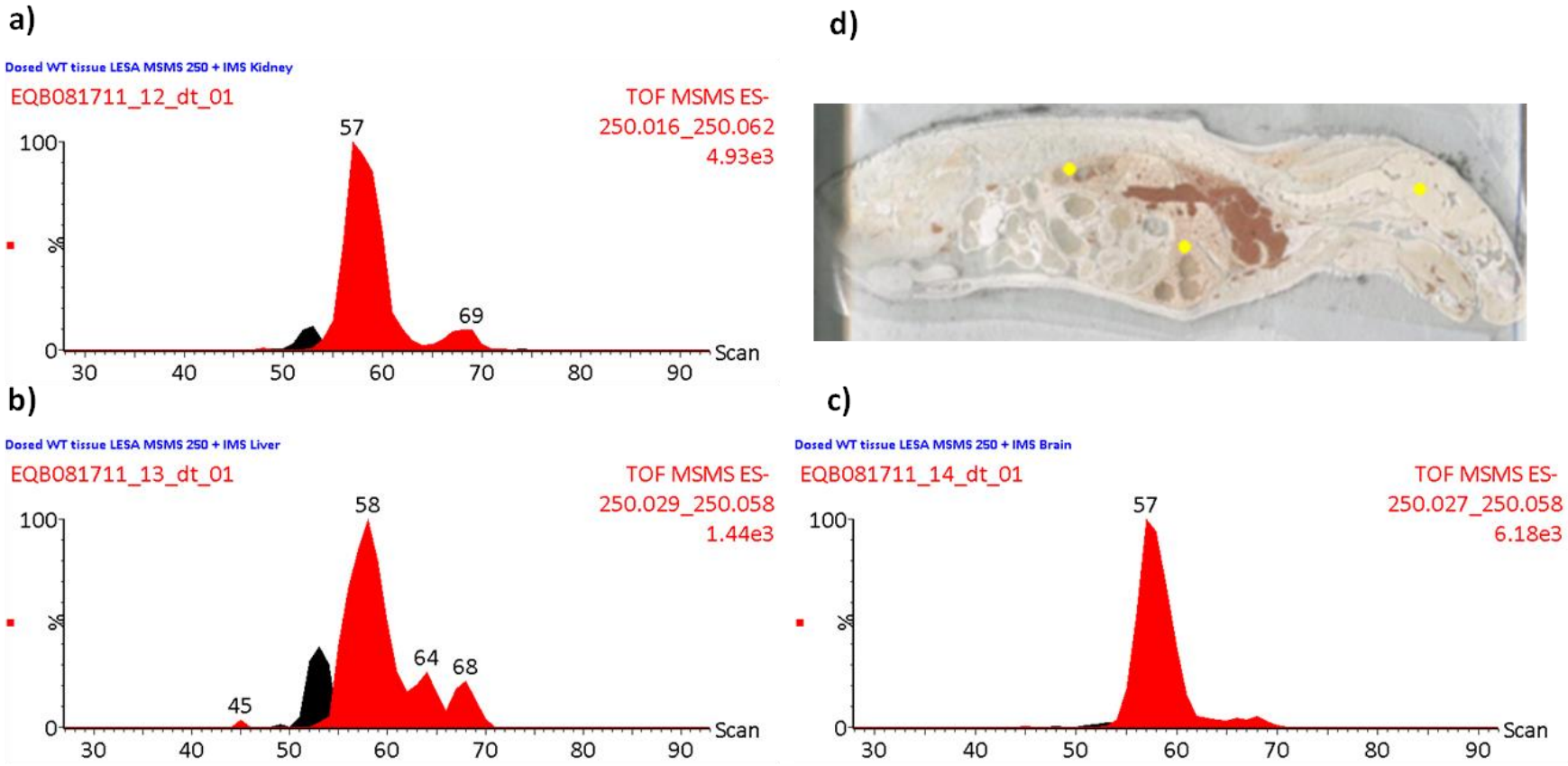

Figure 3.16 LESA-IMS-MS/MS sampling of wild type mouse whole body tissue section 3 hours post-dose**.**
Arrival time distribution of *m/z* 249 (red) and *m/z* 213 (black) from **a)** kidney **b)** liver and **c)** brain. **d)** Optical image of WT whole-body tissue section, with sampling positions highlighted in yellow.

3.5.2 HRN mouse 3 hours post dose

Kidney and liver regions of whole-body tissue sections from dosed HRN mice sacrificed 3 hours post-dose were sampled using LESA-MS. QWBA data from dosed HRN mice indicated moderate radioactivity (from diclofenac or metabolites) in both the kidney and liver, as well as widespread radioactivity. Elevated radioactivity was also seen in the urine and stomach. Again, the brain showed little or no radioactivity and so was included as comparison as a control region.

The extracted ATDs from HRN kidney and liver (Figure 3.17) showed *m/z* 249 and *m/z* 213 present with the same arrival times as that observed from standard diclofenac. The ATD of *m/z* 249 from brain showed a different mobility to that of diclofenac standard, and no ion at *m/z* 213 was present. These results indicated that a small amount of parent diclofenac drug was present in both the kidney and liver of the HRN mouse, but none was present in the brain. This was again consistent with QWBA studies that showed radioactivity distribution in both of these organs, but none in the head region or brain of the mouse.

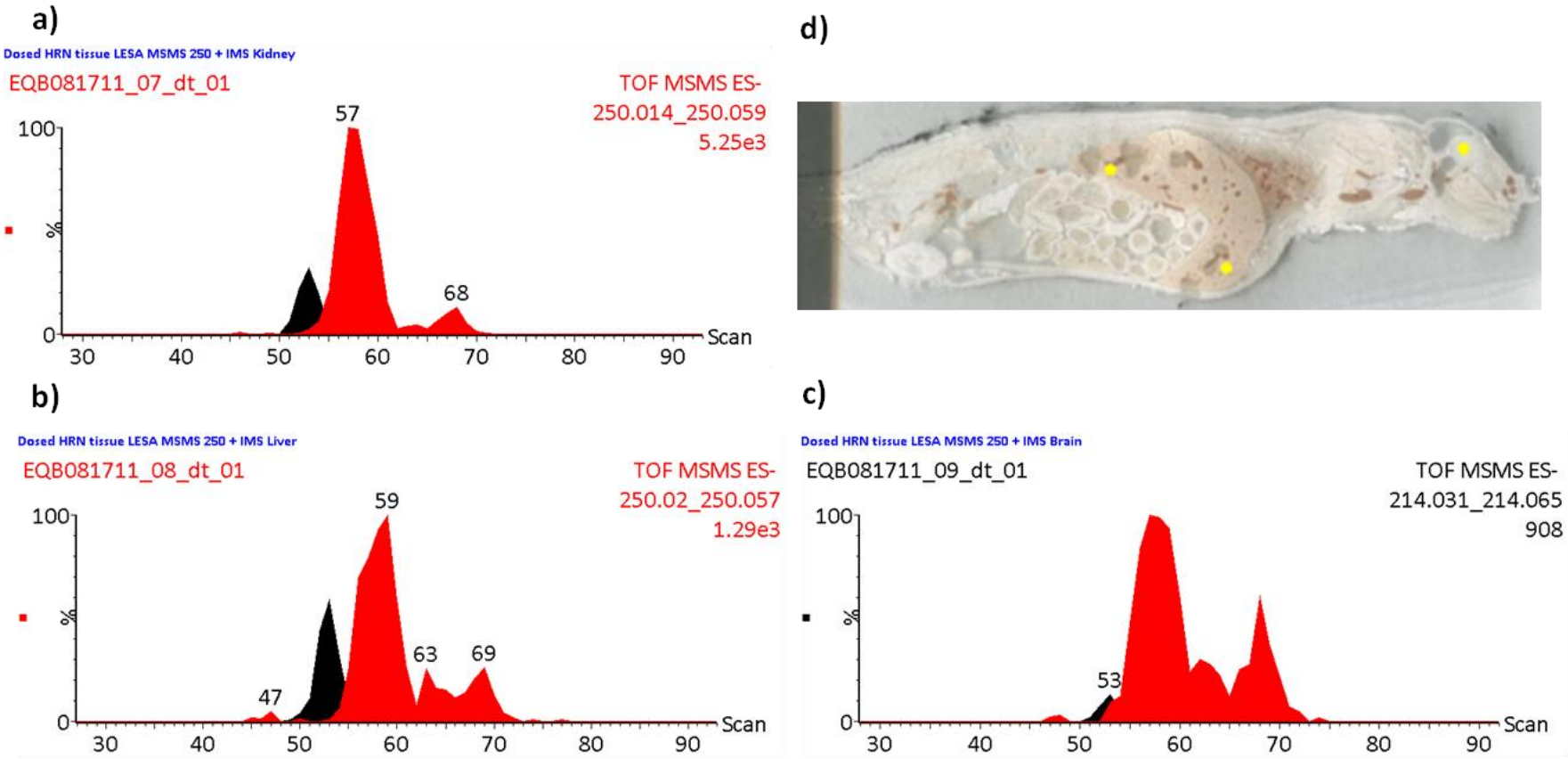

Figure 3.17 LESA-IMS-MS/MS sampling of hepatic P450 null reductase (HRN) mouse whole body tissue section 3 hours post-dose. Arrival time distribution of *m/z* 249 (red) and *m/z* 213 (black) from **a)** kidney **b)** liver and **c)** brain. **d)** Optical image of HRN whole-body tissue section, with sampling positions highlighted in yellow.

3.5.3 Wild type mouse 24 hours post dose

Whole-body tissue sections from dosed WT and HRN mice sacrificed 24 hours post-dose were sampled using LESA-MS. QWBA data indicated radioactivity distribution (from diclofenac or metabolites) in the kidney and liver. A control region showing no radioactivity in the QWBA results, was sampled for comparison. At 24 hours post-dose, more extensive metabolism was expected to have occurred in both the wild type and the HRN mice. Whilst radioactivity was observed in the kidney and liver, QWBA experiments could not distinguish between parent drug and its metabolites.

The ATDs from WT liver and kidney 24 hours post-dose (Figure 3.18) showed the presence of an ion at *m/z* 249 with a similar mobility (ATD scan 55-60) to the standard diclofenac spotted on tissue. The arrival time peak of *m/z* 213, however, was not present in the kidney. The *m/z* 213 peak present in the ATD from the liver was not as distinctive as that from the 3 hour samples, and did not demonstrate a definitive mobility. Neither *m/z* 213 or *m/z* 249 were present with the correct mobility from the LESA sampling of the brain.

Radioactivity distribution was observed in both of these organs from QWBA results. The ATDs obtained by means of a LESA-MS experiment did not indicate the presence of parent diclofenac in the kidney from the wild-type mouse. The ATD from the liver may potentially indicate presence of diclofenac, though this was not a confident assignment. This could indicate that the radioactivity seen in QWBA studies was due to diclofenac metabolites present in these organs rather than parent diclofenac. At 24 hours post-dose this would be consistent with metabolite identification studies from urine samples.

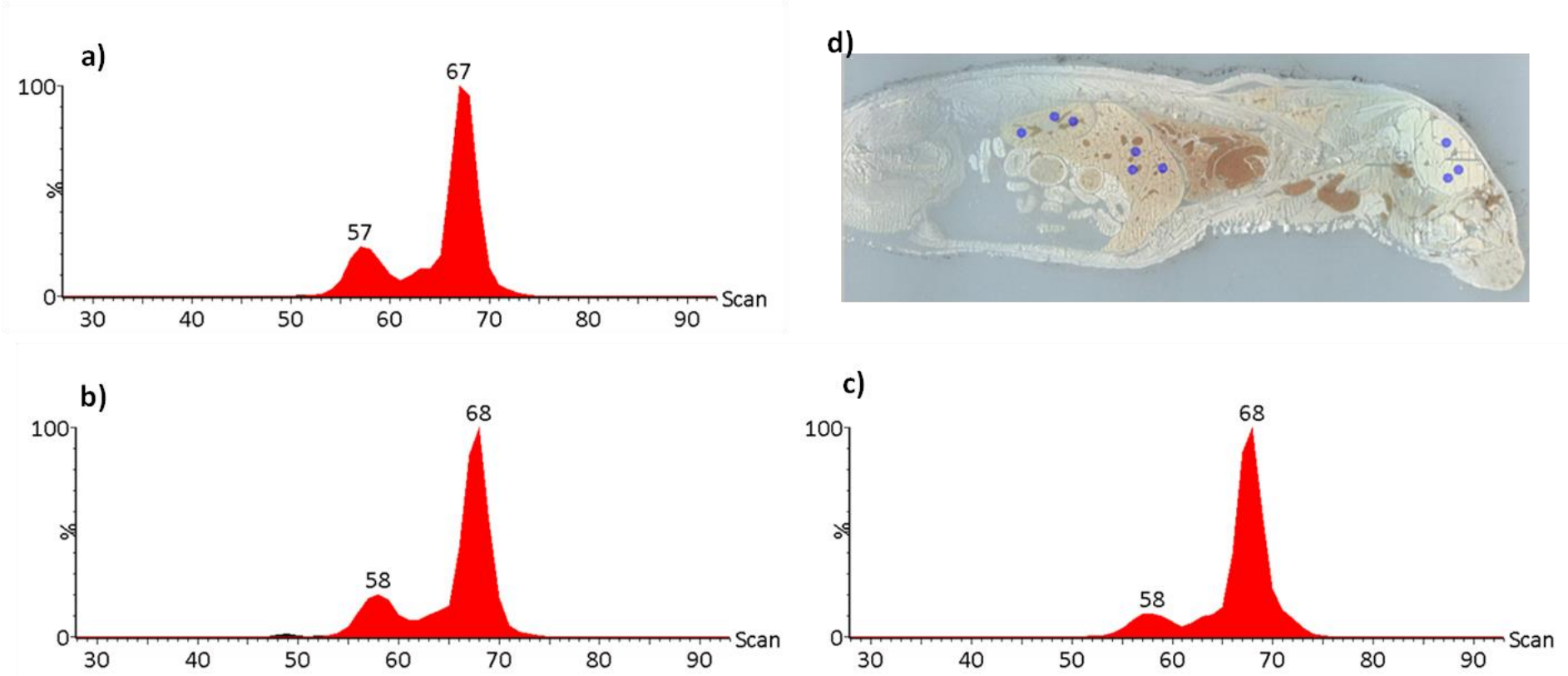

Figure 3.18 LESA-IMS-MS/MS sampling of wild type mouse whole body tissue section 24 hours post-dose.
Arrival time distribution of *m/z* 249 (red) and *m/z* 213 (black) from **a)** kidney **b)** liver and **c)** brain. **d)** Optical image of WT whole-body tissue section, with sampling positions highlighted in blue.

3.5.4 HRN mouse 24 hours post dose

ATDs shown in Figure 3.19 are from HRN liver and kidney 24 hours post-dose. They showed the presence of an ion at *m/z* 249 with a similar mobility to the standard diclofenac spotted on tissue (ATD scan 55-60). The arrival time peak of *m/*z 213, from both the kidney and liver was not as distinctive as that from the 3 hour samples, and did not demonstrate a definitive mobility. Neither *m/z* 213 nor *m/z* 249 were present with the correct mobility from the LESA sampling of the brain.

These results indicated the possible presence of parent diclofenac in the kidney and liver from the HRN mouse. QWBA results showed radioactivity distribution in both organs. Metabolite identification experiments suggested very low levels of both parent diclofenac and metabolites in the urine sampled between 12 and 24 hours from HRN mice.

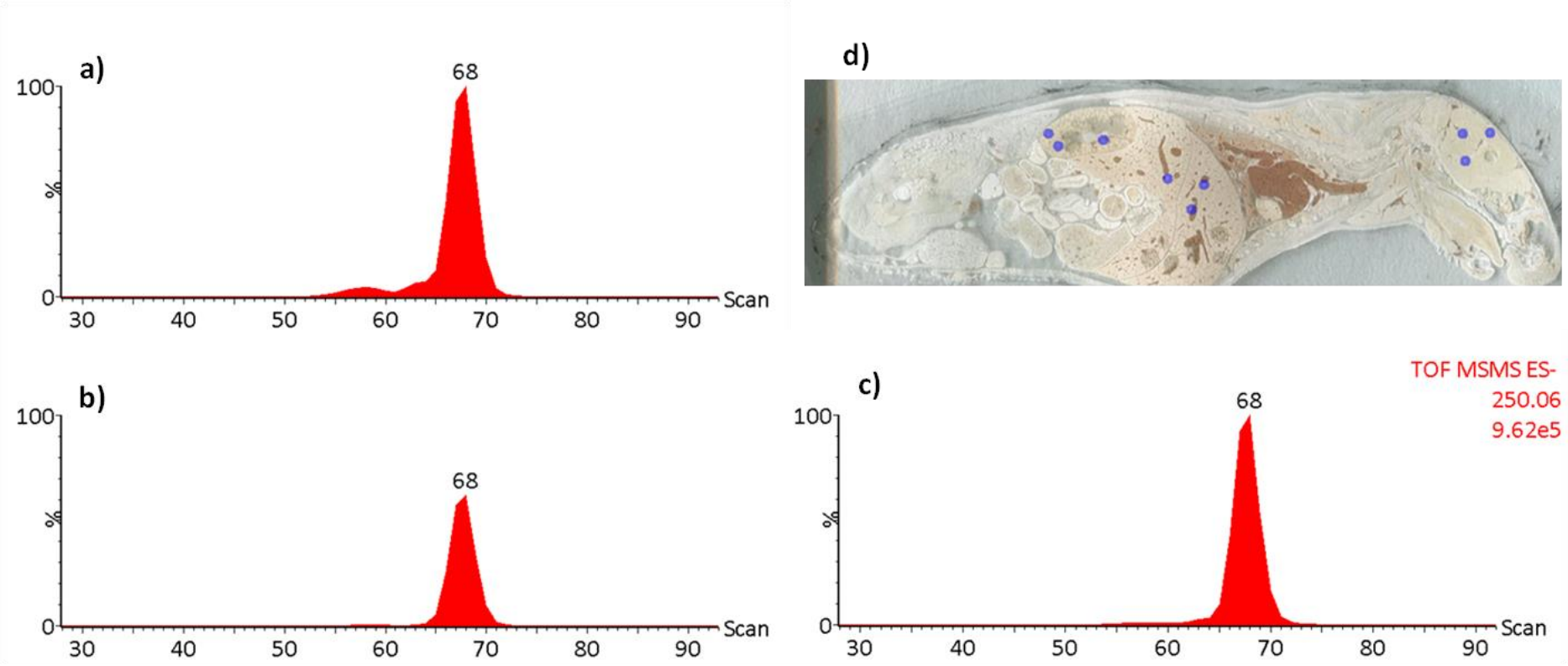

Figure 3.19 LESA-IMS-MS/MS sampling of hepatic P450 null reductase (HRN) mouse whole body tissue section 24 hours post-dose. Arrival time distribution of *m/z* 249 (red) and *m/z* 213 (black) from **a)** kidney **b)** liver and **c)** brain. **d)** Optical image of HRN whole-body tissue section, with sampling positions highlighted in blue.

3.6 MALDI imaging

MALDI-MS methods for the detection and localisation of diclofenac in dosed tissue sections have been optimised using diclofenac standards. MALDI imaging was evaluated for its ability to detect and localise parent drug compound in kidney tissue sections.

3.6.1 MALDI-MS of diclofenac standard

A solution of diclofenac standard was analysed using MALDI-MS, in negative ion mode, prepared with either α-Cyano-4-hudroxycinnamic acid (CHCA) or 2,5-Dihydroxybenzoic acid (DHB) matrix. Deprotonated diclofenac was only detected at *m/z* 293 when CHCA was used as the matrix compound, shown in Figure 3.20 (a). The base peak seen in the CHCA (also present in the DHB spectra) was *m/z* 213, representing the loss of CO_2 and HCl from diclofenac. The decarboxyated diclofenac ion at *m/z* 249 was also present in both spectra. This indicated that in the absence of any collision energy diclofenac will readily fragment in the MALDI experiment to form both the *m/z* 249 and *m/z* 213 ions. In positive ion mode, diclofenac did not readily ionise.

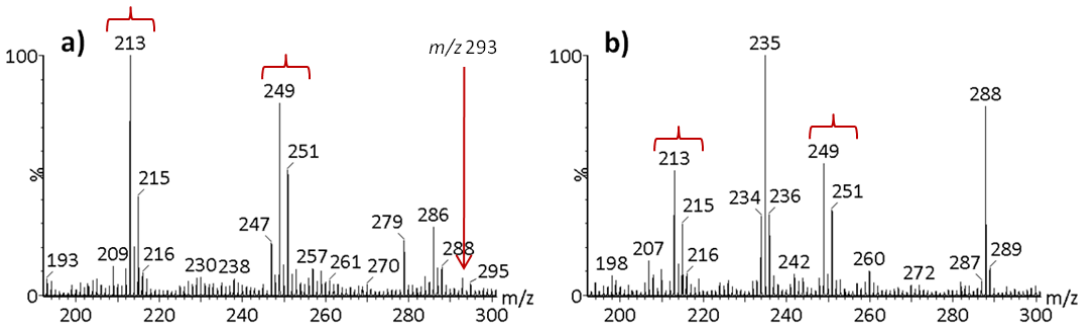

Figure 3.20 Negative ion mode MALDI-MS of diclofenac standard.
MALDI-MS spectra of diclofenac standard in **a)** CHCA matrix and **b)** DHB matrix. With both matrices there is interference from background ions, but diclofenac peaks at *m/z* 213 and *m/z* 249 have better signal to noise ratio with CHCA as the matrix. Very little of the $[M-H]^-$ ion at *m/z* 293 is present in **a)**, and none in **b)**.

CHCA was selected as the matrix of choice, since a better signal-to-noise ratio was obtained for diclofenac related peaks in the spectrum. CHCA produced a more homogenous layer of crystals, important for imaging and profiling experiments.

The most intense diclofenac peak, *m/z* 213 was selected for further fragmentation using MS/MS shown in Figure 3.21 (a). When selected for fragmentation in negative ion mode, there was a further loss of HCl from the *m/z* 213 peak to form *m/z* 177. Analysis of diclofenac using MALDI-MS/MS was carried out, including an ion mobility separation step. This was introduced after fragmentation of *m/z* 213 in the trap cell in order to determine the arrival times of the fragment ions through the mobility cell. The extracted ATDs are shown below in Figure 3.21 (b).

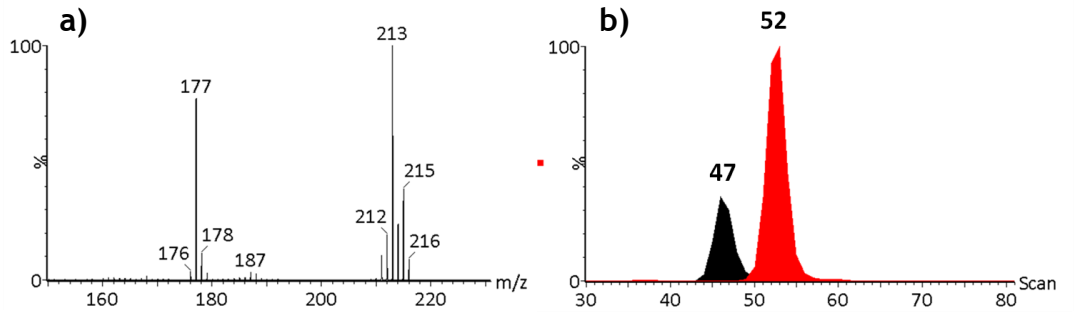

Figure 3.21 MALDI-mobility-MS of diclofenac standard.
a) MALDI-MS/MS of *m/z* 213 results in a loss of HCl to produce *m/z* 177 in negative ion mode.
b) Arrival time distribution of *m/z* 213 (red) and *m/z* 177 (black) when a mobility separation step is included after MS/MS fragmentation.

The extracted ATDs of the *m/z* 213 and *m/z* 177 ions in the MALDI experiment were consistent with those observed in the LESA mobility experiments on the diclofenac standard.

3.6.2 MALDI-MS analysis of diclofenac concentration series

In order to establish limits of detection for the MALDI experiment, six concentrations of diclofenac standard (ranging between 1 µgµL-1 and 10 pgµL^{-1}) were spotted onto a stainless steel target plate, with CHCA as a matrix. A number of different acquisition methods were used to sample across the concentration range of diclofenac, in order to determine the most selective method for detection of diclofenac on target. The most selective method proved to be an MS/MS fragmentation from *m/z* 213 – *m/z* 177. The enhanced duty cycle (EDC) mode of

the instrument was used to improve the selectivity by a factor of ten (compared to MS/MS alone).

To further increase the selectivity of the experiment an ion mobility separation step was included, either before or after fragmentation using EDC MS/MS. These results showed that including an ion mobility separation step prior to fragmentation of *m/z* 213 in the transfer cell improved the selectivity of the experiment by a factor of ten. This allowed diclofenac to be detected at just 100 pg on target.

This enhanced selectivity method can be summarised by the schematic shown in Figure 3.22.

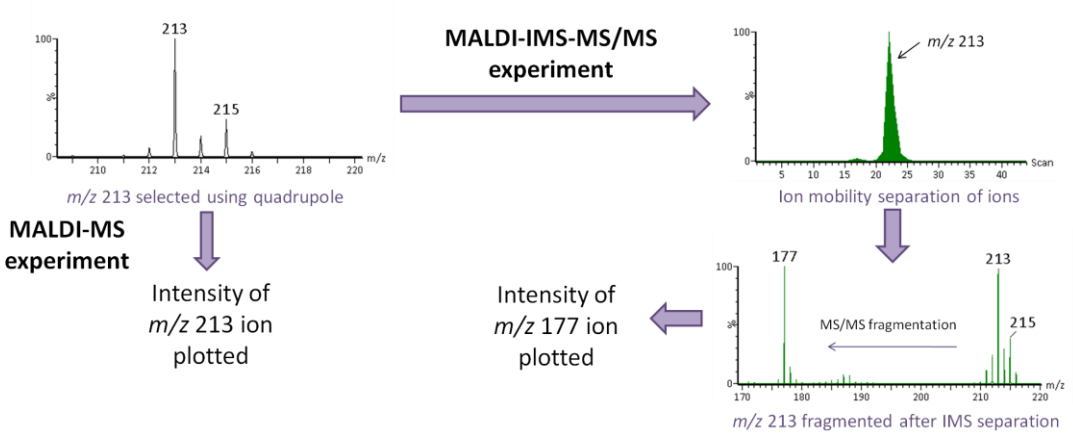

Figure 3.22 Schematic showing differences between a standard MALDI-MS experimental method and an enhanced selectivity MALDI-IMS-MS/MS method.

The selectivity of this method for diclofenac has been demonstrated. Each concentration of diclofenac was spotted onto a stainless steel target plate with an adjacent sample well prepared with matrix alone. A MALDI imaging experiment was used to image two sample wells at a time, one with diclofenac and one without, using the enhanced selectivity method. Figure 3.23 below shows the intensity of the *m/z* 177 ion observed in each experiment. These results demonstrated that this method was selective for diclofenac down to 10 ng on target. This selectivity was not present at concentrations of lower than 10 ng of diclofenac on target.

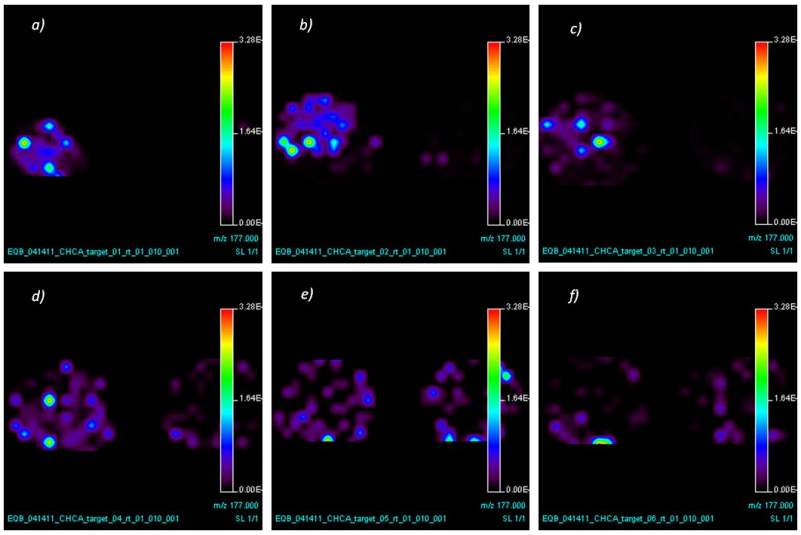

Figure 3.23 MALDI imaging of diclofenac concentration series on target.
Ion intensity map at 150 µm spatial resolution of *m/z* 177 at **a)** 1 µg **b)** 100 ng **c)** 10 ng **d)** 1 ng **e)** 100 pg and **f)** 10 pg of diclofenac on target (left-hand sample well) or CHCA matrix alone (right-hand sample well)

This approach was used to image diclofenac with different levels of diclofenac spotted across control rat kidney tissue. This experiment was performed in order to determine the detection limits and selectivity on tissue. Matrix was applied by spraying using an airbrush, rather than spotting as for a profiling experiment. Each concentration of diclofenac was spotted a number of times across a whole rat kidney section prior to matrix application. The intensity of the *m/z* 177 ion observed across each kidney section is shown in Figure 3.24.

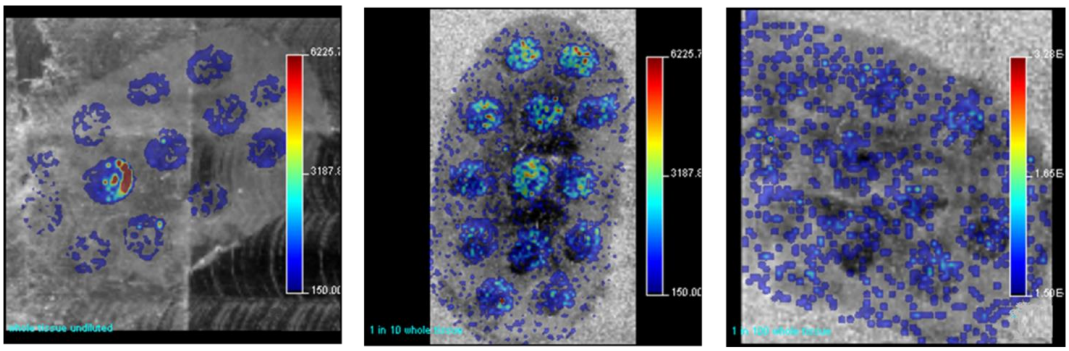

Figure 3.24 MALDI-mobility-MS/MS imaging of diclofenac concentration series on tissue.
Ion intensity map at 150 µm spatial resolution of *m/z* 177 at a) 1 µg b) 100 ng and c) 10 ng of diclofenac spotted on tissue.

Diclofenac was confidently mapped across the kidney sections doped with the two highest concentrations, without interference from background ions. At 10 ng on tissue, diclofenac could not be confidently detected from tissue. This detection limit on tissue was ten-fold higher than for diclofenac spotted on a stainless steel target plate. The loss of sensitivity between target plates and tissue was expected.

The amount of diclofenac at each sampling position (laser spot/pixel) has been estimated, based on the size of the region doped with diclofenac, the spatial resolution and the area of laser ablation at each pixel. 100 ng diclofenac spotted on tissue would give an estimated 600 pg of diclofenac at each pixel. This indicated a detection limit of ~ 600 pg per pixel (where each pixel is 150µm).

In order to demonstrate that the enhanced selectivity method provided an advantage in the MALDI imaging of drug compounds over that obtained using MALDI-MS alone the experiment was repeated, without employing mobility separation or MS/MS fragmentation. The quadrupole was used to select *m/z* 213, but no collision energy was introduced to perform CID.

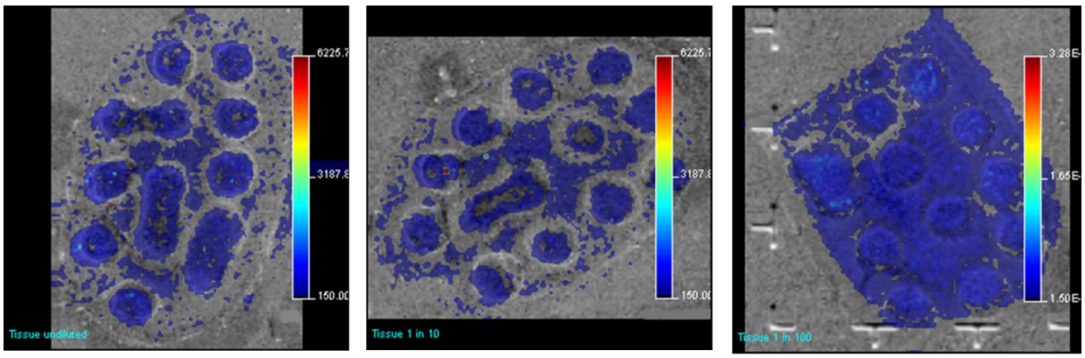

Figure 3.25 MALDI-MS imaging of diclofenac concentration series on tissue. Ion intensity map at 150 µm spatial resolution of *m/z* 213 at a) 1 µg b) 100 ng and c) 10 ng of diclofenac spotted on tissue.

The ion intensity map of m/z 213 is shown in Figure 3.25. This revealed that it was not possible to confidently distinguish between diclofenac and background ions on tissue without the added selectivity of the ion mobility separation. This was true even at high concentrations of diclofenac on tissue.

3.6.3 MALDI imaging of dosed kidney samples

Multiple kidney sections from dosed WT and HRN mice were sampled using MALDI-MS with the selective method previously optimised. At the 10 $mgkg^{-1}$ dose administered to WT and HRN mice, the amount of diclofenac in these dosed kidney sections was roughly estimated to be ~ 6pg per pixel. Based on the previous results, the amount of diclofenac present in the tissues was below the detection limit, 100-fold less than necessary and was unlikely to be detected using a MALDI imaging experiment.

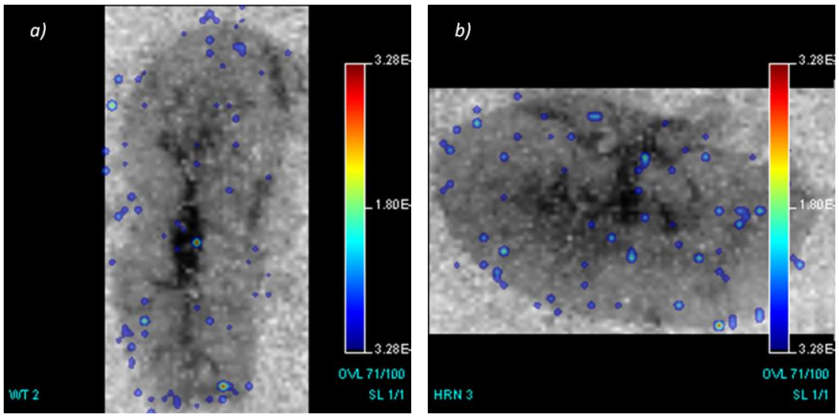

Figure 3.26 MALDI-mobility-MS/MS imaging of *m/z* 213 across dosed kidney sections.
Ion intensity map at 150 µm spatial resolution of *m/z* 177 from a) dosed wild-type mouse kidney and b) dosed HRN mouse kidney.

This has been confirmed by the two example results from MALDI imaging experiments (Figure 3.26). In both images, the intensity of m/z 177 has been plotted, no distinctive presence of m/z 177 was observed anywhere in the tissue, aside from an occasional peak in intensity. These peaks did not indicate the presence of diclofenac within the tissue sections.

3.7 Conclusions

Optimisation experiments have been performed for both mass spectrometry-based imaging experiments. These experiments indicated the importance of enhancing the selectivity of the mass spectrometry imaging experiment for drug localisation studies in tissue. Selectivity has been shown to be greatly improved by coupling an ion mobility separation step with MS/MS fragmentation, for both LESA-MS and MALDI-MS. With the LESA technique, the inclusion of ion mobility separation after MS/MS fragmentation improved the selectivity of the experiment ten-fold. This allowed diclofenac to be identified confidently at 100 pg on tissue. Using the MALDI-MS experiment, ion mobility separation prior to MS/MS fragmentation has been shown to be the most selective method. This allowed for the confident detection of diclofenac at 100 ng on tissue.

The selective approach developed for LESA-MS has been used for the successful identification of diclofenac. This has been achieved in both dosed wild type and HRN mice whole body tissue sections, sacrificed three hours post-dose, and showed data complementary to existing QWBA studies. At 24-hours post dose, parent diclofenac has not been confidently identified from tissue using LESA-MS. QWBA data, however, showed radioactivity at 24 hours in both the kidney and the liver. Since parent diclofenac was not identified by LESA-MS from these tissues, this could suggest that this radioactivity was due to the presence of metabolites in the tissue. Further optimisation would be required to determine the most selective method for the detection of metabolites in tissue for both LESA-MS and MALDI-MS.

Optimisation of the MALDI-MS experiment greatly improved experimental selectivity for compounds of interest. The level of diclofenac estimated to be present in kidney tissue sections was much lower than the limit of detection. This was confirmed using MALDI imaging experiments of dosed wild type and HRN kidney sections. A higher dose of diclofenac would therefore be required to provide a higher concentration of drug within the tissue sections for detection using MALDI imaging.

There were noticeable differences in sensitivity between the two imaging mass spectrometry experiments. The larger sampling area of LESA (1mm) when compared with MALDI (150 μm) provided an inherent advantage for LESA over MALDI. The detection limit of LESA has been shown to be around an order of magnitude lower than for MALDI. This was, however, at the expense of spatial resolution. The choice of technique should therefore be based on the requirements of each experiment. LESA-MS cannot compete with MALDI imaging at present if a high spatial resolution is required. In a profiling-type experiment LESA-MS has been shown to be faster, more sensitive and required much less sample preparation than that of a MALDI imaging experiment.

Chapter 4 Combining industry-standard methods and imaging MS approaches for drug and metabolite distribution in rat

4.1 A combined Met-ID and imaging MS approach to drug and metabolite distribution in rat

Rapid, effective methods for metabolite identification play an important part in the discovery and development phases of new drug compounds. LC-MS approaches are predominantly used for metabolite identification and the introduction of ultra-performance liquid chromatography (UPLC) offers advantages in cases with complex metabolism by providing enhanced component separation prior to MS detection. These approaches are well established for identification and quantitation of metabolites in extracts from tissue homogenates and other biological matrices, but do not contain critical specific localisation information. Combining information from QWBA studies with metabolite identification can offer more information about the distribution of radioactivity, but cannot distinguish spatially between parent compound and metabolites.

The use of LESA profiling and MALDI imaging for targeted detection and localisation of parent drug and metabolites has been evaluated. An established metabolite identification approach was used to determine the metabolism (by LC-MS) of two drug compounds in rat at selected time points post-dose. [^{14}C]-propranolol or [^{14}C]-fenclozic acid were dosed at 25 mgkg^{-1} to two groups of rats, which were sacrificed at 2 hours, 6 hours and 24 hours post-dose, with two rats prepared per time point for each compound. One rat was used to prepare whole-body sections for LESA and MALDI analysis, whilst the other was used for tissue harvesting and metabolite identification. MALDI imaging and LESA profiling were then used for the detection and localisation of parent drug compound and an abundant metabolite in whole body tissue sections. Metabolite characterisation experiments were conducted by Dr. Daniel Weston (AstraZeneca, Alderley Park, Cheshire), and results are used here with permission.

4.1.1 Propranolol

Propranolol (Inderal) is a non-selective β-adrenergic receptor antagonist used for the relief of cardiovascular disorders including hypertension, angina pectoris and cardiac

arrhythmia (Beaudry, Le Blanc et al. 1999). The structure of propranolol is shown in Figure 4.1.

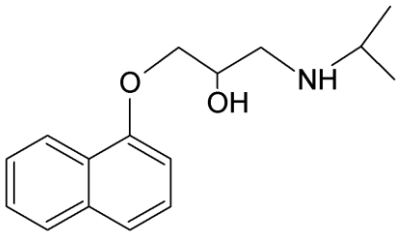

Figure 4.1 Structure of propranolol

The fate of propranolol *in vivo* is complex, with numerous oxidation sites available on the molecule (Athersuch, Sison et al. 2008). Propranolol has been used in a wide range of previous studies in different species, including investigation by imaging mass spectrometry approaches (Kertesz, Van Berkel et al. 2008).

The distribution of [^{14}C]-propranolol was investigated in 1967 using autoradiography. The results demonstrated that radioactivity had disappeared from the blood by 5 minutes post-dose, with extensive uptake into the central nervous system (CNS), lung, liver and kidney. At four hours post-dose this radioactivity remained high in the lung and kidney, but it was not then determined if this was due to metabolites or the parent drug compound (Masuoka and Hansson 1967).

Propranolol is metabolised extensively in the liver, reducing the amount of active drug that reaches the circulatory system. This phenomenon is known as first-pass metabolism and is associated with the oral administration of some drugs. After administration the drug is absorbed by the digestive system and enters the hepatic portal system into the liver where it is metabolised (Schiff and Saxey 1984). This leads to a non-linear relationship between the dose of propranolol and its bioavailability after oral administration, which has previously been described (Shand and Rangno 1972; Routledge and Shand 1979).

Predominant propranolol metabolites produced during phase I metabolism pathways are 4-hydroxypropranolol, via oxidation of the aromatic ring, and *N*-dealkylation followed by side-chain oxidation. Phase II metabolites include direct conjugation of the hydroxyl group on the side chain or sulphate conjugation of 4-

hydroxypropranolol via aromatic oxidation (Baughman, Talarico et al. 2009). Figure 4.2 shows the structures of propranolol metabolites which have been identified in rat cryopreserved hepatocytes.

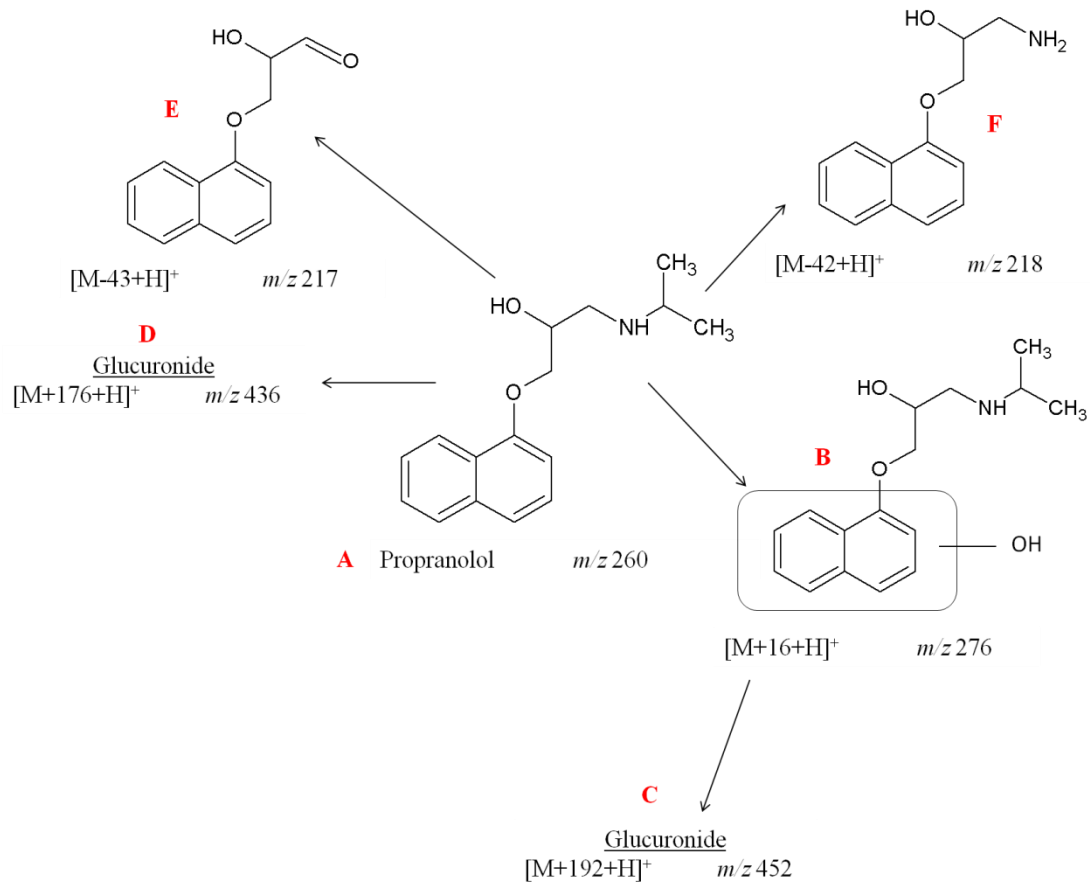

Figure 4.2 Metabolites of propranolol as identified in rat cryopreserved hepatocytes. A) Parent propranolol; B) 4-hydroxypropranolol; C) glucuronide conjugation via oxidation; D) glucuronide conjugate; E) *N*-dealkylation with subsequent oxidation; F) dealkylation. Adapted from Baughman *et al.* 2009.

The phase I metabolite 4-hydroxypropranolol is only produced following oral administration of the drug (Hayes and Cooper 1971). This metabolite has been shown to be active as a β-adrenoceptor blocking drug with a similar potency to that of the parent propranolol (Fitzgerald and O'Donnell 1971). Both parent propranolol and its 4-hydroxypropranolol metabolite were found to bind to a significant extent in tissues, primarily the lung.

4.1.2 Fenclozic Acid

Fenclozic acid was briefly introduced in Chapter 3; further investigations into the metabolism of fenclozic acid have not been published since the 1970s, but it remains an interesting molecule to study due to its hepatotoxicity which caused eventual withdrawal of the drug from market. The structure of fenclozic acid is shown again in Figure 4.3 for reference.

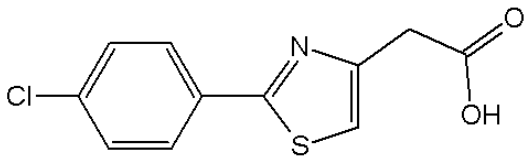

Figure 4.3. Structure of fenclozic acid

Fenclozic acid metabolism studies have identified five metabolites including decarboxylated fenclozic acid; oxidation and hydroxylation of the chlorine atom (Foulkes 1970).

4.2 Results and Discussion

For materials and methods please refer to Chapter 2.

4.3 Radioprofiling of tissue homogenates

One animal at each time point was used to provide tissues for metabolite identification experiments. Tissues were homogenised in distilled water and the level of radioactivity present in each homogenate was determined using oxidation experiments. Radioactivity levels were determined in triplicate using liquid scintillation counting (LSC). Small aliquots of homogenate were weighed and oxidised and [^{14}C] was collected as CO_2 in scintillant solution for LSC. The efficiency of the instrument was evaluated using [^{14}C]-glucose and final radioactivity levels were corrected based on this efficiency value.

Figure 4.4 shows the radioactivity per gram of homogenate measured for each tissue from [^{14}C]-propranolol-dosed rats at each time point. These results show that radioactivity levels are highest at 2 hours post-dose for every tissue homogenate. Liver homogenate contains the highest level of radioactivity per gram at every time point, with the second highest levels of radioactivity being found in the kidney.

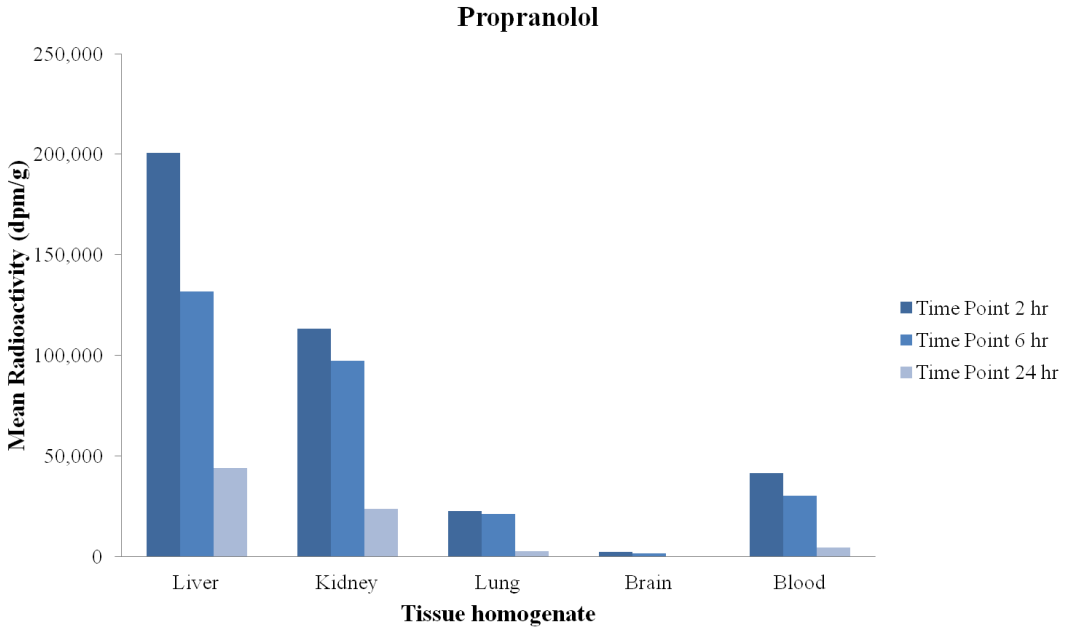

Figure 4.4 Radioactivity levels in tissue homogenate from [^{14}C]-propranolol-dosed rats at 2, 6 and 24 hours post-dose.

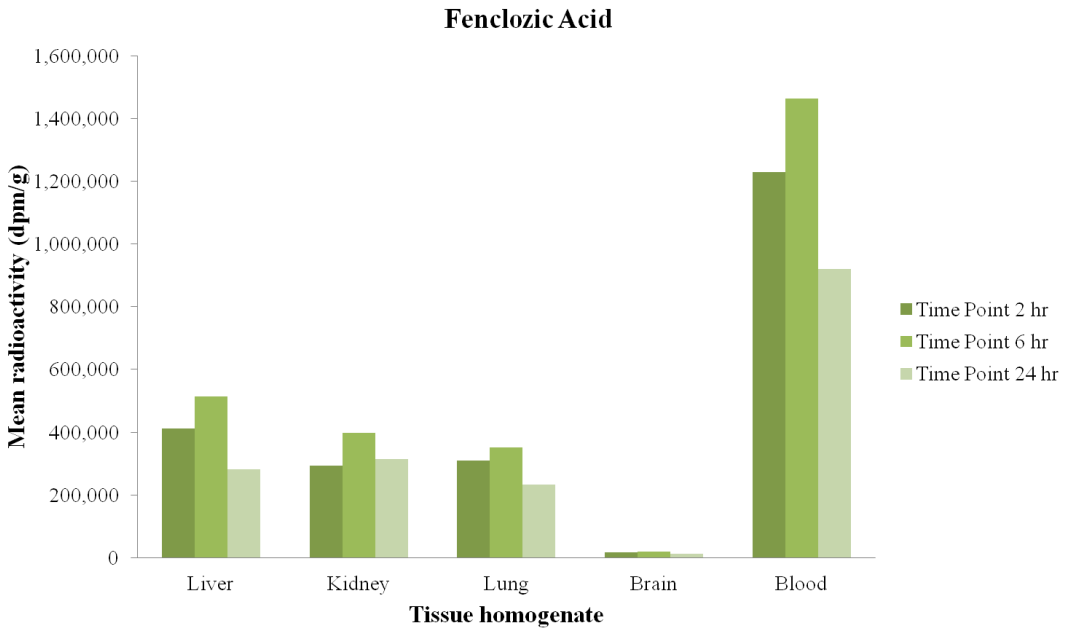

Figure 4.5 Radioactivity levels in tissue homogenate from [^{14}C]-fenclozic acid-dosed rats at 2, 6 and 24 hours post-dose.

Figure 4.5 shows the radioactivity per gram of homogenate measured for each tissue from [^{14}C]-fenclozic acid-dosed rats at each time point. These results show that radioactivity levels are highest at 6 hours post-dose for every homogenate sampled. Blood samples contain the highest level of radioactivity per gram at every time point, with the second highest levels of radioactivity being found in the liver.

The results give an indication of the amount of drug-related material present across the tissue based on total radioactivity. It cannot be established from these results whether the radioactivity is attached to parent drug or metabolites. The radioactivity found in the fenclozic acid dosed tissues is much higher than in the propranolol dosed tissues.

4.4 Tissue extraction and metabolite identification

In order to run metabolite identification experiments, extraction of the drug and metabolites from tissue must be performed. Three extraction solvents were tested for each drug compound to ascertain which solvent gave the best efficiency for extraction of the radioactivity from homogenate. Extraction methods were tested on

homogenates with the highest levels of radioactivity; 2 hour liver for propranolol and 6 hour liver for fenclozic acid.

Figure 4.6 shows the extraction efficiency of these solvents, displayed as a percentage of radioactivity recovered from total homogenate radioactivity for propranolol and fenclozic acid.

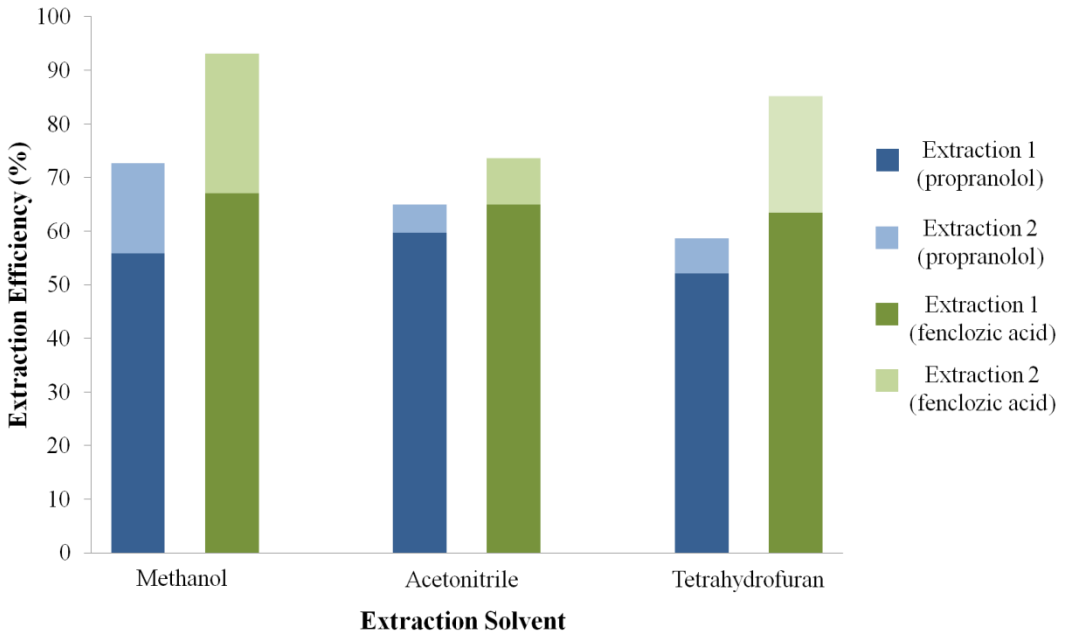

Figure 4.6 Radioactivity extraction efficiency of methanol, acetonitrile and tetrahydrofuran for propranolol and fenclozic acid-dosed tissues. The percentage extraction efficiency for each stage of a two-step extraction is shown for each solvent.

For both propranolol and fenclozic acid, extraction using methanol recovered the highest percentage of total radioactivity. This is therefore assumed to recover the highest levels of drug and metabolite compounds. Extraction efficiency was higher for fenclozic acid dosed tissues than for propranolol. As a second extraction step only recovered relatively small levels of radioactivity, only one extraction step was used.

Methanol extraction was performed on tissue homogenate from both propranolol and fenclozic acid-dosed tissues. Radioactivity levels per extract were measured by liquid scintillation counting. Final radioactivity per gram of tissue extract measured

at each time point for propranolol and fenclozic acid dosed samples prior to metabolite identification are shown in Figure 4.7 and Figure 4.8 respectively.

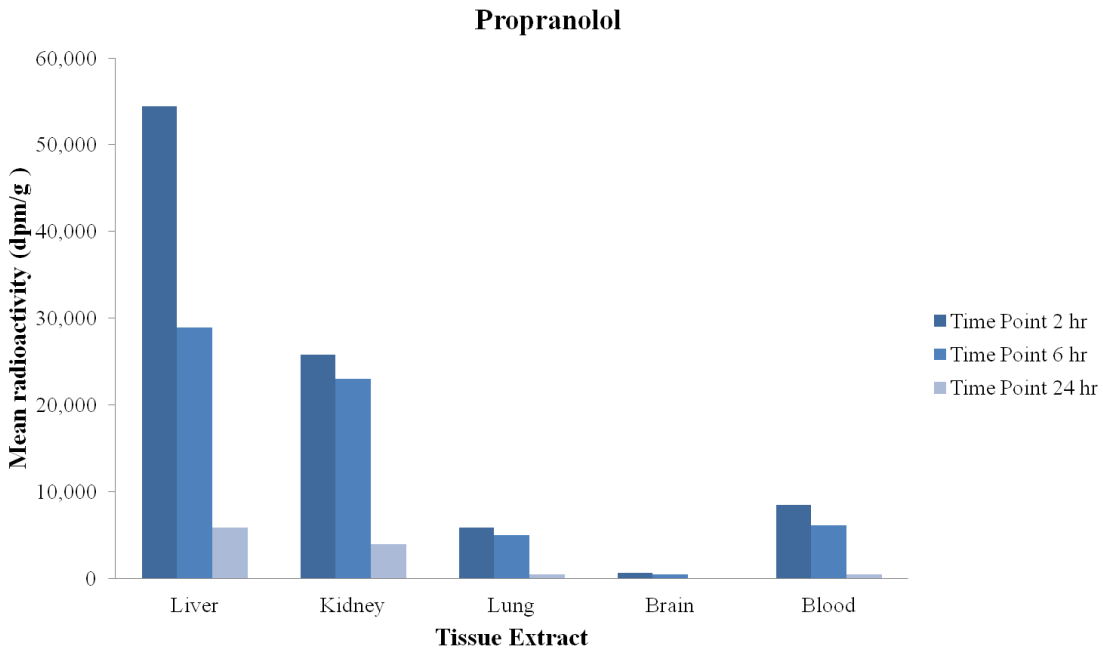

Figure 4.7 Mean radioactivity in propranolol dosed tissue extract following methanol extraction.

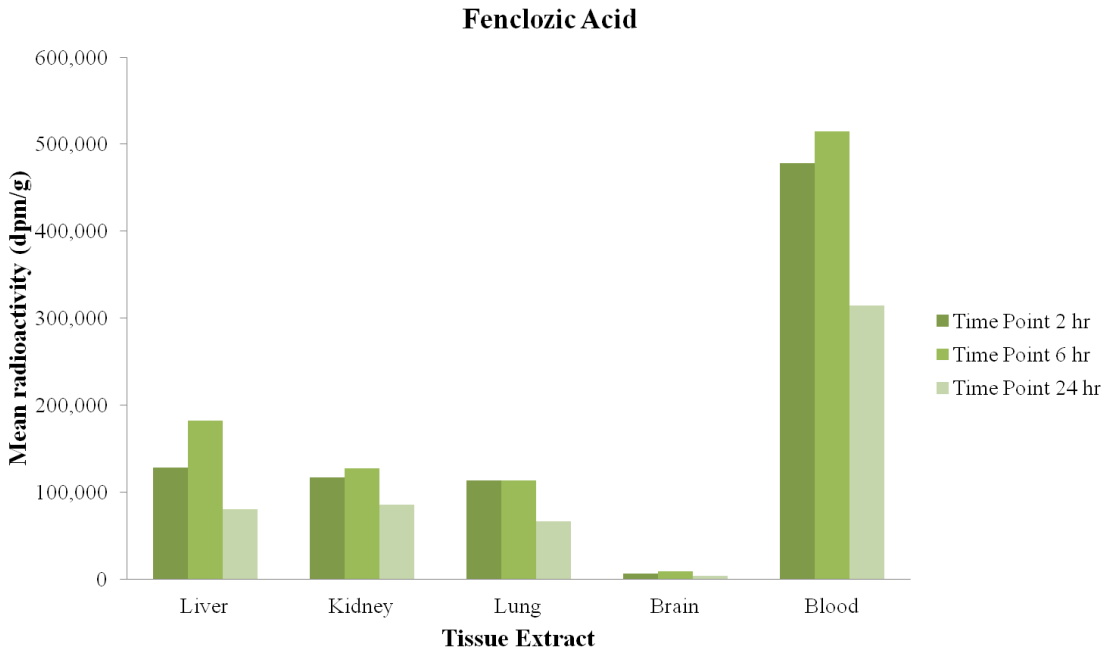

Figure 4.8 Mean radioactivity in fenclozic acid dosed tissue extract following methanol extraction.

These results show a similar overall distribution of radioactivity to the original homogenates. Overall levels of radioactivity per gram are lower and radioactivity levels in the propranolol extracts are lower than that of the fenclozic acid extracts. These results give a good indication of where radiolabelled drug-related material might be found at each time point. This is useful for MALDI or LESA profiling experiments where an organ is targeted for analysis in order to detect parent drug compound or a metabolite.

For metabolite identification approaches UPLC-MS measurements were used to identify metabolites from both drugs in the liver samples from each time point. Fractions were collected using a modified CTC fraction collector and radioactivity in each fraction measured to determine major retention time areas where radioactivity eluted from the UPLC separation. UPLC-MS detection was used for identification of the metabolites by mass spectrometry. Peak alignment between these two techniques allowed interrogation of the MS data to be guided by the peaks in the radiochromatogram (Athersuch, Sison et al. 2008) and gave an indication of relative amounts of each metabolite in the sample.

Attempts to produce a radioflow chromatogram for UPLC of propranolol metabolites by the same methodology were unsuccessful due to the very low radioactivity levels present in the tissue extracts.

4.4.1 UPLC-MS

Metabolite identification was performed using UPLC-MS as described in Chapter 2. Table 4.1 shows metabolites characterised from the propranolol-dosed tissue samples at each time point post-dose.

UPLC-MS/MS data of the hydroxylated glucuronide conjugate (*m/z* 452, RT 7.4 min) showed expected fragment ion transitions of *m/*z 452- *m/z* 276. This is characteristic of intact hydroxylated parent ion following the loss of the glucuronic acid moeity under collision induced dissociation (CID) conditions.

	2 hours post-dose				6 hours post-dose				24 hours post-dose			
	Liver	Lung	Kidney	Brain	Liver	Lung	Kidney	Brain	Liver	Lung	Kidney	Brain
Propranolol	NSR	✓	✓	✓	✓	✓	✓	✓	-	-	-	-
4-hydroxypropranolol	NSR	✓	✓	-	✓	✓	✓	-	-	-	-	-
4-hydroxypropranolol glucuronide	NSR	-	-	-	✓	✓	✓	-	✓	✓	✓	-

Table 4.1. Metabolites observed in selected propranolol-dosed samples.

'✓' = Detection of the metabolite.
'-' = No metabolite detected.
NSR = No sample received for metabolite characterisation.

A single metabolite was characterised from fenclozic acid-dosed samples using UPLC-MS; this had not been previously reported in published fenclozic acid metabolism studies. This metabolite was detected in the liver at 6 hours post-dose and was characterised as a taurine conjugate (*m/z* 361, RT 10.0 min.). Its structure is shown in Figure 4.9.

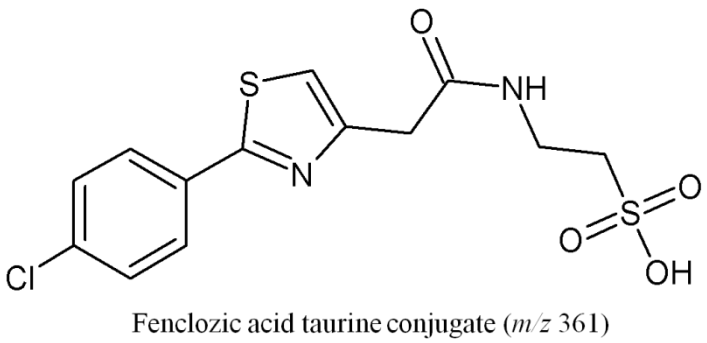

Figure 4.9 Structure of fenclozic acid taurine conjugate.

UPLC-MS/MS data of the taurine conjugate showed expected fragment ion transitions of *m/z* 361→ 254, *m/z* 361 → 236 and *m/z* 361 → 208. These transitions are characteristic of intact molecular ion having lost the taurine under collision induced dissociation (CID) conditions.

4.5 LESA profiling

Standards of both drug compounds were analysed by ESI-MS in order to optimise extraction solvents, ion mobility separation and MS/MS fragmentation parameters and to ascertain the most selective method for detection of these compounds in dosed tissue.

4.5.1 ESI-MS analysis of fenclozic acid standard

A solution of fenclozic acid standard was analysed using ESI-MS in positive ion mode. Protonated fenclozic acid was detected at *m/z* 254 as shown in Figure 4.10 (a), with a corresponding ^{37}Cl isotopic peak at 256 in a characteristic 3:1 ratio. The arrival time distribution through the ion mobility cell is also shown. Fragmentation of fenclozic acid (prior to ion mobility separation) results in the MS/MS spectrum shown in Figure 4.10 (b). Fenclozic acid loses a carboxylic acid side chain to form an intense fragment ion of *m/z* 208, with a corresponding ^{37}Cl isotope at *m/z* 210 in a 3:1 ratio.

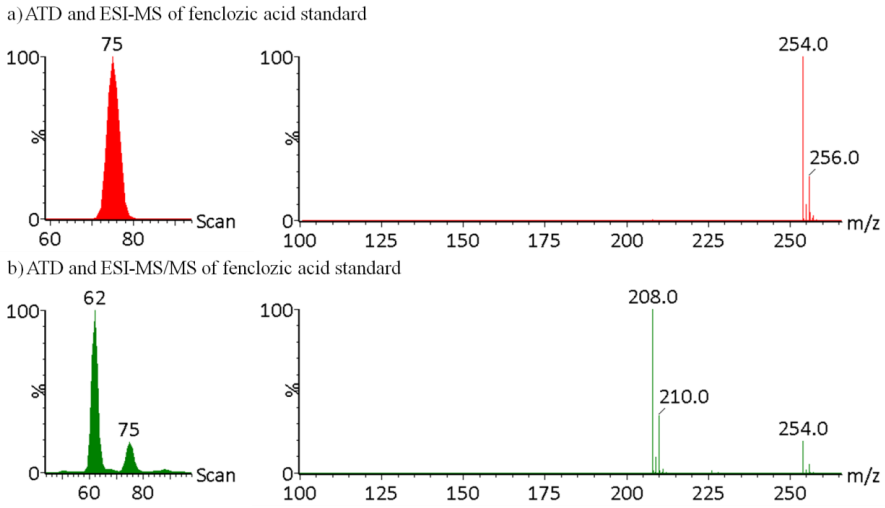

Figure 4.10 Analysis of fenclozic acid standard.
a) ATD and ESI-mobility-MS of fenclozic acid in positive ion mode.
b) ATD and ESI-mobility-MS/MS of fenclozic acid standard in positive ion mode.

A concentration series of fenclozic acid was spotted onto glass slides and control rat kidney tissue to assess the detection limits of the LESA technique on and off tissue. Each position spiked with drug standard was sampled by LESA and analysed using

nano ESI-mobility-MS/MS, with *m/z* 254 selected using the quadrupole (set to also allow through the ^{37}Cl isotope peaks) and with ion mobility separation following MS/MS fragmentation. Non-spiked positions of control tissue were also sampled as a negative control. Fenclozic acid was successfully detected from the glass slide by this method at the lowest amount of fenclozic acid dosed (2.5 pg on slide).

Figure 4.11 shows the mobility resolved MS/MS spectra across the concentration series on tissue. The assignment of the *m/z* 208 ion to fenclozic acid becomes less confident at less than 25 pg on tissue (e-f); with a lack of the ^{37}Cl ion at *m/z* 210 observable.

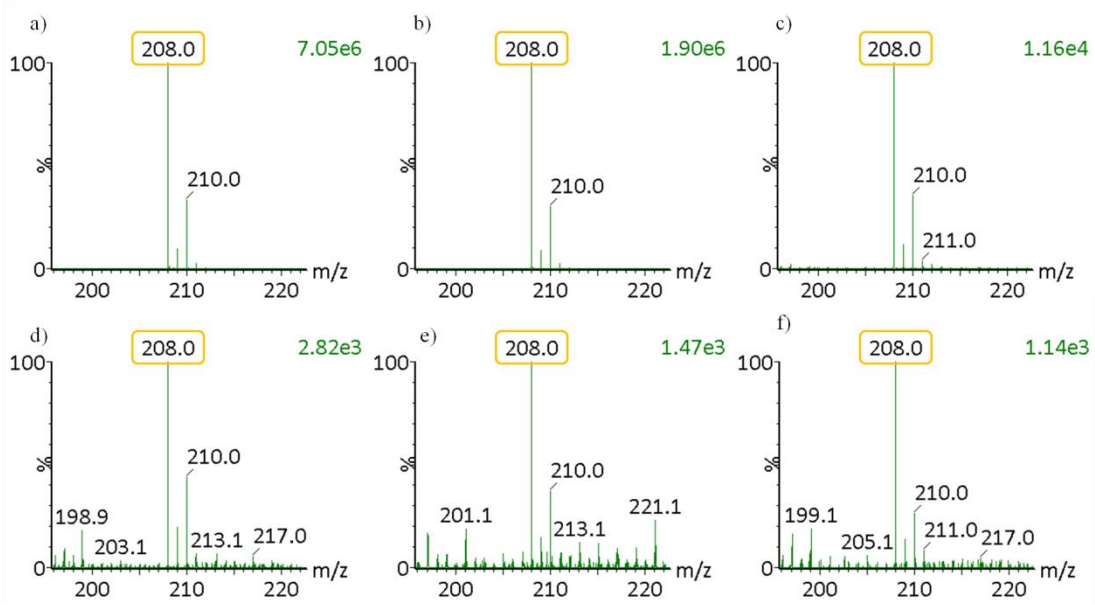

Figure 4.11 LESA-mobility-MS/MS spectra of fenclozic acid concentration series on tissue.
Fenclozic acid was spiked on control rat kidney tissue at **a)** 0.25 µg **b)** 25 ng **c)** 2.5 ng **d)** 250 pg **e)** 25 pg and **f)** 2.5 pg. The *m/z* 208 fragment ion is highlighted in yellow and total ion count for the zoomed spectra is displayed.

The signal intensity of the *m/z* 208 fragment ion at the four lowest concentrations of doped fenclozic acid was plotted against concentration in order to create a calibration curve shown in Figure 4.12. This demonstrates good linearity between the concentration of fenclozic acid and signal intensity when using LESA-mobility-MS/MS.

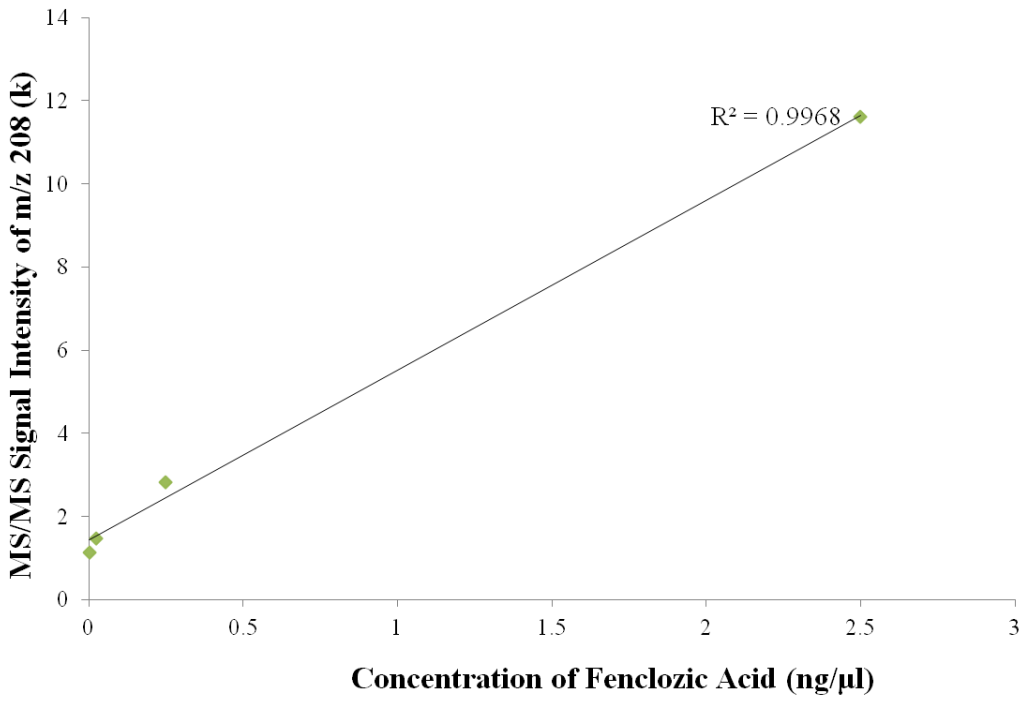

Figure 4.12 Calibration curve of fenclozic acid by LESA-MS/MS.
The signal intensity of the *m/z* 208 MS/MS fragment ion is plotted against a concentration series of fenclozic acid spotted on tissue.

4.5.2 LESA profiling of fenclozic acid dosed tissue sections

The LESA profiling method optimised above was used to sample dosed whole-body tissue sections at three time points post-dose. Liver, lung, kidney, brain and blood were sampled by LESA and analysed using nano ESI-mobility-MS/MS, with fragmentation of *m/z* 254 prior to ion mobility separation. These organs corresponded to those sampled in homogenisation experiments from replicate animals.

Figure 4.13 shows the ATD and LESA-mobility-MS/MS spectra of the *m/z* 208 fragment ion for each tissue at 2 hours post-dose. The *m/z* 208 fragment ion and corresponding ^{37}Cl isotope at *m/z* 210 can be seen confidently in every tissue sampled at this time point. The ATD of *m/z* 208 shows good correlation with that of fenclozic acid standard, allowing confident identification of fenclozic acid in all tissues sampled at 2 hours post-dose.

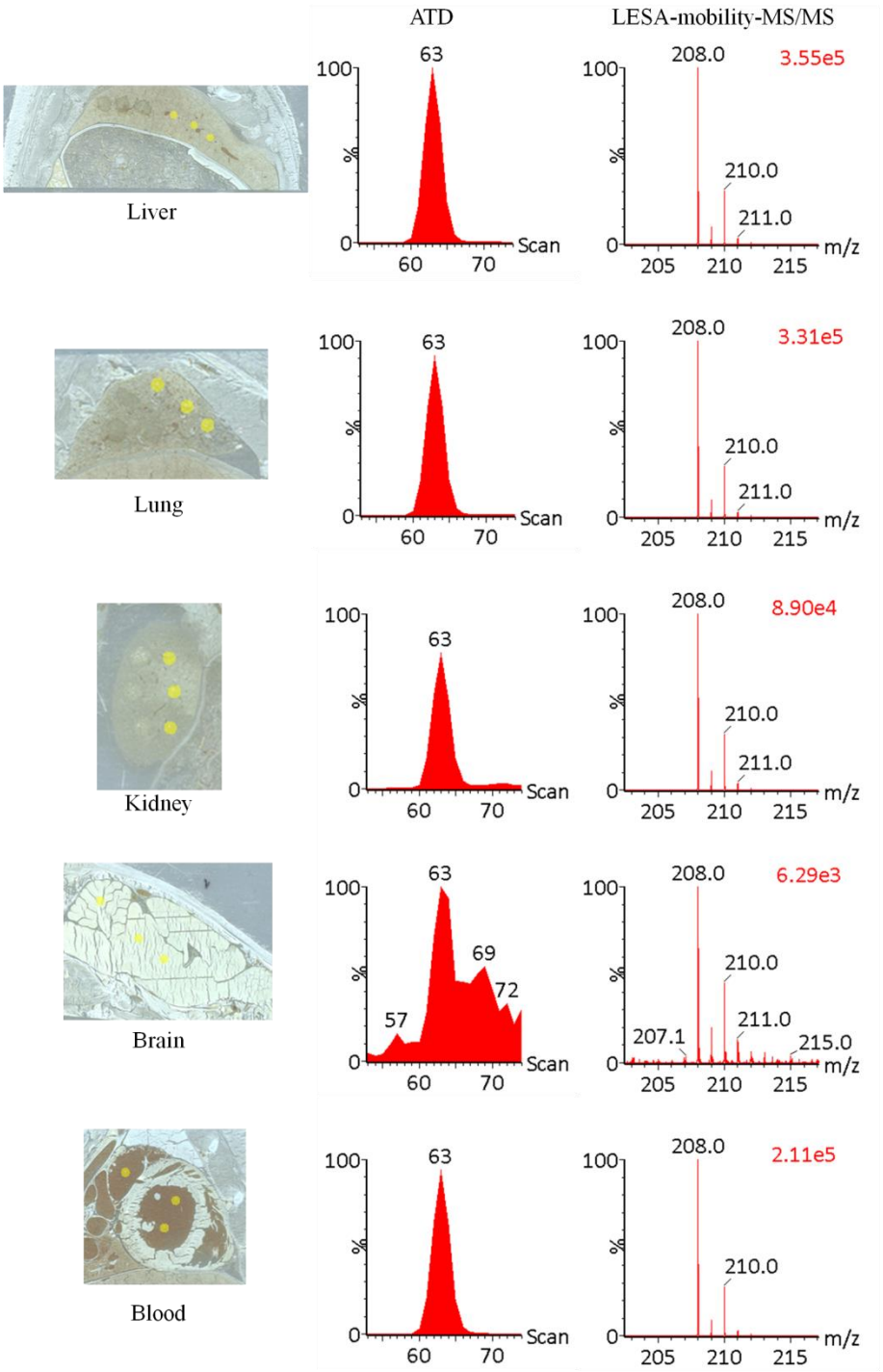

Figure 4.13 LESA-mobility-MS/MS profiling of fenclozic acid dosed rat organs 2 hours post-dose. The tissue sampling positions are indicated in yellow, alongside the extracted ATD and mobility-resolved MS/MS spectra of the fragment ion at *m/z* 208. Total ion counts for each of the zoomed spectra are displayed.

Figure 4.14 shows the ATD and LESA-mobility-MS/MS spectra of the *m/z* 208 fragment ion for each tissue at 6 hours post-dose. The *m/z* 208 fragment ion and corresponding ^{37}Cl isotope at *m/z* 210 can be seen confidently in every tissue. The

ATD of *m/z* 208 shows good correlation with that of fenclozic acid standard, in all tissues. The ATD peak has a lower intensity in brain than in the other tissues, however the mobility MS/MS spectrum clearly indicates the presence of fenclozic acid.

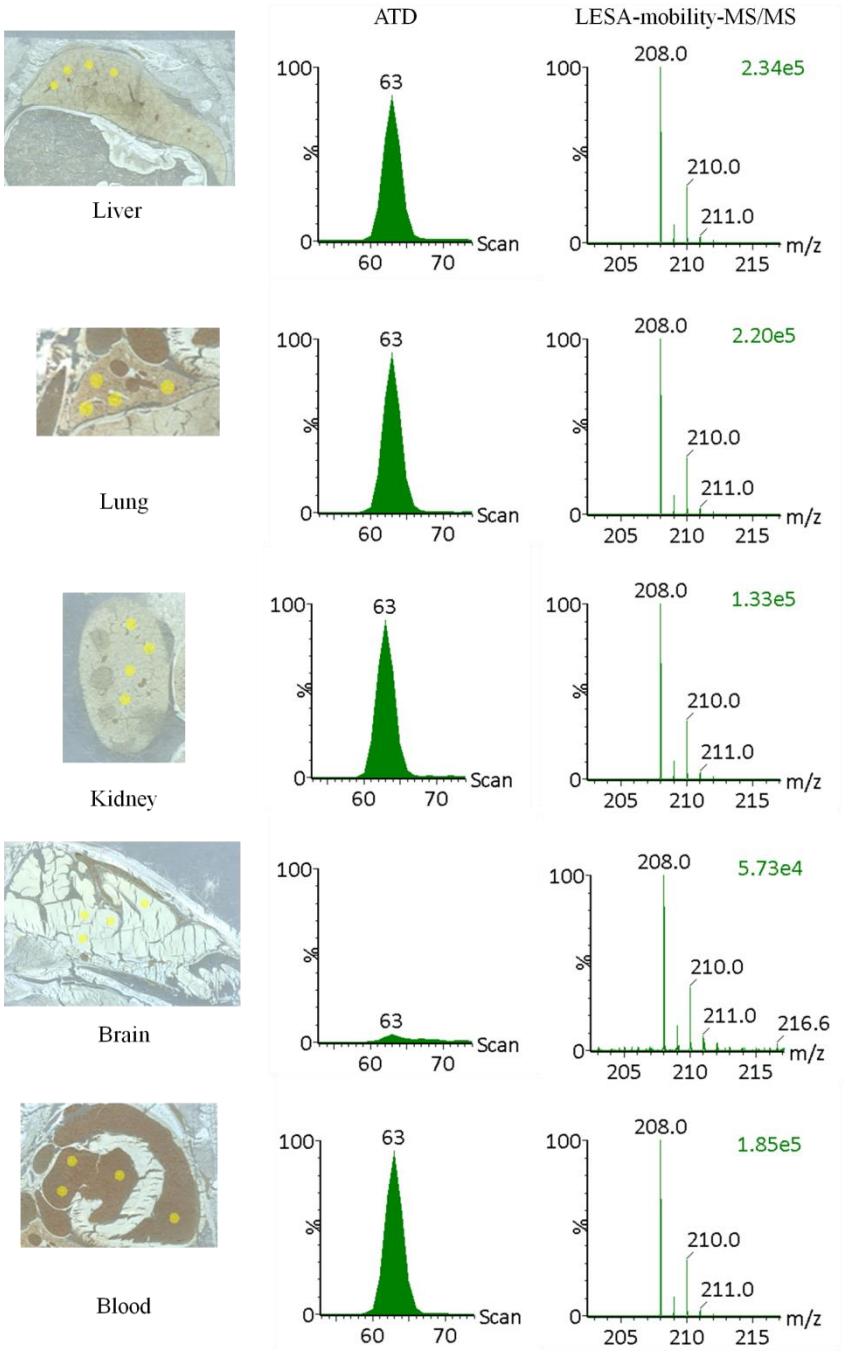

Figure 4.14 LESA-mobility-MS/MS profiling of fenclozic acid dosed rat organs 6 hours post-dose. The tissue sampling positions are indicated in yellow, alongside the extracted ATD and mobility-resolved MS/MS spectra of the fragment ion at *m/z* 208. Total ion counts for each of the zoomed spectra are displayed.

Figure 4.15 shows the ATD and LESA-mobility-MS/MS spectra of the *m/z* 208 fragment ion for each tissue at 24 hours post-dose. The *m/z* 208 fragment ion and corresponding ^{37}Cl isotope at *m/z* 210 are present in every tissue, with the exception of brain. Here, the 3:1 ratio between *m/z* 208 and 210 is not observed, and the ATD has too low an intensity to allow fenclozic acid to be assigned confidently in brain at 24 hours.

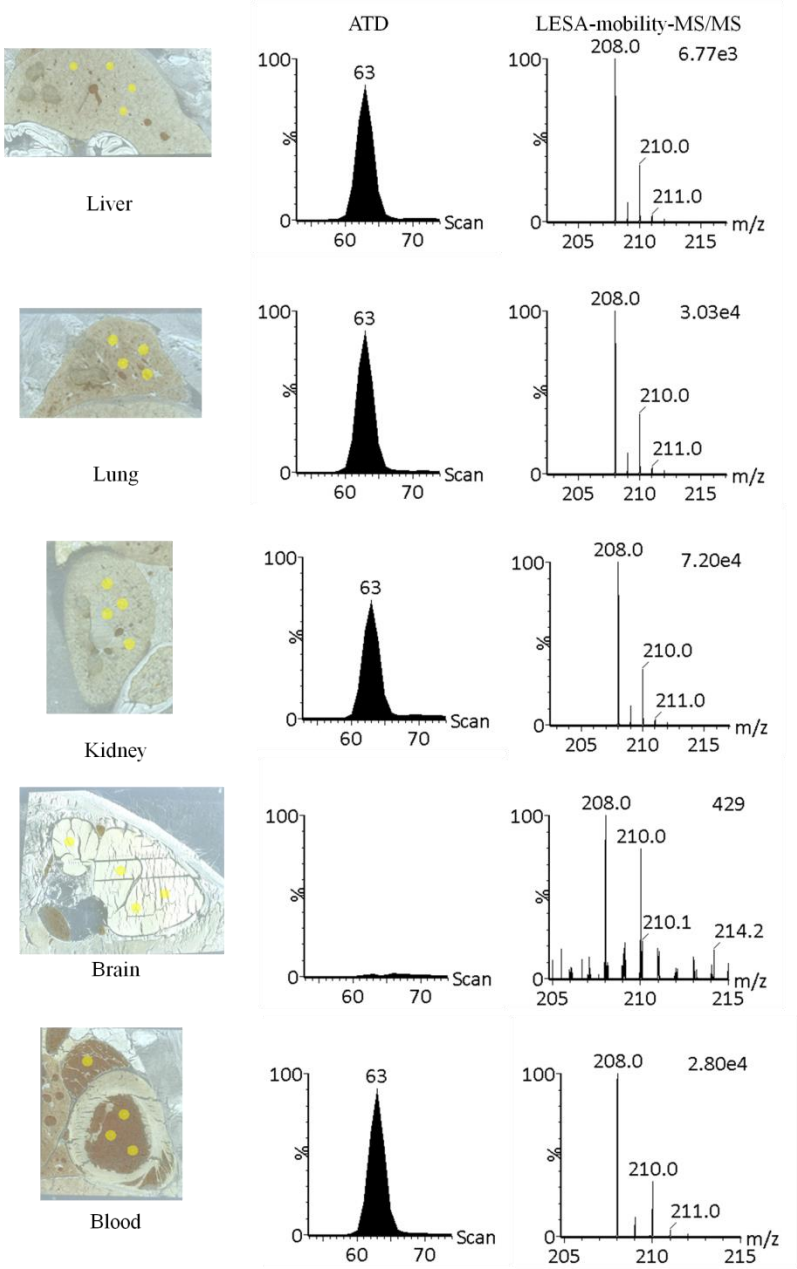

Figure 4.15 LESA-mobility-MS/MS profiling of fenclozic acid dosed rat organs 24 hours post-dose. The tissue sampling positions are indicated in yellow, alongside the extracted ATD and mobility-resolved MS/MS spectra of the fragment ion at *m/z* 208. Total ion counts for each of the zoomed spectra are displayed.

The ATD of *m/z* 208 in the other tissues demonstrates a good correlation with that of fenclozic acid standard. Fenclozic acid can be confidently detected by LESA profiling in liver, lung, kidney and blood 24 hours following administration of the drug.

4.5.3 Detection of fenclozic acid metabolites by LESA-MS

UPLC-MS/MS experiments identified only one metabolite of fenclozic acid in the liver extracts at each of the time points. This metabolite is a taurine conjugate of fenclozic acid, with *m/z* 361. LESA-mobility-MS/MS profiling was used to detect this metabolite in the fenclozic acid dosed liver sections at 2, 6 and 24 hours post-dose. Attempts to detect the taurine conjugate were unsuccessful at all three time points in liver using the LESA profiling approach.

4.5.4 ESI-MS analysis of propranolol standard

A solution of propranolol standard was analysed by ESI-MS using positive ion mode. Protonated propranolol was detected at *m/z* 260 as shown in Figure 4.16 (a). The arrival time distribution through the ion mobility cell is displayed. Fragmentation of propranolol (after ion mobility separation) results in the MS/MS spectrum shown in Figure 4.16 (b). This MS/MS spectrum matches a proposed fragmentation pathway of propranolol.

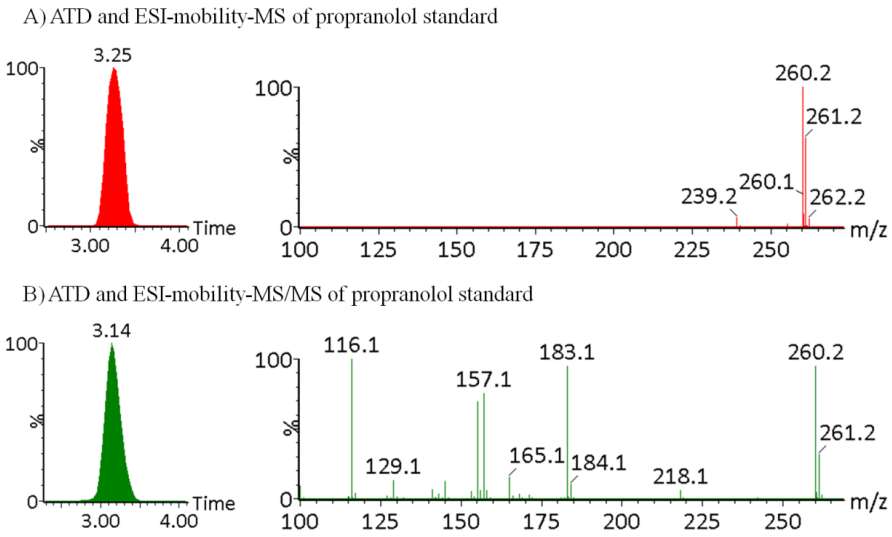

Figure 4.16 Analysis of propranolol standard.
a) ATD and ESI-mobility-MS of propranolol in positive ion mode.
b) ATD and ESI-mobility-MS/MS of propranolol in positive ion mode.

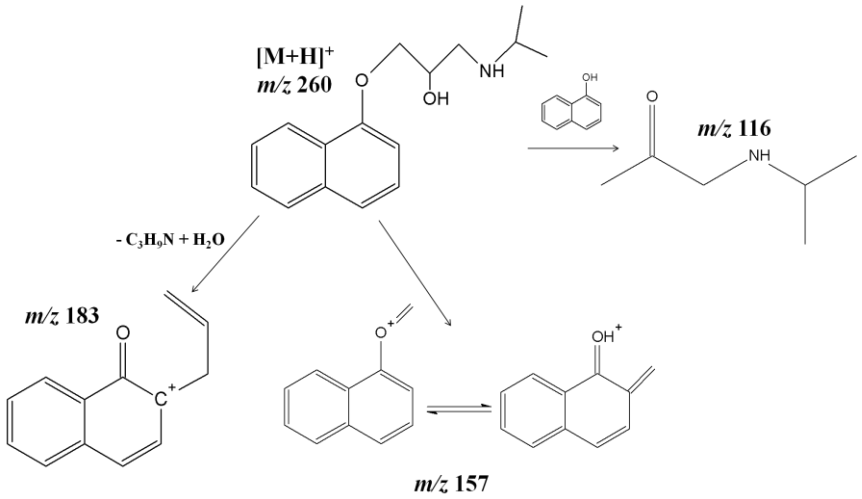

Figure 4.17 Fragmentation pathway of propranolol.
Adapted from Kertesz, Van Berkel *et al.* 2008.

A concentration series of propranolol was spotted onto glass slides and control rat kidney tissue to assess the detection limits of the LESA technique on and off tissue. Each position spiked with propranolol was sampled by LESA and analysed using nano ESI-mobility-MS/MS, with *m/z* 260 selected using the quadrupole. An ion mobility separation step was either included before or after MS/MS fragmentation. Propranolol was successfully detected from the glass slide at 25 pg on slide with ion mobility separation prior to MS/MS fragmentation. With mobility separation after fragmentation, propranolol could only be detected at 250 pg.

Using LESA-mobility-MS/MS with ion mobility separation prior to MS/MS fragmentation, the propranolol concentration series on tissue was sampled. Non-spiked positions of control tissue were also sampled as a negative control. Figure 4.18 shows the mobility resolved MS/MS spectra across the concentration series on tissue. At less than 25 ng on tissue propranolol could not be detected on tissue, showing a drop in detection limit on and off tissue.

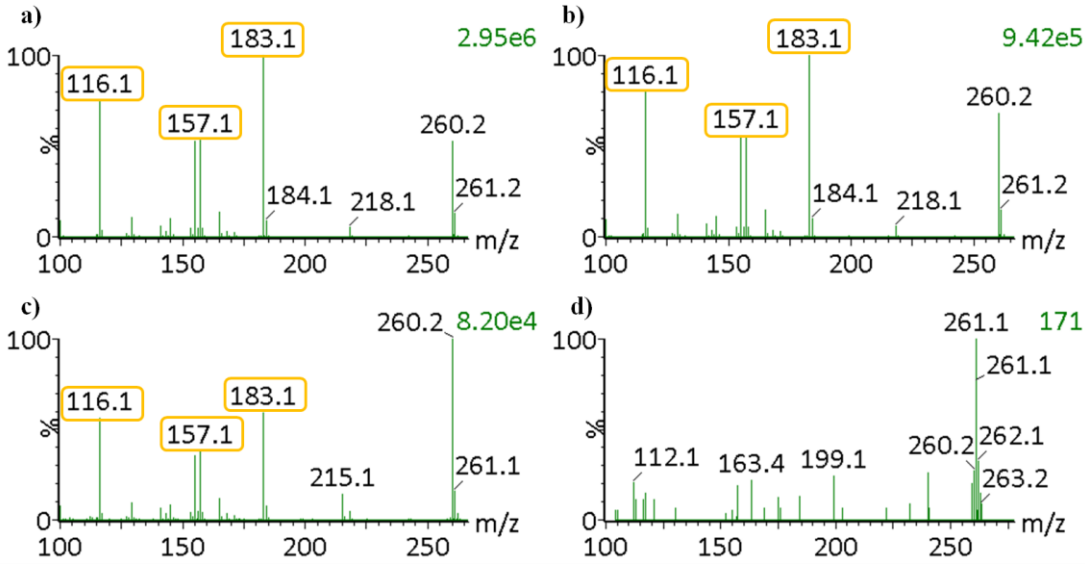

Figure 4.18 LESA-mobility-MS/MS spectra of propranolol concentration series on tissue.
Propranolol was spiked on control rat kidney tissue at a) 2.5 µg b) 0.25 µg c) 25 ng and d) 2.5 ng. The propranolol fragment ions at *m/z* 116, 157 and 183 are highlighted in yellow. The total ion count is displayed.

4.5.5 LESA profiling of propranolol dosed tissue sections

The LESA profiling method optimised above was used to sample dosed whole-body tissue sections at three time points post-dose. Liver, lung, kidney, brain and blood were sampled by LESA and analysed using nano ESI-mobility-MS/MS, with fragmentation of *m/z* 260 after ion mobility separation.

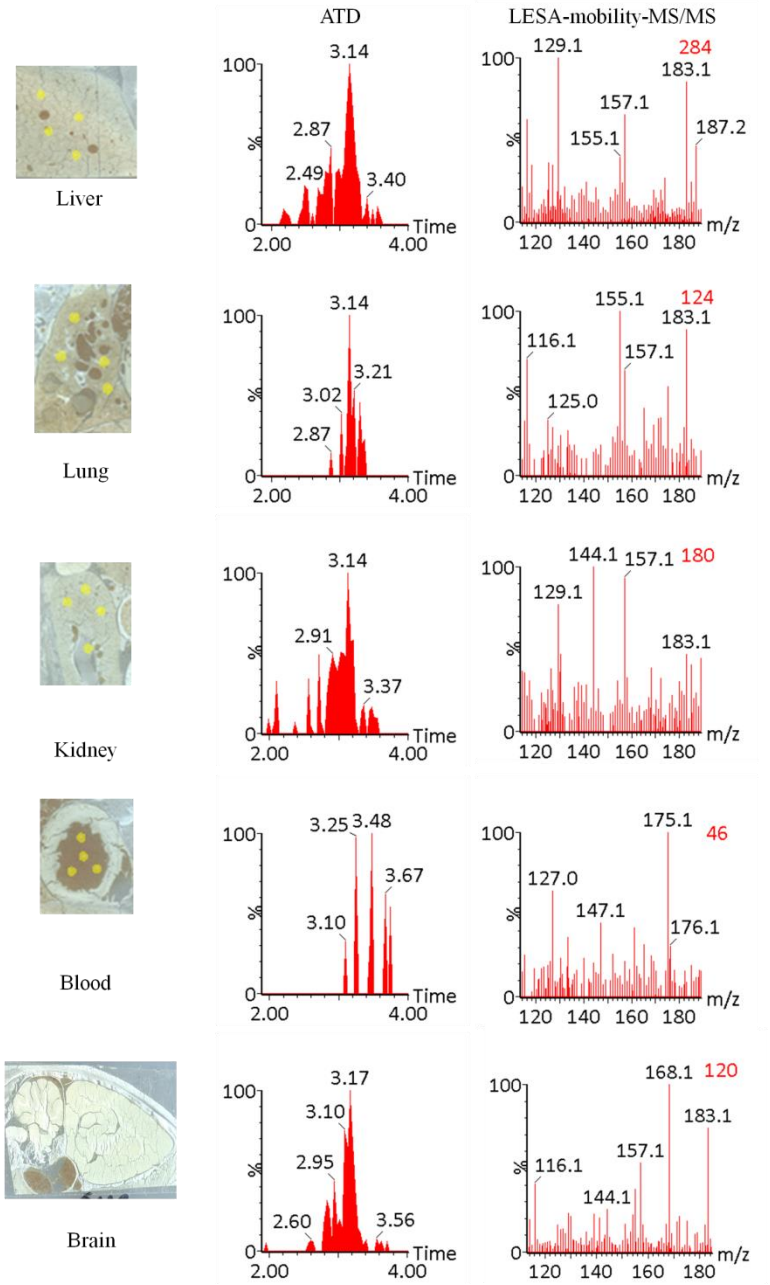

Figure 4.19 LESA-mobility-MS/MS profiling of propranolol dosed rat 2 hours post-dose. Tissue sampling positions are indicated in yellow, alongside extracted ATD of the fragment ion at *m/z* 183 and mobility-resolved MS/MS spectra (*m/z* 115-185 zoom). Total ion counts for each of the zoomed spectra are displayed.

Figure 4.19 shows the ATD and LESA-mobility-MS/MS spectra from fragmentation of a selected *m/z* 260 ion for each tissue at 2 hours post-dose. Extracted ATDs are shown for the propranolol fragment ion at *m/z* 183. MS/MS spectra are shown for the region *m/z* 115-185, where propranolol fragment ions should be found at *m/z* 116, 157 and 183. The extracted ATDs for liver, lung and kidney demonstrate a similar arrival time to that of the parent drug *m/z* 260 ion from the propranolol standard. These ATDs are poorly defined, however, indicating a very low abundance of the ion of interest. MS/MS spectra for all tissues sampled suffer from high background noise, despite using ion mobility to select for the ions of interest. Propranolol fragment ions at *m/z* 116, 157 and 183 can be observed in the MS/MS spectra for liver, lung, kidney and brain. The MS/MS data suggests that propranolol can be detected from these organs at 2 hours post-dose, but the results are less definitive than for fenclozic acid. Propranolol could not be detected in the blood at 2 hours post-dose using LESA.

LESA-mobility-MS/MS was used to sample the liver, kidney, lung and brain in the 6 and 24 hour post-dose tissue sections. Propranolol was identified in the liver and lung at 6 hours post-dose, but not in the kidney or brain. None of the organs sampled at 24 hours post-dose indicated the presence of propranolol.

LESA-mobility-MS/MS was able to detect parent propranolol in some of the organs at 2 hours post-dose. Detection of propranolol was not as confident as that for fenclozic acid, administered at the same dosage. LESA experiments to determine the on-tissue detection limit for each compound show that fenclozic acid can be detected at much lower levels than propranolol. This may in part, account for the less confident detection of propranolol in the dosed tissue sections. Propranolol is known to be metabolised extensively in the liver by first-pass metabolism following oral administration of the drug. This prevents the parent drug from reaching the circulatory system and may help explain a lack of parent compound available in the tissues.

4.5.6 Detection of propranolol metabolites by LESA-MS

To determine if propranolol could not be detected because of extensive metabolism, LESA-mobility-MS/MS profiling was used to sample for known metabolites of propranolol. Two major metabolites of propranolol in rat are 4-hydroxypropranolol and 4-hydroxypropranolol glucuronide (Hayes and Cooper 1971; Baughman, Talarico et al. 2009). The structures of these two metabolites are shown in Figure 4.20.

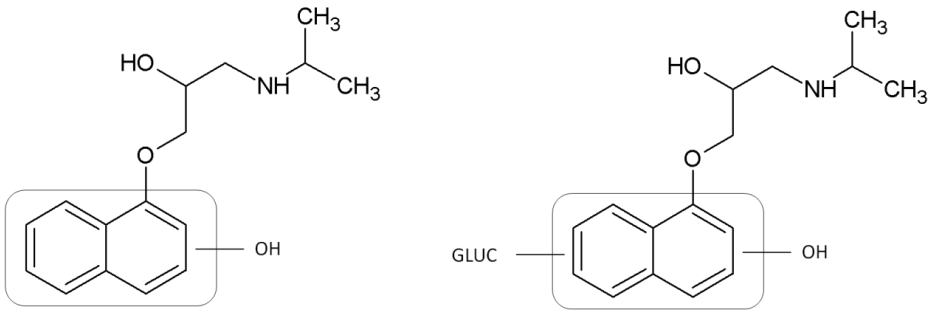

Figure 4.20 Structures of two propranolol metabolites; 4-hydroxypropranolol and 4-hydroxypropranolol glucuronide.

LESA-mobility-MS was used to sample propranolol-dosed liver at 2 hours post-dose. Data were interrogated post-acquisition to search for the two metabolites. Two ions of *m/z* 276 and 452 were detected in the full scan experiment. LESA-mobility-MS/MS experiments were subsequently used to confirm the identities of the two metabolites. Ion mobility separation was performed prior to MS/MS fragmentation with the same conditions as that for parent propranolol. Figure 4.21 shows the extracted ATD and LESA-mobility-MS/MS spectrum of *m/z* 276 (4-hydroxypropranolol).

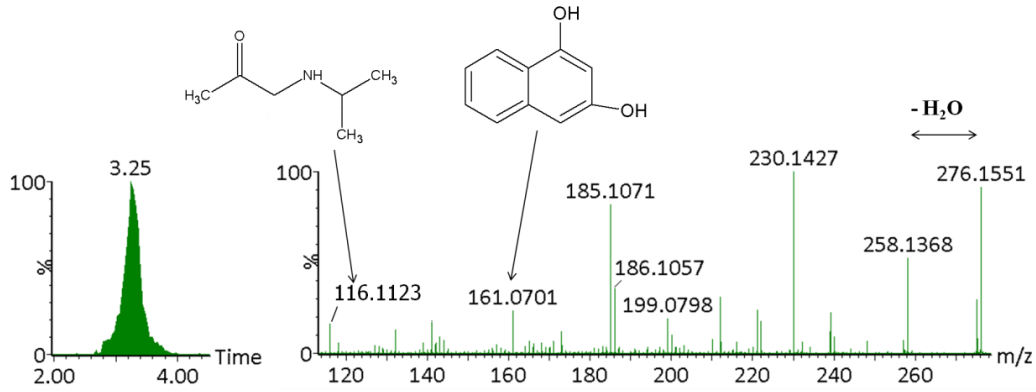

Figure 4.21 Extracted ATD and LESA-mobility-MS/MS of *m/z* 276 from propranolol liver sample 2 hours-post dose.

Despite using ion mobility separation post-acquisiton to help clean up the selection, the resulting MS/MS spectum observed is complex and contains unrelated ions due to isobaric interferences which were not resolved using ion mobility separation. A characteristic fragment ion at *m/z* 116 was used to putatively identify the *m/z* 276 ion as 4-hydroxypropranolol. The fragment ion at *m/z* 116 is a characteristic fragment ion that has previously been used to identify both parent propranolol and metabolites in tissue (Kertesz, Van Berkel et al. 2008). Without standards for the metabolites being available, it is not possible to compare this MS/MS spectrum to that of 4-hydroxypropranolol. Analysis of a metabolite standard would allow LESA profiling methods to be optimised for the metabolite of interest. This would also improve confidence in identification of the metabolite from tissue.

LESA profiling of the *m/z* 452 ion resulted in a more confident identification of a propranolol metabolite. Figure 4.22 shows the extracted ATD and LESA-mobility-MS/MS spectrum of *m/z* 452 (postulated as 4-hydroxypropranolol glucuronide). Fragmentation of *m/z* 452 resulted in an intense fragment ion at *m/z* 276 and two smaller fragment ions at *m/z* 116 and *m/z* 392.

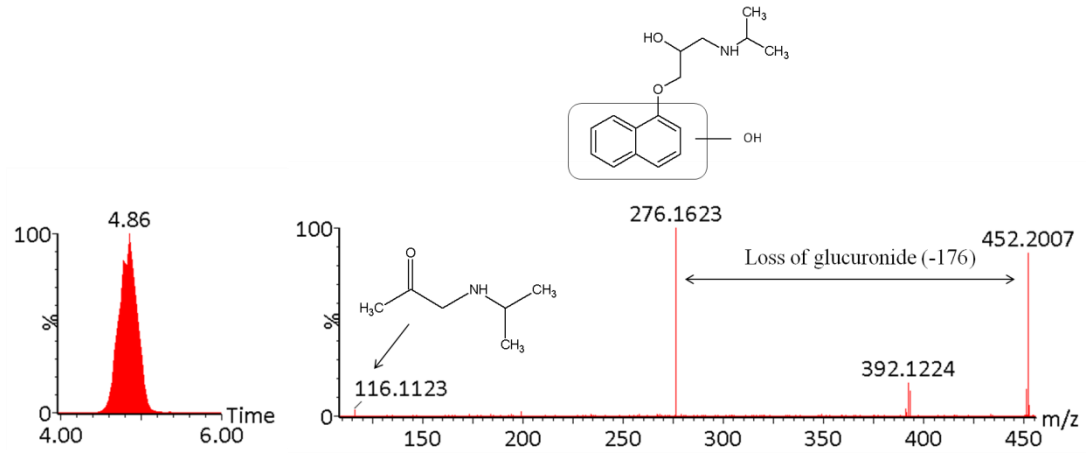

Figure 4.22 Extracted ATD and LESA-mobility-MS/MS of *m/z* 452 from propranolol liver 2 hours post-dose.

The *m/z* 276 fragment ion is formed via the neutral loss of 176 Da, which is characteristic of the loss of a glucuronide group. The 4-hydroxypropranolol glucuronide metabolite is a phase II metabolite formed via conjugation of a glucuronide group to the 4-hydroxypropranolol phase I metabolite. As such, the *m/z* 452 ion detected from tissue can be suggested to be the 4-hydroxypropranolol glucuronide metabolite, due to its MS/MS spectrum showing the loss of glucuronide to form a hydroxylated isomer of propranolol.

LESA-mobility-MS/MS profiling experiments were used to analyse the liver at 6 and 24 hours post-dose. The ATD and LESA-mobility-MS/MS spectra of *m/z* 452 are displayed in Figure 4.23 for propranolol dosed liver at 2, 6 and 24 hours.

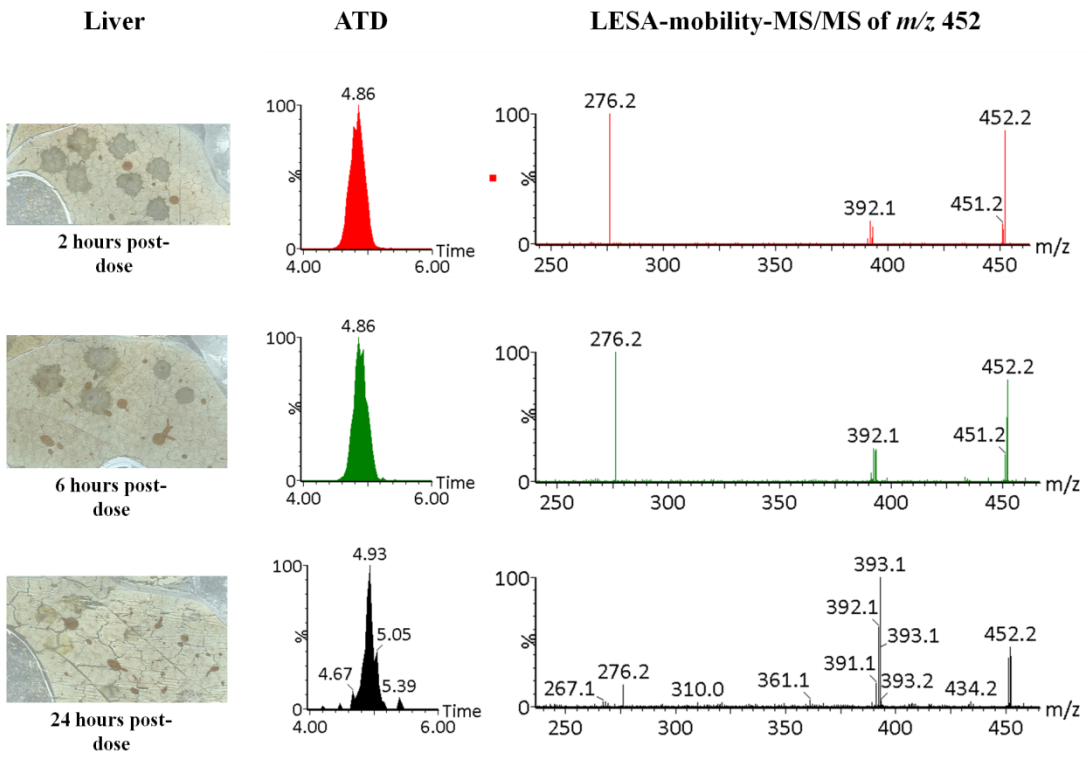

Figure 4.23 Extracted ATD and LESA-mobility-MS/MS profiling of 4-hydroxypropranolol glucuronide in dosed liver at 2, 6 and 24 hours post-dose.

At all three time points the 4-hydroxypropranolol glucuronide metabolite can be confidently identified using LESA profiling. LESA-mobility-MS/MS experiments were also successful in detecting the 4-hydroxypropranolol metabolite at 6 hours post-dose, but at 24 hours post-dose the metabolite could not be detected. The LESA profiling experiments were extended to the kidney, lung and brain at all three time points.

Table 4.2 summarises the LESA profiling results for liver, kidney, lung and brain at 2, 6 and 24 hours post-dose.

	2 hours post-dose				6 hours post-dose				24 hours post-dose			
	Liver	Lung	Kidney	Brain	Liver	Lung	Kidney	Brain	Liver	Lung	Kidney	Brain
Propranolol	✓	✓	✓	✓	✓	✓						
4-hydroxypropranolol	✓				✓	✓				✓		
4-hydroxypropranolol glucuronide	✓	✓	✓		✓	✓	✓		✓	✓	✓	

Table 4.2 Summary of LESA profiling of propranolol dosed tissue sections.
A ✓indicates presence of parent or metabolite; confirmed by MS/MS fragmentation.

Unchanged propranolol is only detected in the 2 and 6 hour tissue sections. At 2 hours post-dose propranolol is detected in the liver, lung, kidney and brain, albeit at low levels. The active phase I metabolite 4-hydroxypropranolol is only seen in liver and lung, whilst the glucuronide conjugate is also identified in the kidney. 4-hydroxypropranolol glucuronide is present in the liver, lung and kidney at 2, 6 and 24 hours post-dose.

These results, together with those from metabolite identification experiments support the hypothesis that parent propranolol was not detected due to extensive metabolism in the liver following oral administration.

4.6 MALDI profiling

MALDI-MS methods were optimised using fenclozic acid and propranolol standards to determine limits of detection and the most selective method for identification and localisation of these drug compounds in dosed tissue. These methods were subsequently used for MALDI profiling experiments to detect parent drug in dosed tissue samples.

4.6.1 MALDI-MS analysis of fenclozic acid

A solution of fenclozic acid standard was analysed by MALDI-MS using positive ion mode, prepared with CHCA matrix. As with ESI-MS experiments, protonated fenclozic acid was detected at *m/z* 254 with a corresponding Cl^{37} isotope at 256. MALDI-MS/MS of fenclozic acid resulted in a major fragment ion observed at *m/z* 208, with a corresponding chlorine isotope peak at *m/z* 210, showing good correlation with analysis using ESI-MS/MS.

Analysis of fenclozic acid by MALDI-MS/MS was repeated using an ion mobility separation step after MS/MS fragmentation. This method was used to sample across a concentration series of fenclozic acid on and off tissue, in order to determine the detection limit for fenclozic acid on tissue using MALDI. MALDI-mobility-MS/MS was successfully used to detect fenclozic acid on tissue at 250 fmol. The MS/MS spectrum of fenclozic acid at 250 fmol on tissue is shown in Figure 4.24, with and without ion mobility separation. Without the added selectivity of the ion mobility separation following MS/MS fragmentation, fenclozic acid cannot be confidently detected at this concentration.

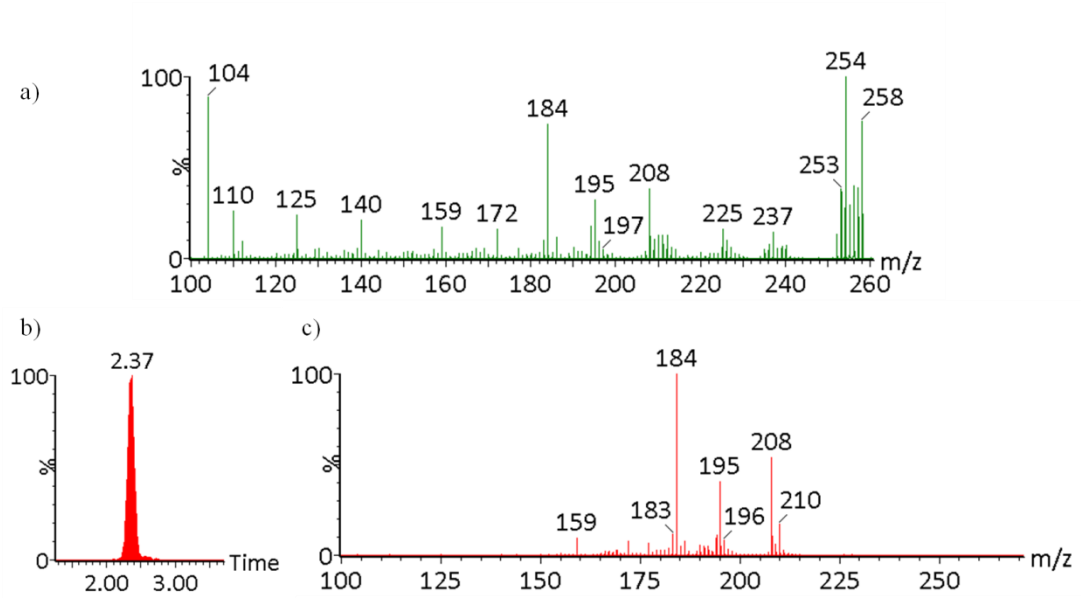

Figure 4.24 MALDI-MS/MS fragmentation of 250 fmol fenclozic acid standard spiked on tissue.
a) MALDI-MS/MS spectra of fenclozic acid on tissue (no mobility).
b) ATD of *m/z* 208 fragment ion.
c) MALDI-mobility-MS/MS spectra of fenclozic acid.

4.6.2 Detection of fenclozic acid in dosed tissue sections

The potential applicability of this selective method for the detection of parent drug compound in dosed tissue samples was tested. Matrix was spotted in discrete regions of dosed whole-body tissue samples. This matrix spot was analysed using MALDI-mobility-MS/MS imaging with ion mobility separation following MS/MS fragmentation.

The sample with the most radioactivity, identified by homogenisation and oxidiser experiments, was selected for initial MALDI profiling experiments. For fenclozic acid dosed tissues, this was the liver of the 6 hour post-dose tissue sample. Matrix was spotted at discrete locations onto 30 µm thick whole-body tissue sections. The parent ion at *m/z* 254 was selected for MS/MS fragmentation, followed by mobility separation. Figure 4.25 shows the extracted ATD of the resulting *m/z* 208 fragment ion and mobility resolved MS/MS spectra of *m/z* 254 from fenclozic acid dosed liver at 6 hours post-dose.

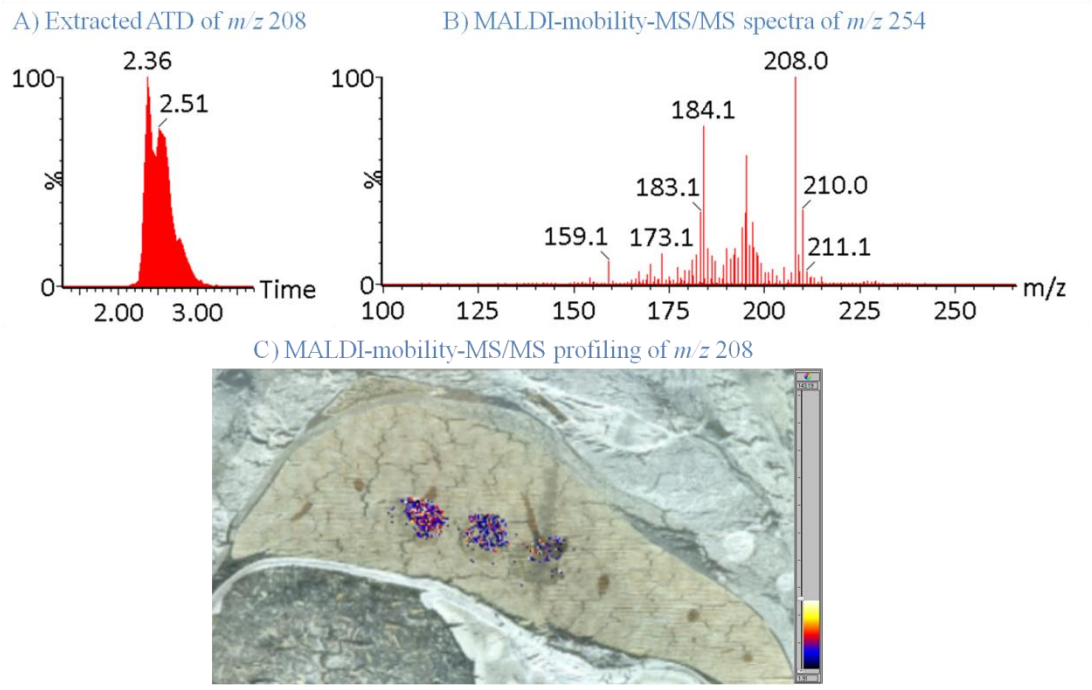

Figure 4.25 MALDI profiling of fenclozic acid dosed rat liver, 6 hours post-dose.
a) Extracted ATD of *m/z* 208 fragment ion.
b) MALDI-mobility-MS/MS spectra for *m/z* 254.
c) MALDI profiling of *m/z* 208 fragment ion on liver section.
Scale bar represents ion intensity, with white being highest and black the lowest.

The mobility resolved MS/MS spectrum shows the resulting fragment ion at *m/z* 208, along with the corresponding ^{37}Cl isotope peak at *m/z* 210. The arrival time distribution of the *m/z* 208 fragment ion is similar to that of the fenclozic acid standard, providing confirmation that fenclozic acid can be detected in dosed tissue sections. The MALDI profiling image shows the intensity of the *m/z* 208 fragment ion in the liver where matrix solution was spotted.

Following successful detection of fenclozic acid using MALDI profiling in the 6 hour post-dose liver sample, MALDI profiling was also used to detect fenclozic acid in the kidney, lung, brain and blood at each time point. The following MALDI profiling images (Figure 4.26, Figure 4.27 and Figure 4.28) show the distribution of the mobility resolved *m/z* 208 fragment ion in these tissues at 2 hours, 6 hours and 24 hours post-dose. Extracted ATDs and mobility resolved MS/MS spectra for each tissue are also shown.

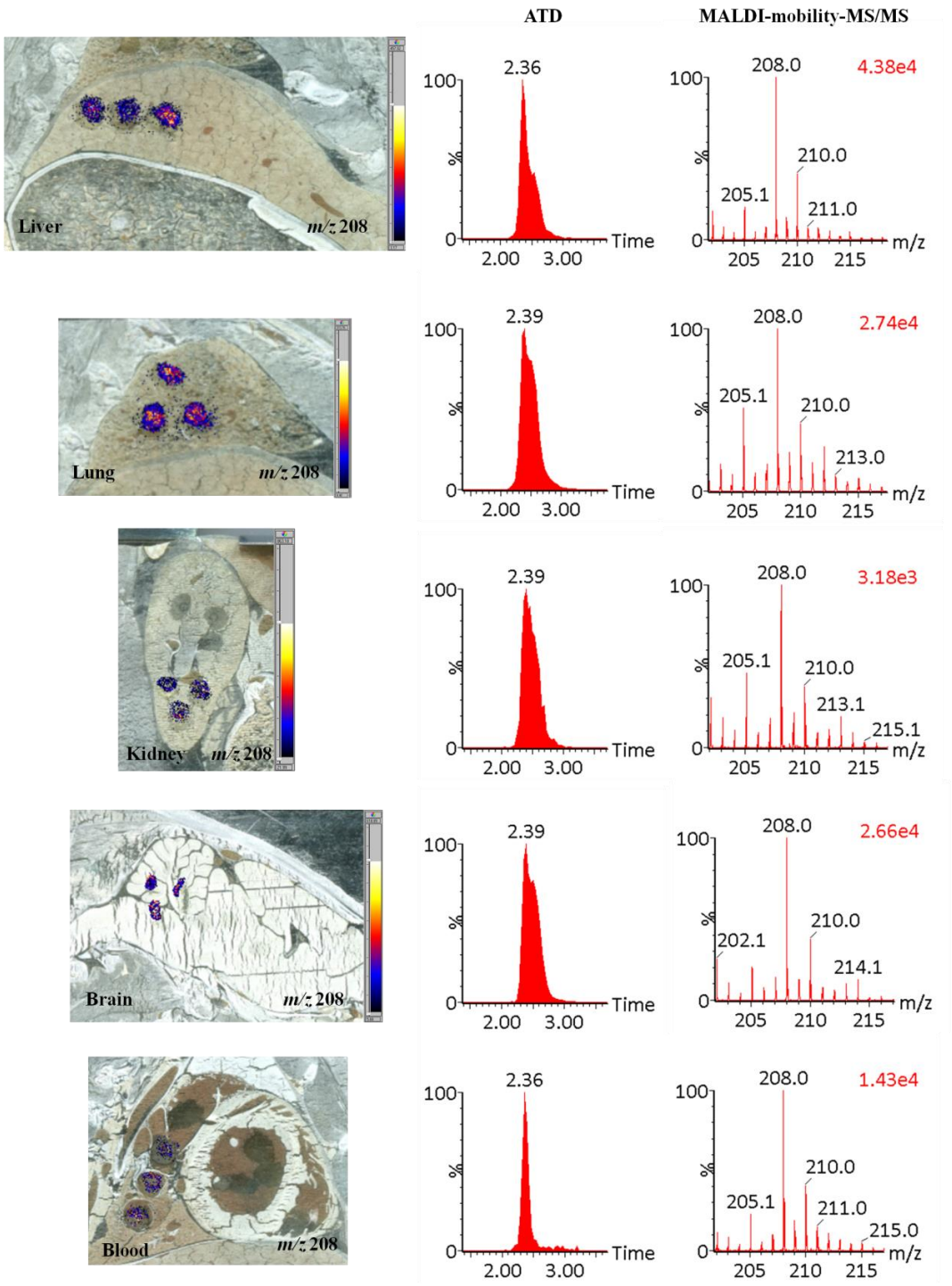

Figure 4.26 MALDI-mobility-MS/MS profiling of *m/z* 208 fragment ion of fenclozic acid 2 hours post-dose. Scale bar represents ion intensity, with white being highest and black the lowest. Total ion counts for each of the zoomed spectra are displayed.

Figure 4.26 shows the clear detection of fenclozic acid in all sampled tissues at 2 hours-post dose. The mobility resolved MS/MS spectra of the combined data for each organ shows clear detection of the *m/z* 208 fragment ion and the corresponding

^{37}Cl ion at *m/z* 210 in a 3:1 ratio. The ATD of *m/z* 208 in each of the tissues is displayed, showing a good correlation with that obtained from fenclozic acid standard. Profiling images of *m/z* 208 in the liver and lung appear to have a higher observable intensity than the other organs.

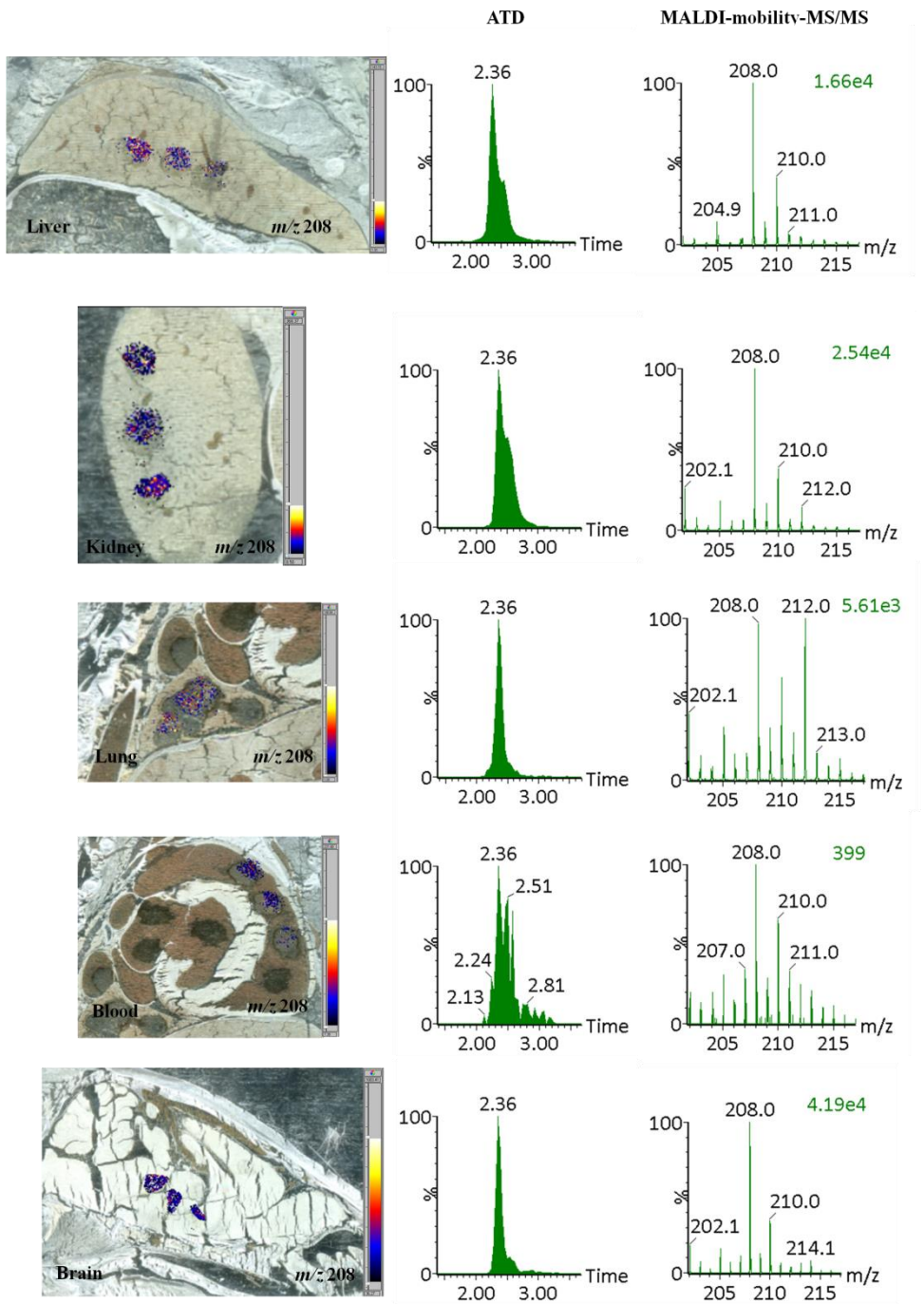

Figure 4.27 MALDI-mobility-MS/MS profiling of *m/z* 208 fragment ion of fenclozic acid 6 hours post-dose. Scale bar represents ion intensity, with white being highest and black the lowest. Total ion counts for each of the zoomed spectra are displayed.

Detection of fenclozic acid in the liver and kidney at 6 hours post-dose is shown in Figure 4.27. Here, the observable intensity of the profiled spots appear to be less intense than in the 2 hour samples, suggesting that lower levels of parent fenclozic acid are present in the 6 hour sample. Identification of fenclozic acid was confirmed by the presence of *m/z* 208 and 210 in the combined mobility resolved MS/MS spectra of all tissue samples 6 hours following administration.

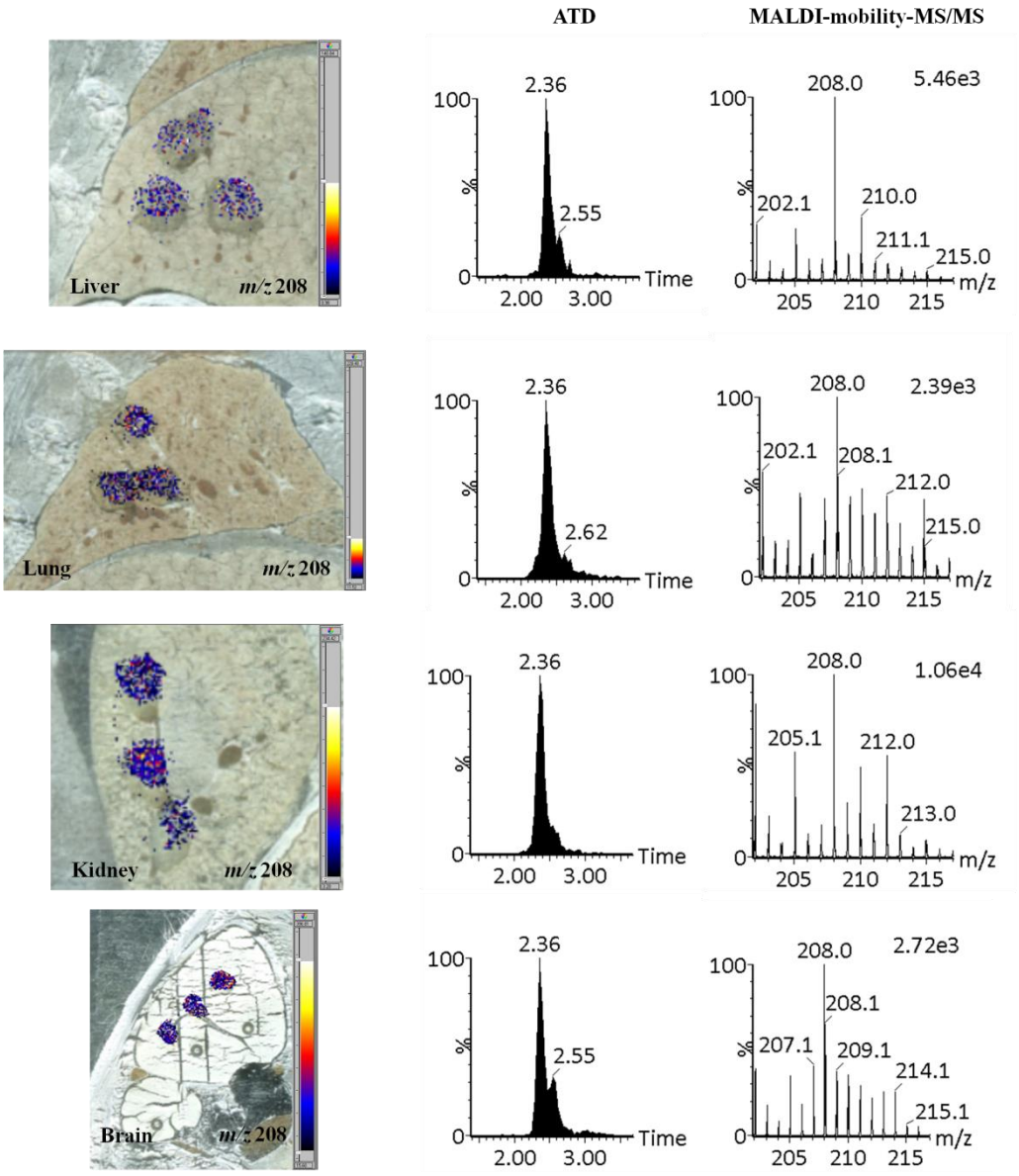

Figure 4.28 MALDI-mobility-MS/MS profiling of *m/z* 208 fragment ion of fenclozic acid 24 hours post-dose. Scale bar represents ion intensity, with white being highest and black the lowest. Total ion counts for each of the zoomed spectra are displayed.

In the 24 hour post-dose sections, Figure 4.28 shows detection of fenclozic acid using MALDI profiling and is supported by the combined MS/MS data with the presence of both *m/z* 208 and 210 observable in a 3:1 ratio. As with the 6 hour sample, the profiled spots appear to be less intense than for the 2 hour sample. Although the ATDs for each tissue suggest successful detection of fenclozic acid, the MS/MS spectra for lung and brain at 24 hours do not show the expected 3:1 ratio of *m/z* 208 and 210, and as such, fenclozic acid cannot be confidently identified in the lung and brain 24 hours following administration of the drug.

Successful detection of parent fenclozic acid using the MALDI-mobility-MS/MS method was achieved at all time points for the fenclozic acid dosed tissue sections. This indicates that MALDI imaging of fenclozic acid in organs of the dosed whole-body sections is possible at this dosage of fenclozic acid.

4.6.3 MALDI-MS analysis of propranolol standard

A solution of propranolol standard was analysed using MALDI-MS in positive ion mode, prepared with CHCA matrix. Protonated propranolol was detected at *m/z* 260, as in the ESI-MS experiments. MALDI-MS/MS of propranolol formed the same fragment ions as for ESI-MS, at *m/z* 116, 157 and 183 (data not shown).

Analysis of propranolol standard by MALDI-MS/MS was repeated with an ion mobility separation step included before and after MS/MS fragmentation. This method was used to sample across a concentration series of propranolol on and off tissue, in order to determine the detection limit on tissue by MALDI. Propranolol was successfully detected at 25 pg on target by MALDI-mobility-MS/MS with ion mobility separation either before or after fragmentation.

On tissue, MALDI-mobility-MS/MS was only successfully able to detect propranolol at 2.5 ng. Unlike the LESA profiling experiments, this was achieved using MS/MS fragmentation prior to ion mobility separation. This method was used for all following MALDI profiling experiments on dosed tissue.

4.6.4 Detection of propranolol in dosed tissue sections

The propranolol dosed sample identified to have the most radioactivity using homogenisation and oxidiser experiments, was the liver of the 2 hour post-dose tissue sample. This was selected for initial MALDI profiling experiments. The limit of detection for propranolol on tissue was previously ascertained to be 2.5 ng on tissue. Matrix was spotted discretely onto 30 µm thick whole-body tissue sections. The parent ion at *m/z* 260 was selected for MS/MS fragmentation, followed by mobility separation. From optimisation experiments on propranolol standard, the most selective method follows the MS/MS transition *m/z* 260 → 183, using an ion mobility separation step to improve selectivity.

Figure 4.29 shows the mobility extracted MS/MS spectra of the *m/z* 260 → 183 transition from MALDI profiling of the 2 hour liver sample. Although an ion at *m/z* 183 can be observed, it is of very low intensity in a noisy region of the spectrum and so cannot be confidently identified as propranolol. No ion at *m/z* 116 was observed in the MS/MS spectrum.

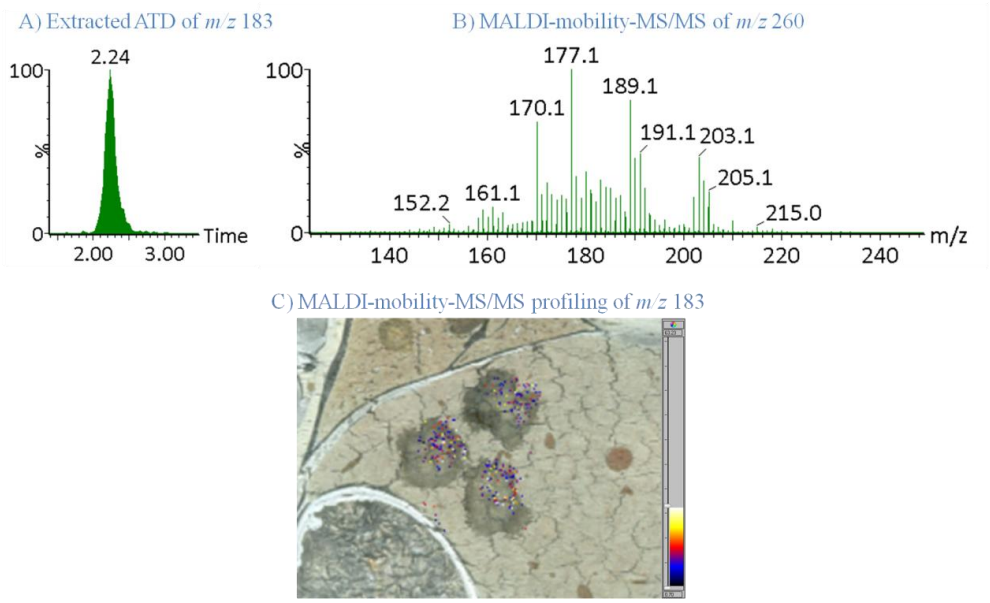

Figure 4.29 MALDI profiling of propranolol dosed rat liver, 2 hours post-dose.
a) Extracted ATD of *m/z* 183 fragment ion.
b) MALDI-mobility-MS/MS spectra for *m/z* 260.
c) MALDI profiling of *m/z* 183 fragment ion on liver section.
Scale bar represents ion intensity, with white being highest and black the lowest.

MALDI-mobility-MS/MS was used to profile the liver, kidney and lung at each time point for propranolol dosed tissues. In all experiments, identification of parent propranolol was unsuccessful, and showed similar results to the 2 hour liver sample above.

4.6.4.1 Detection of propranolol metabolites

A MALDI-mobility-MS/MS profiling approach was used to try to detect propranolol metabolites in dosed liver sections at each time point. As with the LESA profiling results, the metabolites targeted were 4-hydroxypropranolol and 4-hydroxypropranolol glucuronide; selecting *m/z* 276 and 452 for MS/MS fragementation respectively.

Figure 4.30 shows the MALDI-mobility-MS/MS spectrum of *m/z* 452 from the 2 hour liver sample.

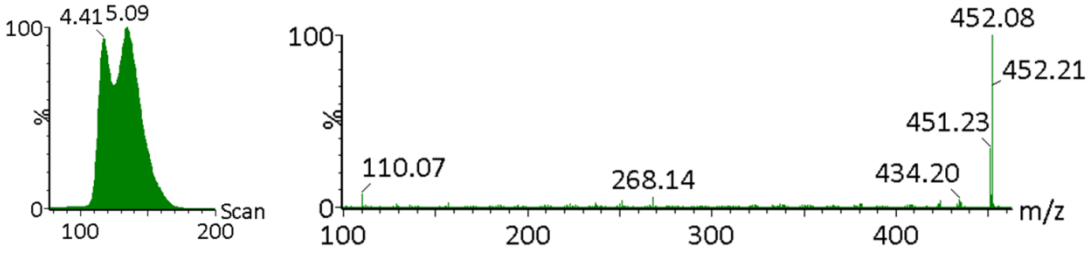

Figure 4.30 ATD and MALDI-mobility-MS/MS spectra of *m/z* 452 from liver 2 hours post-dose.

Although a precursor ion at *m/z* 452 is selected, the resulting MS/MS spectrum does not contain the characteristic *m/z* 276 fragment ion from the loss of the glucuronide group. The ATD also shows a different distribution to that of the 4-hydroxypropranolol glucuronide metabolite identified by LESA profiling experiments. Similar results were seen at 6 and 24 hours post-dose; with the glucuronide conjugate unable to be detected from tissue using the MALDI profiling approach.

MALDI profiling of the 4-hydroxypropranolol metabolite was also unsuccessful at all three time points in liver. Precursor ions were present at *m/z* 276, however the

resulting MS/MS spectra and ATD did not indicate the presence of 4-hydroxypropranolol. In contrast with the parent drug compound, where standards were used to determine the most selective method for detection, standards for the metabolites were not available. As such, it was not possible to confirm whether the lack of detection by MALDI profiling here is due to of low levels of metabolites being present in the tissue or if there are limitations with the matrix or detection method used.

4.7 MALDI imaging

MALDI profiling experiments showed the successful detection of fenclozic acid parent in dosed whole-body tissues at each of the three time points. MALDI imaging was evaluated for the ability to produce distribution images of parent fenclozic acid across different time points. Neither propranolol nor its metabolites were detected in dosed tissue using the MALDI profiling approach. As such, it is unlikely that a MALDI imaging experiment would be effective at this dose of parent compound and so attempts to localise propranolol in dosed tissue sections by MALDI were not performed.

4.7.1 Localisation of fenclozic acid in dosed tissue sections

MALDI imaging was evaluated for localisation of the parent fenclozic acid compound in the dosed tissues at different time points. The more selective MALDI-mobility-MS/MS approach was used, fragmenting the parent *m/z* 254 ion prior to ion mobility separation. The liver was selected for imaging experiments since it had the highest measured levels of radioactivity. A large area incorporating tissue surrounding the liver was selected for MALDI imaging. The distributions of the resulting *m/z* 208 fragment ion from liver at each of the time points are displayed in Figure 4.31. The area of the image corresponding to that of the liver is outlined in red for clarity.

These results show clear localisation of fenclozic acid in the liver at 2 and 6 hours post-dose. Fenclozic acid appears to be localised towards one side of the liver, and this localisation is more pronounced at 6 hours post-dose. The relative intensity of fenclozic acid at 6 hours is also higher at this time point. This could correlate with the higher radioactivity levels measured in liver homogenate and extracts at the 6 hour time point.

At 24 hours post-dose this localisation of fenclozic acid is less clear. A small degree of localisation is observed towards the top of the liver, showing a distribution very different to that of the 2 and 6 hour samples.

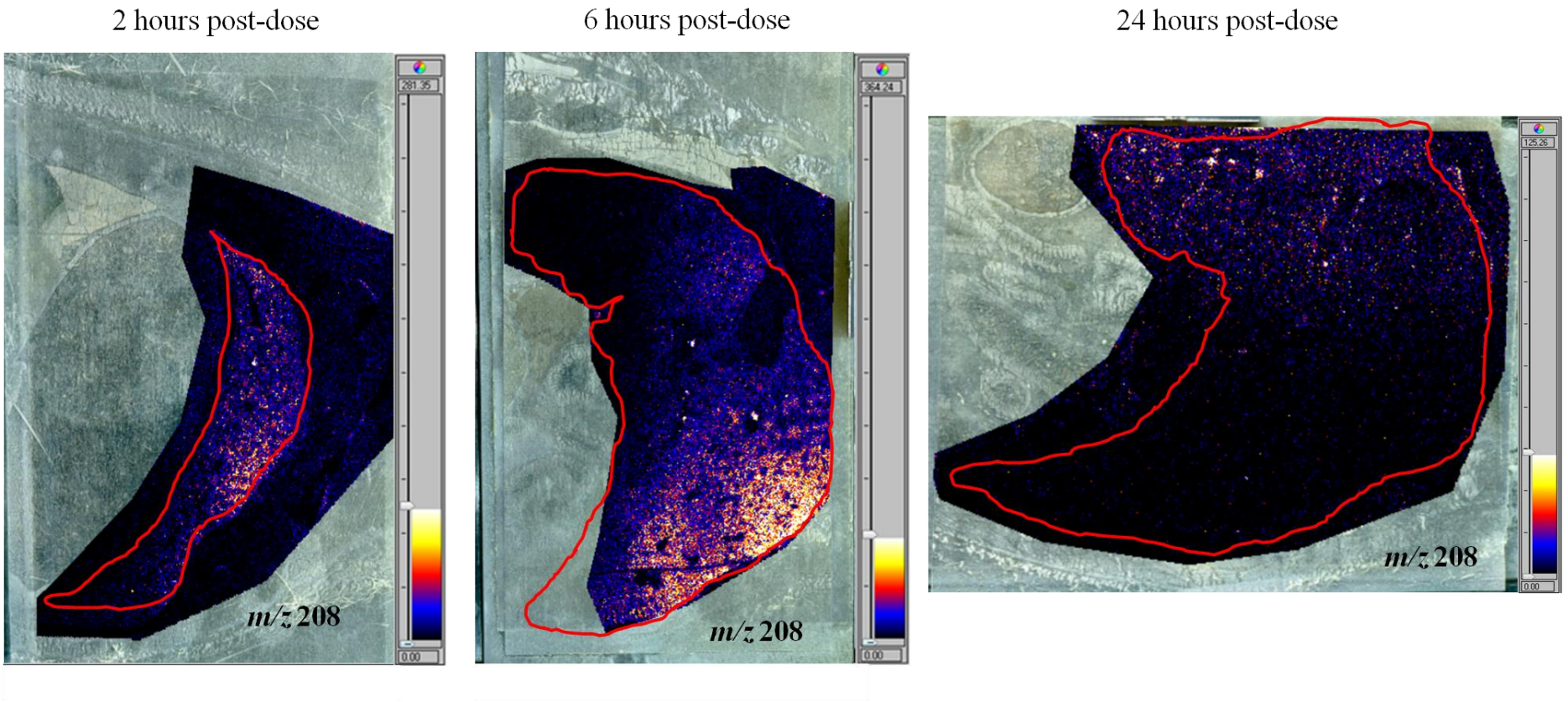

Figure 4.31 MALDI-mobility-MS/MS imaging of fenclozic acid in liver at 2, 6 and 24 hours post-dose.
The liver is outlined in red for clarity. Scale bar represents ion intensity, with white being highest and black the lowest.

Only MALDI imaging of the liver produced ion distribution images of fenclozic acid, despite promising results from MALDI profiling experiments for other tissues. Attempts to localise fenclozic acid using MALDI imaging in the kidney and lung were unsuccessful and as such, brain and blood were not further analysed using MALDI imaging.

4.8 Conclusions

Imaging mass spectrometry approaches have been successfully used for the detection of two selected drug compounds in dosed whole-body rat tissue sections. These experiments were performed alongside an industry-standard metabolite identification experiment to determine the metabolism of each drug compound across a time course in rat liver. This information allowed for a targeted, robust approach for the detection of metabolites in dosed tissue sections using imaging mass spectrometry.

LESA-mobility-MS/MS profiling allowed for the successful detection of fenclozic acid in every tissue sampled at each time point, with the exception of the brain 24 hours post-dose. Confident identification of fenclozic acid was accomplished, using ATD information and MS/MS fragmentation of the *m/z* 254 ion. These results are supported by traditional metabolite identification experiments, which identified mostly parent fenclozic acid in liver extracts across the time course. Attempts to detect a taurine conjugate metabolite of fenclozic acid, identified by UPLC-MS experiments, were unsuccessful using LESA-mobility-MS/MS.

MALDI-mobility-MS/MS profiling experiments used to detect fenclozic acid in dosed tissue sections were also successful. Results were similar to those obtained using the LESA profiling approach, with confident identification of fenclozic acid in all tissues at 2 and 6 hours post-dose. At 24 hours post-dose, however, identification of fenclozic acid was not possible in three of the tissues; brain, blood and lung. LESA profiling experiments were successful in detecting fenclozic acid in blood and the lung. Previous experiments described in Chapter 3 indicated that LESA has a higher overall sensitivity than MALDI. This is due, in part, to the larger area sampled during the LESA experiment and also the ability of the approach to analyse the extracted sample for longer periods of time. This suggests that detection by MALDI profiling might not be possible due to the low levels of the drug present in the lung and blood. This could also be due to poor extraction of fenclozic acid into matrix-analyte crystals during matrix application.

Neither method detected fenclozic acid in the brain 24 hours post-dose. Very low radioactivity levels were also measured in this sample using oxidation experiments. Together these results strongly suggest that fenclozic acid is not present in the brain

24 hours following administration. Both imaging MS approaches and metabolite identification experiments show that parent fenclozic acid is detected in most tissues, even at 24 hours following administration. This suggests that the majority of the radioactivity detected in the tissues is from parent fenclozic acid. Only one metabolite was identified using industry-standard methods, a taurine conjugate, although this could not be detected using the LESA-profiling approach.

MALDI-mobility-MS/MS imaging was successfully used to measure the distribution of fenclozic acid in liver at 2, 6 and 24 hours after administration. Attempts to localise fenclozic acid using MALDI imaging in other organs was not successful, despite the confident detection of fenclozic acid using MALDI profiling. The localisation images show observable changes in the distribution of fenclozic acid in the liver over time. A comparison of these data with results from a QWBA experiment at the same time points could potentially allow further conclusions to be drawn from these results. Further work would be required to interpret these MALDI imaging results in order to draw conclusions regarding the biological significance of these distribution images.

In the propranolol dosed tissues, parent drug was not confidently detected using imaging MS approaches. Metabolite identification experiments identified two metabolites in the liver samples at 2, 6 and 24 hours post-dose. These results suggest that propranolol is metabolised extensively in the liver within 2 hours following oral administration. In light of the metabolite identification results, LESA-mobility-MS/MS was used to profile for major metabolites of propranolol in the tissue samples. Both a hydroxylated metabolite (postulated to be 4-hydroxypropranolol, an active metabolite), and its glucuronide conjugate were successfully detected in dosed tissues using the LESA profiling approach. Attempts to detect these metabolites using MALDI-mobility-MS/MS profiling were unsuccessful. This indicates the importance of understanding the fate of a drug following administration when conducting imaging mass spectrometry experiments. A drug known to be extensively metabolised is increasingly less likely to result in successful detection of the parent drug compound, especially when considering pharmacokinetic parameters, such as metabolic clearance, volume of distribution, or binding in tissue. Instead, major metabolites should be targeted for detection and localisation experiments.

These results demonstrate the added benefit of combining established drug localisation approaches with imaging mass spectrometry for the detection of drug compounds in tissue. Information regarding the distribution of radioactivity in rat organs at each time point post-dose proved useful in initial drug detection experiments. If drug-related material cannot be detected in the organ containing the highest level of radioactivity it is unlikely that drug-related material will be detected in organs with lower radioactivity levels.

More importantly, information regarding the metabolism of each drug compound and what metabolites (if any) were present at each time point allowed for informed decisions regarding which tissues to target for detection of metabolites using imaging MS approaches. Fenclozic acid was not significantly metabolised during the time course of this experiment. As such, parent drug was successfully detected in the tissues known to contain radioactive material. Attempts to detect the taurine conjugate metabolite were not successful using imaging MS approaches. Propranolol dosed tissues were shown to contain much higher levels of metabolites than parent compound, even at 2 hours post-dose in keeping with literature on its *in-vivo* metabolism. This not only allowed for a targeted approach to detect propranolol metabolites in tissue, but also explains the inability of the approach to detect parent propranolol in tissues, even those with rather high total radioactivity.

These results also highlight some of the limitations and issues surrounding label-based approaches to drug localisation, such as QWBA, where the radioactive tag is detected. QWBA results for [^{14}C]-propranolol and [^{14}C]-fenclozic acid would both show widespread radioactivity across the tissues at all three time points, but one is extensively metabolised whilst the other remains relatively unchanged. It is not possible to distinguish between the parent drug and metabolites. LESA profiling is a quick experiment that can be performed on the same tissue sections used for QWBA, in order to determine whether radioactivity is due to a parent drug or a metabolite. The experiments are made significantly easier with information regarding the metabolic profile of each organ at a specific time point, allowing for targeted detection of the compound of interest. Currently, these experiments provide rapid detection of un-labelled compounds in tissue, but this data is qualitative and so alternative experiments are still required in order to obtain quantitative data. This

work shows that LESA combined with ion mobility separation offers a number of advantages for drug distribution experiments, either as a complementary technique to QWBA in an industrial setting or for initial distribution experiments using non-labelled compounds in a drug discovery setting.

Chapter 5 Localisation of adenine nucleotides in mouse brain using ion mobility enabled MALDI imaging

5.1 Metabolic Stress and Neuronal Function

The mammalian brain is very sensitive to metabolic stress (Doyle, Simon et al. 2008). These stresses may include reductions in the supply of oxygen (hypoxia) and glucose (hypoglycemia). There are a large number of incidents during which these stresses can occur, including (but not limited to) strokes, heart attacks or epileptic seizures. Our collaborators in this work, the Frenguelli research group at the University of Warwick, investigate the sequence of cellular and molecular events initiated by cerebral hypoxia/ischemia. Particular interest is given to the role that the adenine nucleotides, specifically adenosine triphosphate (ATP) and the nucleoside adenosine, play in these processes.

The following experiments were undertaken to evaluate the use of MALDI imaging for the localisation of adenine nucleotides in mouse brain. The aims were to assess differences between control mouse brain sections and brain sections subjected to metabolic stress. The rapid post-mortem changes in ATP levels led to a requirement for mass spectrometry-compatible tissue fixation methods to be evaluated. These methods included ethanol fixation and heat stabilisation.

5.1.1 Adenine nucleotides

ATP could be considered one of the best known biological molecules and is commonly referred to as the energy currency of the cell. This is due to the role of ATP as the primary cellular energy source. ATP synthesis occurs during oxidative phosphorylation, where free energy from food and light is transformed into ATP, and glycolysis.

ATP is a nucleotide and the structure of ATP consists of an adenine, a ribose and a triphosphate unit shown in Figure 5.1. When the bonds between phosphate units are broken, energy is readily released through hydrolysis of ATP to form adenosine diphosphate (ADP) and potentially further hydrolysed to form adenosine monophosphate (AMP). This energy release can be utilised to drive processes such as muscle contraction or protein biosynthesis, and is the primary method of energy exchange in biological systems (Lodish, Baltimore et al. 1995; Stryer 2002).

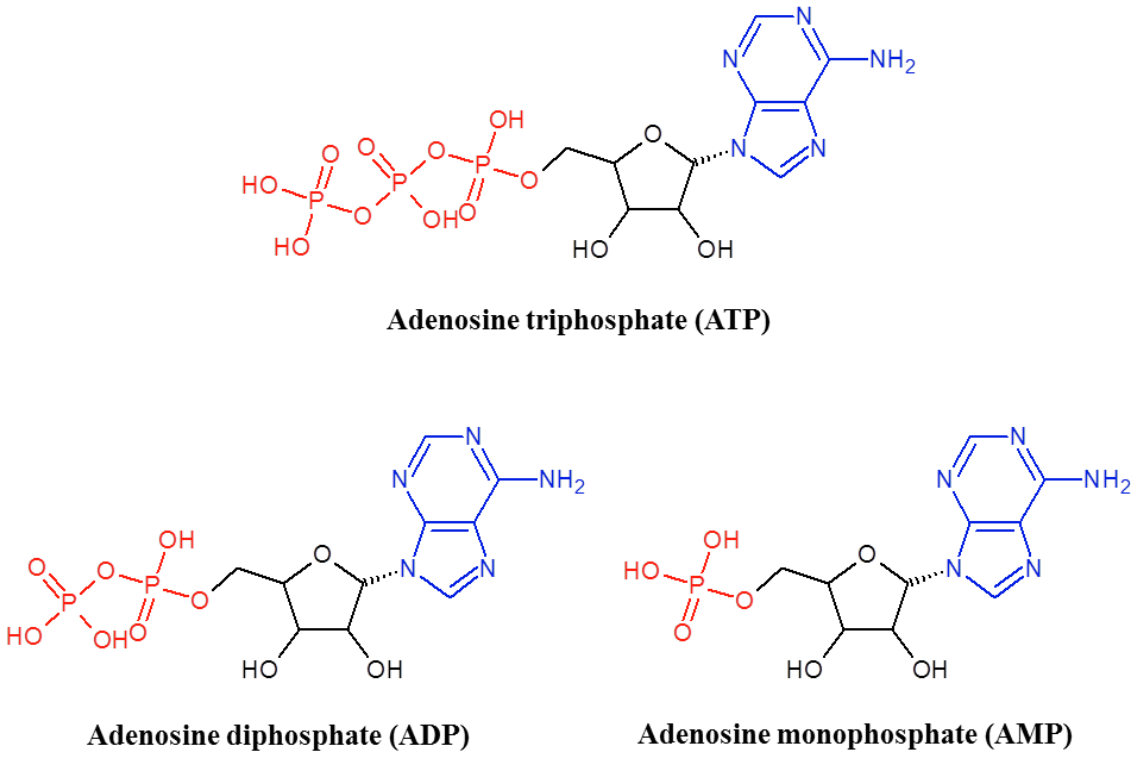

Figure 5.1. Chemical structures of ATP, ADP and AMP.
These adenine nucleotides consist of adenine (blue), a ribose (black) and a tri-, di- or monophosphate unit (red).

A summary of the reactions interconverting ATP, ADP and AMP and the enzymes responsible for these reactions is shown below.

(1) ATPases: ATP →ADP +Pi

(2) Ligases: ATP → AMP + PPi

(3) ATP synthases: ADP + Pi → ATP

(4) Adenylate kinase: 2ADP ↔ ATP + AMP

In a healthy eukaryotic cell these reactions are maintained by the activity of ATP synthases and adenylate kinase (reactions 3 and 4), keeping the ratio of ATP:ADP at around 10:1. Under these conditions, the enzyme adenylate kinase operates to keep the AMP levels in the cell low. In a normal cell, the ratio of ATP:AMP is in the order of 100:1(Hardie and Hawley 2001). Metabolic stresses, such as hypoxia or ischemia, disrupt the balance of adenine nucleotides in the cell. The activity of

ATPases exceeds the activity of ATP synthases to cause hydrolysis of ATP to ADP. This disrupts the equilibrium of the adenylate kinase reaction, causing it to operate to increase the levels of AMP present in the cell.

5.1.2 Metabolic stress and adenine nucleotides

Information regarding the energetic state of tissue is important for a wide range of experimental studies, particularly in the study of metabolic stress. The energetic state of tissues or cells may be assessed by determination of adenine nucleotide (ATP, ADP and AMP) levels. This may be achieved using ultraviolet (UV)-HPLC, which provides quantitative data that can indicate a broad spectrum of metabolic changes, but does not give specific localisation information. Metabolic stress is known to lead to changes in the levels of adenine nucleotides in brain tissue, but little is known regarding relative rates of change of these molecules across the brain during metabolic stress (zur Nedden, Eason et al. 2009).

It is widely recognised by the neuroscience community that adenosine is released during cerebral metabolic stress. ATP release under similar circumstances is less well studied. The direct release of ATP has been demonstrated both *in vivo* and *in vitro* by HPLC studies, but these lack spatial and temporal resolution (Dale and Frenguelli 2009).

The release of ATP and adenosine can initiate both beneficial and damaging cellular cascades. The balance between these can play an important role in post-stress neuronal function. ATP is released from tissue during ischemia; damaging brain tissue through the activation of ATP receptors. Breakdown of ATP produces adenosine, which is believed to be protective through the activation of adenosine A_1 receptors (Frenguelli, Wigmore et al. 2007). Coupling adenine nucleotide localisation information with the localisation of cell-surface receptors for purines could provide insight into these processes. A better understanding of how these processes work may be useful in the treatment of disorders of the central nervous system (CNS).

Determining adenine nucleotide distribution in the brain may provide information regarding areas of the brain more vulnerable to ischemia; such as those with a higher

rate of metabolic activity. These areas may show the fastest decline of ATP levels during metabolic stress and slower recovery times. Establishing this information may prove useful in the explanation of differential vulnerability, recovery of brain regions to metabolic stress and in establishing the potential for neuroprotective or neurorestorative therapies by improving the bioenergetic recovery of brain tissue after injury (zur Nedden, Hawley et al. 2011).

5.1.3 Previous work

A study by Benabdellah *et al.* (Benabdellah, Touboul et al. 2009) demonstrated the applicability of MALDI imaging to the localisation of primary metabolites in rat brain. Using 9-aminoacridine as a matrix compound, thirteen primary metabolites were detected directly from rat brain sections, including ATP, ADP and AMP. The identification of primary metabolites was confirmed using MS/MS experiments. Despite the successful identification of ATP from tissue sections, the distribution of ATP across the brain section was not shown. This was attributed to low sensitivity. In a healthy cell ATP should be 10-fold in excess over ADP, and 100-fold excess over AMP and so it should be possible to detect and image the distribution of ATP in the brain.

Changes in adenine nucleotide levels are known to take place rapidly in the tissue when enzymes (ATPases) are not inactivated. Standard tissue handling and sample preparation protocols for an imaging mass spectrometry experiment require immediate snap freezing of the tissue in liquid nitrogen following dissection. Snap-freezing of tissue has been widely used to prevent enzymatic activity in tissues, but enzymatic activity may be recovered during tissue thawing, leading to the potential for ATP degradation. Tissues can be warmed to around -20 for sectioning, thaw-mounted onto a target and stored again at -80 prior to analysis. The target and tissue are commonly brought to room temperature under vacuum for matrix application. All these tissue handling steps could lead to thawing and recovery of ATPase activity, resulting in changes in the levels of ATP and causing the tissue sample to

become less physiologically relevant. This could explain why, in this work, ATP could not be localised in the mouse brain section.

Work by Setou *et al.* in Japan identified localisation changes in ATP, ADP and AMP in mouse hippocampus following a kainate-induced seizure (Sugiura, Taguchi et al. 2011). Using capillary electrophoresis (CE) MS to quantify the adenine nucleotides, they showed that a reduction in both ATP and ADP in the hippocampus during seizure could be observed. MALDI imaging was used to localise these nucleotides in control mouse brain sections and brains 30 minutes following seizure. The subject of post-mortem degradation of the adenine nucleotides was discussed and *in situ* freezing offered as a potential approach to prevent this. This had been suggested in previous studies (Hattori, Kajimura et al. 2010). The severity of seizures suffered by the kainate-treated mice meant that this was impractical. Instead, the time taken for brain extraction was limited to a maximum of 1 minute prior to snap-freezing. The authors noted that the adenosine nucleotide levels were degraded in these unfixed samples when compared to fixed brains.

Previous studies have indicated the potential of using MALDI imaging for studying the distribution of adenine nucleotides and their changes during times of metabolic stress. It is clear, however that significant experimental challenges remain with regards to the rapid post-mortem changes in these compounds.

5.1.4 Tissue fixation approaches

To prevent loss of ATP during tissue handling and sample preparation, enzymatic activity needs to be prevented following sacrifice of the animal. This may be achieved by fixing the tissue. Traditional tissue fixing procedures do not lend themselves easily towards imaging mass spectrometry experiments. Although there have been examples of successful protein imaging experiments using formalin-fixed paraffin-embedded (FFPE) tissues, these experiments require on-tissue enzymatic digestion prior to analysis (Aoki, Toyama et al. 2007). This method would not be suitable for small molecules such as adenine nucleotides, due to the need for enzymatic digestion.

5.1.4.1 Ethanol fixation

In addition to washing away salts and other contaminants from the tissue surface, washing tissue sections with increasing percentages of ethanol has been used to temporarily fix proteins. An ethanol washing protocol was included during sample preparation for MALDI imaging of proteins in tissue. Washing tissue sections may result in a loss of spatial resolution, especially for small molecules such as drug compounds, that are more susceptible to redistribution. As such, ethanol wash steps have not commonly been used for drug localisation experiments. (Kaletas, van der Wiel et al. 2009; Chughtai and Heeren 2010).

Ethanol can precipitate larger molecular weight proteins in tissue and also dehydrate the tissue, preventing enzymatic activity. This can also lead to shrinkage of the tissue section.

5.1.4.2 Microwave fixation

Focused high-energy microwave irradiation has been used for the sacrifice of mice and rat. This can result in rapid heat inactivation of enzymes in the brain. Microwave irradiation is designed to kill animals very rapidly by heating the brain to temperatures greater than 85 ºC *in situ* (Galli and Racagni 1982).

This method has been used in a number of application areas to maintain physiologically relevant levels of different compounds. These have included peptides, second messengers, neurotransmitters and energy metabolites, including adenine nucleotides. (O'Callaghan and Sriram 2004)

Delaney and Geiger compared the levels of adenosine and adenine nucleotides in rat brain following different methods of sacrifice and tissue preparation. (Delaney and Geiger 1996) The authors demonstrated that using high-energy focused microwave irradiation rapidly inactivated enzymes present in the brain and prevented the breakdown of ATP after death. This enabled more accurate measurements of adenine nucleotides and adenosine in discrete regions of rat brain. Other methods, including decapitation followed by snap-freezing, decapitation into liquid nitrogen and *in situ*

freezing of the brain with liquid nitrogen were found to inactivate enzymes more slowly and resulted in higher levels of AMP and adenosine.

The use of microwave irradiation as a fixation method to prevent post-mortem degradation of adenine nucleotides prior to MALDI imaging was presented at the American Society of Mass Spectrometry annual conference in May 2012 (Sugiura 2012). When compared to *in situ* freezing and snap-freezing methods, microwave irradiation was shown to prevent significant changes in ATP levels due to immediate denaturing of hydrolysis enzymes. The microwave irradiation equipment is expensive to purchase and not currently used as a standard method for the sacrifice of animals for research. This has limited further research into the use of microwave irradiation for preparation of tissues for imaging mass spectrometry, especially within Europe.

5.1.4.3 Heat stabilisation

A heat stabilisation technique for tissue fixation (Stablilizor™, Denator AB, Sweden) has been recently developed by Denator AB. The instrument can handle any type of frozen or fresh tissue sample and is compatible with mass spectrometry analysis. Enzymes are inactivated after sampling by rapidly heating the tissue to 95 ºC using a combination of heat and pressure under vacuum. This raises the temperature quickly, homogenously and reproducibly and prevents the downstream sample degradation commonly encountered with other techniques such as snap-freezing (Svensson, Boren et al. 2009). Evaluation of this heat stabilisation technique has focused predominantly on proteomic analysis and post-mortem changes in protein levels. Heat stabilisation may also be used to prevent metabolism of ATP and other adenine nucleotides, which can be degraded rapidly by enzymes following death.

The potential of this heat stabilisation technique for MALDI imaging experiments has been evaluated by Goodwin *et al* in 2008. Heat treatment at the point of tissue harvesting allowed the retention of a marker ion in mouse brain sections, which was otherwise lost in untreated sections or sections that were heat treated after sectioning and thaw-mounting (Goodwin, Pennington et al. 2008).

This method has been further evaluated in monitoring proteome degradation in mouse brain and evaluating the possible preservation of the sample by heat treatment. Following tissue excision, one hemisphere of the brain was heat treated prior to snap-freezing in liquid nitrogen; the other was immediately snap-frozen without treatment. All samples were processed and analysed by both MALDI imaging and 2D-DIGE. This work highlighted the fact that heat treatment of tissues at the point of excision prevented degradation of proteins in tissues and was compatible with downstream mass spectrometry analyses, including MALDI imaging. The authors have noted issues with the quality of tissue sections following heat treatment, which may affect the spatial information obtained during downstream MALDI imaging experiments. Collecting data from both treated and untreated tissue sections may help to overcome this issue by providing complementary information with regards to spatial resolution and identification (Goodwin, Lang et al. 2010).

The research described here is focused on the evaluation of the potential of mobility enabled MALDI imaging for detection and localisation of the adenine nucleotides in mouse brain samples. The use of ethanol washes and heat-stabilisation as tissue fixation approaches have been investigated, in order to evaluate their potential to prevent rapid degradation of adenine nucleotides following death. This work has been published in the peer-reviewed International Journal of Mass Spectrometry.

5.2 Results and Discussion

For all materials and methods please refer to Chapter 2.

5.2.1 Analysis of adenine nucleotide standards

ATP, ADP and AMP standards were analysed using MALDI-MS in negative ion mode. The samples were prepared with 9-AA matrix to optimise detection of compounds on tissue. Deprotonated ATP, ADP and AMP molecule ions were observed at *m/z* 506, *m/z* 426 and *m/z* 346 respectively. MS/MS fragmentation and mobility separation was optimised for each nucleotide using standards deposited on target. Precursor ions of the adenine nucleotides were selected for MS/MS fragmentation following ion mobility separation. MS/MS spectra were extracted from the arrival time distribution for ATP, ADP and AMP ions, shown in Figure 5.2, Figure 5.3 and Figure 5.4 respectively. Observed MS/MS fragments are displayed above each spectrum.

The majority of fragment ions present in the MS/MS spectrum for ATP correspond to losses from the triphosphate group, including the two most intense fragment ions at *m/z* 158.9 and *m/z* 408.0. A small peak corresponding to a deprotonated adenine fragment was observed at *m/z* 134.

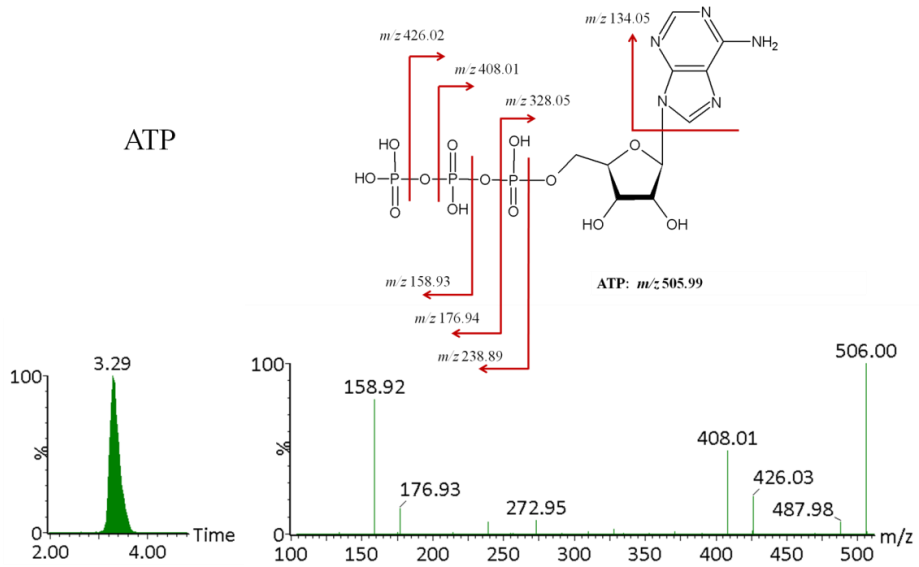

Figure 5.2 Extracted arrival time distribution and mobility-resolved MALDI MS/MS spectra for ATP standard on target.

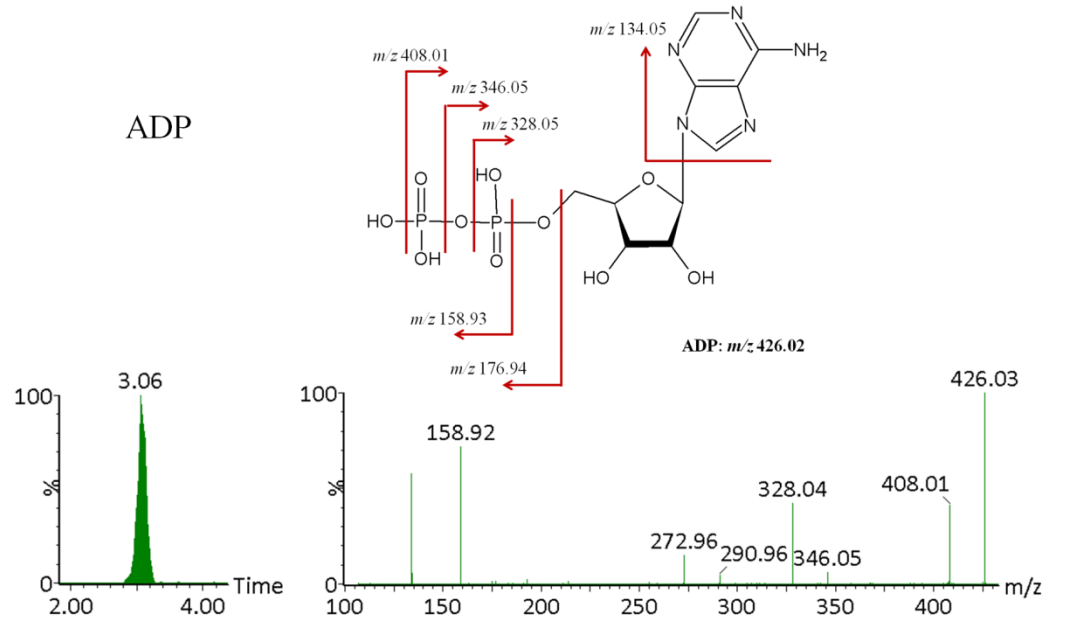

Figure 5.3 Extracted arrival time distribution and mobility-resolved MALDI MS/MS spectra for ADP standard on target.

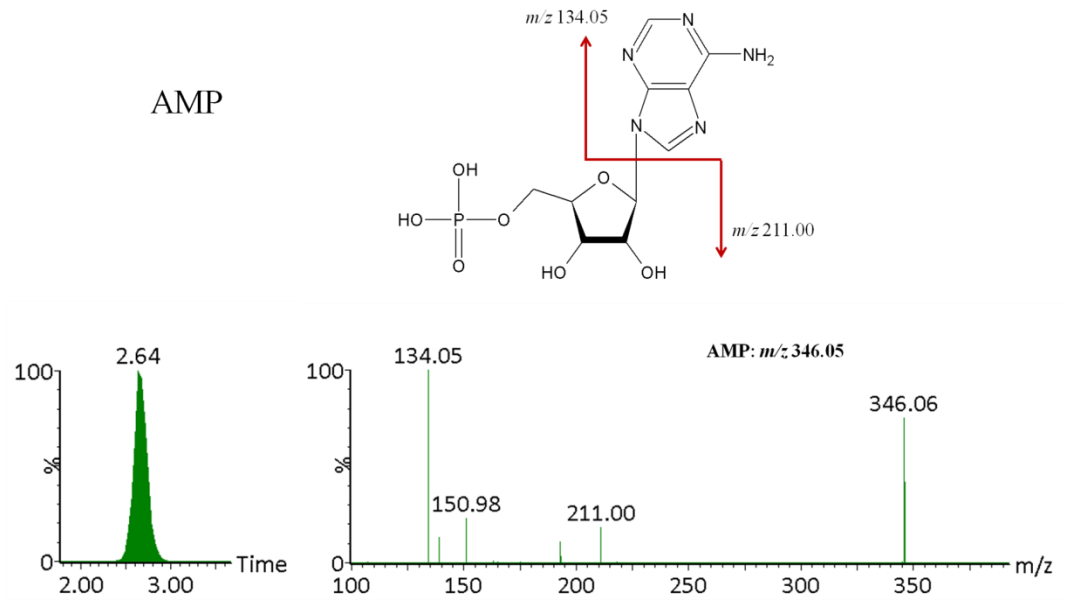

Figure 5.4 Extracted arrival time distribution and mobility-resolved MALDI MS/MS spectra for AMP standard on target.

Many of the fragment ions identified in the ADP MS/MS spectrum (Figure 5.3) were also characteristic of losses from the diphosphate group. The deprotonated adenine ion fragment at *m/z* 134.0 was more intense and the *m/z* 328.0 ion may correspond to a cyclic AMP.

Figure 5.4 shows the MS/MS spectrum obtained from the AMP molecule ion; the fragmentation of AMP was less complex than that observed for the other adenine nucleotides. Little fragmentation was observed from the monophosphate group and the two most intense fragment ions corresponded to a deprotonated adenine fragment (*m/z* 134.0) and loss of adenine (*m/z* 211) from the precursor.

A comparison of spectra obtained from tissue with these extracted ATDs and MS/MS spectra from adenine nucleotide standards may be used in the confident identification of nucleotides from brain tissue sections when using MALDI-mobility-MS/MS.

5.2.2 Identification of adenine nucleotides from a mixture

In order to demonstrate that the MALDI-mobility-MS/MS method is selective for each of the adenine nucleotides, a mixture of ATP, ADP and AMP standards (in a 1:1:1 ratio) were prepared. This mixture was analysed by means of a MALDI-mobility-MS experiment. Figure 5.5 a) shows the ATD and corresponding MS spectrum of the mixture (non-mobility resolved). ATP (*m/z* 506), ADP (*m/z* 426) and AMP (*m/z* 346) are all present in the spectrum, indicating that each nucleotide can be detected within a mixture of the others, as would be the case in tissue.

Ion mobility was used to separate out each of the adenine nucleotides from the mixture, as shown in Figure 5.5 b), c) and d). This demonstrates that ion mobility separation is selective for the adenine nucleotide of interest. Mobility separation was used prior to MS/MS fragmentation to select for the adenine nucleotide of interest from tissue.

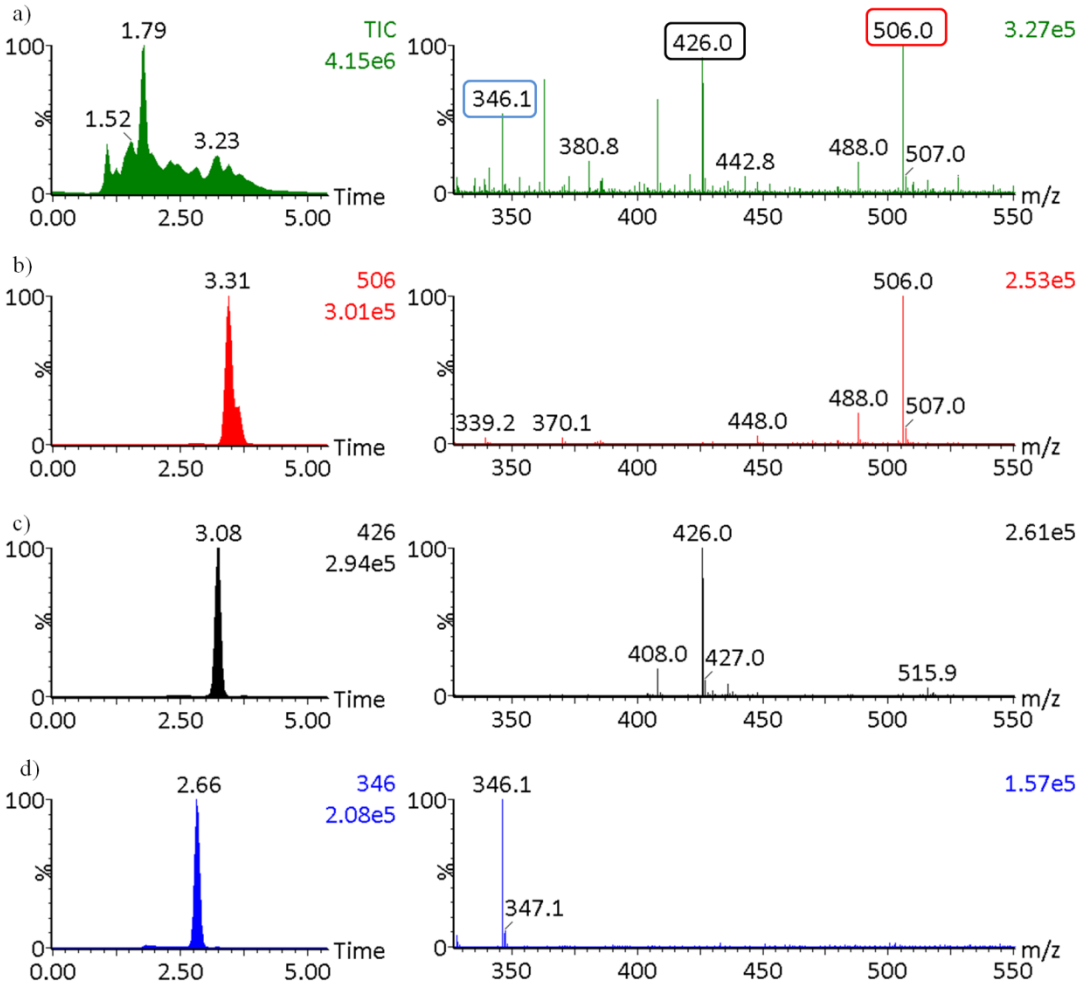

Figure 5.5. Identification of adenine nucleotide standards from a mixture by MALDI-mobility-MS.
a) Full ATD and MS spectrum of an adenine nucleotide mixture by MALDI-mobility-MS. ATP (*m/z* 506, red), ADP (*m/z* 426, black) and AMP (*m/z* 346, blue) are identified in the MS spectrum. Extracted ATDs and MS spectra of b) ATP, c) ADP and d) AMP are shown. Total ion counts for each of the spectra are displayed.

5.2.3 Identification of adenine nucleotides on tissue

Optimised methods for identification of the adenine nucleotides were used to detect ATP, ADP and AMP in 12 µm control, unwashed, mouse brain sections by means of MALDI-mobility-MS/MS imaging experiments. Ions corresponding to the relative precursor ions of each of the adenine nucleotides (*m/z* 506, 426 and 346) were selected from tissue for MS/MS fragmentation following ion mobility separation. Data acquired across a whole brain section were combined and MS/MS spectra were

extracted using mobility data along with the arrival time distribution of the selected parent ion from tissue.

Figure 5.6 shows the MS/MS spectra and extracted arrival time distribution of ATP standard obtained alongside the MS/MS spectra and extracted arrival time distribution for *m/z* 506 identified from mouse brain. The extracted arrival time distribution for *m/z* 506 on tissue showed the same distribution as that for the ATP standard. The MS/MS spectra extracted also matched the mobility-extracted MS/MS spectra of the ATP standard, which allowed for confident identification of the *m/z* 506 from tissue as ATP.

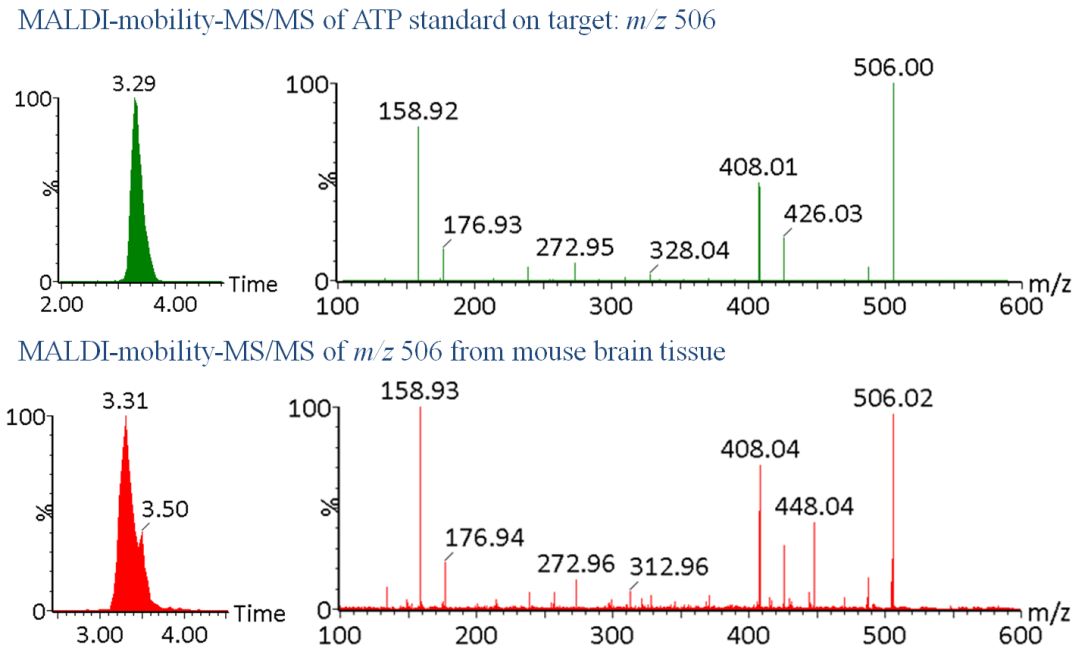

Figure 5.6. MALDI-mobility-MS/MS spectra and extracted arrival time distribution for *m/z* 506 from control mouse brain section and ATP standard.

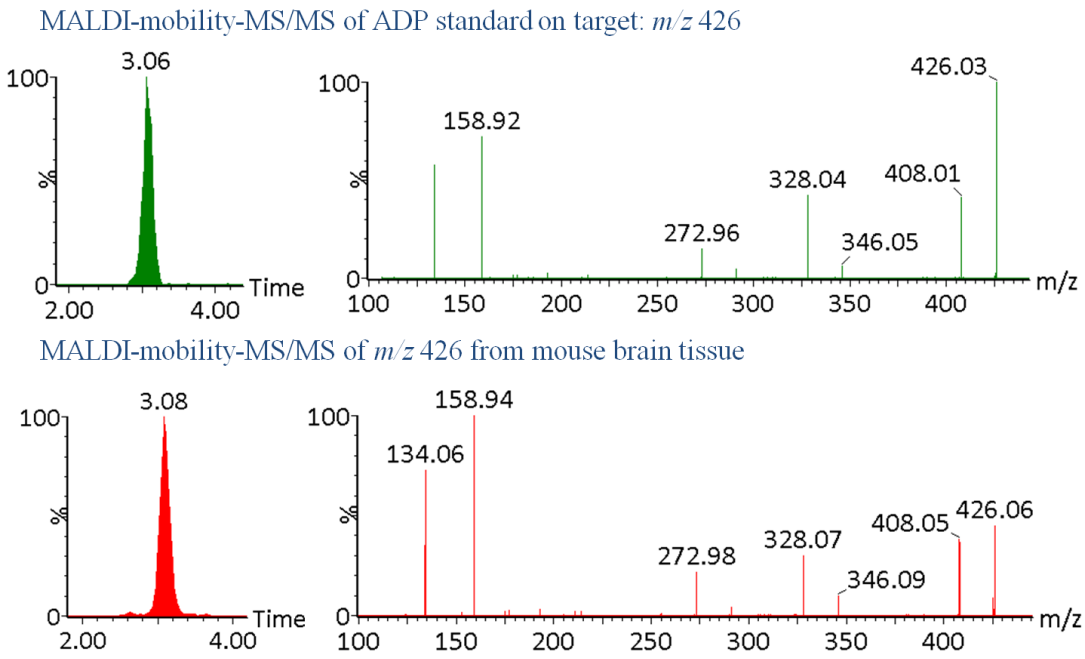

Figure 5.7. MALDI-mobility-MS/MS spectra and extracted arrival time distribution for m/z 426 from control mouse brain section and ADP standard.

Figure 5.7 shows the MS/MS spectra and extracted arrival time distribution of ADP standard alongside the MS/MS spectra and extracted arrival time distribution for *m/z* 426 identified from mouse brain.

The extracted arrival time distribution for *m/z* 426 on tissue showed the same distribution as that for the ADP standard. The MS/MS spectra extracted also matched the mobility-extracted MS/MS spectra of the ADP standard, which allowed for confident identification of the *m/z* 426 from tissue as ADP.

Figure 5.8 shows the MS/MS spectra and extracted arrival time distribution of AMP standard on target alongside the MS/MS spectra and extracted arrival time distribution for *m/z* 346 identified from mouse brain.

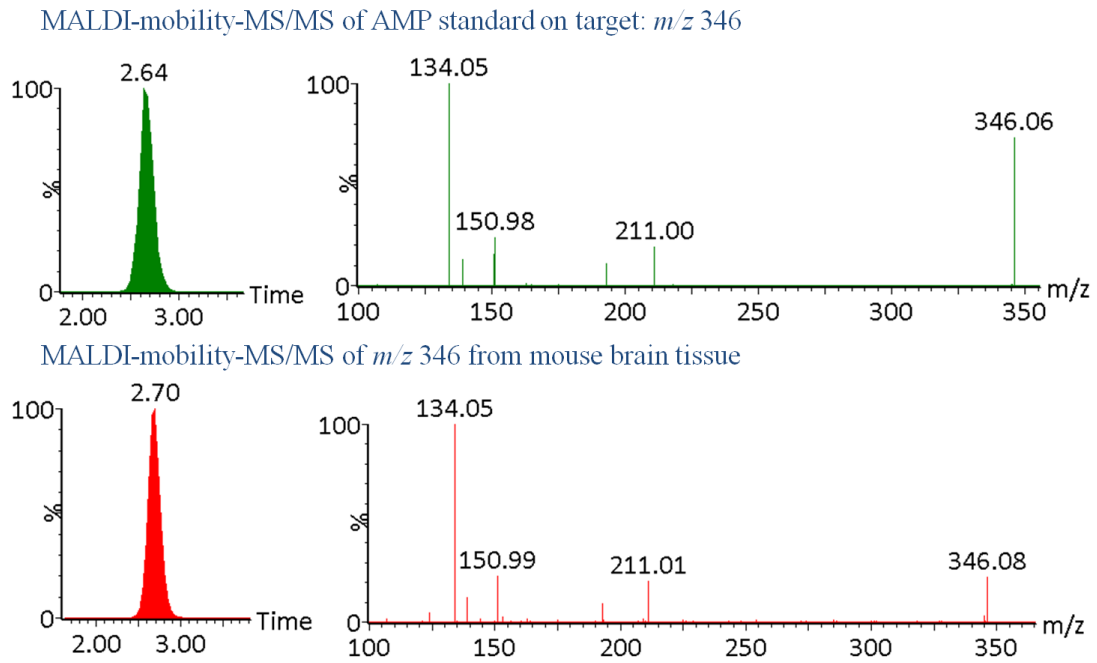

Figure 5.8. MALDI-mobility-MS/MS spectra and extracted arrival time distribution for m/z 346 from control mouse brain section and AMP standard.

The extracted arrival time distribution for *m/z* 346 on tissue showed the same distribution as that obtained from the AMP standard. The MS/MS spectra extracted also matched the mobility-extracted MS/MS spectra of AMP standard, which allowed for confident identification of the *m/z* 346 from tissue as AMP.

5.2.4 Localisation of adenine nucleotides in mouse brain

After carrying out a MALDI-mobility-MS/MS imaging experiment on 12 µm control mouse brain sections, ion distribution images were produced for ATP, ADP and AMP. Using the HDImaging™ software, product ions of interest were selected, with arrival time distributions corresponding to that of the adenine nucleotide of interest. This provided confidence that the ion intensity image produced was that of the compound of interest and not background matrix ions due to endogenous species. MALDI-mobility-MS/MS images of the parent ions of the adenine nucleotides are shown in Figure 5.9.

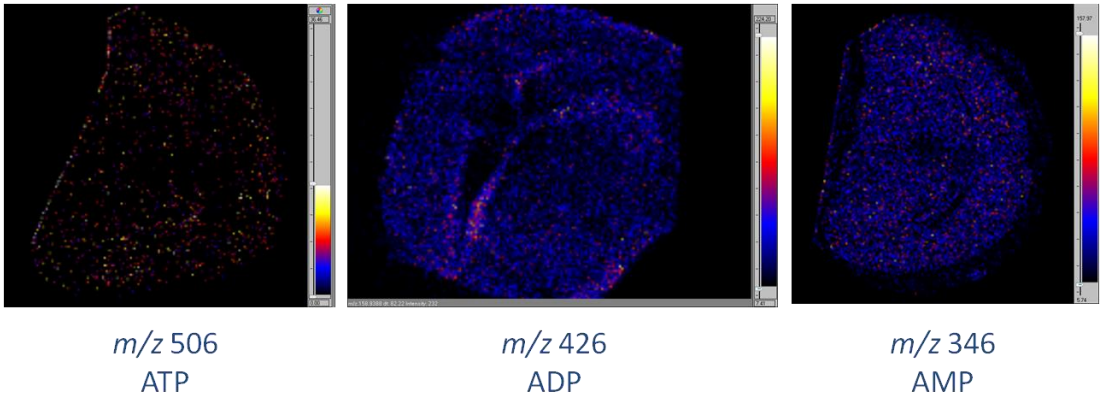

Figure 5.9. MALDI-mobility-MS/MS images from control mouse brain sections at 50 µm spatial resolution. The intensity of parent ions at **a)** m/z 506 (ATP) **b)** m/z 426 (ADP) and **c)** m/z 346 (AMP) in brain are displayed.

Ion distribution images were obtained for both ADP and AMP on unwashed, control tissue sections. Although ATP was successfully identified from the combined data from the same brain sections, localisation of the molecule in the brain was not clear.

In healthy tissue the levels of ATP should be in excess of both that of ADP and AMP. This did not appear to be the case from these images and thus led to questions surrounding the biological relevance of tissues treated in this way. Since ATP is known to be rapidly metabolised following the death of the animal, recovered enzymatic activity as the tissue is thawed to room temperature was suspected to be responsible for the low levels of ATP present in the tissue. A number of tissue fixation methods to prevent enzymatic activity were therefore evaluated.

5.3 Tissue fixation approaches: ethanol wash

Ethanol has been shown to temporarily fix tissue and dehydrate tissue sections, and may be used to prevent ATP hydrolysis from taking place as the tissues are brought to room temperature. In order to test this theory, a sequential wash step utilising increasing percentages of ice-cold ethanol was introduced into the sample preparation procedure, just before the frozen tissue sections were brought to room temperature in the vacuum dessicator.

Apart from the ethanol wash step, control mouse brain sections at 12 µm were analysed in exactly the same way as previously.

The MALDI-mobility-MS/MS ion intensity distribution images for parent ions of ATP, ADP and AMP are shown below in Figure 5.10, alongside corresponding H&E stained optical images.

Figure 5.10 shows that the introduction of an ethanol wash into the sample preparation procedure allowed images of all three adenine nucleotides to be produced. The results for ATP showed a clear distribution in the brain section, whereas no localisation information had been obtained.

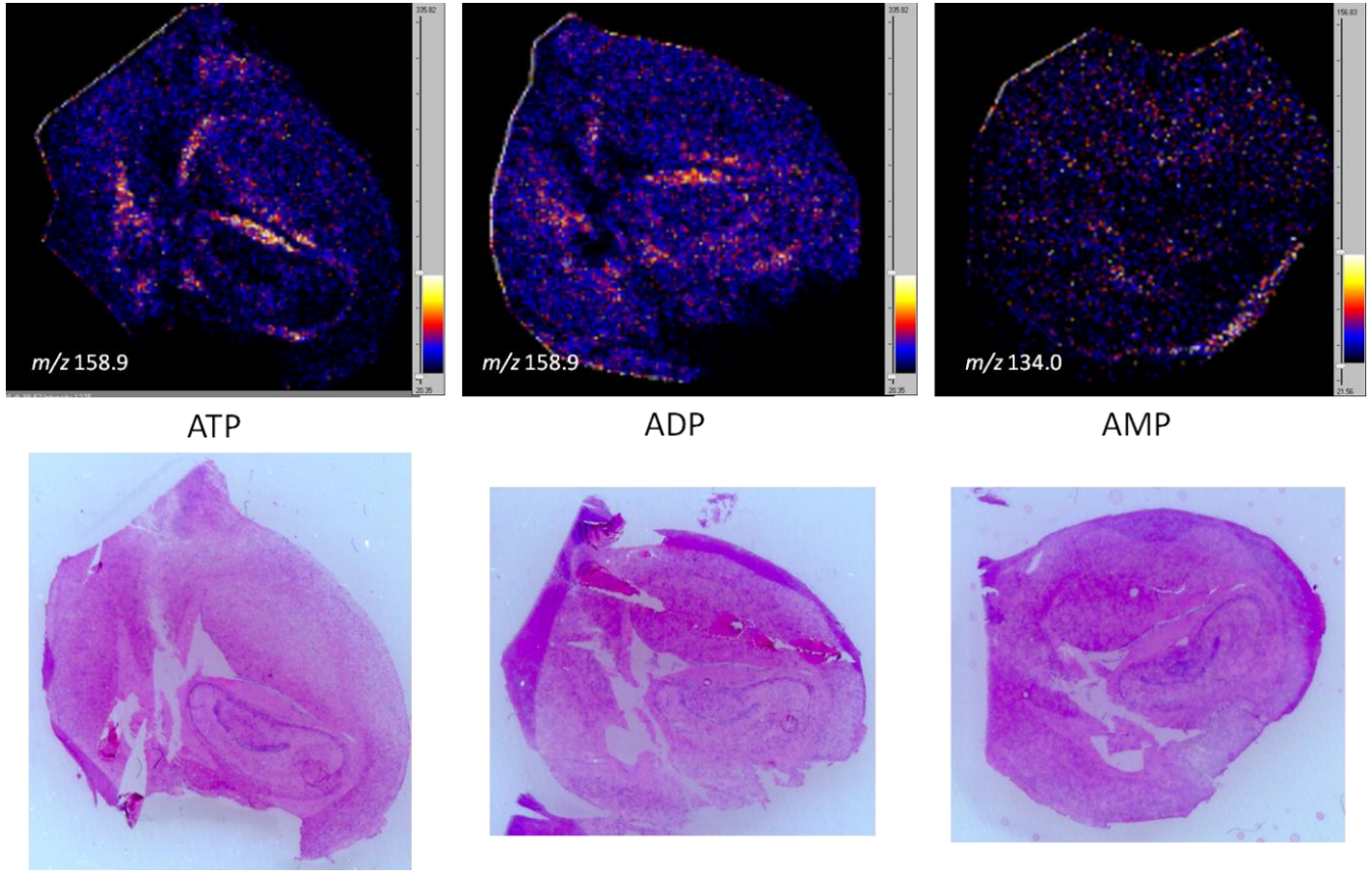

Figure 5.10. MALDI-mobility-MS/MS images from washed control mouse brain sections at 50 µm spatial resolution.
The intensity of MS/MS fragment ions at **a)** *m/z* 158.9 (from ATP) **b)** *m/z* 158.9 (from ADP) and **c)** *m/z* 134.0 (from AMP) in brain are displayed.
The corresponding optical images of HE stained brain sections following acquisition for **d)** ATP, **e)** ADP and **f)** AMP are shown for comparison.

5.3.1 Relative intensity of ATP:ADP:AMP in tissue

The percentage ratio of ATP:ADP:AMP measured in control untreated brain was compared with the percentage ratio of ATP:ADP:AMP from a control brain which had been subjected to an ethanol wash step. Percentage ratios are shown in Figure 5.11.

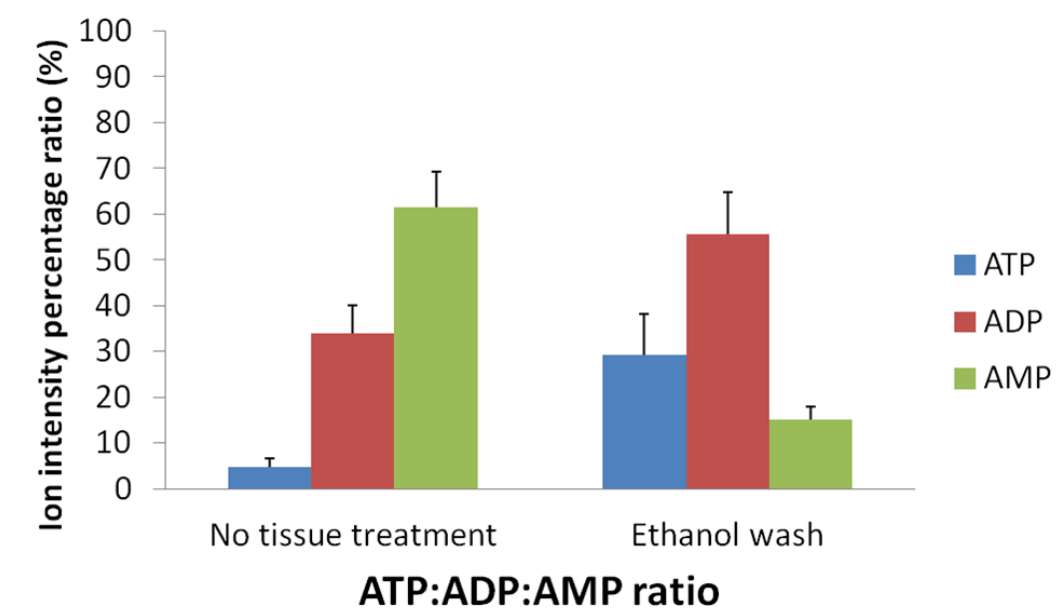

Figure 5.11. Ion intensity percentage ratio of the adenine nucleotides in control brain sections with and without inclusion of an ethanol wash step.
Error bars show the standard deviation in ion intensity for each adenine nucleotide across four brain sections.

The intensity ratios showed an increase in the levels of ATP measured when an ethanol wash step was included in the sample preparation procedure. When the tissue was not treated, very low levels of ATP relative to both ADP and AMP were observed. When an ethanol wash was included in order to to minimise enzymatic degradation of ATP, significant increase in the ATP:AMP ratio in the brain was observed. The levels of ADP present were still higher than that which would be expected in normal tissue.

Figure 5.11 also shows the standard deviations of the ratios measured across four brain sections. It is clear that the method used here for detection and localisation of the adenine nucleotides was reproducible across different samples.

5.3.2 Control vs. stressed tissue

The ability of this approach to determine differences between control and stressed brain sections was assessed, with the inclusion of an ethanol wash during sample preparation. Four control and four stressed brain sections were analysed as previously described, sampling three areas on each brain of identical area targeting each of the adenine nucleotides.

Figure 5.12 shows the average percentage ratio of ATP:ADP:AMP measured in control and stressed brain sections, across the four samples.

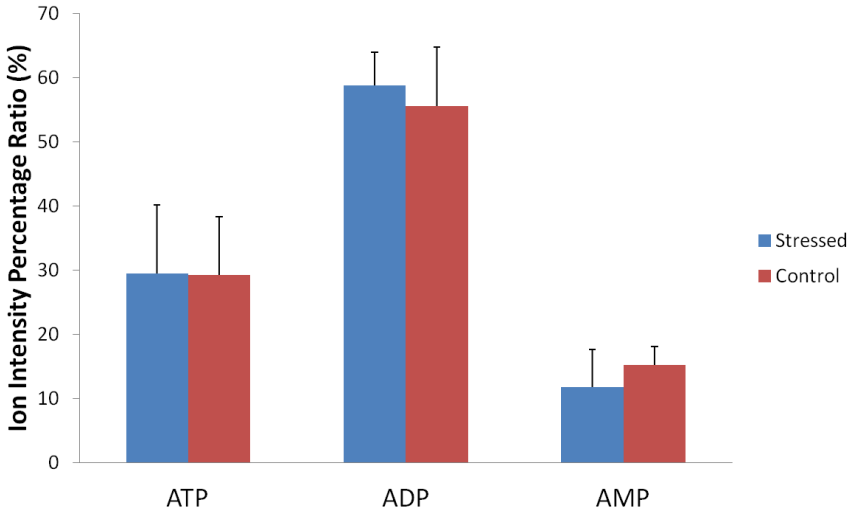

Figure 5.12. Ion intensity percentage ratio of the adenine nucleotides in control and stressed brain sections with the inclusion of an ethanol wash step.
Error bars show the standard deviation in ion intensity for each adenine nucleotide across each of the four brain sections.

Although the ethanol wash step was previously shown to increase the relative levels of intensity of detection of adenine nucleotides in tissue, differences were not detected between control and stressed sections. This result was unexpected, since the stressed brain should contain lower levels of ATP and elevated levels of AMP owing to the fact that ATP is degraded during periods of metabolic stress. This indicated that further metabolism of the adenine nucleotides was potentially taking place following sacrifice and prior to snap-freezing, masking differences between the control and stressed sections caused by metabolic stress. Reproducibility across the

samples was good, indicating the potential of the downstream mass spectrometry experiment for this type of analysis once the sample preparation had been optimised.

5.4 Tissue fixation approaches: heat stabilisation

Heat-stabilisation has been shown to prevent the degradation of proteins in tissue. By heating tissue rapidly to very high temperatures, enzymes may be denatured. This method may prevent ATP hydrolysis from taking place as the tissues are brought to room temperature, by denaturing the enzymes responsible. In order to test this hypothesis brain samples were prepared with and without heat-stabilisation for subsequent mass spectrometry analysis.

Five brain samples were studied; heat-stabilised, snap-frozen, heat-stabilised and left for 30 minutes, left for 30 minutes and heat-stabilised and left for 30 minutes before snap-freezing.

5.4.1 Relative intensity of ATP:AMP

The percentage ratio of ATP:AMP measured in each of the five brain sections are shown in Figure 5.13.

The intensity ratios shown demonstrated an increase in the relative intensity of ATP when the mouse brain was subjected to heat-stabilisation immediately following dissection. There was a significantly higher intensity of ATP relative to AMP in the heat-stabilised sample than in the snap-frozen sample (where AMP was in excess over ATP). This indicated that heat-stabilisation had a significant effect in preventing post-mortem changes in ATP levels. In both samples the standard deviation was small across technical replicates, indicating the relatively good reproducibility of the methods.

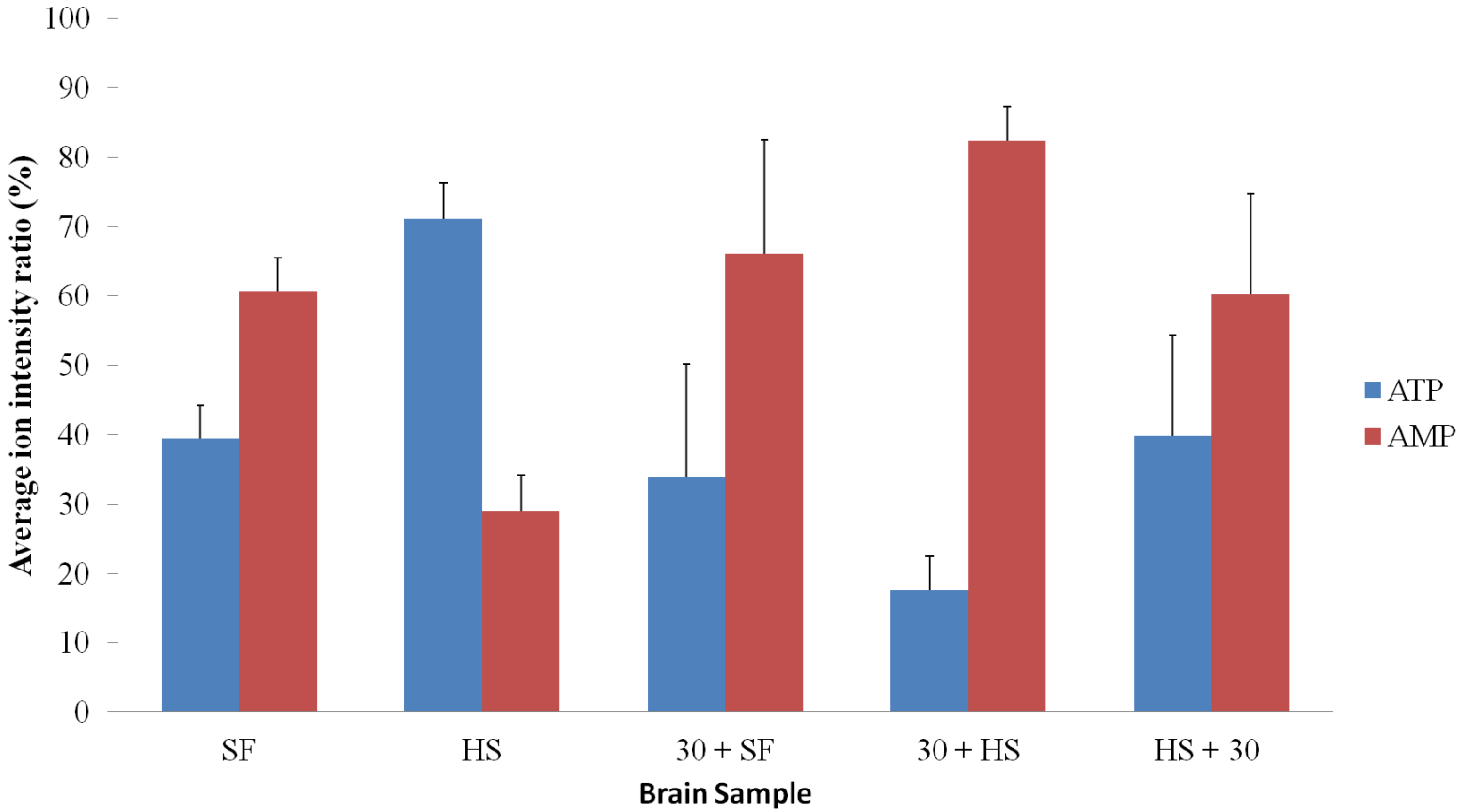

Figure 5.13 Average intensity ratios of ATP:AMP across four mouse brain sections to demonstrate the effect of heat-stabilisation. **SF:** Snap-frozen; **HS:** heat-stabilised; **30+SF:** 30 minutes at room temperature then snap-frozen; **30+HS:** 30 mins at room temperature then heat-stabilised; **HS+30:** heat-stabilised then at room temperature for 30 mins. Error bars represent standard deviation across technical replicates.

In the 30+SF sample, where the brain was left at room temperature for 30 minutes prior to snap freezing, a higher standard deviation was observed across replicates. The ATP:AMP ratio measured was similar to that of the SF sample, but with slightly more AMP observed relative to ATP and greater variation between replicates. Longer periods at room temperature would allow for more enzymatic degradation of ATP to AMP, as indicated by the results shown. Similar results were also observed for the 30 + HS sample, where the brain was left at room temperature for 30 minutes. Here, the brain was heat-stabilised following the waiting period, which would reduce any further changes. AMP was in excess over ATP, but here the standard deviation between replicates was much lower than that observed for the 30+SF sample. This could suggest that, without heat stabilisation, changes in the levels of adenine nucleotides were still occurring in the sample during the sectioning procedure.

An interesting result was observed for the HS+30 sample, which underwent heat-stabilisation and then was left at room temperature for 30 minutes. If heat-stabilisation was successful in permanently preventing enzymatic changes, we would have expected to see a similar ATP:AMP ratio here as observed in the heat-stabilised sample (HS). This was not the case, AMP was observed at a higher relative intensity than ATP. This could indicate that the heat-stabilisation procedure had not fully denatured the enzymes responsible for ATP hydrolysis. The variation between replicates was relatively high, as indicated by the standard deviation, which may skew the results slightly. Another slide with four HS+30 sections was analysed in the same way as previously to probe experimental error, and produced similar results as to those shown.

5.4.2 Ion distribution images of adenine nucleotides

After carrying out a MALDI-mobility-MS/MS imaging experiment on 14 µm heat-stabilised (HS) and snap-frozen (SF) mouse brain sections, ion distribution images were produced for ATP, ADP and AMP. Using the HDImaging™ software, product ions of interest were selected, with arrival time distributions corresponding to that of the adenine nucleotide of interest.

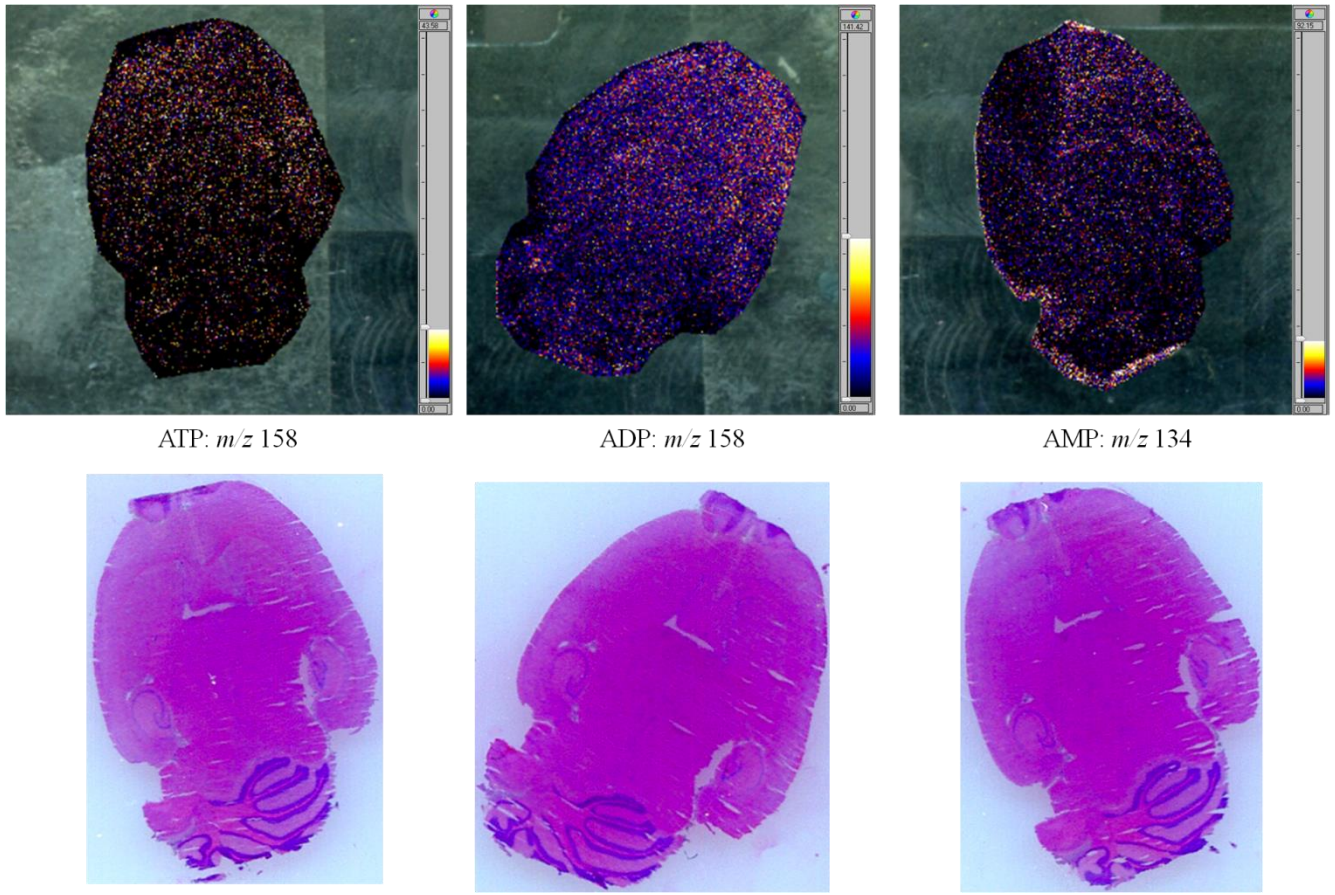

Figure 5.14 MALDI-mobility-MS/MS images of adenine nucleotide localisation in a snap-frozen mouse brain.
Images were acquired at 50 µm spatial resolution and the localisation of the most intense fragment ion for each of ATP, ADP and AMP is displayed. Optical images of the brain sections HE stained following MS analysis are included for comparison.

MALDI-mobility-MS/MS images of the most intense product ions of each the adenine nucleotides from adjacent sections of the snap-frozen brain are shown in Figure 5.14. Optical images of the HE stained sections are included for comparison.

Although all three adenine nucleotides could be successfully identified from snap-frozen tissue and despite the inclusion of an ethanol wash step, localisation of the adenine nucleotide ions across the brain section was unsuccessful. This could be due in part to the method of snap-freezing used for these samples. Brain sections in previous experiments had been snap-frozen by immediate immersion in liquid nitrogen, whereas these brains were frozen on dry ice. This method of freezing was slower than using liquid nitrogen and as such enzymatic degradation would be expected to continue for longer. Freezing on dry ice did have the advantage that it results in less damage to the organ during the freezing process. Here the cerebellum remained intact and attached, whilst previous samples frozen in liquid nitrogen have cracked and the cerebellum had been lost during the freezing process.

MALDI-mobility-MS/MS produced images of the most intense product ions of each the adenine nucleotides from adjacent sections of the heat-stabilised brain are shown in Figure 5.15. Optical images of the HE stained sections are included for comparison.

In the heat-stabilised brain sections all three adenine nucleotides could be confidently identified from tissue sections. Clear distribution images of ATP, ADP and AMP were obtained, with very specific localisation seen in the brain section for ATP. A comparison of these distribution images with a mouse brain atlas (A/J Atlas, section 9, http://www.mbl.org/mbl_main/atlas.html) was made. The areas of highest intensity appeared to correspond to areas of white matter in the brain. The regions that provided the most intense signals were the anterior commissure, the internal capsule and lateral lemniscus. Interestingly, the more vulnerable areas of the brain, including the hippocampi, contained lower levels of ATP. AMP and ADP levels were more widespread throughout the brain section. Some co-localisation was seen between ATP and ADP, in the white matter tracts. These results, alongside the intensity ratio of ATP:AMP obtained demonstrated the advantages of including a tissue fixation step prior to the freezing and sectioning of tissue.

Quantitative ^{31}P-MRSI has previously been used to determine the concentration of ATP in different regions of the human brain. The authors evaluated the tissue-specific concentration differences of ATP between cerebral grey and white matter, and the cerebellum and reported the concentrations to be: 2.19 ± 0.33 mM (cerebral gray matter), 3.41 ± 0.33 mM (cerebral white matter) and 1.75 ± 0.58 mM (cerebellum) (Hetherington, Spencer et al. 2001). The MALDI imaging results presented here are consistent with the ATP concentrations in human brain reported by Hetherington *et al.*; the highest intensity of ATP is observed in the white matter tracts and lowest in the cerebellum.

The HE stained sections highlight a potential limitation of the heat-stabilisation process, i.e. more delicate nature of the tissues following stabilisation. Whilst in Figure 5.14 the snap-frozen sections were intact, here the stabilised tissue sections were damaged and had been torn during the sectioning process. This was found to be characteristic of all stabilised brains and could provide additional challenges when carrying out MALDI imaging analysis.

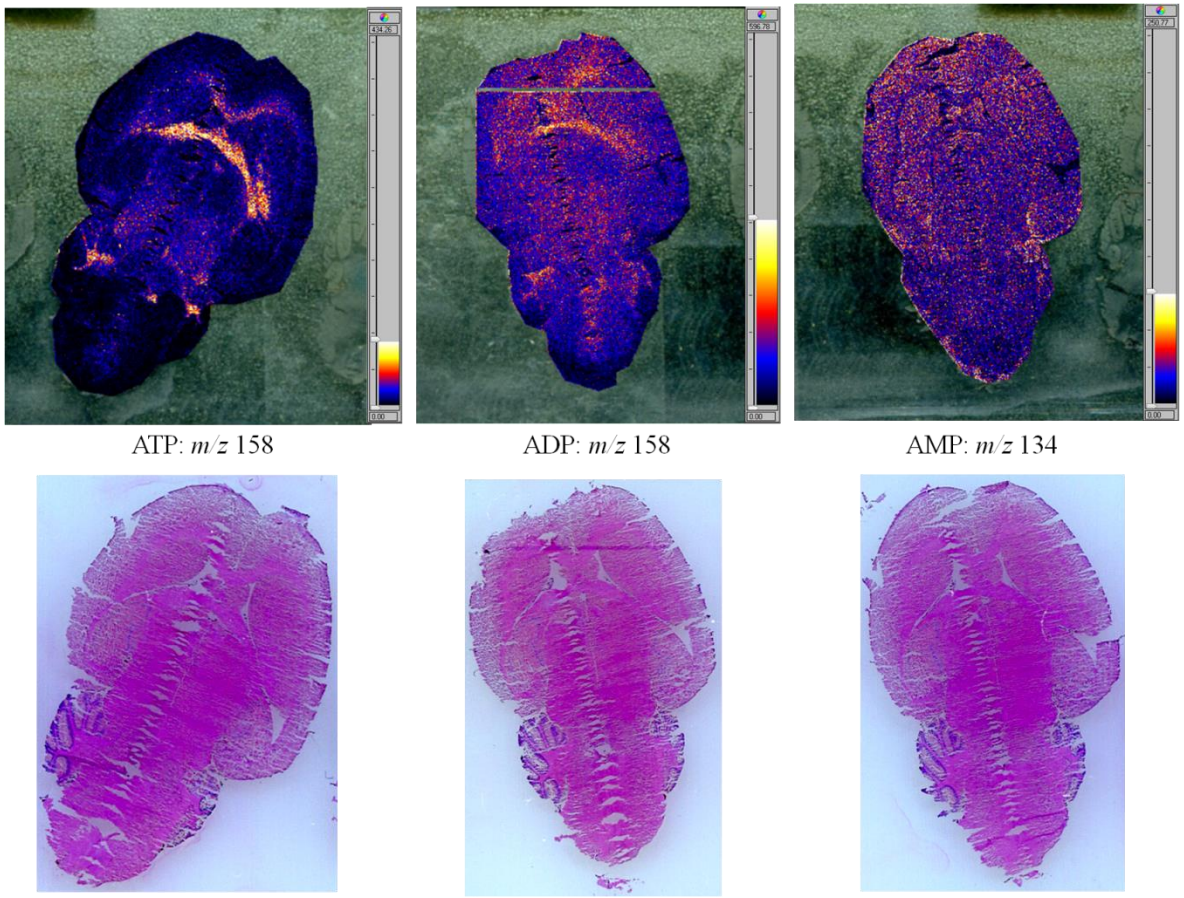

Figure 5.15 MALDI-mobility-MS/MS images of adenine nucleotide localisation in a heat-stabilised mouse brain.
Images were acquired at 50 µm spatial resolution and the localisation of the most intense fragment ion for each of ATP, ADP and AMP is displayed. Optical images of the brain sections HE stained following MS analysis are included for comparison.

5.5 Conclusions

Mobility-MS/MS enabled MALDI imaging has been successfully used for the identification and localisation of the adenine nucleotides in mouse brain tissue. Including an ion mobility separation step in the analysis made this a selective and reproducible method for the detection of these endogenous metabolites from tissue, reducing interference from other background ions. This ion mobility separation step also allowed for improved selectivity during data processing and production of ion intensity images without affecting sample preparation methods or the time of acquisition of the experiment.

It became clear during early experiments that rapid post-mortem changes of adenine nucleotide levels would hinder imaging mass spectrometry approaches for the localisation of these compounds. In order to obtain more biologically relevant distributions of these molecules, two mass spectrometry compatible tissue fixation techniques have been evaluated. The inclusion of an ice-cold ethanol wash step improved the results enough to obtain distribution images of ATP, ADP and AMP. In addition to temporarily fixing tissue prior to thawing to room temperature for matrix application, the ethanol wash step also helped to improve matrix crystallisation by washing salts and other contaminants from the surface of the tissue. Despite achieving localisation images, analysis of control and stressed brain sections did not reveal significant differences in the levels of adenine nucleotides between the two. This is likely due to rapid post-mortem degradation of adenine nucleotides in both samples.

A novel heat-stabilisation technique was evaluated in an attempt to improve the recovery of adenine nucleotides. This technique rapidly heated the tissue at the point of excision in order to denature proteins and enzymes. In these studies, the intensity ratio of ATP:AMP measured in stabilised and snap-frozen tissue was compared, alongside samples which were snap-frozen and heat-fixed following a 30 minute delay. Heat-stabilisation allowed ATP to be successfully detected and localised in brain, with an increased ATP:AMP ratio, compared to snap-frozen tissue. Clear distribution images of ATP could be obtained from heat-stabilised tissue. Tissues analysed following a 30 minute delay indicated that changes in ATP levels had

already occurred by 30 minutes, since little difference was observed between heat-treated and snap-frozen tissues which had been subjected to this wait step.

ATP levels in a heat-stabilised sample that was left for 30 minutes prior to freezing were not that which would be expected. AMP levels were found to be relatively higher than ATP, which suggested that heat-stabilisation had not entirely prevented downstream degradation of ATP to ADP and AMP. This poses questions about the ability of the heat stabilisation technique to permanently fix tissue. Heat-stabilised tissue treated in the same way as fresh-frozen tissue (immediately snap-frozen following fixation) did show relative increases in the levels of adenine nucleotides and could prove useful as a mass spectrometry compatible tissue fixation technique. Issues surrounding the integrity of stabilised tissue during sectioning, raised by Goodwin *et al.* and also during experiments conducted here, do limit the potential usefulness of this technique for MALDI imaging. This is especially true for delicate tissues and for samples where small structural changes may cause significant changes that may mask other changes of biological importance.

MALDI imaging is increasingly being used in biological applications for the detection of important endogenous metabolites. A major potential limitation to any MALDI imaging approach is the need for sufficient selectivity in order to differentiate molecules of interest from matrix compounds and endogenous compounds in the tissue. The use of ion mobility separation during acquisition coupled with MS/MS fragmentation has been shown provide enhanced selectivity without compromising the sensitivity or speed of the experiment.

It is clear that before biological questions can be properly addressed using MALDI imaging, the issue of suitable sample preparation must be addressed. The work presented here demonstrates the need to prevent biological processes continuing prior to data acquisition in order to preserve the integrity of the experiment. A simple ethanol wash is not sufficient to stop enzymatic degradation of adenine nucleotides. Thermal stabilisation of the samples offers a more robust solution, but may cause tissue samples to become more fragile, compromising spatial integrity. Recently, the use of conductive double-sided tape was shown to assist in the support of fragile tissues during sectioning of heat-stabilised brains embedded in CMC. Tissue quality was significantly improved, without an adverse effect on results obtained during MS

analysis (Goodwin, Nilsson et al. 2012). Further investigations of MS compatible tissue fixation techniques, for example microwave fixation, at the point of sacrifice or tissue excision are required. Developments in MALDI-mobility-imaging experiments, coupled with relevant sample preparation will serve to increase our knowledge of metabolite distributions. This may provide experimental data that will help to understand the role these metabolites play in metabolic stress and disease, and the potential for their restoration after brain injury.

Chapter 6 Conclusions and Future Work

The work presented in this thesis has evaluated two imaging mass spectrometry approaches, LESA-MS and MALDI-MS, for the detection and localisation of drug compounds and small molecules in rodent tissue samples. Ion mobility separation was used in conjunction with both methods to improve the selectivity of the experiment.

6.1 Ion mobility separation

The selectivity of an imaging mass spectrometry experiment is often key to the detection of ions with low abundance, or those subject to interference by endogenous ions of similar mass. With some imaging MS instrumentation, high-resolution and/or improved mass accuracy measurements are used to improve selectivity. MS/MS fragmentation has also been used to improve selectivity, but there are potential limitations in the number of analytes that can be successfully sampled at each position before the sample is consumed. At higher spatial resolutions this becomes more pronounced, since the available material at each position for study is decreased. Ion mobility separation has also been used in MALDI imaging experiments to improve selectivity, allowing the compound of interest to be imaged with less interference from background ions of similar mass.

Initial results indicated the importance of enhancing the selectivity of the experiment for drug localisation studies in tissue, using both LESA-MS and MALDI-MS approaches. The selectivity of both experimental methods was greatly improved by combining ion mobility separation with MS/MS fragmentation. This approach allowed drug compounds to be detected at lower concentrations on tissue than using MS/MS fragmentation alone, with lower interference from background ions. Including an ion mobility separation in either a MALDI imaging or LESA profiling experiment does not affect the time of acquisition or change the sample preparation methods required. It does, however, allow for additional selectivity during data interrogation and the production of ion intensity images. Without ion mobility separation, the drug detection experiments presented here for diclofenac and propranolol would not have been possible at the dosing levels provided.

Including an ion mobility separation step in the analysis of the endogenous adenine nucleotides in mouse brain proved useful in confirming the identification of these metabolites in tissue. This extra selectivity is valuable in tissue-based imaging experiments where the sample environment is particularly challenging.

6.2 LESA profiling

LESA-mobility-MS/MS experiments were used for the detection of three of drug compounds in dosed tissue sections. Diclofenac, fenclozic acid and propranolol were all detected in dosed rat or mice tissues using a LESA sampling approach coupled to nESI-MS/MS combined with ion mobility separation. Optimisation experiments demonstrated the importance of enhancing the selectivity of the LESA-MS method using ion mobility separation.

LESA profiling resulted in the successful detection of these drug compounds where MALDI-MS approaches failed to do so. This is due to the larger sampling area of LESA, on the millimetre scale, compared with that of MALDI. This provides an inherent advantage of LESA in terms of sensitivity, but at the expense of spatial resolution. LESA-MS cannot currently be used for producing localisation images with a spatial resolution approaching that of a MALDI imaging experiment. It is important, therefore, to choose a technique based on the requirements of each experiment. For a profiling experiment, LESA-MS is much faster and requires much less sample preparation than for a MALDI imaging experiment.

These experiments illustrate the potential applicability of LESA profiling as a rapid profiling technique employed prior to MALDI profiling or imaging experiments. In all cases examined in this work, if a compound of interest cannot be detected by a LESA profiling experiment it will not be detected using MALDI-MS. MALDI profiling and imaging experiments require more extensive sample preparation and longer acquisition times than for the LESA experiment. It would therefore be advantageous to use LESA-MS as a screening experiment, where sampling and analysis can be performed in a matter of minutes, prior to attempting MALDI experiments where data acquisition and analysis require hours.

6.3 MALDI imaging

MALDI-mobility-MS/MS experiments were evaluated for the detection of three drug compounds in dosed tissue sections. MALDI profiling experiments were performed to assess the ability of the approach to detect each drug compound in tissue. Experimental methods must be optimised for the compound of interest before running an imaging MS experiment. This allows the most selective and sensitive method to be established prior to analysing the dosed sample and also allows detection limits to be determined.

At lower dosing levels, MALDI profiling experiments were not able to detect diclofenac in tissue sections. The amount of drug compound calculated to be present in tissue was determined to be lower than the limit of detection of MALDI-mobility-MS/MS. Higher dosing levels of the drug compounds fenclozic acid and propranolol were much more successful in MALDI profiling experiments. Both drugs were successfully detected in tissue using MALDI-mobility-MS/MS profiling, with confident identification of fenclozic acid in dosed tissue across a time course. A MALDI-mobility-MS/MS imaging experiment showed the distribution of fenclozic acid in rat liver at 2, 6 and 24 hours after administration.

These results demonstrate the ability of MALDI imaging to determine the distribution of a drug compound in dosed tissue sections. This appears to be dependent on a number of factors. The drug must be dosed at a high enough level to allow for successful detection in tissue following administration. This should be established using an initial MALDI profiling approach. Failure to detect the compound of interest during a profiling experiment will result in an unsuccessful imaging experiment. That said, the ability to detect a drug during MALDI profiling experiments does not always indicate that MALDI imaging experiments will be successful.

A biological application of mobility enabled MALDI imaging was also undertaken. MALDI-mobility-MS/MS imaging was successfully used for the identification and localisation of adenine nucleotides in mouse brain tissue. These experiments highlighted another challenge to imaging MS experiments; that of appropriate sample preparation. Rapid changes in these nucleotides were found to occur

following death, preventing biologically relevant distributions of these molecules being obtained. In order to overcome this limitation, a number of tissue fixation approaches were assessed. Heat-stabilisation of tissues at the point of dissection showed an improvement in the levels of adenine nucleotides in measured tissue, but caused tissues to be more fragile which in turn compromised spatial integrity.

6.4 Future directions

The field of imaging mass spectrometry has expanded greatly over the last fifteen years, since the introduction of MALDI imaging in 1997. A range of application areas have been and continue to be explored including proteomics, biomedical analysis, lipidomics and pharmaceutical compounds. A wealth of information can be obtained from a tissue section in a single experiment, without the need for labelling or previous knowledge of the sample. Making sense of this information in order to draw a sensible biological conclusion proves to be a challenge without the input of a pathologist or additional information from complementary techniques.

The incorporation of ion mobility separation into the imaging mass spectrometry experiment provides an enhanced selectivity that can be used to overcome many of the issues that arise when sampling complex biological tissue samples. This technique has not yet been widely adopted in the imaging MS community, despite its noted benefits in an imaging workflow. This is perhaps due in part to the availability of only two ion mobility enabled imaging mass spectrometers, the Synapt and Synapt G2 HDMS.

Sample preparation techniques have not changed significantly from those initially reported, perhaps due to the robust nature of many of these techniques. As imaging mass spectrometry expands across new research areas, however, these sample preparation techniques should continue to be reviewed (Goodwin 2012).

There is the hope that MALDI imaging or other mass spectrometry based imaging approaches will provide a solution to the limitations of QWBA in the field of drug distribution. Radiolabelled drug compounds remain expensive to produce, and so drug localisation studies are often not performed until the later stages of drug development. Imaging mass spectrometry, without the need for labelled compounds,

could be implemented much earlier in the drug development process to provide information on the distribution of a new therapeutic compound with significant financial and research benefits.

Many challenges remain in the field of MALDI imaging of pharmaceuticals, preventing incorporation into the industrial routine of drug development. The analysis of each new compound of interest must be optimised using standards, in order to determine the most selective method for detection and localisation of that compound in tissue. Once these methods have been established, however, it would be possible to set up a routine analysis for detection of that particular drug compound in a tissue section. Imaging experiments are still time-consuming, despite the introduction of faster lasers and rastering speeds. This is a consideration that will remain important in the high-throughput environment of pharmaceutical companies.

Ambient ionisation approaches, such as LESA profiling, offer rapid analysis of samples with little or no need for sample preparation. These methods show great promise in their applicability to be incorporated more easily into a drug development workflow to provide complementary data to industry-standard methods. LESA profiling has still only been used by a few groups for the detection of drug compounds in tissue, with promising results (Eikel, Vavrek et al. 2011; Schadt, Kallbach et al. 2012). Further exposure of this technique is likely to result in a larger research population using LESA for the detection of drug compounds in tissue, where detailed spatial resolution is not required (Prideaux and Stoeckli 2012). Additional research into extraction efficiency from tissue would prove useful in this area, allowing progress to be made in the direction of quantitative analysis using the LESA approach.

6.4.1 Quantitative imaging mass spectrometry

Focus has also turned to the desire to obtain quantitative data through imaging mass spectrometry experiments. There are many issues associated with quantitation of compounds by imaging mass spectrometry. Matrix effects, ionisation efficiency and ion suppression are all factors that prevent measured signal intensity being representative of target compound concentration.

Two software packages have recently been released, which offer potential quantitative analysis of MALDI imaging data. The first, Quantinetix (imaBiotech, France), is available for use with Bruker, Thermo and ABSciex instruments. Quantinetix offers three approaches to quantitation; the use of an on tissue dilution range, the use of an isotopic internal standard or the use of a label-free internal standard. The label-free approach uses a normalisation factor (tissue extinction coefficient, TEC) to compensate for ion efficiency and suppression effects encountered in tissue samples. The TEC is calculated by comparing the intensity signal of a compound of interest on and off tissue at a known concentration. This can be used to evaluate the loss of signal on tissue specific to each compound and tissue type (Hamm, Bonnel et al. 2012).

More recently, MALDI Tools, a freely available imaging MS software, has been presented. This software includes a protocol for the quantitative imaging of drug compounds in tissue. Labelled internal standards, such as deuterated analogues, are incorporated for normalisation and quantitation directly from tissue sections (Kallback, Shariatgorji et al. 2012).

Both approaches described above offer potential solutions for the quantitative analysis of drugs in tissue, however further evaluation of these techniques would be required to confirm their accuracy. These approaches will undoubtedly be tested across a range of compounds and tissue types, provoking debate within the imaging MS community regarding their benefits and disadvantages. They provide the first step into the development of quantitative imaging mass spectrometry methods, which is likely to become a major focus of imaging mass spectrometry research in the future.

6.5 Concluding remarks

Imaging mass spectrometry remains a developing field of research, although it is now considered more mature than a new technology. The number of research articles published in the field continues to grow year on year as shown by Figure 6.1. In the last five years alone, over 3000 articles with imaging and mass spectrometry in the title, keywords or abstract have been published.

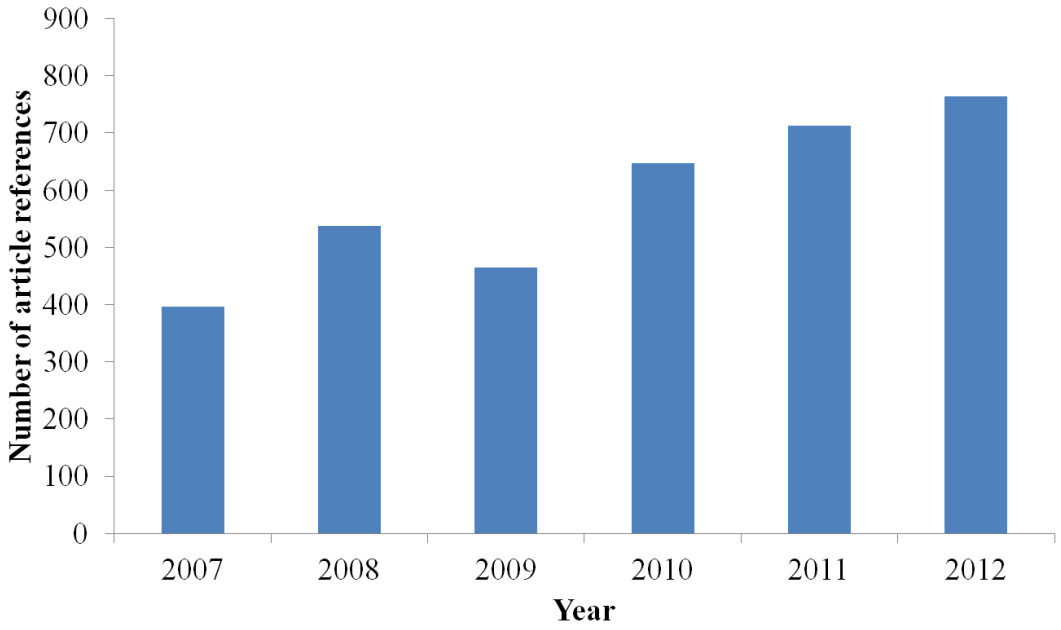

Figure 6.1 Literature search on Scopus (www.scopus.com) using the search terms 'imaging' and 'mass spectrometry' in the title, abstract or keywords. *Results up until 31st December 2012.

These data indicate the increasing interest in the field, but do not begin to represent the diversity of applications that imaging mass spectrometry has been used for. As research continues; in instrumentation through the development of new detectors and progress in sample preparation techniques and improvements in data analysis, the future for imaging mass spectrometry in one form or another looks to be a long and successful one.

Appendix A: References

Aboagye, E. O. (2005). "Positron emission tomography imaging of small animals in anticancer drug development." Molecular Imaging and Biology **7**(1): 53-58.

Aboagye, E. O. and P. M. Price (2003). "Use of positron emission tomography in anticancer drug development." Investigational New Drugs **21**(2): 169-181.

Adams, C. P. and V. V. Brantner (2006). "Estimating the cost of new drug development: Is it really $802 million?" Health Affairs **25**(2): 420-428.

Aoki, Y., A. Toyama, et al. (2007). "A novel method for analyzing formalin-fixed paraffin embedded (FFPE) tissue sections by mass spectrometry imaging." Proceedings of the Japan Academy Series B-Physical and Biological Sciences **83**(7): 205-214.

Aston, F. W. (1919). "A positive ray spectrograph." Philosophical Magazine **38**: 707-714.

Aston, F. W. (1920). "The mass spectra of chemical elements." Philosophical Magazine (Series 6) **39**: 611-625.

Athersuch, T. J., R. L. Sison, et al. (2008). "Evaluation of the use of UPLC-TOFMS with simultaneous [C-14]-radioflow detection for drug metabolite profiling: Application to propranolol metabolites in rat urine." Journal of Pharmaceutical and Biomedical Analysis **48**(1): 151-157.

Atkinson, S. J., P. M. Loadman, et al. (2007). "Examination of the distribution of the bioreductive drug AQ4N and its active metabolite AQ4 in solid tumours by imaging matrix-assisted laser desorption/ionisation mass spectrometry." Rapid Communications in Mass Spectrometry **21**(7): 1271-1276.

Atkinson, S. J., B. Prideaux, et al. (2005). "Imaging Matrix assisted laser desorption ionisation mass spectrometry - A new technique for drug distribution studies." Chimica Oggi-Chemistry Today **23**(6): 5-8.

Barber, M., R. S. Bordoli, et al. (1981). "FAST ATOM BOMBARDMENT OF SOLIDS (FAB) - A NEW ION-SOURCE FOR MASS-SPECTROMETRY." Journal of the Chemical Society-Chemical Communications(7): 325-327.

Baughman, T. M., C. L. Talarico, et al. (2009). "Evaluation of the metabolism of propranolol by linear ion trap technology in mouse, rat, dog, monkey, and human cryopreserved hepatocytes." Rapid Communications in Mass Spectrometry **23**(14): 2146-2150.

Beaudry, F., J. C. Y. Le Blanc, et al. (1999). "Metabolite profiling study of propranolol in rat using LC/MS/MS analysis." Biomedical Chromatography **13**(5): 363-369.

Benabdellah, F., D. Touboul, et al. (2009). "In Situ Primary Metabolites Localization on a Rat Brain Section by Chemical Mass Spectrometry Imaging." Analytical Chemistry **81**(13): 5557-5560.

Blatherwick, E. Q., G. J. Van Berkel, et al. (2011). "Utility of spatially-resolved atmospheric pressure surface sampling and ionization techniques as alternatives to mass spectrometric imaging (MSI) in drug metabolism." Xenobiotica **41**(8): 720-734.

Borsdorf, H. and G. A. Eiceman (2006). "Ion mobility spectrometry: Principles and applications." Applied Spectroscopy Reviews **41**(4): 323-375.

Borsdorf, H., T. Mayer, et al. (2011). "Recent Developments in Ion Mobility Spectrometry." Applied Spectroscopy Reviews **46**(6): 472-521.

Budzikiewicz, H. and R. D. Grigsby (2006). "Mass spectrometry and isotopes: A century of research and discussion." Mass Spectrometry Reviews **25**(1): 146-157.
Bunch, J., M. R. Clench, et al. (2004). "Determination of pharmaceutical compounds in skin by imaging matrix-assisted laser desorption/ionisation mass spectrometry." Rapid Communications in Mass Spectrometry **18**(24): 3051-3060.
Burns, H. D., T. G. Hamill, et al. (1999). "Positron emission tomography neuroreceptor imaging as a tool in drug discovery, research and development." Current Opinion in Chemical Biology **3**(4): 388-394.
Bush, M. F., Z. Hall, et al. (2010). "Collision Cross Sections of Proteins and Their Complexes: A Calibration Framework and Database for Gas-Phase Structural Biology." Analytical Chemistry **82**(22): 9557-9565.
Caprioli, R. M., T. B. Farmer, et al. (1997). "Molecular imaging of biological samples: Localization of peptides and proteins using MALDI-TOF MS." Analytical Chemistry **69**(23): 4751-4760.
Chang, W. C., L. C. L. Huang, et al. (2007). "Matrix-assisted laser desorption/ionization (MALDI) mechanism revisited." Analytica Chimica Acta **582**(1): 1-9.
Chaurand, P., S. A. Schwartz, et al. (2004). "Profiling and imaging proteins in tissue sections by MS." Analytical Chemistry **76**(5): 86A-93A.
Chaurand, P., S. A. Schwartz, et al. (2005). "Imaging mass spectrometry: Principles and potentials." Toxicologic Pathology **33**(1): 92-101.
Chen, Y., M. Monshouwer, et al. (2007). "Analytical tools and approaches for metabolite identification in early drug discovery." Pharmaceutical Research **24**(2): 248-257.
Chughtai, K. and R. M. A. Heeren (2010). "Mass Spectrometric Imaging for Biomedical Tissue Analysis." Chemical Reviews **110**(5): 3237-3277.
Coe, R. A. J. (2000). "Quantitative whole-body autoradiography." Regulatory Toxicology and Pharmacology **31**(2): S1-S3.
Coles, J. and M. Guilhaus (1993). "Orthogonal acceleration — a new direction for time-of-flight mass spectrometry: Fast, sensitive mass analysis for continuous ion sources." TrAC Trends in Analytical Chemistry **12**(5): 203-213.
Creaser, C. S., J. R. Griffiths, et al. (2004). "Ion mobility spectrometry: a review. Part 1. Structural analysis by mobility measurement." Analyst **129**(11): 984-994.
Dale, N. and B. G. Frenguelli (2009). "Release of Adenosine and ATP During Ischemia and Epilepsy." Current Neuropharmacology **7**(3): 160-179.
Dawson, J. H. J. and M. Guilhaus (1989). "Orthogonal-acceleration time-of-flight mass spectrometer." Rapid Communications in Mass Spectrometry **3**(5): 155-159.
de Hoffmann, E. and V. Stroobant (2009). Mass Spectrometry: Principles and Applications. Chichester, England, John Wiley & Sons, Ltd.
Delaney, S. M. and J. D. Geiger (1996). "Brain regional levels of adenosine and adenosine nucleotides in rats killed by high-energy focused microwave irradiation." Journal of Neuroscience Methods **64**(2): 151-156.
Dill, A. L., D. R. Ifa, et al. (2009). "Mass spectrometric imaging of lipids using desorption electrospray ionization." Journal of Chromatography B-Analytical Technologies in the Biomedical and Life Sciences **877**(26): 2883-2889.

DiMasi, J. A., R. W. Hansen, et al. (2003). "The price of innovation: new estimates of drug development costs." Journal of Health Economics **22**(2): 151-185.
Djidja, M.-C., S. Francese, et al. (2009). "Detergent addition to tryptic digests and ion mobility separation prior to MS/MS improves peptide yield and protein identification for in situ proteomic investigation of frozen and formalin-fixed paraffin-embedded adenocarcinoma tissue sections." Proteomics **9**(10): 2750-2763.
Doyle, K. P., R. P. Simon, et al. (2008). "Mechanisms of ischemic brain damage." Neuropharmacology **55**(3): 310-318.
Drexler, D. M., T. J. Garrett, et al. (2007). "Utility of imaging mass spectrometry (IMS) by matrix-assisted laser desorption ionization (MALDI) on an ion trap mass spectrometer in the analysis of drugs and metabolites in biological tissues." Journal of Pharmacological and Toxicological Methods **55**(3): 279-288.
Eberlin, L. S., C. R. Ferreira, et al. (2011). "Desorption electrospray ionization mass spectrometry for lipid characterization and biological tissue imaging." Biochimica Et Biophysica Acta-Molecular and Cell Biology of Lipids **1811**(11): 946-960.
Eberlin, L. S., D. R. Ifa, et al. (2010). "Three-Dimensional Vizualization of Mouse Brain by Lipid Analysis Using Ambient Ionization Mass Spectrometry." Angewandte Chemie-International Edition **49**(5): 873-876.
Eckelman, W. C. (2003). The Use of Positron Emission Tomography in Drug Discovery and Development. Positron Emission Tomography: Basic Sciences, Springer**:** 327-341.
Eikel, D. and J. Henion (2011). "Liquid extraction surface analysis (LESA) of food surfaces employing chip-based nano-electrospray mass spectrometry." Rapid Communications in Mass Spectrometry **25**(16): 2345-2354.
Eikel, D., M. Vavrek, et al. (2011). "Liquid extraction surface analysis mass spectrometry (LESA-MS) as a novel profiling tool for drug distribution and metabolism analysis: the terfenadine example." Rapid Communications in Mass Spectrometry **25**(23): 3587-3596.
Farde, L. (1996). "The advantage of using positron emission tomography in drug research." Trends in Neurosciences **19**(6): 211-214.
Fitzgerald, J. D. and S. R. O'Donnell (1971). "Pharmacology of 4-hydroxypropranolol, a metabolite of propranolol." British journal of pharmacology **43**(1): 222-235.
Fletcher, J. S., N. P. Lockyer, et al. (2009). "DEVELOPMENTS IN MOLECULAR SIMS DEPTH PROFILING AND 3D IMAGING OF BIOLOGICAL SYSTEMS USING POLYATOMIC PRIMARY IONS." Mass Spectrometry Reviews **30**(1): 142-174.
Foulkes, D. M. (1970). "METABOLISM OF C-14-ICI-54,453 (MYALEX) IN VARIOUS SPECIES - AN IN-VIVO NIH SHIFT." Journal of Pharmacology and Experimental Therapeutics **172**(1): 115-&.
Frenguelli, B. G., G. Wigmore, et al. (2007). "Temporal and mechanistic dissociation of ATP and adenosine release during ischaemia in the mammalian hippocampus." Journal of Neurochemistry **101**(5): 1400-1413.
Galli, C. and G. Racagni (1982). "USE OF MICROWAVE TECHNIQUES TO INACTIVATE BRAIN-ENZYMES RAPIDLY." Methods in Enzymology **86**: 635-642.

Giles, K., S. D. Pringle, et al. (2004). "Applications of a travelling wave-based radio-frequencyonly stacked ring ion guide." Rapid Communications in Mass Spectrometry **18**(20): 2401-2414.
Giles, K., J. P. Williams, et al. (2011). "Enhancements in travelling wave ion mobility resolution." Rapid Communications in Mass Spectrometry **25**(11): 1559-1566.
Girod, M., Y. Z. Shi, et al. (2010). "Desorption Electrospray Ionization Imaging Mass Spectrometry of Lipids in Rat Spinal Cord." Journal of the American Society for Mass Spectrometry **21**(7): 1177-1189.
Goodwin, R. J. A. (2012). "Sample preparation for mass spectrometry imaging: Small mistakes can lead to big consequences." Journal of Proteomics **75**(16): 4893-4911.
Goodwin, R. J. A., A. M. Lang, et al. (2010). "Stopping the clock on proteomic degradation by heat treatment at the point of tissue excision." Proteomics **10**(9): 1751-1761.
Goodwin, R. J. A., A. Nilsson, et al. (2012). "Conductive carbon tape used for support and mounting of both whole animal and fragile heat-treated tissue sections for MALDI MS imaging and quantitation." Journal of Proteomics **75**(16): 4912-4920.
Goodwin, R. J. A., S. R. Pennington, et al. (2008). "Protein and peptides in pictures: Imaging with MALDI mass spectrometry." Proteomics **8**(18): 3785-3800.
Griffiths, W. J., A. P. Jonsson, et al. (2001). "Electrospray and tandem mass spectrometry in biochemistry." Biochemical Journal **355**: 545-561.
Groseclose, M. R., M. Andersson, et al. (2007). "Identification of proteins directly from tissue: in situ tryptic digestions coupled with imaging mass spectrometry." Journal of Mass Spectrometry **42**(2): 254-262.
Gross, S. and D. Piwnica-Worms (2006). "Molecular imaging strategies for drug discovery and development." Current Opinion in Chemical Biology **10**(4): 334-342.
Guilhaus, M., D. Selby, et al. (2000). "Orthogonal acceleration time-of-flight mass spectrometry." Mass Spectrometry Reviews **19**(2): 65-107.
Haddon, W. F. and F. W. McLafferty (1968). "Metastable ion characteristics. VII. Collision-induced metastables." Journal of the American Chemical Society **90**(17): 4745-4746.
Hamm, G., D. Bonnel, et al. (2012). "Quantitative mass spectrometry imaging of propranolol and olanzapine using tissue extinction calculation as normalization factor." Journal of Proteomics **75**(16): 4952-4961.
Hardie, D. G. and S. A. Hawley (2001). "AMP-activated protein kinase: the energy charge hypothesis revisited." Bioessays **23**(12): 1112-1119.
Hart, F. D., L. S. Bain, et al. (1970). "HEPATIC EFFECTS OF FENCLOZIC ACID." Annals of the Rheumatic Diseases **29**(6): 684-&.
Hattori, K., M. Kajimura, et al. (2010). "Paradoxical ATP Elevation in Ischemic Penumbra Revealed by Quantitative Imaging Mass Spectrometry." Antioxidants & Redox Signaling **13**(8): 1157-1167.
Hayasaka, T., N. Goto-Inoue, et al. (2008). "Matrix-assisted laser desorption/ionization quadrupole ion trap time-of-flight (MALDI-QIT-TOF)-based imaging mass spectrometry reveals a layered distribution of phospholipid molecular species in the mouse retina." Rapid Communications in Mass Spectrometry **22**(21): 3415-3426.

Hayes, A. and R. G. Cooper (1971). "STUDIES ON ABSORPTION, DISTRIBUTION AND EXCRETION OF PROPRANOLOL IN RAT, DOG AND MONKEY." Journal of Pharmacology and Experimental Therapeutics **176**(2): 302-&.

Heeren, R. M. A., B. Kukrer-Kaletas, et al. (2008). "Quality of surface: The influence of sample preparation on MS-based biomolecular tissue imaging with MALDI-MS and (ME-)SIMS." Applied Surface Science **255**(4): 1289-1297.

Heeren, R. M. A., L. A. McDonnell, et al. (2006). "Why don't biologists use SIMS? A critical evaluation of imaging MS." Applied Surface Science **252**(19): 6827-6835.

Heeren, R. M. A., D. F. Smith, et al. (2009). "Imaging Mass Spectrometry: Hype or Hope?" Journal of the American Society for Mass Spectrometry **20**(6): 1006-1014.

Henry, K. D., E. R. Williams, et al. (1989). "FOURIER-TRANSFORM MASS-SPECTROMETRY OF LARGE MOLECULES BY ELECTROSPRAY IONIZATION." Proceedings of the National Academy of Sciences of the United States of America **86**(23): 9075-9078.

Hepworth, W., B. B. Newbould, et al. (1969). "2-4 CHLOROPHENYLTHIAZOL-4-YL ACETIC-ACID ANTI INFLAM MYALEX ANTI INFLAM A NEW COMPOUND WITH ANTI INFLAMMATORY ANALGESIC AND ANTI PYRETIC ACTIVITY." Nature (London) **221**(5180): 582-583.

Hetherington, H. P., D. D. Spencer, et al. (2001). "Quantitative 31P spectroscopic imaging of human brain at 4 Tesla: Assessment of gray and white matter differences of phosphocreatine and ATP." Magnetic Resonance in Medicine **45**(1): 46-52.

Hilton, G. R., K. Thalassinos, et al. (2010). "Structural Analysis of Prion Proteins by Means of Drift Cell and Traveling Wave Ion Mobility Mass Spectrometry." Journal of the American Society for Mass Spectrometry **21**(5): 845-854.

Holcapek, M., L. Kolarova, et al. (2008). "High-performance liquid chromatography-tandem mass spectrometry in the identification and determination of phase I and phase II drug metabolites." Analytical and Bioanalytical Chemistry **391**(1): 59-78.

Hsieh, Y., R. Casale, et al. (2006). "Matrix-assisted laser desorption/ionization imaging mass spectrometry for direct measurement of clozapine in rat brain tissue." Rapid Communications in Mass Spectrometry **20**(6): 965-972.

Hsieh, Y., J. Chen, et al. (2007). "Mapping pharmaceuticals in tissues using MALDI imaging mass spectrometry." Journal of Pharmacological and Toxicological Methods **55**(2): 193-200.

Hu, Q. Z., R. J. Noll, et al. (2005). "The Orbitrap: a new mass spectrometer." Journal of Mass Spectrometry **40**(4): 430-443.

Jardin-Mathe, O., D. Bonnel, et al. (2008). "MITICS (MALDI Imaging Team Imaging Computing System): A new open source mass spectrometry imaging software." Journal of Proteomics **71**(3): 332-345.

Jennings, K. R. (1968). "Collision-induced decompositions of aromatic molecular ions." International Journal of Mass Spectrometry and Ion Physics **1**(3): 227-235.

Kaletas, B. K., I. M. van der Wiel, et al. (2009). "Sample preparation issues for tissue imaging by imaging MS." Proteomics **9**(10): 2622-2633.

Kallback, P., M. Shariatgorji, et al. (2012). "Novel mass spectrometry imaging software assisting labeled normalization and quantitation of drugs and neuropeptides directly in tissue sections." Journal of Proteomics **75**(16): 4941-4951.
Kanu, A. B., P. Dwivedi, et al. (2008). "Ion mobility-mass spectrometry." Journal of Mass Spectrometry **43**(1): 1-22.
Karas, M. and F. Hillenkamp (1988). "LASER DESORPTION IONIZATION OF PROTEINS WITH MOLECULAR MASSES EXCEEDING 10000 DALTONS." Analytical Chemistry **60**(20): 2299-2301.
Karas, M. and R. Kruger (2003). "Ion formation in MALDI: The cluster ionization mechanism." Chemical Reviews **103**(2): 427-439.
Kertesz, V. and G. J. Van Berkel (2008). "Improved imaging resolution in desorption electrospray ionization mass spectrometry." Rapid Communications in Mass Spectrometry **22**(17): 2639-2644.
Kertesz, V. and G. J. Van Berkel (2010). "Fully automated liquid extraction-based surface sampling and ionization using a chip-based robotic nanoelectrospray platform." Journal of Mass Spectrometry **45**(3): 252-260.
Kertesz, V. and G. J. Van Berkel (2010). "Liquid Microjunction Surface Sampling Coupled with High-Pressure Liquid Chromatography-Electrospray Ionization-Mass Spectrometry for Analysis of Drugs and Metabolites in Whole-Body Thin Tissue Sections." Analytical Chemistry **82**(14): 5917-5921.
Kertesz, V., G. J. Van Berkel, et al. (2008). "Comparison of drug distribution images from whole-body thin tissue sections obtained using desorption electrospray ionization tandem mass spectrometry and autoradiography." Analytical Chemistry **80**(13): 5168-5177.
Khatib-Shahidi, S., M. Andersson, et al. (2006). "Direct molecular analysis of whole-body animal tissue sections by imaging MALDI mass spectrometry." Analytical Chemistry **78**(18): 6448-6456.
Knochenmuss, R. and R. Zenobi (2003). "MALDI ionization: The role of in-plume processes." Chemical Reviews **103**(2): 441-452.
Kolbe, H. and G. Dietzel (2000). "Technical validation of radioluminography systems." Regulatory Toxicology and Pharmacology **31**(2): S5-S14.
Koppenaal, D., C. J. Barinaga, et al. (2005). "Mass spectrometry detectors." Analytical Chemistry **77**(21): 418A-427A.
Kutz, K. K., J. J. Schmidt, et al. (2004). "In situ tissue analysis of neuropeptides by MALDI FTMS in-cell accumulation." Analytical Chemistry **76**(19): 5630-5640.
Landgraf, R. R., M. C. P. Conaway, et al. (2009). "Imaging of Lipids in Spinal Cord Using Intermediate Pressure Matrix-Assisted Laser Desorption-Linear Ion Trap/Orbitrap MS." Analytical Chemistry **81**(20): 8488-8495.
Laskin, J., B. S. Heath, et al. (2011). "Tissue Imaging Using Nanospray Desorption Electrospray Ionization Mass Spectrometry." Analytical Chemistry **84**(1): 141-148.
Lodish, H., D. Baltimore, et al. (1995). Molecular cell biology; Third edition. Molecular cell biology, Third edition.
Luckey, G. W. (1975). Apparatus and Method for Producing Images Corresponding to Patterns of High Energy Radiation. US Patent.

Maas, J., R. Binder, et al. (2000). "Quantitative whole-body autoradiography: Recommendations for the standardization of the method." Regulatory Toxicology and Pharmacology **31**(2): S15-S21.
Makarov, A. (2000). "Electrostatic axially harmonic orbital trapping: A high-performance technique of mass analysis." Analytical Chemistry **72**(6): 1156-1162.
Mamyrin, B. A., V. I. Karataev, et al. (1973). "MASS-REFLECTRON A NEW NONMAGNETIC TIME-OF-FLIGHT HIGH-RESOLUTION MASS-SPECTROMETER." Zhurnal Eksperimentalnoi I Teoreticheskoi Fiziki **64**(1): 82-89.
Manicke, N. E., M. Nefliu, et al. (2009). "Imaging of Lipids in Atheroma by Desorption Electrospray Ionization Mass Spectrometry." Analytical Chemistry **81**(21): 8702-8707.
Marshall, A. G. and C. L. Hendrickson (2002). "Fourier transform ion cyclotron resonance detection: principles and experimental configurations." International Journal of Mass Spectrometry **215**(1-3): 59-75.
Marshall, P., V. Toteu-Djomte, et al. (2010). "Correlation of Skin Blanching and Percutaneous Absorption for Glucocorticoid Receptor Agonists by Matrix-Assisted Laser Desorption Ionization Mass Spectrometry Imaging and Liquid Extraction Surface Analysis with Nanoelectrospray Ionization Mass Spectrometry." Analytical Chemistry **82**(18): 7787-7794.
Masuoka, D. and E. Hansson (1967). "Autoradiographic distribution studies of adrenergic blocking agents. II. 14C-propranolol, a beta-receptor-type blocker." Acta pharmacologica et toxicologica **25**(4): 447-455.
McCullough, B. J., J. Kalapothakis, et al. (2008). "Development of an ion mobility quadrupole time of flight mass spectrometer." Analytical Chemistry **80**(16): 6336-6344.
McDonnell, L. A. and R. M. A. Heeren (2007). "Imaging mass spectrometry." Mass Spectrometry Reviews **26**(4): 606-643.
McDonnell, L. A., A. van Remoortere, et al. (2010). "Automated imaging MS: Toward high throughput imaging mass spectrometry." Journal of Proteomics **73**(6): 1279-1282.
McLean, J. A., W. B. Ridenour, et al. (2007). "Profiling and imaging of tissues by imaging ion mobility-mass spectrometry." Journal of Mass Spectrometry **42**(8): 1099-1105.
McLuckey, S. A. and J. M. Wells (2001). "Mass analysis at the advent of the 21st century." Chemical Reviews **101**(2): 571-606.
Mitra, S. and T. H. Foster (2008). "In vivo confocal fluorescence imaging of the intratumor distribution of the photosensitizer mono-L-aspartylchlorin-e6." Neoplasia **10**(5): 429-438.
Morgan, S., P. Grootendorst, et al. (2011). "The cost of drug development: A systematic review." Health Policy **100**(1): 4-17.
O'Callaghan, J. P. and K. Sriram (2004). "Focused microwave irradiation of the brain preserves in vivo protein phosphorylation: comparison with other methods of sacrifice and analysis of multiple phosphoproteins." Journal of Neuroscience Methods **135**(1-2): 159-168.
O'Halloran, G. J., R. A. Fluegge, et al. (1964). "Report

No.ASD-TDR-62-644 Part I & 2: Determination of chemical species prevalent in a plasma jet." Technical Report prepared by the Bendix Corporation Research

Laboratories Division, Southfield Michigan under Contract Nos AF33(616)-8374 and AF33(657)-11018. A.F. Materials Laboratory Research and Technology Division Air Force Systems Command.

Paul, S. M., D. S. Mytelka, et al. (2010). "How to improve R&D productivity: the pharmaceutical industry's grand challenge." Nature Reviews Drug Discovery **9**(3): 203-214.

Paul, W. and H. Steinwedel (1953). "Ein neues massenspektrometer ohne magnetfeld

(A new mass spectrometer without a magnetic field)." Z. Naturforsch., A: Phys. Sci. **8**: 448-450.

Paul, W. and H. Steinwedel (1960). Apparatus For Separating Charged Particles Of Different Specific Charges. U.S. Patent. **2939952**.

Port, R. E. and W. Wolf (2003). "Noninvasive methods to study drug distribution." Investigational New Drugs **21**(2): 157-168.

Prakash, C., C. L. Shaffer, et al. (2007). "Analytical strategies for identifying drug metabolites." Mass Spectrometry Reviews **26**(3): 340-369.

Prasad, B., A. Garg, et al. (2011). "Metabolite identification by liquid chromatography-mass spectrometry." Trac-Trends in Analytical Chemistry **30**(2): 360-387.

Prideaux, B., V. Dartois, et al. (2011). "High-Sensitivity MALDI-MRM-MS Imaging of Moxifloxacin Distribution in Tuberculosis-Infected Rabbit Lungs and Granulomatous Lesions." Analytical Chemistry **83**(6): 2112-2118.

Prideaux, B. and M. Stoeckli (2012). "Mass spectrometry imaging for drug distribution studies." Journal of Proteomics **75**(16): 4999-5013.

Pringle, S. D., K. Giles, et al. (2007). "An investigation of the mobility separation of some peptide and protein ions using a new hybrid quadrupole/travelling wave IMS/oa-ToF instrument." International Journal of Mass Spectrometry **261**(1): 1-12.

Pysz, M. A., S. S. Gambhir, et al. (2010). "Molecular imaging: current status and emerging strategies." Clinical Radiology **65**(7): 500-516.

Rao, J., A. Dragulescu-Andrasi, et al. (2007). "Fluorescence imaging in vivo: recent advances." Current Opinion in Biotechnology **18**(1): 17-25.

Reyzer, M. L. and R. M. Caprioli (2007). "MALDI-MS-based imaging of small molecules and proteins in tissues." Current Opinion in Chemical Biology **11**(1): 29-35.

Reyzer, M. L., Y. S. Hsieh, et al. (2003). "Direct analysis of drug candidates in tissue by matrix-assisted laser desorption/ionization mass spectrometry." Journal of Mass Spectrometry **38**(10): 1081-1092.

Roach, P. J., J. Laskin, et al. (2010). "Nanospray desorption electrospray ionization: an ambient method for liquid-extraction surface sampling in mass spectrometry." Analyst **135**(9): 2233-2236.

Rodríguez, I., S. Pérez-Rial, et al. (2008). "Magnetic resonance methods and applications in pharmaceutical research." Journal of Pharmaceutical Sciences **97**(9): 3637-3665.

Rohner, T. C., D. Staab, et al. (2005). "MALDI mass spectrometric imaging of biological tissue sections." Mechanisms of Ageing and Development **126**(1): 177-185.

Routledge, P. A. and D. G. Shand (1979). "CLINICAL PHARMACOKINETICS OF PROPRANOLOL." Clinical Pharmacokinetics **4**(2): 73-90.

Rubakhin, S. S., J. C. Jurchen, et al. (2005). "Imaging mass spectrometry: fundamentals and applications to drug discovery." Drug Discovery Today **10**(12): 823-837.
Rudin, M., M. Rausch, et al. (2005). "Molecular imaging in drug discovery and development: Potential and limitations of nonnuclear methods." Molecular Imaging and Biology **7**(1): 5-13.
Rudin, M. and R. Weissleder (2003). "Molecular imaging in drug discovery and development." Nature Reviews Drug Discovery **2**(2): 123-131.
Ruotolo, B. T., K. Giles, et al. (2005). "Evidence for Macromolecular Protein Rings in the Absence of Bulk Water." Science **310**(5754): 1658-1661.
Scarff, C. A., V. J. Patel, et al. (2009). "Probing Hemoglobin Structure by Means of Traveling-Wave Ion Mobility Mass Spectrometry." Journal of the American Society for Mass Spectrometry **20**(4): 625-631.
Schadt, S., S. Kallbach, et al. (2012). "Investigation of Figopitant and Its Metabolites in Rat Tissue by Combining Whole-Body Autoradiography with Liquid Extraction Surface Analysis Mass Spectrometry." Drug Metabolism and Disposition **40**(3): 419-425.
Schiff, A. A. and A. Saxey (1984). "AUTORADIOGRAPHY OF NADOLOL AND PROPRANOLOL IN THE RAT." Xenobiotica **14**(9): 687-691.
Schuerenberg, M., C. Luebbert, et al. (2007). "A New Matrix Application Device for MALDI Tissue Imaging." Bruker Daltonics Technical Note **# 018** (http://www.maldi-msi.org/download/tech18_ImagePrep.pdf) 17th April 2012.
Schwartz, S. A., M. L. Reyzer, et al. (2003). "Direct tissue analysis using matrix-assisted laser desorption/ionization mass spectrometry: practical aspects of sample preparation." Journal of Mass Spectrometry **38**(7): 699-708.
Schweitzer, A., A. Fahr, et al. (1987). "A SIMPLE METHOD FOR THE QUANTITATION OF C-14 WHOLE-BODY AUTORADIOGRAMS." Applied Radiation and Isotopes **38**(5): 329-333.
Setou, M. (2010). Imaging mass spectrometry : protocols for mass microscopy. Tokyo, Springer.
Shand, D. G. and R. E. Rangno (1972). "DISPOSITION OF PROPRANOLOL .1. ELIMINATION DURING ORAL ABSORPTION IN MAN." Pharmacology **7**(3): 159-&.
Shigematsu, A., N. Motoji, et al. (1995). "PROGRESSIVE APPLICATION OF AUTORADIOGRAPHY IN PHARMACOKINETIC AND METABOLIC STUDIES FOR THE DEVELOPMENT OF NEW DRUGS." Regulatory Toxicology and Pharmacology **22**(2): 122-142.
Shimma, S., Y. Sugiura, et al. (2008). "Mass imaging and identification of biomolecules with MALDI-QIT-TOF-based system." Analytical Chemistry **80**(3): 878-885.
Shin, Y. G., T. Dong, et al. (2011). "Determination of Loperamide in Mdr1a/1b Knock-out Mouse Brain Tissue Using Matrix-Assisted Laser Desorption/Ionization Mass Spectrometry and Comparison with Quantitative Electrospray-Triple Quadrupole Mass Spectrometry Analysis." Archives of Pharmacal Research **34**(11): 1983-1988.
Slade, S. E., L. A. Gethings, et al. (2012). Comprehensive characterisation of the sub-proteomes of Myxococcus xanthus using a combination of 1D and 2D-chromatography incorporating mobility-enabled Data Independent

Acquisition. Proceedings of the American Society of Mass Spectrometry Conference, Vancouver, B.C., Canada.
Snel, M., Claude, E., McKenna, T., Langridge, J. (2007) "Advances in MALDI imaging mass spectrometry - adding a new dimension of separation for direct tissue analysis." **Application Note - Waters Corporation, Manchester, UK**.
Solon, E. G. (2012). "Use of Radioactive Compounds and Autoradiography to Determine Drug Tissue Distribution." Chemical Research in Toxicology **25**(3): 543-555.
Solon, E. G., A. Schweitzer, et al. (2010). "Autoradiography, MALDI-MS, and SIMS-MS Imaging in Pharmaceutical Discovery and Development." Aaps Journal **12**(1): 11-26.
Stafford, G. C., P. E. Kelley, et al. (1984). "RECENT IMPROVEMENTS IN AND ANALYTICAL APPLICATIONS OF ADVANCED ION TRAP TECHNOLOGY." International Journal of Mass Spectrometry and Ion Processes **60**(SEP): 85-98.
Stauber, J., L. MacAleese, et al. (2010). "On-Tissue Protein Identification and Imaging by MALDI-Ion Mobility Mass Spectrometry." Journal of the American Society for Mass Spectrometry **21**(3): 338-347.
Stephens, W. (1946). "A pulsed mass spectrometer with time dispersion." Physical Review **69**(11-12): 691.
Stoeckli, M., P. Chaurand, et al. (2001). "Imaging mass spectrometry: A new technology for the analysis of protein expression in mammalian tissues." Nature Medicine **7**(4): 493-496.
Stoeckli, M., D. Staab, et al. (2007). "Compound and metabolite distribution measured by MALDI mass spectrometric imaging in whole-body tissue sections." International Journal of Mass Spectrometry **260**(2-3): 195-202.
Stoeckli, M., D. Staab, et al. (2002). "Molecular imaging of amyloid beta peptides in mouse brain sections using mass spectrometry." Analytical Biochemistry **311**(1): 33-39.
Stryer, L. B., J.M., Tymoczko, J.L. (2002). BIOCHEMISTRY FIFTH EDITION. Stryer, L. Biochemistry, Fifth Edition. Xxxiii+1089p. W. H. Freeman and Co.: New York, New York, USA. Illus.
Sugiura, Y. (2012). An optimized organ fixation technique for imaging and quantitative mass spectrometry for high energy phosphate-metabolites. Proceedings of the American Society of Mass Spectrometry Conference, Vancouver, B.C., Canada.
Sugiura, Y., R. Taguchi, et al. (2011). "Visualization of Spatiotemporal Energy Dynamics of Hippocampal Neurons by Mass Spectrometry during a Kainate-Induced Seizure." Plos One **6**(3).
Svensson, M., M. Boren, et al. (2009). "Heat Stabilization of the Tissue Proteome: A New Technology for Improved Proteomics." Journal of Proteome Research **8**(2): 974-981.
Taban, I. M., A. F. M. Altelaar, et al. (2007). "Imaging of Peptides in the Rat Brain Using MALDI-FTICR Mass Spectrometry." Journal of the American Society for Mass Spectrometry **18**(1): 145-151.
Takats, Z., J. M. Wiseman, et al. (2004). "Mass spectrometry sampling under ambient conditions with desorption electrospray ionization." Science **306**(5695): 471-473.

Tanaka, K., H. Waki, et al. (1988). "Protein and polymer analyses up to m/z 100 000 by laser ionization time-of-flight mass spectrometry." Rapid Communications in Mass Spectrometry **2**(8): 151-153.
Tang, W. (2003). "The metabolism of diclofenac - Enzymology and toxicology perspectives." Current Drug Metabolism **4**(4): 319-329.
Thalassinos, K., M. Grabenauer, et al. (2009). "Characterization of Phosphorylated Peptides Using Traveling Wave-Based and Drift Cell Ion Mobility Mass Spectrometry." Analytical Chemistry **81**(1): 248-254.
Thalassinos, K., S. E. Slade, et al. (2004). "Ion mobility mass spectrometry of proteins in a modified commercial mass spectrometer." International Journal of Mass Spectrometry **236**(1-3): 55-63.
Thomson, J. J. (1912). "Further experiments on positive rays." Philosophical Magazine (Series 6) **24**: 209-253.
Todd, P. J., T. G. Schaaff, et al. (2001). "Organic ion imaging of biological tissue with secondary ion mass spectrometry and matrix-assisted laser desorption/ionization." Journal of Mass Spectrometry **36**(4): 355-369.
Trim, P. J., C. M. Henson, et al. (2008). "Matrix-Assisted Laser Desorption/Ionization-Ion Mobility Separation-Mass Spectrometry Imaging of Vinblastine in Whole Body Tissue Sections." Analytical Chemistry **80**(22): 8628-8634.
Troendle, F. J., C. D. Reddick, et al. (1999). "Detection of pharmaceutical compounds in tissue by matrix-assisted laser desorption/ionization and laser desorption/chemical ionization tandem mass spectrometry with a quadrupole ion trap." Journal of the American Society for Mass Spectrometry **10**(12): 1315-1321.
Ullberg, S. (1954). "Studies on the distribution and fate of S35-labelled benzylpenicillin in the body." Acta radiologica. Supplementum **118**: 1-110.
Upthagrove, A. L., M. Hackett, et al. (1999). "Fragmentation pathways of selectively labeled uropranolol using electrospray ionization on an ion trap mass spectrometer and comparison with ions formed by electron impact." Rapid Communications in Mass Spectrometry **13**(6): 534-541.
Vafadar-Isfahani, B., N. Patel, et al. (2012). The use of an on-line two-dimensional (RP/RP) liquid chromatography mobility-enabled approach for the characterisation of the proteome of bacterial extracts. Proceedings of the American Society of Mass Spectrometry Conference, Vancouver, BC, Canada.
van Duijn, E., A. Barendregt, et al. (2009). "Chaperonin Complexes Monitored by Ion Mobility Mass Spectrometry." Journal of the American Chemical Society **131**(4): 1452-1459.
Vestal, M. L. (2001). "Methods of ion generation." Chemical Reviews **101**(2): 361-375.
Wallace, A. (2010). "A High-Resolution Ion Mobility Mass Spectrometry Platform for Breakthrough Discoveries in Life Science Research and the Pharmaceutical Industry." American Laboratory **42**(6): 13-17.
Walworth, M. J., M. S. ElNaggar, et al. (2011). "Direct sampling and analysis from solid-phase extraction cards using an automated liquid extraction surface analysis nanoelectrospray mass spectrometry system." Rapid Communications in Mass Spectrometry **25**(17): 2389-2396.

Wang, H. Y. J., S. N. Jackson, et al. (2005). "Localization and analyses of small drug molecules in rat brain tissue sections." Analytical Chemistry **77**(20): 6682-6686.

Waters (2011) "A novel High Definition Imaging (HDI) Informatics Platform. Technological Brief, Waters Corporation. (http://www.waters.com/waters/library.htm?locale=en_US&lid=134621461). "

Wiley, W. C. and I. H. McLaren (1955). "Time-of-flight mass spectrometer with improved resolution." Review of Scientific Instruments **26**(12): 1150.

Williams, J. P., M. Grabenauer, et al. (2010). "Characterization of simple isomeric oligosaccharides and the rapid separation of glycan mixtures by ion mobility mass spectrometry." International Journal of Mass Spectrometry **298**(1-3): 119-127.

Wiseman, J. M., D. R. Ifa, et al. (2006). "Tissue imaging at atmospheric pressure using desorption electrospray ionization (DESI) mass spectrometry." Angewandte Chemie-International Edition **45**(43): 7188-7192.

Wiseman, J. M., D. R. Ifa, et al. (2008). "Ambient molecular imaging by desorption electrospray ionization mass spectrometry." Nature Protocols **3**(3): 517-524.

Wiseman, J. M., D. R. Ifa, et al. (2008). "Desorption electrospray ionization mass spectrometry: Imaging drugs and metabolites in tissues." Proceedings of the National Academy of Sciences of the United States of America **105**(47): 18120-18125.

Wiseman, J. M., S. M. Puolitaival, et al. (2005). "Mass spectrometric profiling of intact biological tissue by using desorption electrospray ionization." Angewandte Chemie-International Edition **44**(43): 7094-7097.

Zenobi, R. and R. Knochenmuss (1998). "Ion formation in MALDI mass spectrometry." Mass Spectrometry Reviews **17**(5): 337-366.

zur Nedden, S., R. Eason, et al. (2009). "An ion-pair reversed-phase HPLC method for determination of fresh tissue adenine nucleotides avoiding freeze-thaw degradation of ATP." Analytical Biochemistry **388**(1): 108-114.

zur Nedden, S., S. Hawley, et al. (2011). "Intracellular ATP Influences Synaptic Plasticity in Area CA1 of Rat Hippocampus via Metabolism to Adenosine and Activity-Dependent Activation of Adenosine A(1) Receptors." Journal of Neuroscience **31**(16): 6221-6234.

Appendix B: Dissemination of Work